Saint-Petersburg State University

Petersburg Nuclear Physics Institute
named after B.P. Konstantinov
of National Research Centre "Kurchatov Institute"

Printed as a manuscript

Solovyev Dmitry Anatolyevich

Theoretical particularities of photon scattering processes in applications to precision spectroscopic experiments and astrophysics

1.3.3. Theoretical physics

THESIS
submitted in conformity with the requirements
for the degree of doctor of physico-mathematical sciences

Translation from Russian

Scientific consultant –
doctor of physico-mathematical sciences,
professor,
Labzowsky L.N.

Saint-Petersburg — 2024

Contents

Introduction

Relevance of the work

This dissertation is devoted to the description of photon scattering processes (and, as a consequence, emission or absorption) on simple atomic systems. The simple systems are hydrogen atom or muonic hydrogen, light hydrogen-like ions, and helium atom. The description of one- and multiphoton scattering processes is carried out in the framework of the quantum electrodynamics (QED) theory of bound states and the so-called S-matrix formalism. QED theory is widely spread, being the most rigorous way to describe the processes of radiation and the effects causing the shift of energy levels in neutral and ionized atomic systems. The QED theory, which has become «classical» in scientific research of this kind, is presented in textbooks intended for senior students. As basic books one can refer to such monographs as [1–4] and others. The theory presented in these books provided the basis for further research, which led to the rapid development of atomic physics. Theoretical calculations of the effects associated with photon scattering processes are inherently accompanied by experimental advances aimed at improving the accuracy of measurements and vice versa. Comparison of theoretical and experimental results, in its turn, stimulates further development of theory and methods allowing to carry out competent investigations of this kind.

Since the early days of quantum mechanics (QM), the study of the atomic characteristics [5, 6], such as the energy of bound states, has played a key role in the development of modern quantum field theory and its practical applications in various fields of physics. Subsequent experimental observations and their increasing accuracy required the calculation not only of relativistic correc-

tions, but also the calculation of more complicated effects, such as, for example, various radiative QED corrections [1–4].

Theoretical calculations carried out in the framework of QED and perturbation theory based on certain methods and approaches [7–10] are justified not only by competing experiments in terms of accuracy. The description of increasingly subtle effects in atoms is a means of understanding physical processes, serving, for example, to define fundamental physical constants, see, e.g., [11]. In this regard, experiments conducted with different atomic systems are by far the most accurate. As an example of the success of QED theory one can refer to the work on the calculation and measurement of the g-factor of the electron in multi-charged ions (HCI) [12–15], which allowed to refine the electron mass by an order of magnitude [16]. Improvements are desired for further precision testing of the Standard Model of particle physics [17], as well as determining the value of physical constants such as the fine structure constant, α, and the Rydberg constant, R_∞). With the help of measurements of the g-factor of the electron, one can also establish the constraints on the interaction between the electron and light bosons, which are the basis for the search for «new physics» [18, 19].

Currently, the most accurate atomic experiments can be attributed to measurements of transition frequencies in hydrogen [20, 21] with a relative error of 4.2×10^{-15}, see also [22], in helium [23, 24], where the experimental accuracy reaches the level of 10^{-12}, and in atomic clocks with a precision of about 10^{-17} [25–27]. Such precise experiments required theoretical calculations of various QED effects at $\alpha^6 m^2/M$ and $\alpha^7 m$, see [11], where α is the fine structure constant, m and M are the electron and nucleus masses, respectively. In addition to accurate theoretical calculations of binding energies in the hydrogen atom, the fine structure and isotopic shift of low-lying helium states generally serve as an independent tool to test fundamental interactions. As in the case of well-studied one-electron atomic systems, measured transition frequencies should be compared with theoretical calculations in search of possible discrepancies [28].

The reconciliation of theoretical and experimental studies reveals difficulties, to the solution of which considerable efforts are made. One of the most

prominent ones is the "proton radius puzzle" [29]. Since 2010, the question of the discrepancy between the values of the proton radius obtained by measuring the transition frequencies in electron (H) and muon (μH) hydrogen atoms has been the reason for a detailed theoretical and experimental finding and analysis of the effects to eliminate the discrepancy. At the same time, starting from the work of [29] and subsequent works of [30, 31], the charge radius of the proton extracted from experiments with muon hydrogen remains unchanged. As a result, the puzzle was mostly solved after the publication of data from the experiment [32], matching the value of the proton radius for electron and muon hydrogen. A good agreement of the values was achieved by experimentally accounting for the quantum interference effect (QIE). The latter is the dominant contribution of the nonresonant (NR) corrections arising in the determination of the transition frequency from the cross section of photon scattering on atoms, see the fundamental works in this direction [33–43]and subsequent works [44–53].

Another example is the comparison of theoretical and experimental results in simple atomic systems such as the positronium atom (Ps) and the helium atom (He). Within the framework of QED theory, both atoms are among the most thoroughly studied objects. Comparison of experimental data with the theoretical results, however, revealed significant discrepancies. Since the theory fails to identify the source of possible calculation error and/or to discover (experimentally and theoretically) effects that eliminate such discrepancies, such differences in transition frequencies are used to construct hypotheses about «new physics» and to verify fundamental interactions, see, for example, the work on the helium atom [54–57]. In turn, the positronium atom is the most attractive to theorists, being a purely lepton bound two-charge system. The precision experiments with the Ps atom can be divided into measurements of ortho- and para-positronium lifetime [58], and determination of the frequencies of fine [59] or hyperfine splitting [60] transitions. A comparative analysis of the measured and calculated values in the Ps atom also reveals the discrepancies between theory and experiment [59, 61].

The relevance of the work is emphasized by the fact that in one part of this dissertation a number of applications that can be directly related to precision

spectroscopic measurements of transition frequencies in hydrogen-like atoms will be considered. Due to the parametric estimates given, the effects considered can be applied to light hydrogen-like ions. The restriction to ions with small nuclear charge Z is due to the nonrelativistic limit used in the calculations. Additionally, in this paper the photon scattering process is described in the framework of the dipole approximation, although the discussion of the higher multipole moments of the photon will also be touched upon. The nonrelativistic and dipole approximations used permit us to carry out the leading order estimates of the effects. The relevance of the results obtained is discussed in each respective section, but can be immediately highlighted by the fact that the frequency shifts obtained are at the level of experimental error. Thus, subsequent increases in experimental accuracy will inevitably encounter the issues discussed in the thesis. Detection of such effects is also relevant in connection with the research on the search for dark matter based on precision spectroscopic experiments [62–65].

Among the equally important issues discussed in this dissertation are studies devoted to a detailed comparison of the spectra of hydrogen and anti-hydrogen atoms. The presented theoretical results in this direction are of particular importance in connection with recent outstanding experimental achievements on the synthesis and confinement of anti-hydrogen atoms ($\bar{\mathrm{H}}$) [66]. The latter allowed a number of spectroscopic experiments in anti-proton helium (one of the electrons is replaced by an anti-proton) [67], stimulating the corresponding theoretical studies [68, 69]. The continuous development of experimental techniques for synthesizing anti-hydrogen atoms [70–72] makes it possible to carry out precision experimental measurements of Lyman-α energies, hyperfine, etc. transitions [73–75]. All studies of this kind, on direct comparison of matter and anti-matter spectra, are straight related to the verification of CPT invariance (C-charge, P-space and T-time, respectively) and/or to the search for effects breaking this global symmetry.

Another, no less interesting, direction touched upon in the presented thesis is the description of photon scattering (along with just radiation processes) in application to astrophysical problems. In particular, the considered effects can be related to the study of the cosmic microwave background (CMB). The

theory describing CMB necessarily contains radiation/absorption processes, see, e.g., [76]. Detailed investigations of the properties of the cosmic microwave background were started quite a long time ago [77–79], but only recently the theoretical predictions have been confirmed experimentally, see the RELICT [80] and COBE [81] experiments (the latter was awarded the 2006 Nobel Prize).

By the time the cosmological recombination of the early Universe began, the relict radiation was represented by the Planck frequency distribution, and accounting for the contributions of bound-free and bound-bound transitions in the emerging atomic systems leads to anisotropy in CMB at the $10^{-5} - 10^{-6}$ level, see [77–79]. At the same time, to describe the ionization/recombination processes in the hydrogen atom, the «three-level» approximation - the ground $1s$, the excited $2s$ states, and the continuum - was used in the above works. As in the case of laboratory studies, the experiments [80, 81] (and the subsequent ones based on the WMAP spacecraft - Wilkinson Microwave Anisotropy Probe), having achieved a measurement accuracy of 1%, stimulated the need to develop theoretical methods and calculations. A detailed theory of recombination of hydrogen, singly ionized and neutral helium atoms is given in [76], where the multilevel approximation of atoms was already used, bound-bound and bound-free transitions are included. Since this key work, in this direction foreign and domestic scientists (see the works of the authors: R.A. Sunyaev, V.K. Dubrovich, E.E. Kholupenko, A.V. Ivanchik, D.A. Varshalovich, J. Chluba, C. Hirata, etc.) have been working intensively, with the need to include effects contributing up to the order of 0.1%. To achieve such precision in theoretical calculations, a detailed description and analysis of radiation processes within the framework of atomic physics is required, see, for example, [82–84].

All the above-mentioned directions of research are summarized by the necessity to use the most rigorous theory in describing the processes of emission, absorption and scattering of photons on atoms. In the presented thesis, the theoretical description of the considered effects is given in the framework of the QED theory based on the Line Profile Approach (LPA), see [8]. This approach has the distinct advantage that it was originally formulated with the goal of describing the spectral line profile [85] as accurately as possible. Since most of the thesis is devoted to the study of the effects that cause asymmetry in the

observed line shape, the use of the LPA method is thematically appropriate.

Tasks and objectives of the thesis work

The main **objective** of this thesis is to determine the fundamental principles, detailed description and application to modern precision experiments of the effects associated with the scattering process on simple atomic systems. In addition to laboratory measurements, this thesis aims to discuss a number of issues relevant to astrophysical research involving multiphoton atomic processes. Generally, in the framework of spectroscopic measurements, the use of a resonant spectral line profile is sufficient. The corresponding profile can be correlated to an emission or absorption process. However, the achieved level of accuracy of spectroscopic experiments in conjunction with high-precision QED calculations has led to the need to take into account more and more subtle effects. Their identification, as well as the evaluation of their contribution to the determination of the transition frequency, has become an indispensable part of the determination of fundamental physical constants. Thus, it has recently been shown that the determination of the transition frequency from measured data is significantly refined by theoretical processing of the observed spectral line. As predicted theoretically, a large influence of effects arising outside the resonance approximation has been found experimentally. In turn, a detailed comparison of matter and anti-matter spectra (transition frequencies in particular) is a direct observation of CPT invariance and/or its violation. Similar goals can be set in the astrophysical context, where a detailed description of CMB and its anisotropy necessitates a neat theoretical description of scattering processes. Without solving these problems, the realization of the new physics expected in atomic resonance spectroscopy in the near future, beyond the resonance approximation, is impossible.

The following **problems** had to be solved in order to achieve the goal:

1) In the framework of the strict QED theory, give a detailed description of the process of photon scattering on the atom. Generalize the LPA method to the case of going beyond the resonance approximation.

2) Using the constructed theory within the framework of known approaches and approximations, identify the effects influencing the determination of the transition frequency. To carry out corresponding calculations in applications to modern precision spectroscopic experiments.

3) Carry out theoretical calculations and evaluate the influence of nonresonant and multiphoton radiation processes in astrophysical problems related to the formation of CMB and its anisotropy.

4) Investigate the influence of nonresonant contributions and multiphoton emission processes in an external electric field on the precision determination of transition frequencies in hydrogen and anti-hydrogen atoms.

Scientific novelty of the work

1) As part of the thesis work, an analytical derivation and corresponding numerical calculations of the nonresonant corrections to the transition frequency arising in the total scattering cross section have been presented.

2) For the first time, from the first principles of the QED theory, the frequency dependence for the atomic level width was taken into account. The effect was considered for the calculation of the corresponding shift of the resonance frequency, as well as for the detailed description of the spectral line profile in applications to laboratory experiments and astrophysical problems.

3) Within the framework of the developed approach, the asymmetry of the spectral line profile for the differential scattering cross section was analyzed both analytically and numerically, and the corresponding shifts of the resonance transition frequency were calculated.

4) Using the methods and approaches developed during the thesis work, the influence of broadening effects (due to pressure and external thermal radiation) on the precision determination of the transition frequency has been evaluated.

5) A comparative analysis of the different definitions of transition frequency arising in different approaches has been carried out.

6) For the first time the impossibility of unambiguous separation of radiation and absorption processes is demonstrated (separation is possible only in the framework of the resonance approximation).

7) The thesis presents for the first time results on the study of absorption profile asymmetry induced by cascade radiation processes.

8) Cascade radiation processes in the context of astrophysical research are discussed in detail. In the framework of this issue, the QM and QED approaches are compared, the inseparability of cascade and «pure» radiation, and the interpretation of the contributions of cascade-free «two-photon widths» in cascade processes is discussed.

9) The probabilities of one- and two-photon emission in an external electric field have been calculated. The results are used to compare the spectral characteristics of hydrogen and anti-hydrogen atoms.

10) A comparative analysis of NR effects arising in an external electric field for hydrogen and anti-hydrogen atoms has been carried out.

11) The work considers two-photon emission processes taking into account higher photon multipoles and for highly excited states; its astrophysical application is discussed.

12) The effect of electromagnetic induced transparency (EIT) in the context of astrophysical conditions is investigated for the first time.

Practical significance

The theoretical and practical significance of the thesis is determined, first of all, by the development of the LPA method and its generalization to studies of processes beyond the resonance approximation. The detailed description of photon scattering processes on atoms has gained special importance in the last

few years. Their study has led to the fact that the data obtained in the course of precision spectroscopic experiments must necessarily take into account the effects of spectral line contour asymmetry. As a consequence, the practical validity of the obtained results is expressed in their direct application to experiments on the measurement of transition frequencies. The latter can be achieved in several ways: a) by calculating the corresponding frequency shifts (and then taking them into account in the final result); b) by processing the experimental data by a matched selection of an asymmetric fitting contour and then determining the transition frequency. Being equal (see discussion in the thesis), these two approaches should be used for precise determination of fundamental physical constants.

The description of simple atomic systems (hydrogen atom, hydrogen-like atomic systems, helium) is especially important because in the corresponding experiments the accuracy reaches the level of 10^{-13} relative magnitude (and higher) of [21, 32]. It is shown in the thesis that in order to achieve a higher level of accuracy, consideration of nonresonant effects is required with necessity. It is worth noting that the accuracy of measurements in the hydrogen atom in combination with the available theory makes it possible to accurately determine the fundamental physical constants, and the search for effects contributing at the level of several kilohertz is one of the main goals for solving the problem called the «proton radius puzzle». Finally, it has recently become especially popular to construct theoretical hypotheses and their subsequent experimental verification in search for «new physics». Mainly, such hypotheses are based on detection of discrepancies between the results of theoretical calculations and experimental measurements of transition frequencies. As an example, it is enough to refer to such works as [28] for the helium atom, for positronium [59] and paper establishing experimental constraints on dark matter using atomic clocks [62]. Thus, revealing the effects that remove such divergences is of great practical importance for the further development of fundamental physics.

The second, but no less important circumstance indicating the practical value of the results is the question of a detailed comparison of the spectra of hydrogen and antihydrogen atoms. The studies presented in this work show that even insignificant values of the external electric field available in laboratory

conditions can lead to significant differences in the spectral characteristics in such systems. Thus, when studying the global CPT symmetry and the processes violating it, the examples given demonstrate the necessity of taking into account the presence of stray fields. No less valuable is the question about the search of antimatter in the Universe.

Finally, the astrophysical applications of the theory developed in the thesis should be emphasized. In particular, astrophysical studies have shown the presence of dark matter and dark energy, the search for which is now directed by the efforts of many scientists. As a separate area of research, the thesis deals with a number of effects affecting the formation of anisotropy of cosmic microwave radiation. In particular, the paper proposes new approaches in the description of photon scattering (emission/absorption) processes on the hydrogen atom. As a result of such studies, the question of the influence of appropriate corrections on the recombination of the early Universe is discussed [76].

Methods

Theoretical investigations aimed at studying the spectroscopic properties of various atomic systems, be they ions (with a large or small number of bound electrons) or neutral atoms, use rather well established methods. The theoretical basis for the development of such methods is represented by the QM or QED approaches, see [1–6, 86]. At the same time, there is a number of methods developed by different scientific groups. As the main approaches for solving problems on calculation of energies of atomic levels and/or description of processes accompanied by radiation, the following can be mentioned. Historically, the first and most adapted for these purposes is the adiabatic S-matrix method developed in the [87, 88]. This approach is based on the relativistic quantum field theory presented in the key paper of [89]. A clear advantage of the adiabatic theory (in contrast to the widely used formalism of the «common» S-matrix) is its application to both the case of irreducible and reducible graphs in the framework of the Feynman diagrammatic technique, see [3, 90]. Another method of calculating the energy corrections corresponding to the reduced and irreducible Feynman diagrams, which has become widely used, is the «Two-time

Green's function method» (TTGF) [2, 7, 91]. At present, this approach is the leader in calculations of the atomic structure of highly charged ions [7]. Alternative methods for calculating the spectroscopic properties of atoms and ions are also «covariant evaluation operator method» (CEO) [9, 92] and «line profile approach» (LPA) [8]. Within the scope of the presented thesis, the adiabatic S-matrix method and the spectral line profile approach will be used mainly.

These works, however, represent only a basis for the corresponding calculations and the solution of the stated problems (see section **Aims and Objectives** of the Thesis). The large variety of studies of photon scattering processes on atomic systems available in the modern literature should be extended to the case of nonresonant effects. As a rule, studies of this kind are carried out as follows. First, a theoretical description of the one- or multiphoton scattering process for the atomic system under consideration is given, for example, in the framework of the S-matrix formalism. As a next step, the dominant (resonance) contribution is identified in the obtained expressions. It is usually represented by a singular term in the scattering amplitude. Then, by the methods of QED theory, it is regularized [85]. Finally, the remaining contributions are sequentially evaluated. The corresponding calculations apply to an arbitrary scattering process (e.g., with or without the presence of cascade radiation). Obviously, increasing the number of photons complicates the theoretical description. Problems relating only to radiation processes have another significant simplification. As will be shown later, see, for example, [8], within the resonance approximation, a part of the scattering process (in this case absorption) can be discarded, subjecting to a detailed study the phenomena arising only in the registered radiation. Thus, for example, in astrophysical applications it is the latter circumstance that is used, i.e., the separation of the scattering process into distinct parts, i.e., absorption and emission. As a rule, such approximation is sufficient at the level of modern measurements. A discussion of the validity of such a separation with respect to precision laboratory experiments will be presented in the main text of the thesis.

As part of the research conducted by the author of this thesis, it was shown that well-known effects, for example, in atomic spectroscopy, can also be interesting and important in astrophysical studies of CMB and the interstellar

medium, as well as used to search for antimatter in the Universe. Thus, the density matrix method and the corresponding Liouville quantum equation have been used to apply the EIT [93–95] effect to the search for contributions to the CMB anisotropy, see, e.g., [96,97] and many others. The stationary (*steady state approximation*) approximation [98] was used to solve the above equations. In the framework of this theory, one can directly obtain the absorption profile for the transition in the system under consideration, which is then utilized in the theory of radiative transfer [76,99] by means of the Sobolev approximation [100].

Throughout the thesis, methods of mathematical physics are used and numerical calculations are performed. As a rule, during the whole work analytical expressions are derived, which acquire the most convenient form in the nonrelativistic approximation. On the basis of the nonrelativistic approximation it becomes more simple to carry out numerical calculations, for example, by means of the Green's function method [101]. At the same time for revealing the main contribution in light atomic systems the nonrelativistic approximation is well justified. The thesis will also discuss the dipole approximation and going beyond it (taking into account higher multipoles), and will use the method of B-splines with the imposed condition of dual kinetic balance for summing over the intermediate states of the Dirac energy spectrum [102].

Validity and approbation of the results

The validity of the obtained results is based on the exact correspondence with many conclusions presented in the scientific literature by other authors. Two types of correspondence can be distinguished: a) the result obtained during our research was later confirmed, and b) the effects and values considered earlier by other authors were confirmed in our research in order to further develop them. In addition, the result of the experiment [32], which clearly indicated the presence of line profile asymmetry, its significance and the role of nonresonant effects in precision spectroscopic experiments, should be mentioned separately. Most of the results discussed in this thesis can be attributed to theoretical predictions. The magnitude of the contributions described by the effects is at or close to the level of the present-day precision of the experiments, which allows us to

assert that it is necessary to take them into account. On the other hand, the insignificance of the obtained values relative to the experimental error is also important and shows that the corresponding measurements are not subject to such effects. As such, nonresonant effects that are significant for measurements of transition frequencies in the hydrogen atom and are irrelevant for muonic hydrogen. As an example, one can point out the studies of two-photon emission processes for highly excited states, which qualitatively assess the possibility of limiting the number of transitions necessary for a detailed description of the processes of formation of the cosmic microwave background. Another example can be the results of studies of the electromagnetic induced transparency effect in cosmological conditions of the early Universe or interstellar medium. It was shown that the phenomenon of electromagnetic induced transparency can lead to a distortion of the cosmic background at the level of 1% (the latter represents the modern level of accuracy of the ISM measurements). Finally, studies of radiation processes in an external electric field for the anti-hydrogen atom show that even insignificant ("stray") field values can lead to significant differences between the spectra of the anti-matter and ordinary hydrogen atom. To reveal this effect, the results of well-known works obtained for other purposes were used (see the main text of the thesis and [103–105]).

The results of the work have been repeatedly reported at scientific seminars of the Division of Quantum Mechanics, Department of Physics, SPbSU, working seminars of separate scientific groups of ITMO University, scientific seminars at the theoretical department of PNPI, scientific seminars of foreign universities (Technical University of Dresden and Heidelberg University), as well as at international and domestic conferences:

- «One-, two- and three-photon transitions between 2s-, 2p- and 1s-levels for hydrogen and anti-hydrogen atoms in an external electric field and without it», 22-23 January, 2008, International Workshop "Fock Readings. Modern Problems of Physics", St. Petersburg State University, Department of Physics, St. Petersburg, Russia

- «Two-photon transitions in hydrogen atom: beyond the dipole approximation», Paris Workshop on Cosmological Recombination, Jule 08-10,

2009, Universite Paris-Sud, Paris, France

- «Multiphoton radiation processes with the presence of cascades in cosmological recombination for the atom», 3rd All-Russian Meeting "Precision Physics and Fundamental Physical Constants", The Ioffe Physical-Technical Institute of the Russian Academy of Sciences, 6-10 December 2010, Sankt-Peterburg, Russia.

- «Multiphoton processes in atomic physics and astrophysics», Workshop on the Proton Radius Puzzle, Europian Centre for Theoretical Studies in Nuclear Physics and Related Areas, October 29 - November 2, 2012, Trento, Italy

- «Quantum Optics Effects in Astrophysics», 11th International Colloquium on Atomic Spectra and Oscilator Strengths for Astrophysical and Laboratory Plasmas, University of Mons, August 5-9, 2013, Mons, Belgium

- «Hydrogen and Antihydrogen spectra in presence of external fields», Meeting on Precision Physics and Fundamental Physical Constants, 1-5 December, 2014, Dubna, Russia

- «QED derivation of energy shift and line broadening induced by the BBR for bound electron», «Dark Ages and White Nights (Cosmic Microwave Background Spectroscopy)», 21 June 2016, St. Petersburg, Russia

- «Thermal QED effects in problems of atomic physics and astrophysics», 52nd PNPI Winter School, 26 February - 4 March, 2018, Roshchino, Russia

- «Recombination cross-section for the hydrogen atom in presence of blackbody radiation», 13 th International Colloquium on Atomic Spectra and Oscillator Strengths for Astrophysical and Laboratory Plasmas (ASOS2019), 23-27 June, 2019, Fudan University, Shanghai, China

- «Thermal QED theory for bound states», International Conference on

Natural Sciences and Humanities - «Science SPbU - 2020», 25 December 2020, SPbSU, St. Petersburg, Russia.

- «Thermal shift of atomic levels in hydrogen: influence on the determination of the proton radius», LXXI International Conference on Nuclear Physics « Nucleus-2021. Physics of atomic nucleus and elementary particles. Nuclear Physics Technologies», 20-25 September 2021, St. Petersburg State University, St. Petersburg, Russia.

- «The recombination process of a hydrogen atom in the presence of blackbody radiation», LXXI «Physics and Astrophysics - from Fundamental Constants to Cosmology, In Memory of D.A. Varshalovich», 27-28 September 2021, The Ioffe Physical-Technical Institute of the Russian Academy of Sciences, St. Petersburg, Russia.

- «Thermal QED theory for bound states», School-Conference «Modern Problems of Chemical Physics and Theoretical Chemistry», 25-29 July 2022, Irkutsk, Bolshiye Koty, Russia.

- «Thermal QED theory for bound states», International Conference on Natural Sciences and Humanities - «Science SPbU - 2022», 21 November 2022, SPbU, St. Petersburg, Russia.

- «Radiative corrections to the bound electron g-factor and level width in the presence of a magnetic field combined with blackbody radiation», International Summer Conference on Theoretical Physics (ISCTP-2023), 3-7 July 2023, MIPT Abrikosov Centre for Theoretical Physics, Dolgoprudny, Russia. Abrikosov Centre for Theoretical Physics, Dolgoprudny, Russia.

The results of research have been repeatedly reported in co-authorship by Associate Professor T.A. Zalyalyutdinov, postgraduate student A.A. Anikin, student D.A. Danilov.

Publications

The results presented in the thesis are contained in the form of 39 published articles in peer-reviewed foreign and domestic journals from the list of Scopus, Web of Science and VAK RF. In total, the author has published more than 70 papers in refereed foreign and domestic journals cited by Scopus, Web of Science and VAK RF databases.

The author of the dissertation has developed and registered «Program for calculation of cross sections and recombination coefficients to an arbitrary state of hydrogen atom», registration date 3 March 2020, №2020612747. Right holder: Federal State Budgetary Educational Institution of Higher Professional Education "Saint-Petersburg State University" (SPbSU). Authors: D.A. Solovyev and Y.V. Triaskin.

Personal contribution of the author

The work was carried out at St. Petersburg State University. A number of studies were carried out jointly with A.A. Anikin, T.A. Zalyalyutdinov, G. Plunien, G. Soff and L.N. Labzovsky. Most of the research results presented in the thesis have been published in a hardly separable co-authorship; to exclude ambiguity in the paper, the corresponding references are indicated with a full list of names. At the same time, the presented and put forward for discussion in the theses were obtained personally by the author.

The structure of the dissertation

The thesis consists of an introduction, 10 chapters, a conclusion, a list of abbreviations and symbols, 28 figures, 26 tables, a bibliography of 280 titles and a list of the author's publications of 39 titles. Each chapter discusses the main results obtained. The volume of the thesis is 290 pages.

Thesis statements to be defended

- Nonresonant expansion of the Lorentz contour
- Nonresonant corrections to the total photon scattering cross section
- Nonresonant corrections to the photon scattering differential cross section
- Natural asymmetry of the spectral line profile
- The quantum interference effect
- Relevance of transition frequency definitions beyond the resonance approximation
- Angular correlations in application to precision spectroscopy of the hydrogen atom
- Angular correlations for muonic hydrogen and helium atoms
- Angular correlations in two-photon spectroscopy
- The effect of thermal broadening in nonresonant corrections
- Influence of radiation on the absorption profile beyond the resonance approximation
- Two-photon (multipole) radiation processes
- Two-photon decay processes in an external electric field
- Two-photon decays of highly excited states
- Spectra of hydrogen and anti-hydrogen atoms in an external electric field
- Nonresonant corrections in an external electric field
- Probabilities of two-photon decay with the presence of cascades
- Inseparability of cascade and «pure» radiation

- Two-photon width of the atomic level as an imaginary part of the energy shift
- Electromagnetically induced transparency effect in cosmological conditions of the early Universe
- Electromagnetically induced transparency effect - 21 cm line profile in a hydrogen atom

Principal scientific results

- Nonresonant Lorentz contour extension, see the second chapter in arXiv:2204.12199 [physics.atom-ph], 26 Apr 2022 from the list of publications of the thesis author (all analytical calculations performed personally by the thesis author)
- Nonresonant corrections to the total photon scattering cross section, see Refs. [8, 35–37, 40–42, 106] (personal contribution of at least 80%)
- Nonresonant corrections to the photon scattering differential cross section, see chapter four in arXiv:2204.12199 [physics.atom-ph], 26 Apr 2022 and papers [42, 52, 53, 107] (personal contribution of at least 80%)
- Natural asymmetry of the spectral line profile, see [8, 37] from the list of publications of the author of the thesis (in particular the third paragraph in [37] and section 3.8 in [8]; all analytical and numerical calculations were carried out personally by the author of the thesis)
- Quantum interference effect, see Chapter 4 in arXiv:2204.12199 [physics.atom-ph], 26 Apr 2022; arXiv: 2311.12606 [physics.atom-ph], 21 Nov 2023 (from the list of publications of the thesis author) and papers [52, 53, 108] (personal contribution of at least 80%)
- For consistency of definitions of the transition frequency beyond the resonance approximation, see Section 4.3 in arXiv:2204.12199 [physics.atom-ph], 26 Apr 2022; and arXiv: 2311.12606 [physics.atom-ph], 21 Nov 2023

(from the list of publications of the thesis author, all analytical and numerical calculations were performed personally by the thesis author), papers [52, 53, 108]

- The method of moments adapted to the determination of transition frequencies, see [109] (all analytical and numerical calculations were performed personally by the author of the thesis)

- Angular correlations in application to precision spectroscopy of the hydrogen atom, see sections 4.2, 5.1, 5.2 in arXiv:2204.12199 [physics.atom-ph], 26 Apr 2022; arXiv: 2311.12606 [physics.atom-ph], 21 Nov 2023 and papers [52, 53, 108] (personal contribution of at least 80%)

- Angular correlations with respect to muonic hydrogen and helium atoms, see sections 4.4, 4.5, 5.3 in arXiv:2204.12199 [physics.atom-ph], 26 Apr 2022 (personal contribution of at least 80%)

- Angular correlations in two-photon spectroscopy, see sections 5.1, 5.2, and 5.3 in arXiv:2204.12199 [physics.atom-ph], 26 Apr 2022, and [53, 107] (personal contribution is at least 80%)

- For the effect of thermal broadening in nonresonant corrections, see Section 5.4 in arXiv:2204.12199 [physics.atom-ph], 26 Apr 2022 (all analytical calculations performed personally by the author of this thesis)

- For the effect of radiation on the absorption profile beyond the resonance approximation, see Section 3 of the paper arXiv: 2311.12606 [physics.atom-ph], 21 Nov 2023 (all analytical calculations performed personally by the author of this thesis)

- Two-photon (multipole) radiation processes, see [82, 83, 110–118] (all analytical calculations were performed personally by the author of the thesis, the total contribution can be estimated to be at least 80%)

- One- and two-photon decay processes in an external electric field, see [106, 112–114, 119] (all analytical calculations performed personally by the author of this thesis)

- Two- and multiphoton decays of highly excited states, see Refs. [82–84, 115–125] (personal contribution is at least 80%).
- Spectral characteristics of hydrogen and anti-hydrogen atoms in an external electric field, see [38, 39, 106, 112–114, 119, 126, 127] (personal contribution is at least 80%)
- Nonresonant corrections in the external electric field, see [38, 126] (all analytical and numerical calculations were performed personally by the author of the thesis)
- Two-photon decay probabilities with the presence of cascades, see [82, 84, 115, 116, 118, 120, 121] (personal contribution is at least 80%)
- Inseparability of cascade and «pure» radiation, see [82, 120, 121] (personal contribution is at least 80%).
- «Two-photon approximation» in multiphoton decays, see papers [115, 116, 118, 120] (all analytical calculations were performed personally by the author of the thesis, total contribution is at least 80%)
- Two-photon atomic level width as an imaginary part of the energy shift, see papers [84, 121] (personal contribution is at least 80%)
- The effect of electromagnetically induced transparency in cosmological conditions of the early Universe, see [128, 129] (all analytical calculations were performed personally by the author of the thesis, the total contribution is at least 80%)
- Electromagnetic induced transparency effect - 21 cm line profile in the hydrogen atom, see [130] (all performed personally by the author of this thesis)

Chapter 1.

The role of line profile asymmetry in precision spectroscopy: a review of existing approaches

The quantum mechanical derivation of the natural line profile in atomic physics was introduced by Weisskopf and Wigner [131]. With the development of relativistic quantum field theory, this derivation was revised within the framework of quantum electrodynamics theory (QED) and the S-matrix formalism for one-electron atoms in the pioneering paper by F. Low [85]. Later, the QED theory of the line profile was also reformulated for many-electron atoms [132] and applied to overlapping resonance lines in highly charged ions (HCI) [133]. The combination of these approaches and the corresponding development of the methods started in the [87, 89] was successfully applied to theoretical calculations of radiative QED corrections to energy levels and transition probabilities in atoms and ions in the framework of the Spectral Line Approach (LPA) [8].

The further development of the line profile theory is closely related to the experimental successes in measuring the transition frequency in the hydrogen atom [20, 21, 134], where the absolute value of the $1s - 2s$ frequency of the two-photon transition was established with an accuracy of the order of 10^{-15}

relative magnitude. Such experiments stimulated interest in theoretical studies of effects beyond the resonant approximation, based on results obtained earlier for the HCI [33, 34]. The theoretical analysis of the photon scattering process (within which the QED determination of the spectral line profile arises [85]) was resumed for the hydrogen atom in [35]. One of the most important consequences of LPA theory is the introduction of nonresonant (NR) corrections to the transition frequency arising from nonresonant terms in the scattering amplitude. Various applications of the corresponding corrections to the total cross section can be found in [8, 84], although for the hydrogen atom they are rather beyond the current experimental precision.

NR effects have attracted special interest of researchers in the last decade and have been discussed in a number of theoretical papers [35–37, 43, 135, 136]. This was primarily facilitated by advances in precision spectroscopic experiments [21, 134, 137]. In particular, the experiment [21] to measure the frequency of the $1s - 2s$ transition is one of the most accurate ever performed in the optical domain, with a resulting absolute error of about 10 Hz. The evaluation of the corresponding NR corrections within the framework of the QED theory and LP approach was performed in [37, 40]. An important experimental result was also presented in [137], where the Lyman-α (Ly_α) $1s - 2p$ transition in the hydrogen atom was measured. The corresponding estimates of nonresonant corrections to the frequency of the $1s - 2p$ transition were made in [35–37, 43, 136]. Later, similar calculations were performed taking into account the interference between neighbouring hyperfine components of the $2p$ [41] level.

The continuous development of theory and experiment leads to the appearance of new problems. One of the most striking examples is the problem known in the literature as the «proton radius puzzle», which arose as a result of spectroscopic experiments on muonic hydrogen [29]. The first success in solving this problem was achieved in [32], where the asymmetry of the observed line profile for the $2s - 4p$ transition in hydrogen was taken into account, bringing the charge radius of the proton almost in agreement with the value extracted from muon hydrogen experiments. More recent proton-electron scattering experiments and Lamb shift measurements by [138, 139] also came close to the result of [29].

While the results of the work [32] represent significant progress made by taking into account nonresonant effects in the scattering cross section and, in particular, quantum interference as their most significant part, the issue of similar effects on other precision spectroscopic experiments is widely discussed in the scientific literature at present [51, 140–142]. For example, results from recent work measuring the $2s - 8d$ transition energy in hydrogen again point to inconsistencies in the definitions of the proton charge radius [143]. Similar problems remain in two-photon spectroscopy in measuring the $1s - 3s$ interval [22, 144]. The influence of the quantum interference effect (QIE) within two-photon spectroscopy in determining the frequency of the $1s - 3s$ transition in the hydrogen atom has been studied in detail in [53, 145, 146]. A similar analysis has also been performed for one-photon spectroscopy of the hydrogen atom in [51] and its application to measurements of the Lamb shift and the fine structure of the helium triplet. A detailed analysis of QIE as part of NR effects can be addressed to the papers [50, 147, 148]. In particular, it was shown in [50] that for muonic hydrogen, deuterium, and helium-3 these effects turn out to be either negligible or well below the level of experimental precision. More recently, the line profile asymmetry analysis presented in [49] showed that there are "magic angles" at which quantum interference vanishes (see also [46, 47]). Recently, the effect of quantum interference was also discussed in [148] in an application to spectroscopy of lithium-like highly charged ions.

In spectroscopic studies of many-electron systems, light two-electron atomic systems should be emphasised. The recently achieved accuracy of measurements of the transition frequencies between the energy levels of the helium atom has stimulated a number of theoretical studies on the calculation of QED corrections up to the order of $m\alpha^7$ [54, 149]. A comparative analysis of the theoretical and experimental values revealed a significant discrepancy between the corresponding results for the transition frequency $2^3S_1 - 3^3D_1$ [54]. The corresponding NR corrections for the energy intervals $2^3S_1 - n^3D_1$ ($n = 3,\ 4,\ 5$) were estimated to be [54]. In particular, the analyses revealed that the effect of quantum interference, previously unaccounted for, can at least partially eliminate the existing imbalance between theory and experiment [56].

The study of multiphoton scattering processes and line profile asymmetry

applied to astrophysical problems is also of considerable interest [150–152]. As a powerful tool to investigate the dynamics of the evolution of the Universe at an early stage, accurate calculations of radiative transfer in the interstellar and intergalactic medium with the corresponding estimation of scattering cross sections and derivation of line profiles are extremely important [76, 99]. Until recently, the solution of problems related to radiative transfer was considered only in the resonant approximation [153–155]. In [153] it was shown that the asymmetry of the Ly_α line profile can lead to an underestimation of the redshift of some currently observed astrophysical sources. Accounting for nonresonant effects can lead to redshift bias reaching values of the order of $\delta z \sim 10^{-3} - 10^{-4}$ [156]. In the same context, the effect of electromagnetic induced transparency, which leads to a distortion of the absorption profile has been discussed in [128–130].

The keynote papers [33,35,37,42,85] opened up a whole new field of research devoted to NR effects and their role in modern spectroscopy. Since then, various authors and research groups have been working in this direction [41, 43]. The most important results concern not only the spectroscopy of hydrogen and helium atoms, but also of highly charged ions and mesoatoms. Subsequently, numerous works, see e.g. [36,40,41], have confirmed all the previously predicted features of the NR corrections. Importantly, there is also an influence of the registration method on the measured frequency value [42]. The dependence of the NR corrections on the experimental conditions was also studied in [50, 52, 53, 148].

Since precision spectroscopy of atomic systems is of great importance in modern physics, pursuing the goal, for example, of precision determination of fundamental physical constants, it is becoming increasingly important to take into account not only QED corrections but also NR effects. In the following, recent advances in the study of nonresonant effects and line profile asymmetry using the rigorous theory of quantum electrodynamics are discussed.

Chapter 2.

Spectral line profile asymmetry and nonresonant effects

One of the important features of the line profile theory in QED is the appearance of nonresonant corrections. They were first introduced in [85], where the QED theory of the natural (Lorentzian) line profile was formulated in the application to atomic physics. The NR corrections indicate the limit of applicability of the resonance approximation when only the dominant (resonance) term remains in the process amplitude, for more details see [8, 84]. If the distortion of the Lorentz profile caused by NR contributions is small, the correction can be considered as an additional energy shift of the transition frequency. Unlike all other energy corrections, this correction depends on the specific process of measuring the energy difference between levels, and therefore it should be theoretically calculated each time according to the process used in the experiment.

Below the fully relativistic derivation of the differential and total photon scattering cross sections in the framework of QED theory and the S-matrix formalism is considered, which gives a comprehensive account of nonresonant effects and their influence on the determination of the transition frequency.

2.1. Scattering amplitude of a photon on an atom

First, it is convenient to consider the process of photon scattering on a one-electron atom [85,157]. Following the theory described in [2], the corresponding Feynman diagrams are shown in Fig. 2.1. Here i, n, and f denote the initial, intermediate, and final states of the electron, and $\{\omega j_\gamma m_\gamma s\}$ and $\{\{\omega' j'_\gamma m'_\gamma s'\}$ are the quantum numbers of the initial and final photons, respectively. Here ω is the frequency, $j_\gamma m_\gamma m_\gamma$ denotes the angular momentum of the photon and its projection, and s defines the parity of the photon state.

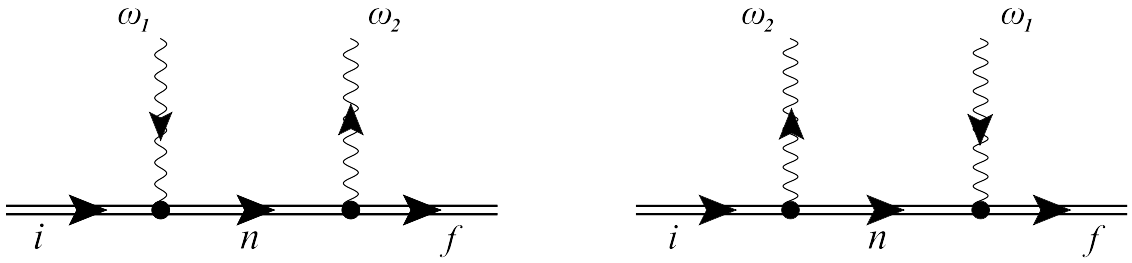

Figure 2.1. Photon scattering on a bound electron. The wavy line denotes absorption, if the arrow is directed to the vertex, or emission, if the arrow is directed away from the vertex, of a photon, and the double solid line denotes a bound electron in the field of the nucleus (Furry picture); ω_1, ω_2 are the frequencies of absorbed and emitted photons, i, n, and f denote the initial, intermediate, and final states of the electron, respectively.

Then the S-matrix element of the scattering process, see [2], is equal to

$$S_{fi}^{(2)} = (-\mathrm{i}e)^2 \int d^4x d^4y \Big[\overline{\psi}_f(x)\gamma^\mu A_\mu^{(\boldsymbol{k}_2,\lambda_2)*}(x) S(x,y)\gamma^\nu A_\nu^{(\boldsymbol{k}_1,\lambda_1)}(y)\psi_i(y) + \overline{\psi}_f(x)\gamma^\nu A_\nu^{(\boldsymbol{k}_1,\lambda_1)}(x) S(x,y)\gamma^\mu A_\mu^{(\boldsymbol{k}_2,\lambda_2)*}(y)\psi_i(y)\Big]. \quad (2.1)$$

Here $\psi_A(x) = e^{-\mathrm{i}E_A t}\psi(\boldsymbol{x})$ is the solution of the Dirac equation for the bound electron in state A and

$$A_\mu^{(\boldsymbol{k},\lambda)}(x) = \sqrt{\frac{2\pi}{\omega}} e_\mu^{(\lambda)} e^{-\mathrm{i}kx}, \quad (2.2)$$

represents the wave function of the photon in the coordinate representation, where $\omega = ||\boldsymbol{k}|$ and $e_\mu^{(\lambda)}$ are the polarisation components of the photon. The complex conjugation of the photon wavefunctions in equation (2.1) means that

the photon is emitted. The normalisation factor in (2.2), $\sqrt{2\pi/\omega}$, is chosen so as to obtain the Coulomb interaction (for the zero component) between the electron and the nucleus as Ze^2/r.

In the expression (2.1), $S(x,y)$ denotes the Feynman propagator of the atomic electron [2], which can be represented using the expansion:

$$S(x,y) = \frac{\mathrm{i}}{2\pi}\int_{\infty}^{-\infty} d\Omega e^{\mathrm{i}\Omega(t_x - t_y)} \sum_n \frac{\psi_n(\boldsymbol{x})\overline{\psi}_n(\boldsymbol{y})}{E_n(1-\mathrm{i}0)+\Omega}. \tag{2.3}$$

Here the summation is performed over the entire Dirac spectrum of the electron in the field of the nucleus. Consideration of real photons leads to the transverse condition with the photon polarisation given by the 3-vector $\boldsymbol{e}$ and the corresponding wave function

$$\boldsymbol{A}_{\boldsymbol{k},\boldsymbol{e}}(\boldsymbol{r}) = \sqrt{\frac{2\pi}{\omega}}\boldsymbol{e}e^{-\mathrm{i}\boldsymbol{k}\boldsymbol{r}}. \tag{2.4}$$

Integration over time variables and frequency Ω in equation (2.1) gives

$$S_{fi}^{(2)} = -2\pi\mathrm{i}\delta(E_i+\omega_1-E_f-\omega_2)U_{fi}^{(2)}, \tag{2.5}$$

where $U_{fi}^{(2)}$ represents the amplitude of the one-photon scattering process $i+\gamma \to f-\gamma$ [8, 84]

$$U_{fi}^{(2)} = e^2\left[\sum_n \frac{\left(\boldsymbol{\alpha}\boldsymbol{A}^*_{\boldsymbol{k}_2,\boldsymbol{e}_2}\right)_{fn}\left(\boldsymbol{\alpha}\boldsymbol{A}_{\boldsymbol{k}_1,\boldsymbol{e}_1}\right)_{ni}}{E_n(1-\mathrm{i}0)-E_i-\omega_1} + \sum_n \frac{\left(\boldsymbol{\alpha}\boldsymbol{A}_{\boldsymbol{k}_1,\boldsymbol{e}_1}\right)_{fn}\left(\boldsymbol{\alpha}\boldsymbol{A}^*_{\boldsymbol{k}_2,\boldsymbol{e}_2}\right)_{ni}}{E_n(1-\mathrm{i}0)-E_f+\omega_1}\right] \tag{2.6}$$

Here we introduce the following notations: $\boldsymbol{\alpha}A_{\boldsymbol{k},\boldsymbol{e}}$ and $\boldsymbol{\alpha}A^*_{\boldsymbol{k},\boldsymbol{e}}$ - photon absorption and emission operators, respectively. Then the differential cross section of the process is defined by the relation:

$$d\sigma_{fi} = 2\pi\left|U_{fi}^{(2)}\right|^2\delta(E_i+\omega_1-E_f-\omega_2)\frac{d^3k_2}{(2\pi)^3}. \tag{2.7}$$

where $d^3k_2 = \omega_2^2 d\omega_2 d\boldsymbol{n}_{k_2}$, $\omega_2 = |\boldsymbol{k}_2|$ is the frequency of the photon and $\boldsymbol{n}_{k_2} = \boldsymbol{k}_2/|\boldsymbol{k}_2|$ defines the unit direction vector of the photon (the latter will also often

be denoted by $\boldsymbol{\nu}$).

The matrix elements (2.6) can be computed using partial decomposition:

$$\boldsymbol{e}e^{-\mathrm{i}\boldsymbol{k}\boldsymbol{r}} = \sum_{j_\gamma m_\gamma s} \left[\boldsymbol{e}\boldsymbol{Y}^{(s)}_{j_\gamma m_\gamma}(\boldsymbol{n}_k)\right] \boldsymbol{A}^{(s)*}_{j_\gamma m_\gamma}(\boldsymbol{n}_r), \tag{2.8}$$

where $\boldsymbol{n}_r = \boldsymbol{r}/|\boldsymbol{r}|$ and $\boldsymbol{A}^{(s)}_{j_\gamma m_\gamma}$ are the components of the vector potential

$$\boldsymbol{A}^{(-1)}_{j_\gamma m_\gamma}(\boldsymbol{n}_r) = \sqrt{\frac{j_\gamma}{2j_\gamma+1}} g_{j_\gamma-1}(kr)\boldsymbol{Y}_{j_\gamma j_\gamma-1 m_\gamma}(\boldsymbol{n}_r) + \sqrt{\frac{j_\gamma+1}{2j_\gamma+1}} g_{j_\gamma+1}(kr)\boldsymbol{Y}_{j_\gamma j_\gamma+1 m_\gamma}(\boldsymbol{n}_r), \tag{2.9}$$

$$\boldsymbol{A}^{(0)}_{j_\gamma m_\gamma}(\boldsymbol{n}_r) = g_{j_\gamma}(kr)\boldsymbol{Y}_{j_\gamma j_\gamma m_\gamma}(\boldsymbol{n}_r), \tag{2.10}$$

$$\boldsymbol{A}^{(+1)}_{j_\gamma m_\gamma}(\boldsymbol{n}_r) = \sqrt{\frac{j_\gamma+1}{2j_\gamma+1}} g_{j_\gamma-1}(kr)\boldsymbol{Y}_{j_\gamma j_\gamma-1 m_\gamma}(\boldsymbol{n}_r) + \sqrt{\frac{j_\gamma}{2j_\gamma+1}} g_{j_\gamma+1}(kr)\boldsymbol{Y}_{j_\gamma j_\gamma+1 m_\gamma}(\boldsymbol{n}_r), \tag{2.11}$$

and $\boldsymbol{Y}^{(s)}_{jm}$ are components of the spherical tensor:

$$\boldsymbol{Y}^{(-1)}_{j_\gamma m_\gamma}(\boldsymbol{n}_k) = \sqrt{\frac{j_\gamma}{2j_\gamma+1}}\boldsymbol{Y}_{j_\gamma j_\gamma-1 m_\gamma}(\boldsymbol{n}_k) - \sqrt{\frac{j_\gamma+1}{2j_\gamma+1}}\boldsymbol{Y}_{j_\gamma j_\gamma+1 m_\gamma}(\boldsymbol{n}_k), \tag{2.12}$$

$$\boldsymbol{Y}^{(0)}_{j_\gamma m_\gamma}(\boldsymbol{n}_k) = \boldsymbol{Y}_{j_\gamma j_\gamma m_\gamma}(\boldsymbol{n}_k), \tag{2.13}$$

$$\boldsymbol{Y}^{(+1)}_{j_\gamma m_\gamma}(\boldsymbol{n}_k) = -\sqrt{\frac{j_\gamma+1}{2j_\gamma+1}}\boldsymbol{Y}_{j_\gamma j_\gamma-1 m_\gamma}(\boldsymbol{n}_k) - \sqrt{\frac{j}{2j+1}}\boldsymbol{Y}_{j_\gamma j_\gamma+1 m_\gamma}(\boldsymbol{n}_k). \tag{2.14}$$

The vector spherical harmonic $\boldsymbol{Y}_{jlm}$ in equations (2.12)-(2.14) is defined as follows:

$$\boldsymbol{Y}_{j_\gamma l_\gamma m_\gamma}(\boldsymbol{n}_k) = \sum_{m_\gamma \mu} C^{j_\gamma m_\gamma}_{l_\gamma m_\gamma 1 \mu} Y_{l_\gamma m_\gamma}(\boldsymbol{n}_k)\boldsymbol{\chi}_\mu. \tag{2.15}$$

Here $\boldsymbol{\chi}_\mu$ is the spin part of the function of the particle with spin one, and Y_{lm} is the spherical harmonic. The function $g_{j_\gamma}(kr)$ in expressions (2.9)-(2.11) is related to the spherical Bessel function $j_{j_\gamma}(kr)$

$$g_{j_\gamma}(kr) = 4\pi \mathrm{i}^{j_\gamma} j_{j_\gamma}(kr). \tag{2.16}$$

Using the expressions (2.9)-(2.11), the operator included in the formula (2.6) can be written as a multipole expansion:

$$\boldsymbol{\alpha}\boldsymbol{A}^*_{\boldsymbol{k},\boldsymbol{e}} = \sqrt{\frac{2\pi}{\omega}} \sum_{j_\gamma m_\gamma s} \left[\boldsymbol{e}\boldsymbol{Y}^{(s)}_{j_\gamma m_\gamma}(\boldsymbol{n}_{\boldsymbol{k}})\right] \boldsymbol{\alpha}\boldsymbol{A}^{(s)*}_{j_\gamma m_\gamma}. \tag{2.17}$$

Finally, by introducing the notation

$$C^{j_{\gamma_1} m_{\gamma_1} s_1}_{j_{\gamma_2} m_{\gamma_2} s_2}(\boldsymbol{e}_1, \boldsymbol{n}_{\boldsymbol{k}_1}; \boldsymbol{e}_2, \boldsymbol{n}_{\boldsymbol{k}_2}) = \left[\boldsymbol{e}_1 \boldsymbol{Y}^{(s_1)}_{j_{\gamma_1} m_{\gamma_1}}(\boldsymbol{n}_{\boldsymbol{k}_1})\right] \left[\boldsymbol{e}_2 \boldsymbol{Y}^{(s_2)}_{j_{\gamma_2} m_{\gamma_2}}(\boldsymbol{n}_{\boldsymbol{k}_2})\right]^*, \tag{2.18}$$

the transition amplitude (2.6) takes the form [158]:

$$U^{(2)}_{fi} = e^2 \frac{2\pi}{\sqrt{\omega_1 \omega_2}} \Bigg[\sum_{\substack{j_{\gamma_1} m_{\gamma_1} s_1 \\ j_{\gamma_2} m_{\gamma_2} s_2}} C^{j_{\gamma_1} m_{\gamma_1} s_1}_{j_{\gamma_2} m_{\gamma_2} s_2}(\boldsymbol{e}_1, \boldsymbol{n}_{\boldsymbol{k}_1}; \boldsymbol{e}_2, \boldsymbol{n}_{\boldsymbol{k}_2}) \times \tag{2.19}$$

$$\left\{ \sum_n \frac{\left(\boldsymbol{\alpha}\boldsymbol{A}^{(s_2)*}_{j_{\gamma_2} m_{\gamma_2}}\right)_{fn} \left(\boldsymbol{\alpha}\boldsymbol{A}^{(s_1)}_{j_{\gamma_1} m_{\gamma_1}}\right)_{ni}}{E_n(1 - \mathrm{i}0) - E_i - \omega_1} + \sum_n \frac{\left(\boldsymbol{\alpha}\boldsymbol{A}^{(s_1)}_{j_{\gamma_1} m_{\gamma_1}}\right)_{fn} \left(\boldsymbol{\alpha}\boldsymbol{A}^{(s_2)*}_{j_{\gamma_2} m_{\gamma_2}}\right)_{ni}}{E_n(1 - \mathrm{i}0) - E_i - \omega_2} \right\} \Bigg],$$

where photons of a certain type are given by the sums in equation (2.19).

In the resonant approximation, it is assumed that in the process $i + \gamma_1 \to f + \gamma_2$ there is an intermediate state b for which the frequency of the absorbed photon ω_1 is equal to the energy difference $E_b - E_i$, and the main contribution to the scattering cross section is given by the term with $n = b$ in the first sum in

the curly braces of the expression (2.19). The resulting divergent contribution should be regularised by including an infinite set of Feynman graphs representing the one-loop self-energy (SE) correction for the bound electron [85]. Thus, the natural level width Γ_b appears in the energy denominator, and the square of the modulus of the resonant regularised contribution determines the line profile of the corresponding emission or absorption process [8].

2.2. QED derivation of the Lorentz profile for the atomic spectral line

To obtain the standard Lorentz form for the spectral line profile in the framework of QED theory, one can consider the resonance process of elastic scattering of a photon on an atomic electron in the state a. According to the construction of perturbation theory within the QED formalism, the state a should be represented by the (meta-)stable (ground) energy level of the atom. In the framework of the resonance approximation, however, this circumstance can be neglected. Using the S-matrix formalism in the Furry picture [2, 3, 159], in the framework of the resonance approximation, the amplitude of the process shown in Fig. 2.1, see Eq. (2.19), can be reduced to the form:

$$U_{aa}^{\rm sc} = \frac{\langle a|\boldsymbol{\alpha}\boldsymbol{A}_{\boldsymbol{k}_2,\boldsymbol{e}_2}|b\rangle\langle b|\boldsymbol{\alpha}\boldsymbol{A}^*_{\boldsymbol{k}_1,\boldsymbol{e}_1}|a\rangle}{E_b - E_a - \omega}. \tag{2.20}$$

According to the expression (2.20), the radiation amplitude, $U_{ba}^{\rm em}$, can be represented as follows:

$$U_{ba}^{\rm em} = \frac{\langle b|\boldsymbol{\alpha}\boldsymbol{A}^*_{\boldsymbol{k}_2,\boldsymbol{e}_2}|a\rangle}{E_b - E_a - \omega}. \tag{2.21}$$

It is assumed that the absorption and emission processes are separated within the resonant approximation, see the discussion in [8], and b represents the excited state defined by the energy conservation law (the frequency of the absorbed photon).

For the resonant excitation process, this expression has a singularity at

$\omega = E_b - E_a$. The regularisation is performed according to the procedure proposed in [85], i.e. by inserting an infinite number of one-loop diagrams for the self-energy of the electron (SE), "loop by loop". The result reduces to a geometric progression [3], which finally leads to the expression

$$U_{ba}^{\rm em} = \frac{\langle b|\boldsymbol{\alpha}\boldsymbol{A}^*_{\boldsymbol{k}_2,\boldsymbol{e}_2}|a\rangle}{E_b - E_a - \omega + \langle b|\hat{\Sigma}\left(E_b\right)|b\rangle}. \tag{2.22}$$

Here $\langle b|\hat{\Sigma}\left(E_b\right)|b\rangle$ is the diagonal matrix element of the operator corresponding to the one-loop diagram for the electron self-energy, $\hat{\Sigma}\left(E_b\right)$:

$$\langle b|\hat{\Sigma}\left(E_b\right)|b\rangle = \frac{e^2}{2\pi \mathrm{i}} \sum_n \langle bn| \frac{1 - \boldsymbol{\alpha}_1\boldsymbol{\alpha}_2}{r_{12}} I_n\left(r_{12}; E_b\right)|nb\rangle. \tag{2.23}$$

The multiplier $1 - \boldsymbol{\alpha}_1\boldsymbol{\alpha}_2$ arises from the product of $\gamma^\mu g_{\mu\nu}\gamma^\nu$ (see [3]) and

$$I_n\left(r_{12}; E_b\right) = \int\limits_{-\infty}^{\infty} \frac{e^{\mathrm{i}|\Omega|r_{12}} d\omega}{E_n(1 - \mathrm{i}0) - E_b - \Omega}. \tag{2.24}$$

Hereinafter the matrix element $\langle cd\left|X\right|dc\rangle$ means

$$\langle cd\left|X\right|dc\rangle = \langle c(1)d(2)\left|X(1,2)\right|d(1)c(2)\rangle \tag{2.25}$$

where the indices 1, 2 refer to the two electron variables in the corresponding vertices of the SE diagram, $\boldsymbol{\alpha}_{1,2}$ represent the Dirac matrices acting on the electron wave functions in the 1 and 2 vertices, $r_{12} = |\boldsymbol{r}_1 - \boldsymbol{r}_2|$. Finally, the summation is performed over the entire Dirac spectrum.

The real part $\langle b|\hat{\Sigma}\left(E_r\right)|b\rangle$ diverges and requires a corresponding renormalisation [92]. The renormalisation results in an energy shift that determines the Lamb shift in the leading order (for the hydrogen atom):

$$\mathrm{Re}\langle b|\hat{\Sigma}_{\rm REN}\left(E_b\right)|b\rangle = L_b^{\rm SE}. \tag{2.26}$$

In our case this circumstance is not important. What is important is that the imaginary part of the matrix element $\langle b|\hat{\Sigma}\left(E_r\right)|b\rangle$ is different from zero.

Analytical calculations for the imaginary part can be found in [3], the result is

$$\mathrm{Im}\langle b|\hat{\Sigma}_{\mathrm{REN}}\left(E_b\right)|b\rangle = -\frac{\Gamma_b}{2}, \tag{2.27}$$

where Γ_b represents the natural width of the excited atomic state (details of the regularisation of the divergent resonance contribution are also presented in [8]).

Substitution of (2.26), (2.27) into (2.22) gives

$$U_{ba}^{\mathrm{em}} = \frac{\langle b|\boldsymbol{\alpha} A^*_{\boldsymbol{k}_2,\boldsymbol{e}_2}|a\rangle}{E_b + L_b^{\mathrm{SE}} - E_a - \frac{\mathrm{i}}{2}\Gamma_b - \omega}. \tag{2.28}$$

The regularised expression (2.28) can be modified both for the case of the state energy shift a and for other QED corrections (not SE), see details in [8, 84]. In the following it will be assumed that the energies include all known atomic level energy shifts. When a transition between two excited states is considered, the widths are represented by the sum of the natural widths. In turn, this gives a clear picture that, when observing a spectral line, the transition frequency includes all "standard" shifts and can be directly compared with the corresponding theoretical value.

To obtain the emission line profile, the amplitude modulus (2.28) should be squared, multiplied by the phase volume $d^3k'/(2\pi)^3$, integrated along the photon emission directions, and summed over the polarisation. The absorption profile can be obtained in a similar way: in this case, the matrix element of the transition $a \to b$ is left in the numerator of the expression (2.20). In the non-relativistic limit, which is obviously valid for the hydrogen atom, $\langle b|\boldsymbol{\alpha}\boldsymbol{A}^*_{\boldsymbol{k},\boldsymbol{e}}|a\rangle = \frac{e}{\sqrt{\omega}}\langle b|\boldsymbol{e}\boldsymbol{p}|a\rangle$, where $\boldsymbol{p}$ is the electron momentum operator and m is the mass of the electron. The coefficient $\frac{1}{\sqrt{\omega}}$ arises from normalising the vector-potential [2, 3]. Then the standard expression for the Lorentz profile is:

$$\phi_{\mathrm{L}}(\omega)d\omega = \frac{1}{\aleph}\sum_{\boldsymbol{e}}\int \frac{\omega d\omega d\boldsymbol{n}_k}{(2\pi)^3}|U_{ba}^{\mathrm{em}}| = \frac{1}{\aleph}\frac{W_{ba}d\omega}{(\omega_0-\omega)^2 + \frac{1}{4}\Gamma_b^2}, \tag{2.29}$$

where

$$W_{ba} = \frac{4}{3}e^2\omega_0|\langle b|\boldsymbol{p}|a\rangle|^2 \tag{2.30}$$

corresponds to the transition probability $b \to a + \gamma$, ω_0 is the resonance frequency equal to $\omega_0 = E_b - E_a$ and $\aleph$ represents the normalisation factor.

In expressions (2.29), (2.30) we put $\omega = \omega_0$ in W_{ba} and Γ_b and take into account that the difference of the Lamb shifts $L_a^{\rm SE}$ and $L_b^{\rm SE}$ can be simply included in the definition of ω_0. If there are no decay channels other than $b \to a$ for state b, then the transition probability coincides with the partial width of level b, $W_{ba} = \Gamma_{ba}$ and transforms to $\Gamma_{ba} = \Gamma_b$ in the case of excited state a. The normalisation factor is defined as follows:

$$\int \phi_{\rm L}(\omega) = 1. \tag{2.31}$$

In the resonance approximation, the integration interval in (2.31) can be extended to $\omega \in (-\infty, \infty)$. Then integration in the complex plane gives $\aleph = \aleph^{(0)} \equiv 1/2\pi$.

2.3. Nonresonant extension of the Lorentz profile

Three types of nonresonant contributions that distort the standard Lorentz profile (2.29) can be distinguished. The first type corresponds to distortion effects arising in external fields. Thus, in an external field, mixing of states of opposite parity [103] occurs. For example, an external electric field leads to overlap of transitions $1s_{1/2} \to 2p_{1/2}$ and $1s_{1/2} \to 2s_{1/2}$ [160]. The second type is represented by the remaining terms in the scattering amplitude (2.19). The study of this set of nonresonant effects is of particular interest in the current experiments [22, 32], as it represents the dominant contribution to the shift of the resonant transition frequency.

In this part of the thesis, a third type occurring for the resonant term is presented. These corrections arise when the frequency dependence in the expression (2.29) is considered for both the transition probability W_{ba} and the natural width Γ_b. The nonresonant expansion of W_{ba} is trivial (see [3]): equation (2.30) should be replaced by

$$W_{ba}(\omega) = \frac{4}{3} e^2 \omega \left| \langle b | \boldsymbol{p} | a \rangle \right|^2 . \tag{2.32}$$

How to determine the dependence of Γ_b on the frequency ω can be found in [3], and the corresponding application to the definition of NR corrections can be found in [8, 37, 160]. In turn, the estimation of the SE contribution should also take into account that initially, within the QED theory, the matrix element $\langle b|\hat{\Sigma}\left(E_a+\omega\right)|b\rangle$ depends on frequency:

$$\langle b|\hat{\Sigma}\left(E_b+\omega\right)|b\rangle = \frac{e^2}{2\pi}\sum_n \langle bn|\frac{1-\boldsymbol{\alpha}_1\boldsymbol{\alpha}_2}{r_{12}} I_n\left(r_{12}, E_b+\omega\right)|nb\rangle. \tag{2.33}$$

Then, the Lorentz profile is represented as:

$$\phi_{\rm L}(\omega) = \frac{1}{\aleph}\frac{W_{ba}(\omega)}{(\omega_0-\omega)^2+\frac{1}{4}\Gamma_b^2(\omega)}. \tag{2.34}$$

To obtain the dependence $\Gamma_b(\omega)$ in explicit form, the integral $I_n\left(r_{12}; E_b+\omega\right)$ should be transformed:

$$I_n\left(r_{12}; E_b+\omega\right) = \int\limits_{-\infty}^{\infty} \frac{e^{{\rm i}|\Omega|r_{12}}d\Omega}{E_n(1-{\rm i}0)-E_b-\omega+\Omega} \tag{2.35}$$

$$= \int\limits_{-\infty}^{\infty} \frac{e^{{\rm i}\Omega r_{12}}d\Omega}{E_n(1-{\rm i}0)-E_b-\omega+\Omega} - \int\limits_{-\infty}^{0} \frac{2{\rm i}\,\sin(\Omega r_{12})d\Omega}{E_n(1-{\rm i}0)-E_b-\omega+\Omega}.$$

Here we assume $E_n-E_b-\omega<0$. In this case, the first contribution (2.35) can be integrated over the variable Ω, closing the contour in the upper half-plane. Then the negative spectrum of Dirac energies does not give a contribution.

It also follows from physical considerations that the wings of the Lorentzian profile cannot be extended to the region of the next (nearest) resonance. Hence, the infinite integration interval for (2.31) should be restricted, $\omega\in[0,\omega_{\rm max}]$, where $\omega_{\rm max}=\omega_0+\frac{1}{2}\Delta_{FS}$, $\Delta_{\rm FS}$ represents the fine splitting interval (for example). Choosing $E_n-E_b-\omega<0$ and $\omega\leqslant\omega_{\rm max}$ leads to contributions only from the positive Dirac spectrum and states below the resonance excited atomic level b. For the hydrogen atom in the state $b=2p_{1/2}$ only $n=1s_{1/2}$ is possible.

Finally, the contribution of the second summand in (2.35) is a purely imaginary quantity. Under the above conditions, the denominator is always different

from zero and, hence, the infinitesimal term in it can be discarded. Hence, the second summand does not contribute to the width $\Gamma(\omega)$. Acting in a similar way, one can obtain that in the case $E_n - E_a - \omega > 0$ the integral (2.35) is zero. A careful calculation of $I_n\left(r_{12}; E_b + \omega\right)$, see [3], leads to the expression:

$$\Gamma_b(\omega) = -2e^2 \sum_{E_n<E_b} \langle bn| \frac{1 - \boldsymbol{\alpha}_1\boldsymbol{\alpha}_2}{r_{12}} \sin\left((E_b - E_n + \omega)r_{12}\right) |nb\rangle. \qquad (2.36)$$

In the nonrelativistic limit one can give the following parametric estimates (in relativistic units): $E_n \approx m(\alpha Z)^2$, $r_{12} \approx 1/m\alpha Z$. Here Z is the charge number of the nucleus, α is the fine structure constant. In the case of decay to the ground state, $n = a$, and hence $\sin\left((E_b - E_n + \omega)r_{12}\right) = \sin\left(\omega r_{12}\right)$.Since the integration interval is bounded, $\omega \leqslant \omega_{\max} \approx m(\alpha Z)^2$, we can decompose $\sin\left(\omega r_{12}\right)$ into a Taylor series. Further, we take into account that there are two contributions in the expression (2.36): dependent and independent of the $\boldsymbol{\alpha}$-matrices.

Using the decomposition of sin it is easy to see that by the property of orthogonality the summand proportional to $r_{12}^2 = r_1^2 + r_2^2 - 2(\boldsymbol{r}_1\boldsymbol{r}_2)$ is different from zero. The result is

$$\Gamma_b'(\omega) = -\frac{2}{3}e^2\omega^3 \left|\langle b|\boldsymbol{r}|a\rangle\right|^2. \qquad (2.37)$$

It is worth noting the $-$ assignment in (2.37), it is the one that leads to the correct $4/3$ factor in the total contribution (certainly positive).

Finally, in the summand depending on $\boldsymbol{\alpha}$-matrices (by order of magnitude) it is enough to restrict to the first term of the expansion sin. Then, in the non-relativistic limit, using the commutation relation $\langle b\left|\boldsymbol{p}\right| a\rangle = -\mathrm{i}\omega_0\langle b\left|\boldsymbol{r}\right| a\rangle$ will result:

$$\Gamma_b''(\omega) = 2e^2\omega\omega_0^2 \left|\langle b\left|\boldsymbol{r}\right| a\rangle\right|^2. \qquad (2.38)$$

Putting together (2.37) and (2.38), the natural level width is represented as:

$$\Gamma_b(\omega) = \Gamma'_b(\omega) + \Gamma''_b(\omega) = \tag{2.39}$$
$$= 2e^2\omega \left[\omega_0^2 - \frac{1}{3}\omega^2\right] |\langle b\,|\boldsymbol{r}|\,a\rangle|^2 \frac{3}{2}\frac{\omega}{\omega_0}\left(1 - \frac{1}{3}\frac{\omega^2}{\omega_0^2}\right)\Gamma_b^{(0)}.$$

Here $\Gamma_b^{(0)} = \frac{4}{3}\omega_0^3 |\langle b\,|\boldsymbol{r}|\,a\rangle|^2$ at the resonance point (see expression (2.32)).

Thus, the imaginary additive in the denominator of the amplitude (2.28) is determined by the linear and cubic in frequency ω contributions, cf. [161]. Introducing the dimensionless variable $x = \omega/\omega_0$, the Lorentz profile with respect to the frequency-dependent level width (Extended) can be represented as follows:

$$\phi_{\rm E}(x) = \frac{1}{\aleph}\frac{x\Gamma_{ba}^{(0)}}{\omega_0^2(x-1)^2 + \frac{9}{16}x^2\left(1 - \frac{1}{3}x^2\right)^2\left(\Gamma_b^{(0)}\right)^2}. \tag{2.40}$$

The normalisation factor $1/\aleph$ is determined from the ratio:

$$\omega_0 \int_0^{\omega_0 x_{\max}} \phi_{\rm E}(x)dx = 1, \tag{2.41}$$

where $x_{\max} = \omega_{\max}/\omega_0$.

In principle, radiative energy corrections can also depend on frequency, for example, $L_b^{\rm SE}(\omega)$. Hence, accounting for such a dependence will also distort the Lorentz profile. The expression for $L_b^{\rm SE}(\omega)$ is more complicated, see Eq. [8], although its ω-dependent part does not diverge and does not require additional renormalisation. However, further the corresponding modification is neglected due to the smallness of the contributions.

The expression (2.40) is a rigorous QED result for the Lorentz profile extended to the "nonresonant case". It may be noted in advance that this nonresonant contour expansion depends only on frequency and therefore cannot be avoided (see the following sections 3, 5, 6). The analytic dependence of Γ_b on ω outside resonance has recently been discussed in [161]. Other forms for the extended Lorentz contour are also presented in the literature [154, 162, 163]. They

are mostly obtained within the framework of the theory of quantum mechanics, i.e. phenomenologically.

2.4. Nonresonant contribution to the red wing profile for the Ly$_\alpha$transition in the expanding Universe

As an application of the modified spectral line contour (2.40), one can consider the cosmological recombination of the hydrogen atom (H) in the early Universe. The breaking of the balance between the original atoms and radiation as the Universe expanded led to the formation of the cosmic microwave background (CMB). One of the most important channels of radiation escape is the shift of the photon frequency towards the red wing of the Lorentz profile for the Ly$_\alpha$ line of the [164, 165]. When the photon frequency reaches a critical value ω_c, below which the absorption probability becomes too small, the photon no longer participates in scattering processes on atoms. Mainly, the redshift of the photon frequency occurs during the propagation of the photon from one atom to another. Consequently, the escape probability should depend on the density of hydrogen atoms during the cosmological recombination period. Strictly speaking, the study of the radiation escape from matter is a separate complex problem, which are carried out in the framework of the theory of radiation transfer, see, for example, [166]. However, the task can be greatly simplified by the fact that the spectral line profile is directly included in the definition of the optical depth [100]. Consequently, the influence of the extended profile can be analysed by comparing it with the "standard" profile. Such a comparison allows us to point out the significance of nonresonant effects for the theory of cosmological recombination.

A detailed analysis of photon scattering in the Ly$_\alpha$ and 21 cm lines covers a wide range of studies related to the evolution of the Universe [167, 168]. An important characteristic of photon scattering on hydrogen clouds in the interstellar medium (ISM) is the optical depth, τ, which depends directly on the line profile and is proportional to the column density of atoms (neutral

hydrogen in this case). In the standard analysis of radiation transfer in the Ly_α line in the expanding Universe from a source with redshift z_s to an observer with redshift $z_0 = 0$, the following expression is used [162, 169]:

$$\tau(z) = N_{\mathrm{HI}} \int_0^{z_\mathrm{s}} dz \sigma(n)(1+z)^2 \left[\frac{H(z)}{H_0}\right]^{-1}. \tag{2.42}$$

Here N_{HI} is the characteristic mean column density of atomic hydrogen, $\sigma(n)$ is the scattering cross section, $n = c(1+z)/\lambda_{\mathrm{obs}}$, H_0 is the Hubble constant and $H(z)$ is the Hubble factor. In the case of Ly_α scattering the cross section $\sigma(n)$ in the vicinity of resonance is equal to

$$\sigma(\omega) = \frac{3\lambda_\alpha^2 \Gamma_{2p}}{4} \phi(\omega), \tag{2.43}$$

where ϕ denotes the line profile of a single atom, and $\lambda_\alpha = c/\omega_0$ is the wavelength of the $2p \to 1s$ transition. Several approximations [77, 153–155, 163, 170] have been proposed in the last decade to describe the line profile with large redshift. Then, the profiles obtained under the different approximations are compared.

In the classical theory, the natural line broadening is described by a damped harmonic oscillator with a periodic dipole driving force. Then the angular integration of the time-averaged intensity gives the known ω^4 dependence for Rayleigh scattering

$$\phi_{\mathrm{R}}(\omega) = \frac{1}{2\pi} \frac{\Gamma_{2p}(4\omega^4/\omega_0^2)}{(\omega_0^2 - \omega^2)^2 + \Gamma_{2p}^2 \omega^2}. \tag{2.44}$$

Another form of ϕ, based on the two-level approximation, was introduced in the [77]:

$$\phi_{\mathrm{P}}(\omega) = \frac{1}{2\pi} \frac{\Gamma_{2p}(\omega/\omega_0)^4}{(\omega_0 - \omega)^2 + \Gamma_{2p}^2 (\omega/\omega_0)^6/4}. \tag{2.45}$$

Recently, the Ly_α scattering cross section of a photon was obtained in the framework of QM nonstationary perturbation theory in [154, 163]. As a conse-

quence, the expression (2.45) was modified as follows:

$$\phi_{\rm QM}(\omega) = \phi_{\rm R}(1 + f(\omega)) = \phi_{\rm L}\frac{4(\omega/\omega_0)^4}{(1+\omega/\omega_0)^2}(1 + f(\omega)), \qquad (2.46)$$

where $f(\omega) = a(1 - e^{-bx}) + cx + dx^2$, $a = 0.376$, $b = 7.666$, $c = 1.922$, $d = -1.036$, and $x = \omega/\omega_0$ as before. The absorption profiles (2.29), (2.40) and (2.44), (2.45), (2.46) are presented in the graph 2.2 (was constructed by T.A. Zalialialiutdinov). In particular, it follows from Fig. 2.2 that the red wing of

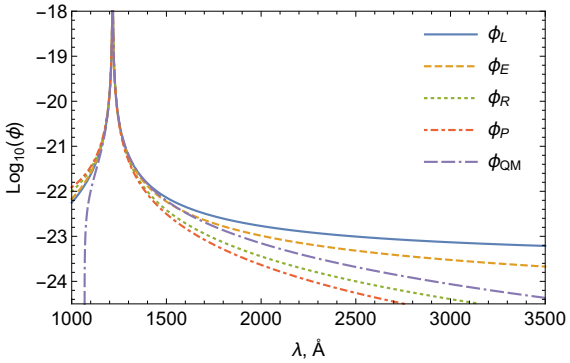

Figure 2.2. Comparison of Ly_α line profiles in the red wing for the absorption profiles given by the expressions (2.29), (2.40), (2.44), (2.45), (2.46) as a function of the wavelength λ. The normalisation factor $\aleph = 2\pi$ is chosen for profiles defined according to (2.29) and (2.40). The peak corresponds to the resonance wavelength $\lambda_\alpha = 1216$ Å.

the Lorentz profile extended to the nonresonant case, $\phi_{\rm E}(\omega)$, lies much higher than in the previously proposed models. The $\phi_{\rm E}(\omega)$ contour is obtained in the framework of the QED theory and agrees with [161].

Chapter 3.

Nonresonant effects for the total Ly$_\alpha$-scattering cross section

3.1. Nonresonant contributions in the total scattering cross section

In this section nonresonant corrections arising for the total cross section of the one-photon scattering process on the hydrogen atom are considered. If to neglect the hyperfine structure, the set of quantum numbers for a particular atomic state is $nljm$, where n is the principal quantum number, l is the angular momentum of the electron, j is the total angular momentum ($\boldsymbol{j} = \boldsymbol{l} + \boldsymbol{s}$) and m_j its projection.

The total cross section of the single-photon scattering process is obtained by integrating the expression (2.19) along the directions of the emitted photon $\boldsymbol{n}_{\boldsymbol{k}_2}$ and summing over the photon polarisation. If the incident radiation is isotropic and unpolarised, then an additional integration over $\boldsymbol{n}_{\boldsymbol{k}_1}$ and averaging over the polarisation $\boldsymbol{e}_1$ should be performed. Integrating along the photon directions, summing over the photon polarisations and projections of the final state m_{j_f}, averaging also over the projections of the initial state m_{j_f}, the total photon

scattering cross section on an atom is reduced to the form:

$$\sigma_{fi}(\omega) = C \sum_{\substack{m_{j_f} m_{j_i}}} \sum_{\substack{j_{\gamma_1} m_{\gamma_1} s_1 \\ j_{\gamma_2} m_{\gamma_2} s_2}} \left| \sum_{m_a} \frac{\left(\boldsymbol{\alpha} \boldsymbol{A}^{(s_2)*}_{j_{\gamma_2} m_{\gamma_2}}\right)_{fa} \left(\boldsymbol{\alpha} \boldsymbol{A}^{(s_1)}_{j_{\gamma_1} m_{\gamma_1}}\right)_{ai}}{E_a - E_i - \omega - \frac{\mathrm{i}}{2}\Gamma_a} \right. \tag{3.1}$$

$$\left. + \sum_{n \neq a} \frac{\left(\boldsymbol{\alpha} \boldsymbol{A}^{(s_2)*}_{j_{\gamma_2} m_{\gamma_2}}\right)_{fn} \left(\boldsymbol{\alpha} \boldsymbol{A}^{(s_1)}_{j_{\gamma_1} m_{\gamma_1}}\right)_{ni}}{E_n - E_i - \omega} + \sum_{n} \frac{\left(\boldsymbol{\alpha} \boldsymbol{A}^{(s_1)}_{j_{\gamma_1} m_{\gamma_1}}\right)_{fn} \left(\boldsymbol{\alpha} \boldsymbol{A}^{(s_2)*}_{j_{\gamma_2} m_{\gamma_2}}\right)_{ni}}{E_n - E_f + \omega} \right|^2,$$

$$C = \frac{e^4}{(2\pi)^3} \frac{\omega(\omega_0 - \omega)}{(2j_i + 1)(2j_{\gamma_2} + 1)}.$$

Here and further (unless separately specified) a means the resonance atomic level, $\omega_0 \equiv E_a - E_i$ (it is implied that the energies take into account all possible relativistic and QED corrections). Also, the frequency dependence of the natural width Γ_a is discarded further. The influence of the $\Gamma_a(\omega)$ dependence on the precision determination of the transition frequency will be shown in one of the following sections of the thesis.

After extracting the resonant summand (and appropriate regularisation) in the scattering amplitude, the total scattering cross section can be represented as two summands:

$$\sigma_{fi}(\omega) = \sigma^{(0)}_{fi}(\omega) + \sigma^{(1)}_{fi}(\omega), \tag{3.2}$$

where $\sigma^{(0)}_{fi}$ refers to the resonance contribution

$$\sigma^{(0)}_{fi}(\omega js) = \frac{e^4 \omega_{ai} \omega_{af}}{(2\pi)^4} \frac{2j_a + 1}{(2j_\gamma + 1)(2j_i + 1)} \frac{\Gamma_{fa} W_{ia}(js)}{(\omega_0 - \omega)^2 + \frac{\Gamma_a^2}{4}}, \tag{3.3}$$

and $\sigma^{(1)}_{fi}$ is the corresponding nonresonant contribution:

$$\sigma^{(1)}_{fi}(\omega js) = 2e^4 \frac{\omega_{ai} \omega_{af}}{(2\pi)^4} \frac{2j_a + 1}{(2j_\gamma + 1)(2j_i + 1)} \times \tag{3.4}$$

$$\Re \left[\sum_{n \neq a} \frac{\Gamma_{af;fn} W_{ia;ni}(js)}{(\omega_0 - \omega - \frac{\mathrm{i}}{2}\Gamma_a)(E_n - E_a)} + \sum_{n} \frac{\Gamma_{af;ni} W_{ia;fn}(js)}{(\omega_0 - \omega - \frac{\mathrm{i}}{2}\Gamma_a)(E_n - E_f + \omega_0)} \right].$$

In the expressions (3.3) and (3.4), see [35], the following notations are introduced:

$$W_{ab;cd}(j_\gamma s) = \frac{2\pi}{2j_d+1}\sum_{\substack{m_a m_b\\ m_c m_d}}\sum_{m_\gamma}\left(\boldsymbol{\alpha}\boldsymbol{A}^{(s)*}_{j_\gamma m_\gamma}\right)_{ab}\left(\boldsymbol{\alpha}\boldsymbol{A}^{(s)}_{j_\gamma m_\gamma}\right)_{cd}, \tag{3.5}$$

$$W_{ab} \equiv W_{ab;ba}(j_\gamma s), \tag{3.6}$$

$$\Gamma_{ab;cd} = \sum_{j's'} W_{ab;cd}(j'_\gamma s'), \tag{3.7}$$

so that $\Gamma_{ab;ba} \equiv \Gamma_{ab}$ is the partial width of level a, $\Re$ denotes the real part of the expression given in square brackets.

The resonant frequency of the transition $i+\gamma_1 \to a$ can be determined from the condition of the maximum of the scattering cross section $\sigma_{fi}(\omega)$. In the case of the resonance approximation, $\sigma_{fi}(\omega) \to \sigma^{(0)}_{fi}(\omega)$, the resonant frequency is strictly equal to ω_0. However, given the second summand in (3.2), see [35, 43], there is an additive to ω_0 - the NR correction:

$$\delta_{\rm NR} = -\frac{1}{4}\frac{\Gamma_a^2}{\Gamma_{fa}W_{ia}}\Re\left[\sum_{n\neq a}\frac{\Gamma_{af;fn}W_{ia;ni}(j_\gamma s)}{E_n-E_a} + \sum_n \frac{\Gamma_{af;ni}W_{ia;fn}(j_\gamma \lambda)}{E_n-E_f+\omega_0}\right]. \tag{3.8}$$

The parametric estimate of $\delta_{\rm NR}$ in relativistic units is given by the relation:

$$|\delta_{\rm NR}| \sim \frac{\left[m\alpha(\alpha Z)^4\right]^2}{m(\alpha Z)^2} = m\alpha^2(\alpha Z)^6, \tag{3.9}$$

where the denominator estimates the energy difference in (3.8) and the numerator represents a parametric estimate of the width (partial transition probability).

For the Ly_α transition in the hydrogen atom ($i = f = 1s_{1/2}$, $a = 2p_{1/2}$), the calculation of the resulting expression (3.8) was performed in [35]. The

numerical value of the NR correction is

$$\delta_{\rm NR} \equiv \delta_{1s,1s}^{(2p_{1/2})} = -2.93 \text{ Hz}. \tag{3.10}$$

Since the Ly_α resonance corresponds to two transitions to different levels of fine structure ($j_a = 1/2, 3/2$), as an example, calculations were performed for the transition $2s_{1/2} \to 2p_{3/2} \to 1s_{1/2}$:

$$\delta_{2s,1s}^{(2p_{3/2})} = -1.51 \text{ Hz}. \tag{3.11}$$

The values given in (3.10) and (3.11) are an order of magnitude lower than the highest accuracy of modern measurements of the transition frequencies in the hydrogen atom. For instance, the frequency of the $2s - 1s$ two-photon transition is determined with an experimental error of the order of 10 Hz (the relative error is a few fractions of 10^{-15} [20,21]). In turn, the Ly_α transition was measured with a much larger error (about 1 MHz) [137]. Applying the formula (3.8) for the $2s - 1s$ transition, a negligibly small value of the NR correction can be found, see [37]. Thus, one can conclude that the corrections in the total scattering cross section lead to effects that are negligibly small compared to the present level of experimental precision.

3.2. Green function method

It is worth mentioning separately a very efficient method for performing summation over intermediate states arising in the framework of second-order perturbation theory (see, for example, the expression (3.8) and expressions for the probabilities of two-photon transitions below). The Green function method (GFM) can be used not only in appropriate numerical calculations, but has also been shown to be effective in analytical calculations. The Green function method was intensively developed at the end of the last century and can be found in many textbooks, see, for example, [101, 171]. Applications of this method to the calculation of the nonresonant correction (3.8) and other effects can be found in [172]. In this thesis the use of GFM is restricted to the non-

relativistic case, since its applications are considered for the hydrogen atom, but it is worth noting the relativistic approach as well, see for example [173–176] (as well as the thesis of [177] and the relevant references therein).

The Coulomb Green's function, $G_E(\boldsymbol{r}, \boldsymbol{r'})$, is a solution of

$$\left(\hat{H} - E\right) G_E(\boldsymbol{r}, \boldsymbol{r'}) = \delta\left(\boldsymbol{r} - \boldsymbol{r'}\right), \tag{3.12}$$

where the standard notations for the Hamilton operator, $\hat{H}$, energy E and δ-function are introduced. The Coulomb Green's function can be represented as a spectral decomposition:

$$G_E(\boldsymbol{r}, \boldsymbol{r'}) = \sum_n \frac{\psi_n^*(\boldsymbol{r})\psi_n(\boldsymbol{r'})}{E_n - E}. \tag{3.13}$$

The sum extends to the entire spectrum of the Hamiltonian $\hat{H}$, including the continuous spectrum.

The expression (3.13) is not much suitable for practical purposes. For most applications, it is desirable to have close expressions for the radial part of the function $G_E(\boldsymbol{r}, \boldsymbol{r'})$ defined by the partial wave decomposition:

$$G_E(\boldsymbol{r}, \boldsymbol{r'}) = \sum_{lm} \frac{1}{r\, r'} G_{El}(r, r') Y_{lm}^*(\Omega) Y_{lm}(\Omega'). \tag{3.14}$$

Omitting for brevity the intermediate calculations, the following representation for the radial part of the Coulomb Green's function can be found (see [101]):

$$\frac{1}{r\, r'} G_{El}(r, r') \equiv g_l(E; r, r') = \frac{Z}{\nu} \sum_{m=l+1}^{\infty} \frac{m^4}{m - \nu} R_{ml}\left(\frac{2Zr}{\nu}\right) R_{ml}\left(\frac{2Zr'}{\nu}\right) \tag{3.15}$$

where $\nu = Z/\sqrt{-2E}$. The radial functions $R_{ml}(x)$, $x = 2Zr/\nu$, can be represented as

$$R_{ml}(x) = \frac{2}{m^2} \sqrt{\frac{(m - l - 1)!}{(m + l)!}} x^l e^{-\frac{x}{2}} L_{m-l-1}^{2l+1}(x), \tag{3.16}$$

$L_n^a(x)$ is the connected Laguerre polynomial [178].

The expression (3.15) has poles of the Green's function corresponding to hydrogen energy levels (as in the case of resonance in the amplitude (3.1)). In this connection, the representation for the "reduced" Green's function, in which the " resonant" state is singled out, is very convenient. The final expression corresponding to (3.15) can be represented in the form, [101]:

$$g_l^{(n)}(E;r,r') = \frac{Z}{n}\sum_{\substack{m=l+1\\ m\neq n}} \frac{m^4}{m-\nu} R_{ml}(x)R_{ml}(x') + \qquad (3.17)$$

$$n^2 R_{nl}(x)\left[\frac{5}{4}R_{nl}(x') + x'\frac{d}{dx'}R_{nl}(x')\right] + n^2 R_{nl}(x')\left[\frac{5}{4}R_{nl}(x) + x\frac{d}{dx}R_{nl}(x)\right].$$

The representation of the Coulomb Green's function in the form of an expansion by connected Laguerre polynomials is convenient for several reasons. First, in the case of an integer value of ν, the radial functions $R_{ml}(x)$ coincide with the corresponding hydrogen functions. Second, the series on m converges absolutely as $1/m^{3/2}$ for real values of ν.

It is the decompositions (3.17) and (3.15) that were used to calculate the first and second summands in (3.8), respectively. Using the first eight summands of m, an accuracy of the order of five significant digits was obtained.

3.3. "Quadratic" nonresonant correction in the total scattering cross section due to fine structure of levels

For the full scattering cross section, the "quadratic" nonresonant correction can be found (it does not disappear after integration over the angles of the incident photon). As was noted in [43], being dependent on the energy difference in the denominator, the NR correction can be significant for close values of E_n and E_a. By discarding the interference terms in the expression (3.1) and considering only the corresponding squared modulus for the levels separated by the fine structure [36,37], one can obtain the NR correction to the transition frequency

ω_0 in the form:

$$\delta_{\rm NR}^{\rm (sq)} = \frac{\Gamma_a^4}{16\Delta^3}, \tag{3.18}$$

where Δ corresponds to the interval of fine splitting of atomic levels. For hydrogen-like atoms, the parametric estimate of this correction is given by the relation:

$$\delta_{\rm NR}^{\rm (sq)} \sim \frac{\left[m\alpha(\alpha Z)^4\right]^4}{\left[m(\alpha Z)^4\right]^3} = m\alpha^4(\alpha Z)^4. \tag{3.19}$$

Thus, on the order of smallness, the NR correction $\delta_{\rm NR}^{\rm (sq)}$ is the same as $\delta_{\rm NR}$, according to the estimate (3.9) for the hydrogen atom ($Z = 1$).

For Ly$_\alpha$ resonance in hydrogen, see [8, 36, 37], the result for $\delta_{\rm NR}^{\rm (sq)}$ is

$$\delta_{\rm NR}^{\rm (sq)} = 4.70 \text{ Hz}. \tag{3.20}$$

3.4. Nonresonant correction in the total scattering cross section due to the frequency dependence of $\Gamma_a(\omega)$

Considering the Ly$_\alpha$ transition in the hydrogen atom as the simplest example (there is only one decay channel), the dependence of the natural width on the frequency should be taken into account. According to section 2.3, in the framework of QED theory, this dependence can be obtained from the imaginary part of the one-loop SE of the bound electron correction. However, for simplicity of presentation and revealing of the leading order, it is sufficient to restrict ourselves to the linear dependence, which immediately follows from the definition of the level width as the sum of probabilities of transitions to lower states, see [8, 37]. We note at once that the order of magnitude of such a correction is similar to (3.9) for the hydrogen atom.

Consider that in the radiation theory the transition probability is determined by an expression in the velocity form. Then for the Ly$_\alpha$ transition in

the hydrogen atom $\Gamma_a(\omega_0) = (2/3)^8\, m\alpha(\alpha Z)^4$ (in relativistic units) should be replaced by $\Gamma_a(\omega) = \omega\,(2^{11}/3^9)\, m\alpha(\alpha Z)^4$ [8,37]. Leaving only the resonant scattering cross section $\sigma_{fi}^{(0)}$ and substituting the width in the numerator according to the above, it follows from the extremum condition that

$$\delta_{\rm NR}^{\rm (fr)} = \frac{1}{8}\Gamma_a(\omega_0)\left[\frac{d\Gamma_a(\omega)}{d\omega}\right]_{\omega=\omega_0}. \tag{3.21}$$

The parametric estimate $\delta_{\rm NR}^{\rm (fr)}$ is immediately obtained similarly with (3.9). Its numerical value is

$$\delta_{\rm NR}^{\rm (fr)} = 1.007\ \text{Hz}. \tag{3.22}$$

Accounting for the frequency dependence in the denominator according to section 2.3 leads to a much smaller NR correction to the resonant frequency of the Ly_α transition.

Thus, the total contribution for the line $2p_{1/2} - 1s_{1/2}$ is determined by

$$\delta_\Sigma = \delta_{\rm NR} + \delta_{\rm NR}^{\rm (sq)} + \delta_{\rm NR}^{\rm (fr)} = -2.93Z^6 + 4.70Z^4 + 1.007Z^6\ \text{Hz}. \tag{3.23}$$

3.5. Nonresonant correction for hyperfine structure (HFS)

An important case for the precise determination of the frequency of the Ly_α transition in the hydrogen atom is the consideration of the hyperfine structure (HFS). Line profile distortion estimates were first presented in [41], see also [40]. As an example, the process used in [137] to measure the frequencies of the two transitions $1s_{1/2}(F=1) \to 2p_{3/2}(F=1)$ and $1s_{1/2}(F=0) \to 2p_{3/2}(F=1)$ (F is the total atomic moment, $\boldsymbol{F} = \boldsymbol{j} + \boldsymbol{I}$, I is the spin of the nucleus, and j is the total angular momentum of the atom as before). The hyperfine structure of the $2p_{3/2}$ level is experimentally intractable for the reason that the splitting corresponding to HFS is much smaller than the natural width of the atomic level: $\Gamma_{2p} \approx 100$ MHz, whereas $\Delta_{\rm HFS}(2p_{3/2}) = E(2p_{3/2}, F=2) - E(2p_{3/2}, F=$

1) ≈ 23.7 MHz. This is a typical case of overlapping resonances of two hyperfine sublevels, see the theory in [133]. However, due to the presence of interference terms, the line shape is different from the overlap of just two Lorentz profiles. The corresponding line shape can be represented by the expression:

$$\phi_{\rm HFS}(\omega) \approx \frac{f(F,F')}{(\omega-\omega_0)^2+\frac{1}{4}\Gamma_{2p}^2} + \frac{f(F,F'')}{(\omega-\omega_0-\Delta_{\rm HFS})^2+\frac{1}{4}\Gamma_{2p}^2} + 2\Re\frac{g(F,F',F'')}{(\omega-\omega_0-\frac{\rm i}{2}\Gamma_{2p})(\omega-\omega_0-\Delta_{\rm HFS}-\frac{\rm i}{2}\Gamma_{2p})}, \tag{3.24}$$

where $\omega_0 = E(2p_{3/2}, F=1) - E(1s_{1/2}, F=1)$, F, F', F'' denote the total atomic momentum including the spin of the nucleus for the corresponding state. In (3.24) f, g represent the factors arising in the framework of angular momentum theory (see [179]). A detailed calculation of the coefficients f, g was carried out by G. Shchedrin and presented in Refs. [40, 41].

Angular factors play a crucial role in determining the line shape (3.24). The result can be represented as: $f(1,2) : f(1,1) : g(1,2,1) = 181 : 1 : 0.307$. Thus, the spectral line shape exhibits a single-peak structure to a high degree (the larger peak completely screens the smaller one - 181 : 1, and the interference contribution is even an order of magnitude smaller). The asymmetry due to the overlap of the two Lorentz profiles is determined by the interference term and can be estimated on the order of magnitude as $0.307/181 \approx 0.17\%$. Then the NR correction to the transition frequency $E(2p_{3/2}) - E(1s_{1/2}, F=1)$ can be estimated as follows: $0.0017\Gamma_{2p} \approx 0.17$ MHz. The existence of an interference contribution distorting closely lying resonant lines is well known (see, e.g., [180]). However, in [180] this distortion has been included in the range of experimental error in determining the transition frequency, by analogy with other contributions of purely technical origin, such as, for example, the distribution and spread of atomic velocities. At present, the technical capabilities of the experiment have grown considerably and allow a significant suppression of these effects. It is worth noting that the contribution of the effect represented by the expression (3.24) is close in magnitude to the esperimental error, ~ 6 MHz [137], and is thus observable. The main conclusion, however, is that using the "correct" line contour (e.g., the expression (3.24) for the experiment [137])

can significantly increase the accuracy of the experimental determination of the transition frequency. A detailed discussion of the latter will be presented in the following sections of the thesis.

3.6. Conclusion on NR corrections for the Ly_α line in the total scattering cross section

The resonant approximation, which reduces the description of the spectral line profile to the usual Lorentz contour, represents an important milestone of all modern measurements of the transition frequency in resonance experiments. In the resonant approximation, the line profile is described by two parameters: the resonant frequency ω_0 and the natural width of the atomic level (Γ_a in the above cases). According to the resonant approximation, the resulting Lorentz profile is symmetric about ω_0. As pointed out in [85], the resonant approximation is valid only up to a certain accuracy limit, which is given by nonresonant corrections. Beyond this limit, the line profile acquires an asymmetric shape and the determination of the transition frequency becomes ambiguous. In addition, the NR corrections depend on the process used in the experiment. The latter determines the limit of achievable accuracy of the resonant frequency measurement. Beyond this limit, the spectral line profile can no longer be described by two parameters (ω_0 and Γ_a); only the line profile itself (but not the frequency) remains an observable quantity to be compared with the corresponding theoretical calculations.

The magnitude of the NR corrections according to F. Low [85] turns out to be small, $\sim \alpha^6$ for the hydrogen atom. However, the order of magnitude is competitive with the "usual" relativistic QED corrections, the calculation of which is necessary at the current level of experimental precision, see e.g. [28, 54, 69, 149, 181]. In the last two decades, NR corrections have played an important role and have been investigated both in a number of theoretical and direct experimental works [32,43,46,47,50,51,145–148] (see also the works of the author of this thesis and the relevant references therein). The reassessment of the importance of NR effects in the early 2000s was triggered by high-precision

experiments [134,137,182]. In particular, the experiments [134,182] are the most accurate in the optical domain: with an absolute accuracy for the frequency of the $1s-2s$ transition of about ± 46 Hz or a relative accuracy of the order of 10^{-14}. At present, the accuracy of the measurement of the frequency of the $1s-2s$ transition is of the order of 10 Hz or $\sim 10^{-15}$ relative magnitude [20,21]. However, the experimental scheme for measuring the $1s-2s$ transition frequency in the hydrogen atom poses serious difficulties for the theoretical description of the line contour asymmetry. Relevant estimates will be given in the following sections of the thesis.

An important experimental result was obtained in [137], where the Lyman-alpha $2p-1s$ transition was measured for the first time with an accuracy that allowed one to observe the natural line profile and to determine its characteristics. These measurements had a resonant character. Due to the absence of external fields, the estimation of NR corrections and the determination of the corresponding asymmetry are simpler in this case and were carried out in theoretical works [35–37,40–43]. As a result, the potential for experimental precision achievable within the framework of experiments [137] was underestimated.

Chapter 4.

Nonresonant effects for the $1s-2s$ transition frequency

The experimental measurement of the $1s-2s$ transition frequency represents a significant result, since the achieved accuracy of $10^{-14}-10^{-15}$ is currently unrivalled for the hydrogen atom [183]. From the point of view of theoretical description, the scheme of the experiment [134, 182] has not undergone significant changes at the present time [20, 21]. Thus, according to experiments [134, 182] hydrogen atoms are excited by laser radiation by two-photon absorption from the ground $1s$ state to the $2s$ state. This excitation occurs in a region in which there are no external fields. Within about 10^{-3} s, the excited atoms move to another region where they are subjected to a weak electric field. In the presence of such a field, the $2s$ and $2p$ states mix, and the atoms decay via the Ly_α $2p-1s$ transition. The corresponding emission is detected as a function of the frequency of the incident laser radiation, thus forming the absorption line profile. In the case of the rest frame of an atom, this looks like excitation occurs in the absence of an electric field and then the electric field is switched on. In terms of quantum electrodynamics, the initial and final states of the atom are described by the time-dependent Hamiltonian $\hat{H}(t)$ with different Hamiltonians $\hat{H}_{\mathrm{in}}$ and $\hat{H}_{\mathrm{in}}$ at asymptotic times t_{in} and t_{out}, respectively.

4.1. NR corrections to the $1s - 2s$ transition frequency for spontaneous decay combined with decay in an external electric field

In [36, 37], estimates of NR corrections to the $1s - 2s$ transition frequency were presented on the basis of the effect of mixing of $2s$ and $2p$ states for an atom in an external electric field. For the total scattering cross section, the NR corrections were negligibly small (as in the case of the decay of the $2s$ state unstimulated by an external field (spontaneous)), i.e., of the order of 10^{-14} Hz and less.

So for spontaneous decay, i.e., the process schematically depicted in Fig. 4.1, the expression for the NR correction can be estimated as

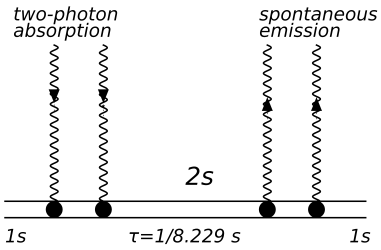

Figure 4.1. The process of two-photon absorption accompanied by spontaneous decay. The transition to the metastable state $2s$ of a hydrogen atom ($n = 2s$ in the notations of Fig. 2.1) is considered, the lifetime of the state $2s$ $\tau = 1/8.229$ seconds, the initial and final states are represented by the ground state $1s$.

$$|\delta| = \frac{\Gamma^2_{2s,2\gamma}}{\Delta E} \sim \frac{\left[m\alpha^2(\alpha Z)^6\right]^2}{m(\alpha Z)^2} = m\alpha^4(\alpha Z)^{10}. \tag{4.1}$$

This estimate was given in [43], and, in particular, it is pointed out that such an NR correction for the $1s + 2\gamma \to 2s$ transition turns out to be of the order of 10^{-14} Hz and is thus negligible at the current and predicted level of experimental accuracy.

The correction (4.1) corresponds to the process described by the Feynman graph shown in Fig. 4.1. However, the experiment is based on a different process. In it, the width of the $2s$ level is determined by the travel time to the region where the external electric field leads to an impurity $2p$

state. As a result, a photon corresponding to the Ly_α transition $2p-1s$ is emitted. For a weak electric field, the Stark parameter (mixing parameter) is $\xi_\mathrm{S} = \langle 2s|\boldsymbol{d}\boldsymbol{\mathcal{E}}|2p\rangle/\Delta E_L \ll 1$, where $\boldsymbol{d}$ is the electric dipole moment operator, $\boldsymbol{\mathcal{E}}$ is the electric field strength, ΔE_L is the Lamb shift for the states $2s$ and $2p$. In the experiments [20, 21, 134, 182] the excitation region is separated in space from the signal detection region. Therefore, the Stark shift is not included in the excitation condition: $2\omega = E_{2s} - E_{1s}$. The width of the resonance is determined by the time delay required for the atom to reach the detection region: at $\xi_\mathrm{S} \sim 0.1$ the damping time in the electric field is $\xi_\mathrm{S}^{-2}\Gamma_{2p,1\gamma}^{-1} \sim 10^{-7}$ s. This is a very small time compared to the fly-by time: the characteristic velocities of the atoms are 10^4 cm/s, and the spatial separation of the excitation and registration regions is of the order of 13 cm [134, 182]. Thus, the time delay is about 10^{-3} s - this corresponds to the experimental resonance width $\Gamma_\mathrm{exp} \sim 1$ kHz.

The main nonresonant contribution (differential cross section) is given by the level $2p$. By order of magnitude, it is defined by the relation:

$$|\delta| = \frac{\Gamma_\mathrm{exp}^2}{\Delta E_L} \sim 10^{-3}\ \mathrm{Hz}. \tag{4.2}$$

In turn, considering an atom placed in an external electric field, we can represent the excited state as $2s' = 2s + \xi_\mathrm{S} 2p$. Then the scattering cross section can be written as [37]:

$$\sigma \sim \frac{\Gamma_{2s,2\gamma}\Gamma_\mathrm{exp}}{(E_{2s} - E_{1s} - 2\omega)^2 + \frac{1}{4}\Gamma_\mathrm{exp}^2} + \frac{\Gamma_{2p',2\gamma}\Gamma_{2p,1\gamma}}{(E_{2p} - E_{1s} - 2\omega)^2 + \frac{1}{4}\Gamma_{2p,1\gamma}}. \tag{4.3}$$

Here, the second summand represents the nonresonant contribution arising due to mixing $2p' = 2p + \xi_\mathrm{S} 2s$, and $\Gamma_{2p',2\gamma}$ is the two-photon level width $2p$. The interference contribution between the resonant and nonresonant summands is absent in the total cross section, but may be present in the differential cross section.

In the case of measuring the total cross-section, the correction from the

expression (4.3) can be found in the form:

$$|\delta| = \frac{\Gamma_{2p',2\gamma}\Gamma_{2p,1\gamma}}{\Gamma_{2s,2\gamma}\Gamma_{\rm exp}} \frac{\left(\frac{1}{2}\Gamma^2_{\rm exp}\right)^4}{\Delta E_L^3} \tag{4.4}$$

and turns out to be negligibly small.

For the differential scattering cross section one can find

$$|\delta| = \frac{1}{2}\left(\frac{\Gamma_{2p',2\gamma}\Gamma_{2p,1\gamma}}{\Gamma_{2s,2\gamma}\Gamma_{\rm exp}}\right)^{\frac{1}{2}} \frac{\Gamma^2_{\rm exp}}{\Delta E_L} \sim 10^{-2}\ \text{Hz}. \tag{4.5}$$

Thus, a correction $\sim 10^{-2}$ [37] was obtained for the differential scattering cross section, which is three orders of magnitude lower than the experimental error. Nevertheless, the above estimates for the NR corrections are rather rough. The main reason for this statement is the separated excitation and de-excitation regions of the atom in the experiments [20, 21, 134, 182]. Next, the evaluation of the NR correction carried out in the framework of the strict QED approach at "finite times" will be presented. In this part of the paper a formalism was used when the external field potentials are "off" at $t_{\rm in}$ (initial state) and "on" at $t_{\rm out}$ (final state), and they correspond to different $\hat{H}_{\rm in}$ and $\hat{H}_{\rm out}$, see [184].

4.2. In and out QED formalism

The QED theory with different in and out Hamiltonians was developed by Fradkin, Gitman, and Shvartsman [184]. In the framework of this theory it becomes possible to operate with two complete sets of eigenfunctions belonging to in and out Hamiltonians. This theory follows the standard QED approach in a generalised form: the S-matrix, field operators in Fock space, four-dimensional perturbation decomposition for elements of the S-matrix, Wick's theorem and Feynman diagrammatic technique. In fact, the only new element to be used in the framework of the problems is the generalised electron propagator. This propagator connects two vertices described by in and out Hamiltonians.

Applied to the case of two-photon $1s-2s$ resonant absorption [20, 21, 134, 182], this means the absence or presence of an electric field in $\hat{H}_{\rm in}$ and $\hat{H}_{\rm out}$,

respectively. Then the electron propagator, $S^{\rm FGS}$, looks like

$$S^{\rm FGS}(x_1,x_2) = \theta(t_1-t_2)\sum_{\substack{\tilde{m},n\\ E_{\tilde{m},n}>0}} \psi_{\tilde{m}}(x_1)\omega_{\tilde{m},n}\overline{\psi}_n(x_2) - \theta(t_2-t_1)\sum_{\substack{\tilde{m},n\\ E_{\tilde{m},n}<0}} \psi_n(x_1)\omega_{n,\tilde{m}}\overline{\psi}_{\tilde{m}}(x_2). \tag{4.6}$$

The first sum in (4.6) describes the propagation of the electron from the spacetime point x_2, where there is no additional external field (in-space), to the spacetime point x_1, where the field is included (out-space). The eigenfunctions ψ_n, ψ_m correspond to in- and out-spaces: $\psi_m(x)$ are solutions of the Dirac equation for the electron in the field of the nucleus and the external electric field, $\psi_n(x)$ represent solutions in the absence of the field, E_m and E_n are the corresponding eigenvalues. The matrices $\omega_{m,n}$ are defined according to [184] (see also [42]):

$$\omega_{\tilde{m},n} = \langle \cdots \tilde{m} \cdots | \hat{\tilde{a}}^\dagger \hat{a} | \cdots n \cdots \rangle, \tag{4.7}$$

where $\langle \cdots \tilde{m} \cdots |$ denotes the out-state vector in Fock space with an electron in state $\tilde{m}$, $| \cdots n \cdots \rangle$ denotes the in-state vector in Fock space with an electron in state n, $\hat{\tilde{a}}^\dagger$ is the creation operator in out- Fock space, and $\hat{a}$ is the annihilation operator in in- Fock space.

In the simple case when electric fields do not create particles, the matrix $\omega_{\tilde{m},n}$ reduces to the overlap integral:

$$\omega_{\tilde{m},n} = \int d\boldsymbol{x}\psi^\dagger_{\tilde{m}}(\boldsymbol{x})\psi_n(\boldsymbol{x}) \equiv \langle \tilde{m}|n\rangle. \tag{4.8}$$

In the nonrelativistic limit, obviously valid for the neutral hydrogen atom, the Dirac wave functions are replaced by the Schr?dinger ones and the contribution of negative energies to (4.6) is discarded.

An important question is the definition of the transition probability in the framework of [184] theory. In particular, how to relate an element of the S-matrix to the decay probability (or cross section of the process)? In standard

QED this problem is solved as follows: due to the law of conservation of energy, the S-matrix element between the initial i and final f states can always be reduced to the process amplitude by the relation

$$S_{if} = -2\pi \mathrm{i}\delta(E_i - E_f)U_{if}, \tag{4.9}$$

where E_i, E_f are the energies of the initial and final states, and U_{if} is the amplitude of the process. The square of $\delta(E_i - E_f)$ is represented as

$$\delta(E_i - E_f)\frac{1}{2\pi}\int\limits_{-T/2}^{T/2} dt\, e^{\mathrm{i}(E_i - E_f)t} = \frac{T}{2\pi}\delta(E_i - E_f). \tag{4.10}$$

Here T can be interpreted as the observation time. Then the transition rate (transition probability per unit time) can be determined by the formula:

$$dW_{if} = \frac{|S_{if}|^2}{T} = 2\pi\delta(E_i - E_f)\,|U_{if}|^2\,. \tag{4.11}$$

In the in- and out-formalism the energy is not conserved and the definition (4.11) for the transition probability is in principle not fulfilled. However, in the case of a weak field, if one neglects the Stark shifts, energy conservation is actually realised. Then one can retain the standard formulation (4.11) for the estimation of transition probabilities and the standard Feynman diagram technique, using, however, wave functions perturbed by the electric field.

In the following, the usual Feynman diagrams will be used, taking into account the propagator (4.6). The solid line will represent the electron in the nucleus field only, and the double solid line will describe the electron propagating in the nucleus field together with an additional external electric field. The vertex corresponding to the Hamiltonian $\hat{H}_{\mathrm{out}}$ is further denoted by the "normal" point, and the vertex corresponding to the Hamiltonian $\hat{H}_{\mathrm{in}}$ is denoted by the "punched out" point. The new diagram element is shown in Fig. 4.2.

The applicability of the [184] theory to the problem of delayed decay of the resonance state in an atom is determined by two inequalities: $\tau_{\mathrm{at}} \ll \tau_{\mathrm{field}} \ll \tau_{\mathrm{d}}$. Here τ_{field} is the time showing how fast the field changes in the rest frame

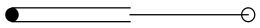

Figure 4.2. Schematic representation of the electron propagator $S^{\mathrm{FGS}}(x_1, x_2)$ (4.6) in coordinate space. The double solid line and the "normal" dot represent a vertex and an electron propagating in out-space. the single solid line and the "punched out" dot represent a vertex and an electron propagating in in-space. It is assumed that the corresponding in and out states are characterised by the same set of quantum numbers.

of the atom, τ_{at} is the characteristic atomic time required for the formation of stationary atomic states, τ_{d} is the decay time of the atomic level. The inequality $\tau_{\mathrm{at}} \ll \tau_{\mathrm{field}}$ means that the field changes slowly enough not to destroy the stationary states of the atom. The other inequality $\tau_{\mathrm{field}} \ll \tau_{\mathrm{d}}$ implies that the field varies rather sharply in space (and, consequently, in time in the atom's rest frame), so that the recorded signal has a peak structure that allows us to accurately determine the frequency. Obviously, the second inequality $\tau_{\mathrm{field}} \ll \tau_{\mathrm{d}}$ is fulfilled in the experiments [20, 21, 134, 182]. To estimate τ_{at}, one has to consider that the decay time of the $2p$ level is about 10^{-9} s ($\tau_{2p} = 1/\Gamma_{2p} \approx 1/(6.26 \times 10^8)$ c); the same damping time has $2s$ level in the critical field $\mathcal{E}_c = 475$ V/cm (full mixing of $2s$, $2p$ levels [103]). Assuming that the "weak field" in the experiments of [134, 182] is an order of magnitude smaller than $\mathcal{E}_c$, and considering that the admixture of the $2s$ state in the external electric field is proportional to $\mathcal{E}^2$, we obtain $\tau_{\mathrm{d}} \sim 10^{-7}$ s. Thus, both inequalities mentioned above are compatible [42].

In the framework of the [184] theory, the cross section of resonance scattering of two equivalent laser photons with frequency ω by a hydrogen atom followed by "delayed" decay in an external electric field, $a + 2\gamma \to a', \tilde{a}' \to \tilde{a} + \gamma$, is as follows (see [40–42]):

$$d\sigma^{(\mathrm{FGS})}_{\tilde{a}a} = \frac{1}{2\pi} \frac{W^{(\mathrm{em})}_{\tilde{a}\,\tilde{a}'} \, |\langle \tilde{a}' | a' \rangle|^2 \, W^{(2\gamma\,\mathrm{abs})}_{a'\,a}}{(E_{a'} - E_a - 2\omega)^2 + \frac{1}{4}\Gamma^2_{a'}} S^{2\gamma}_{a\,a'}. \tag{4.12}$$

Here $W^{(2\gamma\,\mathrm{abs})}_{a'\,a}$ is the two-photon absorption probability, $W^{(\mathrm{em})}_{\tilde{a}\,\tilde{a}'}$ is the decay probability of the $\tilde{a}'$ state, $S^{2\gamma}_{a\,a'}$ is the angular coefficient requiring computation, and tildes denote states for an atom in an external field. The resonance condition is satisfied by $E_{a'} - E_a = 2\omega$.

This theory is then used to describe the NR corrections in the two-photon $1s-2s$ resonance experiment.

4.3. Two-photon $1s-2s$ excitation followed by decay in an external electric field

The computations of the matrix elements presented in this part of the thesis were performed jointly with G. Shchedrin and E. Chernovskaya. A detailed description of the photon scattering process on an atom, including two-photon scattering followed by "delayed" decay in an external electric field, was presented in the most general form in [42]. In this part of the thesis, the latter is discussed.

The process of resonant scattering of two photons on an atom with subsequent "delayed" decay in an external electric field can be represented by the following Feynman diagram, Fig. 4.3:

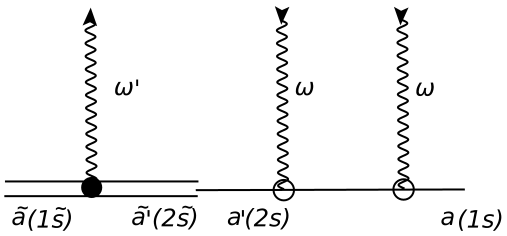

Figure 4.3. The process of two-photon excitation of a $1s-2s$ hydrogen atom with subsequent decay in an external electric field. The single solid lines describe the wave functions of the electron and the propagator in the absence of an external electric field. The compound inner electron line represents the electron propagator in the framework of the theory [184], see Fig. 4.2. The outer double solid line corresponds to an atomic electron propagating in an external electric field. As in the standard theory, the wavy lines describe photons. The two absorbed photons are laser photons with frequency $\omega = 1/2(E_{2s} - E_{1s})$, where E_i are the energies of the atomic electron states in the absence of an external field (eigenstates of the in-Hamiltonian). The emitted photon has frequency ω'. The designations of states with a tilde ($\tilde{a} = 1\tilde{s}$, $\tilde{a}' = 2\tilde{s}$) correspond to the electronic states in an external field (eigenstates of the out-Hamiltonian); in particular, the $2\tilde{s}$ state arises from the $2s$ state in the presence of a field.

The main contribution to the NR corrections comes from the interference

of the resonant and nonresonant terms in the expression for the scattering amplitude [35, 43]. Only nonresonant terms with the same symmetry as the resonant term have been included in the [35] (see section 3). As noted in [43], the most important contribution arises from the interference between the resonant term and nonresonant terms with a different symmetry: as an example, the contribution of the $2p_{3/2}$ nonresonant state to the $1s - 2p_{1/2}$ resonance was considered. It was found that this contribution arises only for the differential cross section of resonant photon scattering on the atom (depending on the directions of the incoming and emitted photons). It is further shown that for the case of two-photon $1s-2s$ excitation with subsequent decay in the external electric field NR contributions of this type are preserved both in the differential and in the total cross section, provided that the shape of the resonance line is quite natural (see the applicability of the theory of [184] in the previous section). It is also assumed that the external electric field is weak and one can neglect the Stark shifts and the corresponding level splitting. The criterion for a weak field is $\mathcal{E} \ll \mathcal{E}_c = 475$ V/cm, where $\mathcal{E}$ is the electric field strength. In the field $\mathcal{E} = \mathcal{E}_c$, the matrix element for the linear Stark shift is equal to the Lamb splitting, and the levels $2s$ and $2p$ are completely mixed [5].

Taking into account nonresonant contributions, the scattering cross section of two equivalent photons with subsequent "delayed" decay in an external electric field can be represented as follows:

$$d\sigma^{(\mathrm{FGS})}_{\tilde{a}a} = \frac{1}{2\pi}\frac{W^{(\mathrm{em})}_{\tilde{a}\,\tilde{a}'}\,|\langle\tilde{a}'|a'\rangle|^2\,W^{(2\gamma\,\mathrm{abs})}_{a'\,a}}{(E_{a'}-E_a-2\omega)^2+\frac{1}{4}\Gamma^2_{a'}}S^{2\gamma}_{a\,a'}+ \tag{4.13}$$

$$\frac{1}{2\pi}2\Re\left[\frac{A^{(\mathrm{em})*}_{\tilde{a}\,\tilde{a}'}\langle\tilde{a}'|a'\rangle^* A^{(\mathrm{em})}_{\tilde{a}\,\tilde{a}''}\langle\tilde{a}''|a''\rangle A^{(2\gamma\,\mathrm{abs})*}_{a'\,a}A^{(2\gamma\,\mathrm{abs})}_{a''\,a}}{(E_{a'}-E_a-2\omega-\frac{\mathrm{i}}{2}\Gamma_{a'})(E_{a''}-E_a-2\omega-\frac{\mathrm{i}}{2}\Gamma_{a''})}S^{2\gamma}_{a\,a''}\right],$$

where $A^{(2\gamma\,\mathrm{abs})*}_{a'\,a}$, $A^{(2\gamma\,\mathrm{abs})}_{a''\,a}$ are the reduced two-photon amplitudes obtained by the Eckart-Wigner theorem [179].

In a weak electric field

$$\begin{aligned} \psi_{\tilde{a}} &= \psi_a, \\ \psi_{\tilde{a}'} &= \psi_{a'} + |\xi_{\mathrm{S}}|\psi_{a''}, \\ \psi_{\tilde{a}''} &= \psi_{a''} - |\xi_{\mathrm{S}}|\psi_{a'}. \end{aligned} \tag{4.14}$$

Here the sign of the modulus for the ratio of the Stark shift to the Lamb shift, ξ_{S} (see above for the definition) stands for the corresponding number to be positive. Then the overlap integrals in (4.13) $\langle\tilde{a}'|a'\rangle = \langle\tilde{a}''|a''\rangle = 1$.

Next, introducing the notation $E_{a'} - E_a \equiv \omega_0$, we find $E_{a''} - E_a - 2\omega = E_{a''} - E_a - 2\omega \pm E_{a'} = \omega_0 - \Delta E_L - 2\omega$ for the second denominator in the nonresonant summand of the expression (4.13). The ΔE_L in the general case is identically equal to $E_{a''} - E_{a'}$ and represents the Lamb shift for the excitation of the $2s$ state (further the contribution of the hyperfine level splitting to the Lamb shift is neglected in view of the estimative nature of the correction). Considering the excitation process $1s_{1/2} + 2\gamma \to 2s_{1/2}$, one should set $a = \tilde{a} = 1s_{1/2}$, $a' = 2s_{1/2}$, $a'' = 2p_{1/2}$, and the tilde states are defined according to (4.14). The above choice is schematically illustrated in Fig. 4.4.

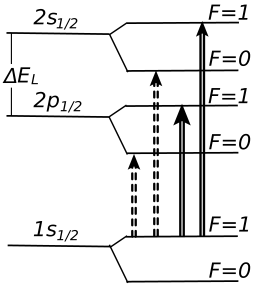

Figure 4.4. Level scheme of the two-photon $1s-2s$ transition taking into account the hyperfine splitting. Vertical double dashed lines denote allowed two-photon transitions. Vertical double dashed lines denote two-photon transitions forbidden by the Landau-Yang theorem [122, 124, 125]. The contribution to the NR correction to the $1s - 2s$ transition frequency arises from the permitted transition $1s - 2p$.

For the following evaluations, it is considered that $\Delta E_L \approx 10^9$ Hz, the level width $\Gamma_{a'}$ is determined by the experimental conditions and $\Gamma_{a'} = \Gamma_{\mathrm{exp}} \approx 10^3$ Hz. Given the expressions (4.14), the amplitudes included in (4.13), can be

estimated as follows: $A^{(\mathrm{em})}_{\tilde{a}\,\tilde{a}'} \approx |\xi_{\mathrm{S}}|\Gamma^{1/2}_{2p}$, $A^{(\mathrm{em})}_{\tilde{a}\,\tilde{a}''} \approx \Gamma^{1/2}_{2p}$, where Γ_{2p} is the natural width of the $2p$ level in the hydrogen atom.Then the maximum of the line profile (4.14) can be found shifted from the frequency ω_0 (in modulus) by

$$\delta^{(\mathrm{FGS})} \approx \frac{1}{4}\frac{\Gamma^2_{\mathrm{exp}}}{\Delta E_L}\left(\frac{W^{(2\gamma)}_{1s,2p}}{W^{(2\gamma)}_{1s,2s}}\right)^{1/2}\frac{1}{\xi_{\mathrm{S}}}\frac{S^{2\gamma}_{a\,a''}}{S^{2\gamma}_{a\,a'}}. \tag{4.15}$$

The coefficients $S^{2\gamma}_{a\,a'}$, $S^{2\gamma}_{a\,a''}$ were calculated for the case $F = F' = F'' = 1$ [41]: their ratio is $S^{2\gamma}_{a\,a''}/S^{2\gamma}_{a\,a'} = 18/11$. An estimate of the ratio of the two-photon absorption probabilities can be calculated taking into account the calculations carried out in [110] (see also the following sections of the thesis, works [83, 106, 111, 112, 114, 117] and references therein): the well-known two-photon absorption probability $W^{(2\gamma)}_{1s,2s} \approx 8.226\ \mathrm{s}^{-1}$, and $W^{(2\gamma)}_{1s,2p} = W^{(E1M1)}_{1s,2p} + W^{(E1E2)}_{1s,2p} \approx 1.089\times10^{-5}$ s^{-1}. Then, at $\xi_{\mathrm{S}} = 0.1$ (in the field $\mathcal{E} \approx 47.5$ V/cm),

$$\delta^{(\mathrm{FGS})} \approx 10^{-5}\ \mathrm{Hz}. \tag{4.16}$$

The choice of the total atomic momentum (taking into account the spin of the nucleus) for the states a, a', a'' $F = F' = F'' = 1$ is due, firstly, to experiments on measuring the frequency of the $1s - 2s$ transition [20, 21, 134, 182], and, second, by the fact that the transfer of the total momentum of two photons equal to unity is strictly forbidden according to the Landau-Yang theorem [122, 124, 125].

It is also important to note that the $1/\xi_{\mathrm{S}}$ dependence in (4.15) cannot be used in the zero-field case. The implied limit here is given by the field in which the decay rate of the $2s$ level due to the $2p$ state admixture becomes equal to the natural decay width of the $2s$ state. This limiting field strength will be so small that it cannot be used in a real experiment.

The situation in hydrogen appears to be very fortunate for an accurate measurement of the resonance frequency because of the absence of a transition to another hyperfine sublevel ($F' = F'' = 0$) of the $2s$ or $2p$ states. For comparison, in deuterium, where the values of the total angular momentum of the atom for levels $1s$ and $2s$ are $F = 1/2,\ 3/2$, respectively, transi-

tions with different total atomic momenta are allowed (for $F = 3/2$ we have $|3/2 - 0(2)| \leq F' \leq 3/2 + 0(2) \Rightarrow F' = 1/2, 3/2, 5/2, 7, 2$). The NR correction for a similar experiment (see [185]) is of order of magnitude equal to

$$\delta^{(\mathrm{D})} \sim \frac{1}{4} \frac{\Gamma_{\mathrm{exp}}^2}{\Delta E_{\mathrm{HFS}}}, \tag{4.17}$$

where $\Delta E_{\mathrm{HFS}}^{(\mathrm{D})} = E_{2s_{1/2}(F=3/2)} - E_{2s_{1/2}(F=1/2)} \approx 40.9$ MHz is the hyperfine structure interval for the $2s$ level in the deuterium atom (according to [186] $\Delta E_{\mathrm{HFS}}^{(\mathrm{D})} = 40\,924\,454(7)$ Hz). Taking the same value of $\Gamma_{\mathrm{exp}} \approx 10^3$ as for the hydrogen atom, a rough estimate (4.17) leads to $\delta^{(\mathrm{D})} \sim 10^{-2}$ Hz, which is three orders of magnitude larger than for hydrogen. This is not that far from the experimental accuracy of about 7 Hz [186].

4.4. Conclusion on NR corrections to the $1s - 2s$ two-photon excitation frequency

The estimates of the asymmetry of the observed spectral line arising for the $1s - 2s$ transition in the hydrogen atom carried out in sections 4.1, 4.3 have shown their insignificance. Thus, the upper limit of the nonresonant contribution is at 10^{-2}, which is three orders of magnitude smaller than the measurement error (about 10 Hz) in modern spectroscopic experiments [20,21,134,182]. This is primarily due to the specificity of the metastable $2s$ atomic level and, secondly, to the absence of close lying states that can be efficiently excited in a "two-photon" way. Since the NR corrections to the transition frequency are proportional to the square of the width and inversely proportional to the splitting energy of neighbouring resonance states (in leading order), and $\Gamma_{2s} \approx 1.31$ Hz, their smallness is understandable. The main difficulty for the accurate calculation of NR corrections to the $1s - 2s$ transition frequency is the experimental conditions. According to [20, 21, 134, 182], in such experiments the excitation and deexcitation regions are spatially separated, which makes "standard" methods unsuitable for analysis. Therefore, the QED formalism with in- and out-Hamiltonians was used [184]. Calculations of NR corrections for frequency

measurements based on two-photon excitation of the $1s-2s$ transition followed by decay in an external electric field were presented in Refs. [37, 40–42].

Two types of possible resonant optical experiments should be distinguished. All processes consist of three stages: excitation of a certain intermediate state, its propagation and its decay. The coherence in the sum over the intermediate state can be destroyed by collisions (the first type of experiments) or preserved (the second type of experiments). The analysis shows that the NR corrections in the case of the first type of resonance experiments are significantly smaller than for the second type of experiments [42]. However, in the limiting case where a natural line profile can be observed and there are no distortions due to the above effects, the two types of resonance experiments actually coincide and the NR corrections to the frequency for both experiments are the same. In the thesis only this situation is considered with the following reasoning: when the natural line profile is not observed, i.e., shielded by collision, time-of-flight, Doppler broadening, etc. [134, 182], then it is these effects that determine the possible uncertainty in the experimental determination of the transition frequency. This uncertainty is obviously larger than the nonresonant profile asymmetry, but it can be reduced by technical improvements. The distortion of the line profile caused by nonresonant effects is an inevitable systematic effect that requires a case-by-case theoretical analysis of the measurement process used in the experiment.

The work of [42] (with the valuable contribution of E. Chernovskaya) is worth mentioning because it presents the results of analytical calculations of the total and differential cross sections of one-photon scattering for both arbitrary parity (electric and magnetite types) and arbitrary multipoles of photons. The derived expressions can be used in the corresponding NR corrections analysis. In the following sections, specific examples of the calculation of NR corrections arising from the differential scattering cross section and, as a consequence, depending on angles will be discussed. In addition, taking into account the effect of an external electric field on the transition frequency measurements has opened up the possibility of a different kind of research. A comparative analysis of the spectral characteristics (transition frequency and level width) of hydrogen atoms (H) and anti-hydrogen atoms ($\bar{\text{H}}$) exposed to an external

electric field will be presented in one of the next sections of the thesis.

Chapter 5.

The quantum interference effect (QIE)

5.1. Differential scattering cross section: two close resonances

The photon scattering amplitude, see (2.19), can be conveniently represented as:

$$U_{fi}^{(2)} = \sum_{\substack{j_{\gamma_1} m_{\gamma_1} s_1 \\ j_{\gamma_2} m_{\gamma_2} s_2}} C_{j_{\gamma_2} m_{\gamma_2} s_2}^{j_{\gamma_1} m_{\gamma_1} s_1}(\boldsymbol{e}_1, \boldsymbol{n}_{\boldsymbol{k}_1}; \boldsymbol{e}_2, \boldsymbol{n}_{\boldsymbol{k}_2}) \left[\sum_{m_a} \frac{\left(\boldsymbol{\alpha} \boldsymbol{A}_{j_{\gamma_2} m_{\gamma_2}}^{(s_2)*}\right)_{fa} \left(\boldsymbol{\alpha} \boldsymbol{A}_{j_{\gamma_1} m_{\gamma_1}}^{(s_1)}\right)_{ai}}{E_a - E_i - \omega_1 - \frac{\mathrm{i}}{2}\Gamma_a} + \right. \tag{5.1}$$

$$\left. \sum_{n \neq a} \frac{\left(\boldsymbol{\alpha} \boldsymbol{A}_{j_{\gamma_2} m_{\gamma_2}}^{(s_2)*}\right)_{fn} \left(\boldsymbol{\alpha} \boldsymbol{A}_{j_{\gamma_1} m_{\gamma_1}}^{(s_1)}\right)_{ni}}{E_n - E_i - \omega_1} + \sum_{n} \frac{\left(\boldsymbol{\alpha} \boldsymbol{A}_{j_{\gamma_1} m_{\gamma_1}}^{(s_1)}\right)_{fn} \left(\boldsymbol{\alpha} \boldsymbol{A}_{j_{\gamma_2} m_{\gamma_2}}^{(s_2)*}\right)_{ni}}{E_n - E_i - \omega_2} \right] \frac{2\pi e^2}{\sqrt{\omega_1 \omega_2}}.$$

Here in the nonresonant summands, the infinitesimal parts $(1 - i0)$ in the denominators are omitted because there are no divergent contributions. In the resonance approximation, it is assumed that Γ_a is independent of ω_1, and the photon emission operators given by the expression (2.17) are taken at fixed transition energies, i.e., at $\omega_1 = E_a - E_i$ and $\omega_2 = E_a - E_f$. Keeping only the first (resonance) term in (5.1), after integrating over ω_2 in (2.7), the corresponding scattering cross section presents a line profile symmetric with respect to the

resonance frequency $\omega_0 \equiv E_a - E_i$:

$$\frac{d\sigma_{fi}(\omega_1)}{d\boldsymbol{n}_{k_2}} = \text{const}\frac{f_{fi}^{(1\gamma)}(a,a)}{(\omega_1-\omega_0)^2+\frac{\Gamma_a^2}{4}}, \tag{5.2}$$

where

$$f_{fi}^{(1\gamma)}(a,a') = \tag{5.3}$$
$$\left(\sum_{\substack{j_{\gamma_1}m_{\gamma_1}s_1\\ j_{\gamma_2}m_{\gamma_2}s_2}} C^{j_{\gamma_1}m_{\gamma_1}s_1}_{j_{\gamma_2}m_{\gamma_2}s_2}(\boldsymbol{e}_1,\boldsymbol{n}_{\boldsymbol{k}_1};\boldsymbol{e}_2,\boldsymbol{n}_{\boldsymbol{k}_2})\sum_{m_a}\left(\boldsymbol{\alpha}\boldsymbol{A}^{(s_2)*}_{j_{\gamma_2}m_{\gamma_2}}\right)_{fa}\left(\boldsymbol{\alpha}\boldsymbol{A}^{(s_1)}_{j_{\gamma_1}m_{\gamma_1}}\right)_{ai}\times\right)$$
$$\left(\sum_{\substack{j'_{\gamma_1}m'_{\gamma_1}s'_1\\ j'_{\gamma_2}m'_{\gamma_2}s'_2}} C^{j'_{\gamma_1}m'_{\gamma_1}s'_1}_{j'_{\gamma_2}m'_{\gamma_2}s'_2}(\boldsymbol{e}_1,\boldsymbol{n}_{\boldsymbol{k}_1};\boldsymbol{e}_2,\boldsymbol{n}_{\boldsymbol{k}_2})\sum_{m_{a'}}\left(\boldsymbol{\alpha}\boldsymbol{A}^{(s'_2)*}_{j'_{\gamma_2}m'_{\gamma_2}}\right)_{fa'}\left(\boldsymbol{\alpha}\boldsymbol{A}^{(s'_1)}_{j'_{\gamma_1}m'_{\gamma_1}}\right)_{a'i}\right)^*.$$

Here "const" - is a constant of no interest for further calculations. Thus, when only the resonance term is taken into account, the spectral line profile has a Lorentzian shape with a maximum at $\omega = \omega_0$. The frequency of the resonance transition ω_{res} can be defined as the maximum of the expression (5.2). For a symmetric profile, the definitions through the maximum and the "line centre" (see [32]) coincide.

Taking into account the other (nonresonant) terms in (5.1) leads to the asymmetry of the line profile. If the asymmetry is negligible, the resonance transition frequency ω_{res} can be determined from $d\sigma_{if}$ as $\omega_{\text{res}} = \omega_{\max}$, where $\omega_{\max}$ corresponds to the maximum value of $\sigma_{if}(\omega)$, see [43,49,50,53,148]. As long as the line profile is symmetric about $\omega = \omega_{\max}$, the definition of the maximum remains equivalent to any other way of extracting ω_{res} from the line profile. In the case of small asymmetry, the extremum condition leads to an biased value, i.e., $\omega_{\max} = \omega_{\text{res}} + \delta_{\text{NR}}$, where δ_{NR} is determined by the nonresonant terms in Eq. (5.1). The restriction imposed on the determination of the resonance frequency in the presence of asymmetry follows from the relation $\delta_{\text{NR}} \ll \Gamma_a$.

It is assumed that in the process of resonant absorption $i + \gamma_1 \to a$ the

selection rules also allow another (close) transition $i+\gamma_1 \to a'$ [122, 124, 125]. Then two summands can be distinguished in (5.1) - resonant and near-resonant:

$$U_{fi}^{(2)} = e^2 \frac{2\pi}{\sqrt{\omega_1\omega_2}} \sum_{\substack{j_{\gamma_1} m_{\gamma_1} s_1 \\ j_{\gamma_2} m_{\gamma_2} s_2}} C_{j_{\gamma_2} m_{\gamma_2} s_2}^{j_{\gamma_1} m_{\gamma_1} s_1}(\boldsymbol{e}_1, \boldsymbol{n}_{\boldsymbol{k}_1}; \boldsymbol{e}_2, \boldsymbol{n}_{\boldsymbol{k}_2}) \times \tag{5.4}$$

$$\left[\sum_{m_a} \frac{\left(\boldsymbol{\alpha} \boldsymbol{A}_{j_{\gamma_2} m_{\gamma_2}}^{(s_2)*}\right)_{fa} \left(\boldsymbol{\alpha} \boldsymbol{A}_{j_{\gamma_1} m_{\gamma_1}}^{(s_1)}\right)_{ai}}{E_a - E_i - \omega_1 - \frac{\mathrm{i}}{2}\Gamma_a} + \sum_{m_{a'}} \frac{\left(\boldsymbol{\alpha} \boldsymbol{A}_{j_{\gamma_2} m_{\gamma_2}}^{(s_2)*}\right)_{fa'} \left(\boldsymbol{\alpha} \boldsymbol{A}_{j_{\gamma_1} m_{\gamma_1}}^{(s_1)}\right)_{a'i}}{E_{a'} - E_i - \omega_1} \right.$$

$$\left. + \sum_{n \neq a,a'} \frac{\left(\boldsymbol{\alpha} \boldsymbol{A}_{j_{\gamma_2} m_{\gamma_2}}^{(s_2)*}\right)_{fn} \left(\boldsymbol{\alpha} \boldsymbol{A}_{j_{\gamma_1} m_{\gamma_1}}^{(s_1)}\right)_{ni}}{E_n - E_i - \omega_1} + \sum_{n} \frac{\left(\boldsymbol{\alpha} \boldsymbol{A}_{j_{\gamma_1} m_{\gamma_1}}^{(s_1)}\right)_{fn} \left(\boldsymbol{\alpha} \boldsymbol{A}_{j_{\gamma_2} m_{\gamma_2}}^{(s_2)*}\right)_{ni}}{E_n - E_i - \omega_2} \right],$$

The last two terms in (5.4) represent nonresonant contributions to the amplitude. Their consideration in the determination of the transition frequency was presented in section 3.1 (see the expression (3.8) for δ_{NR}). Here and below they can be neglected. After integrating over ω_2 in (2.7), the corresponding cross section can be reduced to the form:

$$\frac{d\sigma_{fi}}{d\boldsymbol{n}_{k_2}} = \mathrm{const} \left(\frac{f_{fi}^{(1\gamma)}(a,a)}{(\omega_0 - \omega_1)^2 + \frac{\Gamma_a^2}{4}} + \frac{2 f_{fi}^{(1\gamma)}(a,a')(\omega_0 - \omega_1)}{\left((\omega_0 - \omega_1)^2 + \frac{\Gamma_a^2}{4}\right)(\omega_0 - \omega_1 + \Delta)} \right), \tag{5.5}$$

where $\Delta \equiv E_{a'} - E_a$, and only the interference contribution besides the quadratic contribution from the second summand in (5.4) is left.

The nonresonant leading-order correction to the transition frequency $i + \gamma_1 \to a$ arises from the extremum condition and is equal to

$$\frac{d\sigma_{if}(\omega_1)}{d\omega_1} = -\frac{1}{(\omega_0 - \omega_1 + \Delta)^2 \left((\omega_1 - \omega_0)^2 + \frac{\Gamma_a^2}{4}\right)^2} \times \tag{5.6}$$

$$8 \left[f_{fi}^{(1\gamma)}(a,a') \left((\omega_1 - \omega_0)^2 - \frac{\Gamma_a^2}{4} \right) \Delta - 2 f_{fi}^{(1\gamma)}(a,a')(\omega_1 - \omega_0)^3 + \right.$$

$$\left. f_{fi}^{(1\gamma)}(a,a)(\omega_1 - \omega_0)(\omega_0 - \omega_1 + \Delta)^2 \Delta \right].$$

Expanding the numerator in (5.6) into a Taylor series in the vicinity of ω_0, in

the leading order one can set

$$-8f_{fi}^{(1\gamma)}(a,a')\,\Gamma_a^2\,\Delta - 32f_{fi}^{(1\gamma)}(a,a)\,(\omega_1-\omega_0)\,\Delta^2 = 0. \tag{5.7}$$

Finally, solving the equation (5.7) with respect to ω_1, the following is obtained

$$\omega_{\rm max} = \omega_0 - \delta_{\rm NR}, \tag{5.8}$$

$$\delta_{\rm NR} = \frac{f_{fi}^{(1\gamma)}(a,a')}{f_{fi}^{(1\gamma)}(a,a)}\frac{\Gamma_a^2}{4\Delta}. \tag{5.9}$$

The expression (5.9) arises as the higher order of the Γ_a/Δ expansion and represents a part of the NR corrections arising due to the interference of transitions to nearby (with resonance) states. Due to the origin, the effect is called quantum interference (QIE). The approximations used above assume that the parameter $\Gamma_a/\Delta < 1$ is small, e.g. for close neighbouring components of the fine structure (see specific examples below). The parameter Γ_a/Δ can also be small for two neighbouring hyperfine sublevels and in this case requires a special study, see section 3.5 and [42].

The next-order contribution can be obtained (see section 3.3) by retaining the remaining terms in (5.6) and taking into account the square of the second summand in (5.4). Then the nonresonant correction to the transition frequency can be found in the form:

$$\delta_{\rm NR} = \frac{f_{fi}^{(1\gamma)}(a,a')}{f_{fi}^{(1\gamma)}(a,a)}\frac{\Gamma_a^2}{4\Delta} - \frac{\left(f_{fi}^{(1\gamma)}(a,a')\right)^2\left(2f_{fi}^{(1\gamma)}(a,a)+f_{fi}^{(1\gamma)}(a,a')\right)}{f_{fi}^{(1\gamma)}(a,a)^3}\frac{\Gamma_a^4}{16\Delta^3}. \tag{5.10}$$

The first term in (5.10) coincides with (5.9), and the second term is proportional to the ratio $\Gamma_a^4/(16\Delta^3)$. In most cases, the second contribution is a small addition to the leading-order NR correction (5.9). The expressions (5.9), (5.10) can be used to estimate the magnitude of the corrections given that $\Gamma_a \sim m\alpha(\alpha Z)^4$ and the fine splitting interval $\Delta \sim m(\alpha Z)^4$ are in relativistic units (electron mass is given for clarity). Then $\Gamma_a^2/\Delta \sim m\alpha^2(\alpha Z)^4$, and $\Gamma_a^4/\Delta^3 \sim m\alpha^4(\alpha Z)^4$, i.e. α^2 times smaller. Although the factors in (5.10) are dimensionless, they

can vary considerably and should be calculated for each case separately. Another way to estimate the corrections in (5.10) corresponds to the direct use of tabulated values of level widths and splitting intervals.

As follows from expression (5.8), the NR correction depends on the experimental setup, i.e., on the angular and polarisation correlations between incident and escaping photons. All information about such correlations is given by the relation $f_{fi}^{(1\gamma)}(a,a')/f_{fi}^{(1\gamma)}(a,a)$. Since the coefficients in (5.3) depend on the quantum numbers (angular momenta) of particular atomic states and the mutual orientation of the vectors $\boldsymbol{e}_1$, $\boldsymbol{n}_{\boldsymbol{k}_1}$, $\boldsymbol{e}_2$, $\boldsymbol{n}_{\boldsymbol{k}_2}$, the resulting value of the NR correction is determined by the geometry of the experiment and the photon registration method [43, 52]. Before proceeding to particular examples, it is necessary to write down the scattering amplitude. In the nonrelativistic limit and the dipole approximation [2, 3]:

$$\frac{U_{fi}^{(2)}}{2\pi e^2\sqrt{\omega_1\omega_2}} = \sum_n \frac{\left(\boldsymbol{r}\boldsymbol{e}_2^*\right)_{fn}\left(\boldsymbol{r}\boldsymbol{e}_1\right)_{ni}}{E_n(1-\mathrm{i}0)-E_i-\omega_1} + \sum_n \frac{\left(\boldsymbol{r}\boldsymbol{e}_1\right)_{fn}\left(\boldsymbol{r}\boldsymbol{e}_2^*\right)_{ni}}{E_n(1-\mathrm{i}0)-E_f+\omega_1}, \quad (5.11)$$

where now the summation is performed over the Schr?dinger spectrum.

5.2. Angular correlations: the effect of quantum interference

Unlike the resonant transition frequency value, the NR corrections depend on the excitation and deexcitation processes of the atomic level, the type of experiment, and the way the transition frequency value is extracted from the experimental data. For all cases mentioned in the previous sections, the NR corrections were found to be negligible. In particular, according to [42], this was also the case for the measurement of the frequency of the $1s-2s$ two-photon transition in hydrogen. The situation changed when the results of high-accuracy measurements of the frequencies of the $2s_{1/2}^{F=0} \to 4p_{1/2}^{F=1}$ and $2s_{1/2}^{F=0} \to 4p_{3/2}^{F=1}$ transitions in the hydrogen atom were presented [32]. The uncertainty of these measurements is much smaller than the observed effects of quantum interfer-

ence. To achieve an accuracy of a few kilohertz, the observed asymmetric line profile has been fit with the corresponding theoretical contour (see [43]). The result is the extraction of the symmetric part and the subsequent determination of the "line centre". According to the line profile theory, this indicates the existence of nonresonant corrections.

In this section, the expressions for the cross section of resonant one-photon scattering on the hydrogen atom are presented, taking into account the fine and hyperfine structure of the atomic levels [32]. The corresponding expressions for the amplitudes contain dependences on the directions and polarisations of incident (absorbed) and outgoing (emitted) photons. Thus, they can be used to describe different experiments, with different correlations between the directions and/or polarisations of photons. The scattering cross sections arising from the amplitudes are used to obtain NR corrections. The influence of the latter on the determination of the transition frequency is the main objective.

Following [52], the NR corrections arising from taking into account the adjacent components of the fine structure levels are considered. According to the experiment [32], the mutual influence of the transitions $2s^{F=0}_{1/2} \to 4p^{F=1}_{1/2}$ and $2s^{F=0}_{1/2} \to 4p^{F=1}_{3/2}$ was detected and accounted for according to the theory, presented in the supplementary materials of [32] and is in good agreement with the theoretical analysis presented in [43]. First, consider the NR corrections to the $2s^{F=0}_{1/2} \to 4p^{F=1}_{1/2}$ transition due to quantum interference with the $2s^{F=0}_{1/2} \to 4p^{F=1}_{3/2}$ transition. The corrections to the other transition $2s^{F=0}_{1/2} \to 4p^{F=1}_{3/2}$ are found in a similar way. Thus it will be shown that the NR corrections for transitions to a fixed final hyperfine sublevel do not depend on the type of experiment and the "geometry" of the experiment. However, they depend on the choice of the decay channel: the NR corrections are different if the registration process ends with states with $F = 0, 1$ or 2. When the frequency of the escaping photon is not recorded at all, the measurement result starts to depend both on the type of experiment and on the experiment scheme (geometry), which is in good agreement with [32].

Once again, the type of experiments can be graded. In the first type of experiment, the directions of photon propagation are fixed: the direction of the incident photon $\boldsymbol{n}_{k_1}$ coincides with the direction of the laser beam, and

the direction of the exiting photon $\boldsymbol{n}_{k_2}$ is determined by the detector position. In the second type of experiments, the polarisation of the incident photon $\boldsymbol{e}_1$ and the direction of the outgoing photon $\boldsymbol{n}_{k_2}$ are fixed; this is the case in the experiment [32].

In the nonrelativistic limit the matrix elements of the scattering amplitude defined by expressions (5.11) do not depend explicitly on directions of photons $\boldsymbol{n}_{k_1}$ and $\boldsymbol{n}_{k_2}$. This dependence arises from the transversality condition. Since the transversality condition will be fulfilled automatically in the laser beam, the direction of this beam in the experiment of type 2 can be chosen arbitrarily. The dependence on $\boldsymbol{n}_{k_1}$, $\boldsymbol{n}_{k_2}$ becomes explicit after summing over the photon polarisations. Then, for the experiment of type 1 one needs to derive $\sum\limits_{\boldsymbol{e}_1,\boldsymbol{e}_2} d\sigma_{if}$, and for the experiment of type 2 one needs to obtain $\sum\limits_{\boldsymbol{e}_2} d\sigma_{if}$, where the differential cross section is defined according to (5.5). In the nonrelativistic limit the corresponding factors $f_{fi}(a,a')$ in the cross section (5.5) for the experiment of the first and the second type are given by the following expressions [52]:

$$f_{fi}^{(1)}(a,a') = 36\sum_{xy}(-1)^{F_{a'}-F_a+x+y}\Pi_x^2\Pi_y \begin{Bmatrix} 1 & x & 1 \\ F_{a'} & F_f & F_a \end{Bmatrix} \begin{Bmatrix} 1 & x & 1 \\ F_{a'} & F_i & F_a \end{Bmatrix} \tag{5.12}$$
$$\times \begin{Bmatrix} 1 & 1 & y \\ 1 & 1 & x \end{Bmatrix} \begin{Bmatrix} 1 & 1 & x \\ 1 & 1 & 1 \end{Bmatrix}^2 \left\{ \left\{ v_1^{(1)} \otimes w_1^{(1)} \right\}_y \otimes \left\{ v_1^{(1)} \otimes w_1^{(1)} \right\}_y \right\}_{00}$$
$$\times \langle n_f l_f j_f F_f || r || n_a l_a j_a F_a \rangle \langle n_a l_a j_a F_a || r || n_i l_i j_i F_i \rangle$$
$$\times \langle n_i l_i j_i F_i || r || n_{a'} l_{a'} j_{a'} F_{a'} \rangle \langle n_{a'} l_{a'} j_{a'} F_{a'} || r || n_f l_f j_f F_f \rangle,$$

$$f_{fi}^{(2)}(a,a') = 6\sum_{xy}(-1)^{F_{a'}-F_a+y}\Pi_x^2\Pi_y \begin{Bmatrix} 1 & x & 1 \\ F_{a'} & F_f & F_a \end{Bmatrix} \begin{Bmatrix} 1 & x & 1 \\ F_{a'} & F_i & F_a \end{Bmatrix} \tag{5.13}$$
$$\times \begin{Bmatrix} 1 & 1 & y \\ 1 & 1 & x \end{Bmatrix} \begin{Bmatrix} 1 & 1 & x \\ 1 & 1 & 1 \end{Bmatrix} \left\{ \left\{ v_1^{(2)} \otimes w_1^{(2)} \right\}_y \otimes \left\{ v_1^{(2)} \otimes w_1^{(2)} \right\}_y \right\}_{00}$$
$$\times \langle n_f l_f j_f F_f || r || n_a l_a j_a F_a \rangle \langle n_a l_a j_a F_a || r || n_i l_i j_i F_i \rangle$$
$$\times \langle n_i l_i j_i F_i || r || n_{a'} l_{a'} j_{a'} F_{a'} \rangle \langle n_{a'} l_{a'} j_{a'} F_{a'} || r || n_f l_f j_f F_f \rangle,$$

where $v_1^{(1)} = \boldsymbol{n}_{k_1}$, $v_1^{(2)} = \boldsymbol{e}_1$, $w_1^{(1)} = w_1^{(2)} = \boldsymbol{n}_{k_2}$ and $\Pi_x = \sqrt{2x+1}$. In (5.12),

(5.13) the coefficient $\left\{v_1^{(1,2)} \otimes w_1^{(1,2)}\right\}_y$ denotes the tensor product of rank y for two tensors $v_1^{(1,2)}$ and $w_1^{(1,2)}$ of rank 1 each [179]. This tensor product completely determines the angular correlations in the scattering cross section.

Determining the transition frequency through the extremum condition for the cross section, the corresponding leading-order NR correction takes the form:

$$\delta_{\mathrm{NR}}^{(1,2)} = \frac{f_{fi}^{(1,2)}(a,a')}{f_{fi}^{(1,2)}(a,a)} \frac{\Gamma_a^2}{4\Delta}. \tag{5.14}$$

Here $\Delta = E_{a'} - E_a$ represents the fine splitting for the levels $4p_{1/2}^{F=1}$ and $4p_{3/2}^{F=1}$. The correction (5.14) may depend on the experimental setup, i.e., on the angle between the vectors $\boldsymbol{n}_{k_1}$ and $\boldsymbol{n}_{k_1}$ in a type 1 experiment or on the angle between the vectors $\boldsymbol{e}_{k_1}$ and $\boldsymbol{n}_{k_2}$ in a type 2 experiment. This dependence was discussed in detail in [52]; it is usually reduced to $1 + 3\cos 2\vartheta$ for dipole electric photons when the fine structure of the levels is taken into account [43]. However, being determined by the set of quantum numbers of the particular states under consideration, taking into account the hyperfine structure can violate the latter (see below).

5.3. Application to hydrogen spectroscopy

To determine the transition frequency $2s_{1/2}^{F=0} \to 4p_{1/2}^{F=1}$ taking into account NR corrections originating from the neighbouring $4p_{3/2}^{F=1}$ level [32, 52] one should consider for the initial state $n_i l_i = 2s$, $j_i = 1/2$, $F_i = 0$, the resonant state is defined by the set $n_a l_a = 4p$, $j_a = 1/2$, $F_a = 1$, and, correspondingly, for the closest state leading to QIE $j_{a'} = 3/2$, $F_{a'} = 1$. The numerical values of the nonresonant corrections in $2s_{1/2}^{F_a=0} \to 4p_{1/2}^{F_a=1}(4p_{3/2}^{F_{a'}=1}) \to f$ photon scattering process with a fixed final state f are presented in Table 5.1.

To calculate the NR corrections (5.12), (5.13), and (5.14), the theoretical values given in the [187], which include relativistic QED corrections, corrections for hyperfine structure, and finite nucleus size, were used. The same is valid for the fine structure interval $\Delta = E_{4p_{3/2}^{F_{a'}=1}} - E_{4p_{1/2}^{F_{a'}=1}} = 1367433.3$ kHz, the width

Table 5.1. NR corrections in kHz to the transition frequency $2s_{1/2}^{F_i=0} \to 4p_{1/2}^{F_a=1}$ ($\nu_{1/2}$ in [32]) taking into account the interfering transition to the $4p_{3/2}^{F_{a'}=1}$ state for the type 2 experiment ($\boldsymbol{e}_1\boldsymbol{n}_{k_2}$ correlation) and $2s_{1/2}^{F_i=0} \to 4p_{3/2}^{F_a=1}$ ($\nu_{3/2}^{F_a=1}$ ($\nu_{3/2}$ in the notation [32]) taking into account the condition $4p_{1/2}^{F_{a'}=1}$. The same values are obtained for the type 1 experiment ($\boldsymbol{n}_{k_1}\boldsymbol{n}_{k_2}$ correlation).

Final state f	$\delta_{\rm NR}^{(2)}$ to $\nu_{1/2}$ (kHz)	$\delta_{\rm NR}^{(2)}$ to $\nu_{3/2}$ (kHz)
$1s_{1/2}^{F_f=0}$	60.7127	-15.1782
$1s_{1/2}^{F_f=1}$	-30.3563	30.3563
$2s_{1/2}^{F_f=0}$	60.7127	-15.1782
$2s_{1/2}^{F_f=1}$	-30.3563	30.3563
$3s_{1/2}^{F_f=0}$	60.7127	-15.1782
$3s_{1/2}^{F_f=1}$	-30.3563	30.3563
$3d_{3/2}^{F_f=1}$	30.3563	30.3563
$3d_{3/2}^{F_f=2}$	6.0713	-151.7819

value $\Gamma_a = \Gamma_{4p_{1/2}^{F_a=1}} = 1.2941 \times 10^7$ Hz. These values give a reasonably accurate result for $\delta_{\rm NR}$, to four digits after the decimal point. The parameter Γ_a/Δ in this case is 0.00946, so the expansion by powers of this parameter is valid.

As it turned out, the NR corrections to the transition frequency $2s_{1/2}^{F_i=0} \to 4p_{1/2}^{F_a=1}$ do not depend on the type of experiment and, moreover, on the "geometry" (angles) of the experiment. However, these corrections strongly depend on the method of frequency registration, i.e., on the choice of the state into which the $4p_{1/2}^{F_a=1}$ excited level finally decays. Moreover, this dependence is determined only by the quantum numbers of the final state, and the result is practically independent of the frequency of the outgoing photon. The latter circumstance is understandable, since according to (5.14) the NR corrections are proportional to the ratio $f_{\rm nr}/f_{\rm res}$, where the corresponding energy differences are compensated. When the hyperfine structure of finite levels is resolved, the NR corrections differ only in the values of the total angular momentum F_f of the final hyperfine sublevel. This can be seen from the closed expressions (5.12),

(5.13), (5.13), (5.14) defined via $6j$-symbols.

The obtained transition frequencies for the partial channels are summarised in Table 5.2, which shows the partial scattering channels to different final states (first column), the transition frequencies ω_0 as eigenvalues of the Hamiltonian [187] (second column), the nonresonant corrections (third column) see Table 5.1. in Table 5.1, and the resulting transition frequencies $\omega_{\rm res}^{\max\,(1,2)}$ (fourth column). Results are presented for both measured in [32] transition frequencies $\nu_{1/2} \to 2s_{1/2}^{F_i=0} - 4p_{1/2}^{F_{a'}=1}$ and $\nu_{3/2} \to 2s_{1/2}^{F_i=0} - 4p_{3/2}^{F_{a'}=1}$ (top and bottom of Table 5.2, respectively).

Focusing on the frequency $\nu_{1/2}$, for the transition $2s_{1/2}^{F_i=0} \to 4p_{1/2}^{F_a=1}$ three different values of $\omega_{\rm res}^{\max\,(1,2)}$ corresponding to $F_f = 0,\, 1,\, 2$, can be obtained for both types of experiment using ω_0 from the [187] and NR corrections from Table 5.1:

$$\begin{aligned} F_f = 0 \quad & \omega_{\rm res}^{\max\,(1,2)} = 616520152619.2 \text{ kHz}, \\ F_f = 1 \quad & \omega_{\rm res}^{\max\,(1,2)} = 616520152528.1 \text{ kHz}, \\ F_f = 2 \quad & \omega_{\rm res}^{\max\,(1,2)} = 616520152564.6 \text{ kHz}. \end{aligned} \tag{5.15}$$

The values above can equally be used as a determination of the $2s_{1/2}^{F=0} \to 4p_{1/2}^{F=1}$ transition frequency (by the maximum of the line profile - the most probable frequency), i.e., they represent an unambiguously reproducible result for strictly defined conditions (fixed final state). Then, the three transition frequencies in (5.15) differ from each other by more than 50 kHz. This is 15 times greater than the accuracy of the measurements in [32] (3 kHz) and shows the applicability region of the resonance approximation. Moreover, the frequency difference in (5.15) demonstrates the ambiguity in determining the transition frequency from the observed line profile due to the existence of nonresonant contributions in the scattering cross section. It is worth noting that a similar conclusion will follow for the frequency corresponding to the full-width-half-maximum of the observed contour, see [43]. It will be shown below that this fact is only relevant to the question of definition.

However, ω_0 is of interest, since this value should correspond to the theoretical value (the difference of eigenvalues of the Hamiltonian). Exactly ω_0

Table 5.2. Numerical values of the frequency $\omega_{\rm res}^{\max\,(1,2)}$. The first column indicates the partial scattering channel, the second column gives the values of ω_0 used in the calculations for $\nu_{1/2}$ and $\nu_{3/2}$, see [187], the third column shows the corresponding nonresonant correction values, and the last column shows the $\omega_{\max}$ values. All values are given in kHz.

Transition, $\nu_{1/2}$	ω_0, kHz [187]	$\delta_{\rm NR}^{(1,2)}$, kHz	$\omega_{\rm res}^{\max\,(1,2)}$, kHz
$2s_{1/2}^{F_i=0} \to 4p_{1/2}^{F_a=1} \to 1s_{1/2}^{F_f=0}$	616520152558.5	60.7127	616520152619.2
$2s_{1/2}^{F_i=0} \to 4p_{1/2}^{F_a=1} \to 1s_{1/2}^{F_f=1}$		−30.3563	616520152528.1
$2s_{1/2}^{F_i=0} \to 4p_{1/2}^{F_a=1} \to 2s_{1/2}^{F_f=0}$	616520152558.5	60.7127	616520152619.2
$2s_{1/2}^{F_i=0} \to 4p_{1/2}^{F_a=1} \to 2s_{1/2}^{F_f=1}$		−30.3563	616520152528.1
$2s_{1/2}^{F_i=0} \to 4p_{1/2}^{F_a=1} \to 3s_{1/2}^{F_f=0}$	616520152558.5	60.7127	616520152619.2
$2s_{1/2}^{F_i=0} \to 4p_{1/2}^{F_a=1} \to 3s_{1/2}^{F_f=1}$		−30.3563	616520152528.1
$2s_{1/2}^{F_i=0} \to 4p_{1/2}^{F_a=1} \to 3d_{3/2}^{F_f=1}$	616520152558.5	−30.3563	616520152528.1
$2s_{1/2}^{F_i=0} \to 4p_{1/2}^{F_a=1} \to 3d_{3/2}^{F_f=2}$		6.0713	616520152564.6
Transition, $\nu_{3/2}$	ω_0, kHz [187]	$\delta_{\rm NR}^{(1,2)}$, kHz	$\omega_{\rm res}^{\max\,(1,2)}$, kHz
$2s_{1/2}^{F_i=0} \to 4p_{3/2}^{F_a=1} \to 1s_{1/2}^{F_f=0}$	616521519991.8	−15.1782	616521519976.6
$2s_{1/2}^{F_i=0} \to 4p_{3/2}^{F_a=1} \to 1s_{1/2}^{F_f=1}$		30.3563	616521520022.2
$2s_{1/2}^{F_i=0} \to 4p_{3/2}^{F_a=1} \to 2s_{1/2}^{F_f=0}$	616521519991.8	−15.1782	616521519976.6
$2s_{1/2}^{F_i=0} \to 4p_{3/2}^{F_a=1} \to 2s_{1/2}^{F_f=1}$		30.3563	616521520022.2
$2s_{1/2}^{F_i=0} \to 4p_{3/2}^{F_a=1} \to 3s_{1/2}^{F_f=0}$	616521519991.8	−15.1782	616521519976.6
$2s_{1/2}^{F_i=0} \to 4p_{3/2}^{F_a=1} \to 3s_{1/2}^{F_f=1}$		30.3563	616521520022.2
$2s_{1/2}^{F_i=0} \to 4p_{3/2}^{F_a=1} \to 3d_{3/2}^{F_f=1}$	616521519991.8	30.3563	616521520022.2
$2s_{1/2}^{F_i=0} \to 4p_{3/2}^{F_a=1} \to 3d_{3/2}^{F_f=2}$		−151.7819	616521519840.0

should be used for, e.g., determination of fundamental physical constants. All three numbers in (5.15) can be reduced to ω_0 by simple subtraction of $\delta_{\rm NR}$. This is possible because the correction does not depend on any angles, which in turn demonstrates the advantage of recording the radiation corresponding to a transition to a particular final state.

If in the process of frequency measurement radiation is registered without fixing its frequency, then summation over all final states should be performed.

This summation is as follows:

$$\delta_{\rm NR}^{(1,2)} = \frac{\sum\limits_{n_f l_f j_f F_f} f_{\rm nr}^{(1,2)}}{\sum\limits_{n_f l_f j_f F_f} f_{\rm res}^{(1,2)}} \frac{\Gamma_a^2}{4\Delta}. \tag{5.16}$$

Now the NR correction depends on the type of experiment and on the angle between the vectors $\boldsymbol{n}_{k_1}$, $\boldsymbol{n}_{k_2}$ in the experiment of the first type or between the vectors $\boldsymbol{e}_1$, $\boldsymbol{n}_{k_2}$ in the experiment of the second type. For a set of quantum numbers $n_i l_i = 2s$, $j_i = 1/2$, $F_i = 0$, $n_a l_a = 4p$, $j_a = 1/2$, $F_a = 1$, $j_{a'} = 3/2$, $F_{a'} = 1$, one can find $\delta_{\rm NR}^{(2)} \approx -0.23983(1 + 3\cos 2\vartheta)\Gamma_a^2/\Delta$. For brevity, only the result for the second type of experiment is written out here, the details are given in [52], and the numerical factor arises from the radial integrals. Solving the equation $1 + 3\cos 2\vartheta = 0$ for the variable ϑ, it is easy to find that the correction goes to zero at angles $\vartheta = (1/2)(\pm \arccos(1/3) + 2\pi n)$ (with arbitrary integer n). This result can be obtained for the scattering of photons corresponding to a dipole transition with an arbitrary set of quantum numbers of initial and intermediate states. The difference will be in the numerical multiplier. The latter means that nonresonant corrections should be considered separately for each particular transition. The corrections $\delta_{\rm NR}^{(1,2)}$ in the expression (5.16) as a function of the angle ϑ are shown in Fig. 5.1 for the transition $2s_{1/2}^{F_i=0} \to 4p_{1/2}^{F_a=1}$.

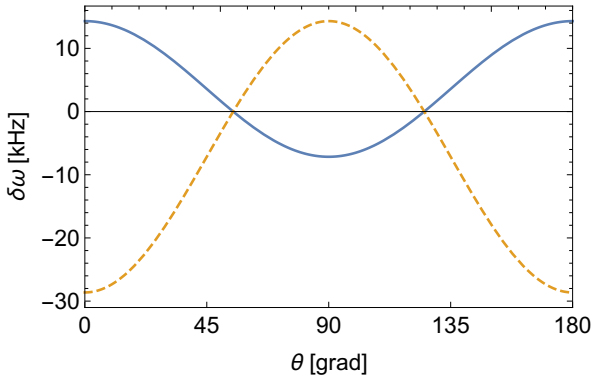

Figure 5.1. NR correction to the transition frequency $2s_{1/2}^{F_i=0} \to 4p_{1/2}^{F_a=1}$ as a function of the angle between vectors $\boldsymbol{n}_{k_1}$, $\boldsymbol{n}_{k_2}$ for experiment type 1 (solid line) and as a function of the angle between vectors $\boldsymbol{e}_1$, $\boldsymbol{n}_{k_2}$ in experiment type 2 (dashed line) according to the expression (5.16).

According to the above, the NR correction is zero for certain ("magic") angles $\theta_1 = 54.7^\circ$ and $\theta_2 = 125.3^\circ$, which are the same for both types of experiment. The possible use of "magic angles" to determine transition frequencies in atoms was pointed out in [51,187]. It was pointed out in [51] that the method of extracting the transition frequency value from experimental data used in [32] is actually equivalent to using "magic angles". Specifically, the amplitude (5.11) was used to construct the fitting contour in [32] (see also [51]), the first summand in which leads to the symmetric part of the profile. The non symmetric part of the profile was obtained in the linear approximation, see [43], by taking the resonant term in the amplitude (5.11) as a common factor and expanding the additional term (nonresonant) in a series on the parameter Δ. Then, a convolution of the profile derived in this way (Fano profile) with a Gaussian contour (Fano-Voigt profile) [188] was taken. With this in mind, the "theoretical" profile much more accurately fit the observed profile, allowing the asymmetry parameters to be determined. In turn, the arising asymmetry parameters are zero for the "magic angle" and define the " line centre", which was determined as the transition frequency in [32].

Calculations of atomic transition frequencies using "magic angles" were considered in [49], which coincide with those given above for corresponding transitions. The value of the transition frequency $2s_{1/2}^{F_i=0} - 4p_{1/2}^{F_a=1}$ (5.16) for "magic angles" and the theoretical values of ω_0, Γ_a and Δ are equal to

$$\omega_{\rm res}^{\max\,(1,2)} = 616520152558.5 \text{ kHz}. \tag{5.17}$$

Similarly, for the transition frequency $2s_{1/2}^{F_i=0} - 4p_{3/2}^{F_a=1}$ one can find

$$\omega_{\rm res}^{\max\,(1,2)} = 616521519991.8 \text{ kHz}. \tag{5.18}$$

5.4. Relationship between the definitions of transition frequency

According to the theory presented in the previous section, the transition frequency can be determined by various experiments. In one of them it is proposed

to record the radiation associated with a fixed final hyperfine state. Obviously, it is preferable to use some sublevel of the ground state, since its hyperfine splitting is experimentally resolvable [137]. The advantage in this case is the angle-independent nonresonant correction, which can be simply subtracted from the determined result for the most probable transition frequency. However, in the experiment [32] a different scheme was used: the whole emission was recorded. Consequently, the resulting asymmetry of the line profile becomes angle dependent (in the experiment [32] it corresponds to the angle between the polarisation vector of the incident photon and the direction vector of the emitted photon). Since this angle is not fixed, a different interpretation of the experimental data is required. In other words, the nonresonant correction calculated at a fixed angle cannot be subtracted from the experimentally determined transition frequency.

To avoid the problems associated with an asymmetric line profile, in [32] the observed profile was fit with a Fano-Voigt profile. As a result of this treatment, the "line centre" of the symmetric part of the line profile was defined as the transition frequency. Finally, the values determined in [32] for $\nu_{1/2} = 616\,520\,152\,555.1(3.0)$ kHz (numbers in brackets denote the established experimental error) and $\nu_{3/2} = 616\,521\,519\,990.8(3.0)$, were used to calculate the weighted average hyperfine centroid ν_{2s-4p} corrected for hyperfine shift (denoted here as Δ_{HFS}).

$$\nu_{2s-4p} = \frac{1}{3}\nu_{1/2} + \frac{2}{3}\nu_{3/2} - \Delta_{\mathrm{HFS}} = 616\,520\,931\,626.8 \ \text{kHz}, \qquad (5.19)$$
$$\Delta_{\mathrm{HFS}} = 132\,552.092(75) \ \text{kHz}.$$

The values of $\nu_{1/2}$, $\nu_{3/2}$ agree with the values of (5.17), (5.18) within the experimental error.

Thus, two methods are available to determine the transition frequency. The first method corresponds to the theory discussed above and involves identifying the peak of the line profile, determining the transition frequency as the most probable, followed by estimating nonresonant corrections. The second method is based on the "symmetrization" procedure described in [32,51]. At first glance, these definitions may seem completely different and lead to deviations in transition frequency values of the order of tens of kHz (before subtracting nonresonant

corrections, as shown in (5.15)). Moreover, a direct comparison of the experimental results for $\nu_{1/2}$ and $\nu_{3/2}$ and the values of (5.17) and (5.18) shows a significant discrepancy. Currently, this discrepancy may play a decisive role in determining the Rydberg constant and the charge radius of the proton.

To demonstrate the absence of a contradiction in these definitions, one can use the averaging procedure for $\omega_{\max}$ corresponding to a fixed finite hyperfine sublevel, see Table 5.2. By emphasizing their angular independence, it is assumed that measurements can be made for each specific transition. The determined values can then be averaged in various ways. For example,

$$\omega_{\text{av}} = \sum_{F_f, j_f} \frac{2F_f + 1}{(2j_f + 1)(2I + 1)} \omega_{\max}, \tag{5.20}$$

where I is the spin of the nucleus.

Another scheme can be used with the same success. When estimating nonresonant corrections, additional averaging can be carried out over the projections of the total moment of the resonant state j_a. Then, according to the expression (5.8),

$$\omega_{\text{av}} = \omega_0 + \frac{1}{2j_a + 1} \sum_{F_f, j_f} \frac{2F_f + 1}{(2j_f + 1)(2I + 1)} \delta_{\text{NR}}. \tag{5.21}$$

Averaging (5.21) is due to the fact that practically in experiment one observes radiation for which the resonant state is "pseudo-initial".

Turning again to the case of a fixed final state $1s_{1/2}^{F_f=0}$, the averaged centroid (5.20) can be found according to the expression (5.19): $\nu_{2s-4p} = 616\,520\,931\,638.7$ kHz with the same result for the $1s_{1/2}^{F_f=1}$ state (for δ_{NR} values see Table 5.1). Additional averaging over the j_r projections for the nonresonant correction leads to $\nu_{2s-4p}^{(F_f=0)} = 616\,520\,931\,630.5$ kHz and $\nu_{2s-4p}^{(F_f=1)} = 616\,520\,931\,628.6$ kHz, and therefore $\nu_{2s-4p} = 616\,520\,931\,629.1$ kHz. Finally, the center of gravity averaged as (5.21) for frequencies (5.17), (5.18) can be found equal to $616\,520\,931\,628.6$ kHz. All these values, within the error, agree with the value (5.19) obtained experimentally.

Thus, there is a range of options for determining the transition frequency.

The first is to determine the maximum of the observed profile and then subtract the nonresonant shift from the resulting value. However, in view of possible angular correlations caused by the interference effect, from all the observed radiation it is worth choosing the one that corresponds to a specific hyperfine sublevel of the final state. This can be achieved by detecting photons of only a certain frequency. In this case, the nonresonant shift is a constant and can be determined theoretically. Another option is to average the measured values. Finally, one can apply the "symmetrization" procedure described in [32,43]. Averaging experimentally determined transition frequencies is preferable because subtraction is always less accurate. All of them have their own difficulties associated with the accuracy of the described process for determining the transition frequency. In turn, these problems are caused by going beyond the resonant approximation, when it is necessary to take into account the asymmetry of the observed spectral line profile. However, the main conclusion that follows from the above discussion is the consistency of definitions through the "maximum" or "line center". Deviations of the corresponding values (albeit coinciding with high accuracy) are precisely associated with going beyond the limits of the resonant approximation.

Another, no less important, circumstance indicating the advantage of the partial decay channel (namely, the detection of radiation corresponding to decay into a certain hyperfine sublevel of the ground state) is discussed in the next section.

5.5. Participation of the emission process in determining the absorption frequency

The fundamental principles governing the detailed description of the observed line profile require careful consideration of all processes involved in the measurements. For example, evaluation of nonresonant contributions to the photon scattering cross section shows a clear difference for the cases when all outgoing photons are detected or when a partial scattering process is used to determine the transition frequency [52]. The QED formulation of the line profile

theory itself and the use of the resonant approximation for the photon scattering cross section require consideration of the process from stable state to stable state. To a fairly good approximation, the use of a metastable state is also permissible (the lifetime of the metastable state should significantly exceed the measurement time). In turn, the determination of the $2s - 4p$ absorption frequency is not limited to the $2s \to 4p \to 1s(2s)$ scattering process, but also involves transitions to the $3s$ and $3d$ states, which then decay through two-photon emission (including cascade and "pure" radiation) into a stable state $1s$ (metastable state $2s$) [32]. A discussion about the ambiguity of separating cascades from "pure" (see [82]) two-photon radiation will be presented in one of the following sections of the thesis. Here this circumstance is neglected, assuming that the interference between these two types of probabilities is small. Accordingly, the determination of the frequency of the $2s - 4p$ transition can be correctly described only taking into account the following cascade processes: $2s + \gamma \to 4p \to 3s(3d) + \gamma \to 2p(3p) + \gamma \to 1s(2s) + \gamma$. Next, the case of cascade radiation only into the $1s$ state is considered, but in conjunction with accounting for the hyperfine structure of levels.

It can be noted at once that the cascade radiation is also subject to the quantum interference effect if we consider the interference for the corresponding hyperfine sublevels of the fine structure (similarly $4p_{1/2}^{F=1}$ and $4p_{3/2}^{F=1}$). In the framework of the above approximations (see also [49, 50]) the detailed description of the cascade transition $2s + \gamma \to 4p \to 3s(3d) + \gamma \to 2p(3p) + \gamma \to 1s(2s) + \gamma$ should include the states $4p_{1/2}^{F=1}$, $4p_{3/2}^{F=1}$ as resonant (denoted below as state r), states $3s_{1/2}$ and $3d_{3/2}$, $3d_{5/2}$ as the first cascade state (denoted below as state a), and then levels $2p_{1/2}$, $2p_{3/2}$, $3p_{1/2}$, $3p_{3/2}$ (denoted below as state b). In further calculations, the summation on the total atomic momentum F for states a and b is carried out. Leaving a resonance term in the cross section for the transition to the $4p_{1/2}^{F=1}$ or $4p_{3/2}^{F=1}$ state, for details see [189], the influence of quantum interference in the cascade can be described by considering in the amplitude, in addition to the resonance (cascade) states, also the states nearest in energy. The amplitude will now contain three energy denominators, each of which can be reduced to the denominator of the absorption resonance using the energy conservation law. Then QIE due to cascade radiation arises for states

a and b in the same way as for states r with corresponding widths and energy intervals between resonant and neighbouring nonresonant states.

Considering first the cascade through the $3s$ state, it can be found that the absorption frequency, determined from the extremum condition [189], is

$$\omega_{\max} = \omega_0 + \delta\omega_r + \delta\omega_a + \delta\omega_b, \tag{5.22}$$

where ω_0 represents $\nu_{1/2}$ or $\nu_{3/2}$, according to the notations in [32], and $\delta\omega_i$ is defined by the expression:

$$\delta\omega_i = \frac{f_{\rm nr}^{(c)}}{f_{\rm res}^{(c)}} \frac{\Gamma_r^2}{4\Delta_i} \Upsilon, \tag{5.23}$$

$$\Upsilon = \frac{(\Gamma_r+\Gamma_a)^2(\Gamma_a+\Gamma_b)^2}{(\Gamma_r+\Gamma_a)^2(\Gamma_a+\Gamma_b)^2 + (\Gamma_r+\Gamma_a)^2\Gamma_r^2 + (\Gamma_a+\Gamma_b)^2\Gamma_r^2}.$$

Here i is one of the states labelled r, a, b. The value $f_{\rm res}^{(c)}$ is defined through the numerator of the resonant amplitude. In the case of a cascade passing through the $3s_{1/2}$ state, this amplitude corresponds to $2s_{1/2}^{F=0} + \gamma \to 4p_{1/2(3/2)}^{F=1} \to 3s_{1/2} + \gamma \to 2p_{1/2} + \gamma \to 1s_{1/2} + \gamma$ transition and $f_{\rm nr}^{(c)}$ corresponds to one of the nonresonant contributions $2s_{1/2} + \gamma \to 4p_{1/2(3/2)}^{F=1} \to a + \gamma \to b + \gamma \to 1s_{1/2} + \gamma$, Δ_i represents the energy splitting between the r states, a or b (as, for example, $\Delta_r \equiv E_{4p_{3/2}^{F=1}} - E_{4p_{1/2}^{F=1}}$), and the correction $\delta\omega_i$ is written out in leading order.

Assuming that all outgoing photons are directed to the same detector (i.e., the photon direction vectors, $\boldsymbol{\nu}$, are co-directional, $\boldsymbol{\nu}_{4p-3s} \parallel \boldsymbol{\nu}_{3s-2p(3p)} \parallel \boldsymbol{\nu}_{2p-1s}$), the NR corrections are

$$\delta\omega_r = -\frac{1}{2}(1 - 3\cos 2\theta)\frac{\Gamma_r^2}{4\Delta_r}\Upsilon, \tag{5.24}$$

$$\delta\omega_a = 0,$$

$$\delta\omega_b = 2\frac{\Gamma_r^2}{4\Delta_b}\Upsilon.$$

Here and below θ denotes the angle between the incident photon polarisation vector and the direction vector of the emitted photons (this corresponds to the conditions of the experiment [32]), and the numerical factors arise from the ratio

of the radial parts of the amplitudes. It can be noted that when F_f is fixed, the results of [52] are recovered. The angular dependence in the expression (5.24) is due to the summation over the total atomic moments in the $f_{\rm res}^{(c)}$ and $f_{\rm nr}^{(c)}$.

Thus, it is obtained that the correction $\delta\omega_a$ is equal to zero. This holds only when the photons are registered in one direction, otherwise the correction is different from zero. It also follows from (5.24) that $\delta\omega_b$ is independent of the correlation angle, θ. Using the values $\Gamma_r = 1.2941 \times 10^7$ Hz, $\Delta_r = 1\,367\,433.3$ kHz, $\Gamma_{3d} = 1.0295 \times 10^7$ Hz, $\Gamma_{3p} = 3.0208 \times 10^6$ Hz, $\Gamma_{3s} = 1.0054 \times 10^6$ Hz, $\Gamma_{2p} = 9.97624 \times 10^7$ Hz, $\Delta_{3p} = 3\,241\,327.3$ kHz, $\Delta_{2p} = 10\,939\,469.7$ kHz [187], frequency shifts are given in Table 5.3 for different angles θ.

As follows from (5.24), the correction $\delta\omega_r$ is zero at angles $\theta = \pm 1/2 \arccos(1/3) + \pi k$ (k is an integer), instead of the magic angle $\theta_{\rm m} = \arccos(1/\sqrt{3})$. By solving the equation for the total correction $\delta\omega_\Sigma(\theta_0) = \delta\omega_r + \delta\omega_{2p} = 0$, one can find the angle at which it goes to zero (if it exists). According to [32], the fraction of the cascade process is about 4% of all photons detected by the detector. The corresponding value can be found as the ratio of the partial transition probability to the level width: $W_{4p-3s}/\Gamma_{4p} \approx 0.0377$, $W_{4p-3d}/\Gamma_{4p} \approx 0.0043$, which were used to calculate the total contribution $\delta\omega_\Sigma$.

Repeating the calculations for the cascade transition through the state $3d_{3/2}$ for the frequency $\nu_{1/2}$, one obtains

$$\begin{aligned} \delta\omega_r &= \frac{1}{20}\,(1 - 3\cos 2\theta)\,\frac{\Gamma_r^2}{4\Delta_r}\Upsilon, \\ \delta\omega_a &= 0, \\ \delta\omega_b &= \frac{1}{5}\frac{\Gamma_r^2}{4\Delta_b}\Upsilon. \end{aligned} \tag{5.25}$$

Here, the resonant amplitude corresponds to $2s_{1/2}^{F=0} + \gamma \to 4p_{1/2}^{F=1} \to 3d_{3/2} + \gamma \to 2p_{1/2} + \gamma \to 1s_{1/2} + \gamma$ and nonresonant amplitudes are related to i) $2s_{1/2}^{F=0} + \gamma \to 4p_{3/2}^{F=1} \to 3d_{3/2} + \gamma \to 2p_{1/2} + \gamma \to 1s_{1/2} + \gamma$, $\Delta_r \equiv E_{4p_{3/2}^{F=1}} - E_{4p_{1/2}^{F=1}}$ and ii) $2s_{1/2}^{F=0} + \gamma \to 4p_{1/2}^{F=1} \to 3d_{3/2} + \gamma \to 2p_{3/2} + \gamma \to 1s_{1/2} + \gamma \to$

[1] There is no decay to the $3p_{3/2}$ state.

Table 5.3. Numerical values of nonresonant shifts and the total contribution $\delta\omega_\Sigma$ multiplied by the cascade fraction factor $W_{4p-n_a l_a}/\Gamma_{4p}$. The angle at which the maximum ($\theta_{\max}$), minimum ($\theta_{\min}$) values are reached, and NR correction at the "magic angle" ($\theta_{\rm m}$) are given. The highlighted line shows the values of the angle at which the total contribution is zero (θ_0), if it exists, the cascade fractions and the process under consideration. All values are given in kHz.

Angle	$\delta\omega_r + \delta\omega_{3p}$ (kHz)	$\delta\omega_r + \delta\omega_{2p}$ (kHz)	$\delta\omega_\Sigma$ (kHz)
$2s^{F=0}_{1/2} \to 4p^{F=1}_{1/2} \to 3s_{1/2} \to 2p_{1/2} \to 1s_{1/2}$; $\theta_0 = \pm 0.403619$; $2s^{F=0}_{1/2} \to 4p^{F=1}_{1/2} \to 3s_{1/2} \to 3p_{1/2} \to 1s_{1/2}$; $W_{4p-3s}/\Gamma_{4p} \approx 0.0377$			
$\theta_{\min} = 0$	-3.388	-17.342	-0.781
$\theta_{\max} = \pi/2$	61.587	52.008	4.282
$\theta_{\rm m}$	39.942	28.898	2.595
$2s^{F=0}_{1/2} \to 4p^{F=1}_{1/2} \to 3d_{3/2} \to 2p_{1/2} \to 1s_{1/2}$; $\theta_0 = \pm 0.403605$; $2s^{F=0}_{1/2} \to 4p^{F=1}_{1/2} \to 3d_{3/2} \to 3p_{3/2} \to 1s_{1/2}$; $W_{4p-3s}/\Gamma_{4p} \approx 0.0043$			
$\theta_{\min} = 0$	-0.339	-1.734	$-9. \times 10^{-3}$
$\theta_{\max} = \pi/2$	6.164	5.203	4.9×10^{-2}
$\theta_{\rm m}$	3.997	2.890	3.0×10^{-2}
$2s^{F=0}_{1/2} \to 4p^{F=1}_{1/2} \to 3s_{1/2} \to 2p_{3/2} \to 1s_{1/2}$[1]; $\theta_0 = \pm 0.637414$; $W_{4p-3d}/\Gamma_{4p} \approx 0.0377$			
$\theta_{\min} = 0$	$--$	-21.679	-0.817
$\theta_{\max} = \pi/2$	$--$	43.343	1.634
$\theta_{\rm m}$	$--$	21.675	0.817
$2s^{F=0}_{1/2} \to 4p^{F=1}_{1/2} \to 3d_{3/2} \to 2p_{3/2} \to 1s_{1/2}$; $2s^{F=0}_{1/2} \to 4p^{F=1}_{1/2} \to 3d_{3/2} \to 3p_{3/2} \to 1s_{1/2}$; $W_{4p-3d}/\Gamma_{4p} \approx 0.0043$			
$\theta_{\max} = 0$	-224.435	-74.460	-1.285
$\theta_{\min} = \pi/2$	-218.192	-67.534	-1.229
$\theta_{\rm m}$	-220.274	-69.843	-1.247

$1s_{1/2} + \gamma$, $\Delta_b \equiv E_{2p_{3/2}} - E_{2p_{1/2}}, E_{3p_{3/2}} - E_{3p_{1/2}}$ decay channels. The numerical values multiplied by a factor of 0.0043 according to the contribution of the cascade in the transition frequency measurements in [32] are collected in the second segment of Table 5.3. When the resonant channel is considered as passing through the $2p_{3/2}(3p_{3/2})$ state, numerical results are presented in the third and

fourth segments of Table 5.3 (the corresponding graphs are presented in the appendix of the paper [189]).

From the values given in the table, one can conclude that the contribution of QIE due to the cascade is in general significant, but is suppressed by the relative fraction of the cascade process in the total emission. Nevertheless, the interfering links in the cascade process affect the absorption line profile at the level of a few kilohertz. This asymmetry can be expressed through a nonresonant correction to the transition frequency, defined here through the maximum of the line profile (as the most probable value). These corrections do not vanish at the magic angle, see Table 5.3. Practically, this means that the symmetrization procedure applied in [32] reduced the contribution of the cascading ECI to the value estimated here for the magic angle, since an appropriate asymmetry parameter was used. Although the $\delta\omega_\Sigma$ value is within the experimental uncertainties, a frequency shift at the kHz level can be expected for the "central" value with the same uncertainty.

An analysis of the measurement of the transition frequency $\nu_{1/2}$ was presented above as a demonstration. Similar calculations can be performed for the transition frequency $\nu_{3/2}$. Omitting for brevity the details of the calculations, the numerical results are presented in Table 5.4.

In addition to the results above, it is necessary to point out the importance of the QIE arising in cascade emission for measuring the frequencies of two-photon transitions: $n_i s + 2\gamma \rightarrow n_a s/n_a d \rightarrow 1s$. Recently, the corresponding calculations were performed and published in Ref. [190].

However, the main conclusion of this section, which follows from the analysis of the cascade QIE, is that the Fano profile obtained by the cascade process should be taken into account in the symmetrization procedure [32]. For example, in order to best fit the experimental data, several parameters related to the asymmetry of the line profile due to different processes should be used. The asymmetry parameters do not necessarily depend equally on the angle and, in principle, can be considered as independent of each other. In fact, it can be

[2]There is no decay to the $3p_{3/2}$ state.

Table 5.4. Numerical values of nonresonant shifts for given cascade transitions corresponding to the frequency $\nu_{3/2} = E_{4p^{F=1}_{3/2}} - E_{2s^{F=0}_{1/2}}$ and the total contribution $\delta\omega_\Sigma$ multiplied by the factor W_{4p-nl}/Γ_{4p}. The designations are the same as in Table 5.3. All values are in kHz.

Angle	$\delta\omega_r + \omega_{3p}$ (kHz)	$\delta\omega_r + \omega_{2p}$ (kHz)	ω_Σ (kHz)
$2s^{F=0}_{1/2} \to 4p^{F=1}_{3/2} \to 3s_{1/2} \to 2p_{1/2} \to 1s_{1/2}$; $2s^{F=0}_{1/2} \to 4p^{F=1}_{3/2} \to 3s_{1/2} \to 3p_{1/2} \to 1s_{1/2}$; $W_{4p-3s}/\Gamma_{4p} \approx 0.0377$			
$\theta_{\max} = 0$	39.954	28.902	2.596
$\theta_{\min} = \pi/2$	7.446	−5.780	6.3×10^{-2}
θ_{m}	11.058	−1.927	0.344
$2s^{F=0}_{1/2} \to 4p^{F=1}_{3/2} \to 3s_{1/2} \to 2p_{3/2} \to 1s_{1/2}$[2]; $\theta_0 = 0.528655$;			
$\theta_{\max} = 0$	−−	21.679	0.817
$\theta_{\min} = \pi/2$	−−	−13.006	−0.490
θ_{m}	−−	−9.152	−0.345
$2s^{F=0}_{1/2} \to 4p^{F=1}_{3/2} \to 3d_{3/2} \to 2p_{1/2} \to 1s_{1/2}$; $\theta_0 = 0.651478$; $2s^{F=0}_{1/2} \to 4p^{F=1}_{3/2} \to 3d_{3/2} \to 3p_{1/2} \to 1s_{1/2}$; $W_{4p-3s}/\Gamma_{4p} \approx 0.0043$			
$\theta_{\max} = 0$	9.571	8.836	7.9×10^{-2}
$\theta_{\min} = \pi/2$	−106.438	−114.926	−0.952
θ_{m}	−16.235	−18.690	−0.150
$2s^{F=0}_{1/2} \to 4p^{F=1}_{3/2} \to 3d_{3/2} \to 2p_{3/2} \to 1s_{1/2}$; $2s^{F=0}_{1/2} \to 4p^{F=1}_{3/2} \to 3d_{3/2} \to 3p_{3/2} \to 1s_{1/2}$; $W_{4p-3s}/\Gamma_{4p} \approx 0.0043$			
$\theta_{\max} = 0$	−37.927	−6.192	−0.190
$\theta_{\min} = \pi/2$	−153.437	−129.889	−1.218
θ_{m}	−63.665	−33.709	−0.419

stated that modern spectroscopic experiments represent a frontier leading to the next generation of experiments in which the problem of resonance approximation will play a crucial role.

As a consequence, consideration of the cascade process affecting the determination of the absorption transition frequency shows the inseparability of the absorption and emission processes in describing the line profile beyond the resonance approximation. The "central" value can be expected to be shifted at the kHz level. Summarising the results of this study, it can be seen that the photon

scattering process used in the [32] experiment is quite complex and should include, with necessity, an analysis of the observed asymmetry of the line profile. This asymmetry is caused not only by the effect of quantum interference at resonant absorption, but also by cascade emission processes. Assuming the need to increase the accuracy of the experiment (e.g., for the precise determination of physical constants), the analysis of cascade processes will be increasingly required for experiments of the type [32] (when all radiation is detected). However, for the measured $2s - 4p$ line in the experiment [32], one can distinguish a case that is not affected by the QIE in the cascade. The main contribution to the emission comes from the $4p - 1s$ emission line, which lacks the cascade. Hence, this scattering channel is the preferred one for determining the transition frequency. An appropriate experiment can be performed by recording emitted photons with a certain energy equal to $4p - 1s$. Such experiments should be more accurate.

5.6. Application to muon hydrogen spectroscopy

Following the analyses in 5.2 and 5.3, here we consider QIE in the framework of one-photon fluorescence spectroscopy of muonic hydrogen using the example of the $2s^{F_i=0,1}_{1/2} \to 2p^{F_a}_{j_a}$ transitions. In this particular case, nonresonant corrections to the transition frequencies arise due to interference between $2p^{F_r}_{j_r}$ sublevels (states of fine and hyperfine structure), for which dipole (according to the selection rules) transitions $2s^{F_i=0,1}_{1/2} \to 2p^{F_a}_{j_a}$ and $2s^{F_i=0,1}_{1/2} \to 2p^{F_{a'}}_{j_{a'}}$ are possible, $j_{a'}F_{a'} \neq j_aF_a$. The physical process described here includes one-photon scattering, see 2.1. The hyperfine states of muonic hydrogen are separated by several hundred GHz [191–193] and have line widths of several tens of GHz [194]. In particular, the natural widths $2p$ of the fine and hyperfine sublevels are roughly equivalent: $\Gamma_{2p^{F=1}_{3/2}} \approx \Gamma_{2p^{F=1}_{1/2}} \approx \Gamma_{2p^{F=2}_{3/2}} \approx \Gamma_{2p^{F=0}_{1/2}} = 116.49 \times 10^9$ s^{-1} or 18.54 GHz. The energies of the atomic states of muonic hydrogen used are listed in Table 5.5.

As in the case discussed in section 5.2, the description of one-photon scattering on muon hydrogen is related to the geometry of the experiment when the polarisation vector $\boldsymbol{e}_1$ of the incident photon is fixed. Then the NR correction

Table 5.5. Energies of atomic states of muonic hydrogen in meV (10^{-3} eV) and Hz. All values are borrowed from [194].

State	meV	Hz
$1s^{F=0}_{1/2}$	-2047.75	-4.95144×10^{14}
$1s^{F=1}_{1/2}$	-1865.3	-4.51028×10^{14}
$2s^{F=0}_{1/2}$	-244.37	-5.90804×10^{13}
$2s^{F=1}_{1/2}$	-221.532	-5.35662×10^{13}
$2p^{F=0}_{1/2}$	-30.9524	-7.48426×10^{12}
$2p^{F=1}_{1/2}$	-23.3505	-5.64613×10^{12}
$2p^{F=1}_{3/2}$	-18.7182	-4.52604×10^{12}
$2p^{F=2}_{3/2}$	-15.6775	-3.7908×10^{12}

can be found to depend on the angle θ between the vector $\boldsymbol{e}_1$ and the direction of emitted photon $\boldsymbol{n}_{k_2}$. Table 5.6 collects the results for the NR correction to the transition frequency $2s^{F_i=0,\,1}_{1/2} \to 2p^{F_a}_{j_a}$ for different final states and angles $\theta = 0,\ \pi/2$.

Thus, for muonic hydrogen, the effect of quantum interference plays a minor role (it is at the level of experimental error [30, 31]) and cannot be the source of the so-called "proton radius puzzle" [29], see also [50]. Nevertheless, this systematics requires careful evaluation and amounts, as the result is close to the sixth-order QED corrections [195].

5.7. Spectroscopy of the ^{3}He isotope

The interest in the two-electron helium-3 atom, ^{3}He, as well as in ^{4}He, is primarily due to the estimation of the rms charge radii of the nuclei and the present discrepancy between experimental results and theory for the transition frequencies, see, e.g., [196–198]. In this section an analysis of NR effects is presented with respect to the experiment [196], where transitions between different hyperfine sublevels of the atom were observed.

Following the work of [196], the atomic level of the helium isotope is labelled as follows: $n^{\kappa}L^{F}_{J}$, where n is the principal quantum number and $\kappa = 2S + 1$ is

Table 5.6. The partial contributions $\delta_{\rm NR}(i \to a[a'])$ to the total correction for the singlet ($F_i = 0$) and triplet ($F_i = 1$) lines $i \to a$ arising from interference with the $i \to a'$ transition in the muon hydrogen atom. The angle between the polarisation vector of the incident photon and the propagation vector of the outgoing photon is denoted θ, which corresponds to a type II experiment according to section 5.2, the energy splitting is defined as $\Delta \equiv E_{n_a l_a j_{a'} F_{a'}} - E_{n_a l_a j_a F_a}$. Results are presented for two different cases: 1) when the final states are assumed to be fixed; 2) summation over all resolved final states is performed. The cases independent of θ are given without specifying the angle.

i	a	a'	f	Δ, Hz	$\delta_{\rm NR}(i \to a[a'])$, Hz	$\delta_{\rm NR}(i \to a[a'])$, meV
$2s_{1/2}^{F_i=0}$	$2p_{3/2}^{F_a=1}$	$2p_{1/2}^{F_{a'}=1}$	$1s_{1/2}^{F_f=0}$	-1.12009×10^{12}	-3.71×10^{7}	-1.53×10^{-4}
–	–	–	$1s_{1/2}^{F_f=1}$		7.41×10^{7}	3.06×10^{-4}
–	–	–	$2s_{1/2}^{F_f=0}$		-3.60×10^{7}	-1.49×10^{-4}
–	–	–	$2s_{1/2}^{F_f=1}$		7.18×10^{7}	2.97×10^{-4}
–	–	–	$\sum_{\substack{n=1,2\\F_f=0,1}} ns_{1/2}^{F_f}$, $\theta = 0$		7.40×10^{7}	3.06×10^{-4}
–	–	–	$\sum_{\substack{n=1,2\\F_f=0,1}} ns_{1/2}^{F_f}$, $\theta = \frac{\pi}{2}$		-1.94×10^{7}	-8.02×10^{-5}
$2s_{1/2}^{F_i=1}$	$2p_{3/2}^{F_a=2}$	$2p_{3/2}^{F_{a'}=1}$	$1s_{1/2}^{F_f=1}$, $\theta = 0$	-7.35238×10^{11}	2.63×10^{7}	1.09×10^{-4}
–	–	–	$1s_{1/2}^{F_f=1}$, $\theta = \frac{\pi}{2}$		-7.28×10^{6}	-3.01×10^{-5}
–	–	–	$2s_{1/2}^{F_f=1}$, $\theta = 0$		2.58×10^{7}	1.07×10^{-4}
–	–	–	$2s_{1/2}^{F_f=1}$, $\theta = \frac{\pi}{2}$		-7.13×10^{7}	-2.95×10^{-4}
–	–	–	$\sum_{n=1,2} ns_{1/2}^{F_f=1}$, $\theta = 0$		2.63×10^{7}	1.09×10^{-4}
–	–	–	$\sum_{n=1,2} ns_{1/2}^{F_f=1}$, $\theta = \frac{\pi}{2}$		-7.27×10^{6}	-3.01×10^{-5}
$2s_{1/2}^{F_i=1}$	$2p_{3/2}^{F_a=2}$	$2p_{1/2}^{F_{a'}=1}$	$1s_{1/2}^{F_f=1}$, $\theta = 0$	-1.85532×10^{12}	2.01×10^{7}	8.31×10^{-5}
–	–	–	$1s_{1/2}^{F_f=1}$, $\theta = \frac{\pi}{2}$		-5.55×10^{6}	-2.29×10^{-5}
–	–	–	$2s_{1/2}^{F_f=1}$, $\theta = 0$		1.91×10^{7}	7.90×10^{-5}
–	–	–	$2s_{1/2}^{F_f=1}$, $\theta = \frac{\pi}{2}$		-5.28×10^{6}	2.18×10^{-5}
–	–	–	$\sum_{n=1,2} ns_{1/2}^{F_f=1}$, $\theta = 0$		2.00×10^{7}	8.27×10^{-5}
–	–	–	$\sum_{n=1,2} ns_{1/2}^{F_f=1}$, $\theta = \frac{\pi}{2}$		-5.54×10^{6}	2.29×10^{-5}
$2s_{1/2}^{F_i=1}$	$2p_{3/2}^{F_a=2}$	$2p_{1/2}^{F_{a'}=0}$	$1s_{1/2}^{F_f=1}$, $\theta = 0$	-3.69345×10^{12}	6.30×10^{6}	2.61×10^{-5}
–	–	–	$1s_{1/2}^{F_f=1}$, $\theta = \frac{\pi}{2}$		-1.74×10^{6}	-7.20×10^{-6}
–	–	–	$2s_{1/2}^{F_f=1}$, $\theta = 0$		5.68×10^{6}	2.35×10^{-5}
–	–	–	$2s_{1/2}^{F_f=1}$, $\theta = \frac{\pi}{2}$		-1.57×10^{6}	-6.49×10^{-6}
–	–	–	$\sum_{n=1,2} ns_{1/2}^{F_f=1}$, $\theta = 0$		6.28×10^{6}	2.60×10^{-5}
–	–	–	$\sum_{n=1,2} ns_{1/2}^{F_f=1}$, $\theta = \frac{\pi}{2}$		-1.73×10^{6}	-7.15×10^{-6}

the level multiplicity (S is the total spin momentum), L is the total orbital momentum of the two electrons, J is the total angular momentum of the electrons and F is the total angular momentum of the atom ($\boldsymbol{F} = \boldsymbol{J} + \boldsymbol{I}$, where $\boldsymbol{I}$ is the spin of the nucleus (equal to 1/2 for helium-3). In the case of the $2^3S - 2^3P$ transition, quantum interference arises due to transitions from the 2^3S state to hyperfine components of the fine structure of the 2^3P level. Since the experiment [196] concerns a one-electron excitation, the use of the expressions (5.12), (5.13), and (5.14) is justified in the evaluation of the NR correction for ^{3}He. The latter arises as

$$\delta_{\rm NR}(2^3S_1^{F_i} - 2^3P_{J_r}^{F_r}) = \sum_{J_{a'}F_{a'} \neq J_aF_a} \delta_{\rm NR}(2^3S_1^{F_i} \to 2^3P_{J_a}^{F_a}[2^3P_{J_{a'}}^{F_{a'}}]), \qquad (5.26)$$

where $\delta_{\rm NR}(2^3S_1^{F_i} \to 2^3P_{J_a}^{F_a}[2^3P_{J_{a'}}^{F_{a'}}])$ denotes the partial contributions from the interference of one-photon transitions to sublevels with J_aF_a and $J_{a'}F_{a'}$.

The energies of ^{3}He from the [199] and natural level widths taken from the *NIST Atomic Spectra Database*[3] were used to calculate the corresponding NR corrections, listed in Table 5.7.

Table 5.7. Energies in MHz and natural widths in Hz for some states of ^{3}He.

State	Energy, MHz	Level width, Hz
$2^3P_0^{F=1/2}$	5068832675.730	1625926.899
$2^3P_1^{F=1/2}$	5068804582.860	1626002.179
$2^3P_1^{F=3/2}$	5068800070.670	
$2^3P_2^{F=3/2}$	5068805250.892	1625932.103
$2^3P_2^{F=5/2}$	5068798289.789	

Restricting ourselves to the second type of experiment, see section 5.3, all possible 2^3S-2^3P transitions are considered below, and the NR corrections are evaluated according to the expressions (5.12), (5.13), and (5.14). The numerical results are presented in the form of graphs shown in Fig. 5.2.

Seven dipole transitions were observed in the 2^3S-2^3P transition (the intensity of two lines is strongly suppressed due to the dominance of the hyperfine in-

[3]https:// www.nist.gov/pml/atomic-spectra-database

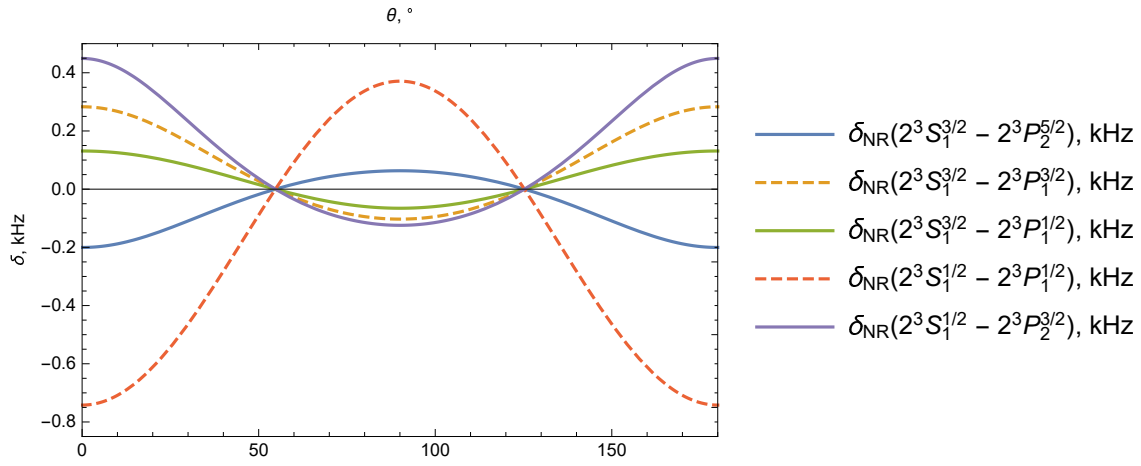

Figure 5.2. NR corrections in kHz for the [196] transitions studied in the experiment as a function of the angle between the polarisation vector of the absorbed photon and the propagation vector of the emitted photon, $\boldsymbol{e}_1$, $\boldsymbol{n}_{\boldsymbol{k}_2}$. The graphs corresponding to $2^3S_1^{3/2} \to 2^3P_0^{1/2}$ and $2^3S_1^{1/2} \to 2^3P_0^{1/2}$ are omitted due to their smallness.

teraction over the fine structure interaction [200]) [196]. It follows from the analysis that for the transitions $2^3S_1^{F_i=3/2} \to 2^3P_0^{F_a=1/2}$ and $2^3S_1^{F_i=1/2} \to 2^3P_0^{F_a=1/2}$ the NR corrections are negligible (therefore the corresponding plots are omitted). As before, all values of δ_{NR} are proportional to the factor $1 + 3\cos 2\theta$, so the intersection of all curves occurs at values of the angle equal to the magic angle. Comparing the values of the NR corrections presented in Fig. 5.2 with the Zeeman shift and the corresponding experimental errors (about 0.5 and 2 kHz, respectively, see [196]), one can find that nonresonant effects lead to a comparable shift.

Using the energy values for the hyperfine components of the fine structure of the 2^3S and 2^3P levels, the so-called "centroid" energy can be obtained. According to [196] it is given by the expression:

$$E\left(n^{\kappa}L\right) = \frac{\sum_{J,F}\left(2F+1\right)E\left(n^{\kappa}L_J^F\right)}{\left(2I+1\right)\left(2S+1\right)\left(2L+1\right)}. \tag{5.27}$$

Performing the corresponding averaging to obtain the "centroids" of the levels

2^3S, 2^3P, the transition frequency is determined by the expression:

$$\Delta E^{^3\mathrm{He}}_{\mathrm{centr}} \equiv E\left(2^3P\right) - E\left(2^3S\right) = \quad (5.28)$$
$$\frac{1}{6}\left\{\frac{1}{3}\left[\omega\left(2^3P_1^{1/2} - 2^3S_1^{1/2}\right) + \omega\left(2^3P_0^{1/2} - 2^3S_1^{1/2}\right) + \omega\left(2^3P_1^{1/2} - 2^3S_1^{3/2}\right) + \right.\right.$$
$$\left.\omega\left(2^3P_0^{1/2} - 2^3S_1^{3/2}\right)\right] + \frac{4}{3}\left[\omega\left(2^3P_2^{3/2} - 2^3S_1^{1/2}\right) + \omega\left(2^3P_1^{3/2} - 2^3S_1^{3/2}\right)\right] +$$
$$\left.2\omega\left(2^3P_2^{5/2} - 2^3S_1^{3/2}\right)\right\} = 276\,702\,827\,204\,.8 \text{ kHz},$$

where $\omega\left(2^3P_{J_r}^{F_a} - 2^3S_{J_i}^{F_i}\right)$ denotes the frequency of the partial $2^3P_{J_r}^{F_a} - 2^3S_{J_i}^{F_i}$ transition. Further, assuming that each of the seven values of ω included in (5.28) incorporates the corresponding NR correction δ_{NR}, the total "centroid" energy shift can be calculated. The corresponding correction δ_{centr} is equal to

$$\delta_{\mathrm{centr}} \equiv \frac{1}{6}\left\{\frac{1}{3}\left[\delta_{\mathrm{NR}}\left(2^3P_1^{1/2} - 2^3S_1^{1/2}\right) + \delta_{\mathrm{NR}}\left(2^3P_0^{1/2} - 2^3S_1^{1/2}\right)\right.\right. \quad (5.29)$$
$$+\delta_{\mathrm{NR}}\left(2^3P_1^{1/2} - 2^3S_1^{3/2}\right) + \delta_{\mathrm{NR}}\left(2^3P_0^{1/2} - 2^3S_1^{3/2}\right)\Big] +$$
$$+\frac{4}{3}\left[\delta_{\mathrm{NR}}\left(2^3P_2^{3/2} - 2^3S_1^{1/2}\right) + \delta_{\mathrm{NR}}\left(2^3P_1^{3/2} - 2^3S_1^{3/2}\right)\right] +$$
$$\left.2\delta_{\mathrm{NR}}\left(2^3P_2^{5/2} - 2^3S_1^{3/2}\right)\right\},$$

where each value of δ_{NR} for the specified partial transition can be calculated according to the expression (5.14) in section 5.1.

It is easy to notice that δ_{centr}, as well as partial NR corrections (5.26) are equal to zero at the "magic angle". Being much lower than the relativistic and QED corrections, the values of δ_{NR} are close to 1 kHz (see Fig. 5.2) and approach the contribution from the polarisability of the nucleus, which is -1.1 kHz for the "centroid" energy, $2^3P - 2^3S$, see [196], "screening" the latter. It is important to note that the value of δ_{NR} also depends on experimental parameters such as the density of atoms in the beam, blackbody radiation, etc., see below.

Chapter 6.

Two-photon spectroscopy of hydrogen and helium

Following the analysis of nonresonant effects in one-photon spectroscopy described in 5.2, special attention should be paid to the interference arising in the measurement of the two-photon frequency of $2s \to ns/nd$ ($n = 4, 6, 8, 12$ is the principal quantum number) transitions in the hydrogen atom. In such experiments, atoms in the beam are populated into the $2s_{1/2}^{F_i=1}$ state and then excited to the $ns_{1/2}^{F_a=1}$ or $nd_{3/2}^{F_a=2}$ state by absorption of two polarised laser photons propagating in opposite directions. The detection of the excited ns/nd fraction of atoms can be observed by its fluorescence (i.e., decay to the $2p$ state) [201] or by the decreasing registration of atoms in the $2s$ state [202, 203].In both cases there is interference between different fine sublevels of $nd_{3/2}^{F_a=2}$ and $nd_{5/2}^{F_{a'}=2}$, which leads to asymmetry of the line profile. It has been shown in [201] that detection of the excited ns/nd fraction of atoms by their fluorescence has a much higher potential accuracy than experiments to control the extinction rate of metastable states [204, 205]. The latter is limited by the large background of unexcited $2s$ atoms. Recently, it has been shown in [107] that nonresonant corrections to the frequency of the $2s_{1/2}^{F_i=1} - nd_{3/2(5/2)}^{F_a=2}$ transition measured in experiments like [204, 205] reach the level of several kHz. Their combination with the extrapolation of the hyperfine structure performed in [187] turns out to be important for the determination of the proton charge radius r_p and the Rydberg constant R_∞ (although the NR corrections contribute in the following

order with respect to HFS).

This part of the thesis was carried out with the inseparable participation of T.A. Zalialiutdinov and A.A. Anikin.

6.1. Amplitude and cross section of two-photon scattering followed by one-photon emission

In 5.2, it was shown that for certain geometries the influence of NR effects in one-photon spectroscopy can be significantly reduced [43, 49, 52]. Developing this approach, here expressions for the cross section of the corresponding resonant two-photon scattering on the hydrogen atom are presented, taking into account the fine and hyperfine structure of the levels. As before, these expressions depend on the directions and polarisations of the incident (absorbed) and outgoing (emitted) photons. Therefore, the different correlations between directions and polarisations should be considered within the framework of the three-photon scattering process (two photons are absorbed and one is emitted). The results of the evaluation are then used to obtain NR corrections to the two-photon absorption cross section and to determine the frequencies of $2s-ns/nd$ transitions.

In full analogy with the results of section 5.2, such a scattering process is described by the Feynman diagram shown in Fig. 6.1, which corresponds to the process of two-photon absorption by an atom followed by emission of a photon.

The corresponding S-matrix element is

$$S_{fi}^{(3)} = (-\mathrm{i}e)^3 \int d^4x_3 d^4x_2 d^4x_1 \overline{\psi}_f(x_3)\gamma_{\mu_3} A^*_{\mu_3}(x_3) \times S(x_3,x_2)\gamma_{\mu_2} A_{\mu_2}(x_2) S(x_2,x_1)\gamma_{\mu_1} A_{\mu_1}(x_1)\psi_i(x_1), \tag{6.1}$$

with all notations given in 2.1. Integration over the time variables in (6.1) leads

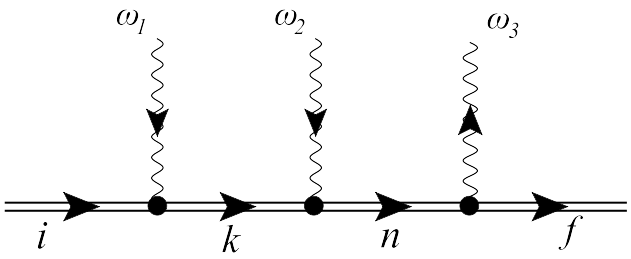

Figure 6.1. Two-photon excitation process of a bound electron. A wavy line indicates absorption or emission of a photon. The double solid line denotes the bound electron; ω_1, ω_2 are the frequencies of the absorbed photons, and ω_3 is the frequency of the emitted photon. The indices i, n, k, f correspond to the initial, two intermediate, and final states of the electron, respectively. According to Feynman's rules, there are 5 more diagrams related to photon permutations, which are omitted here for brevity.

to the amplitude:

$$U_{fi}^{(3)} = e^3 \sum_{nk} \frac{\langle f|\boldsymbol{\alpha} \boldsymbol{A}^*_{\boldsymbol{k}_3,\boldsymbol{e}_3}|n\rangle\langle n|\boldsymbol{\alpha} \boldsymbol{A}_{\boldsymbol{k}_2,\boldsymbol{e}_2}|k\rangle\langle k|\boldsymbol{\alpha} \boldsymbol{A}_{\boldsymbol{k}_1,\boldsymbol{e}_1}|i\rangle}{(E_n - E_f - \omega_3)(E_k - E_i - \omega_2)} + (5 \text{ terms from photon permutations}). \tag{6.2}$$

The permutations in (6.2) should be understood as all possible permutations of the indices 1, 2, 3 denoting the corresponding photons. Then, the differential cross section of the scattering process is defined by the expression:

$$\frac{d\sigma_{fi}}{d\boldsymbol{n}_{k_3}} = 2\pi\delta(E_f - E_i + \omega_3 - \omega_1 - \omega_2) \left|U_{fi}^{(3)}\right|^2 \frac{\omega_2^2 d\omega_2}{(2\pi)^3} \frac{\omega_3^2 d\omega_3}{(2\pi)^3}. \tag{6.3}$$

Here $\boldsymbol{n}_{\boldsymbol{k}}$ denotes the solid angle in $\boldsymbol{k}$-space for the corresponding photon. In the framework of the nonrelativistic limit and the dipole approximation (in the length form, see, e.g., [84])

$$U_{fi}^{(3)} = e^3 (2\pi)^{3/2} \sqrt{\omega_1\omega_2\omega_3} \sum_{nk} \frac{\langle f|\boldsymbol{e}_3^*\boldsymbol{r}|n\rangle\langle n|\boldsymbol{e}_2\boldsymbol{r}|k\rangle\langle k|\boldsymbol{e}_1\boldsymbol{r}|i\rangle}{(E_n - E_f - \omega_3)(E_k - E_i - \omega_2)} + \dots. \tag{6.4}$$

The case when two incident photons are absorbed into the resonant state n, i.e., $\omega_1 + \omega_2 = E_n - E_i$, is of interest. In the resonance approximation, this intermediate state gives the dominant contribution, and the remaining nonresonant

terms in the scattering amplitude can be omitted. Such an approximation is justified by the fact that the corresponding nonresonant corrections are beyond the accuracy of the experiments [84]. Then, assuming that the frequencies of two incident laser photons are equal, i.e., $\omega_1 = \omega_2 \equiv \omega$, the cross section (6.3) with the scattering amplitude (6.4) can be reduced to

$$\frac{d\sigma_{fi}}{d\boldsymbol{n}_{k_3}} = \frac{e^6}{(2\pi)^5}\omega^6(E_i + 2\omega - E_f)^3 \left| \sum_{nk} \frac{\langle f|\boldsymbol{e}_3^*\boldsymbol{r}|n\rangle}{E_n - E_i - 2\omega - \frac{\mathrm{i}}{2}\Gamma_n} \times \left(\frac{\langle n|\boldsymbol{e}_2\boldsymbol{r}|k\rangle\langle k|\boldsymbol{e}_1\boldsymbol{r}|i\rangle}{E_n - E_i - \omega} + \frac{\langle n|\boldsymbol{e}_1\boldsymbol{r}|k\rangle\langle k|\boldsymbol{e}_2\boldsymbol{r}|i\rangle}{E_k - E_n + \omega} \right) \right|^2, \tag{6.5}$$

where the divergent denominator regularisation procedure and the relation $\langle a|\mathbf{p}|b\rangle = \mathrm{i}(E_a - E_b)\langle a|\mathbf{r}|b\rangle$ [8] were used. The appearance of the imaginary part leads to the formation of the absorption line profile [8]. The regularisation in the case of two-photon absorption repeats the "one-photon calculations", see section 2.2, and allows nonresonant extension, see section 2.3.

To introduce the leading-order nonresonant correction for the cross section given by the expression (6.5), in the sum over n the nearest-energy terms should be considered, i.e., in the case of two neighbouring states it is $n = a$ (the main resonant term to which the NR correction applies) and $n = a'$ (the one closest in energy to the resonant state) [33, 35, 37, 43]. The set of quantum numbers for the a' state has to permit the absorption of two electric dipole photons (as for the resonance state) and hence has to be allowed by the two-photon selection rules. Then, using the same approximations as for the one-photon correction, i.e., neglecting the quadratic nonresonant contribution (see (5.10)), the dominant contribution can be found quite simply.

Further, the standard set of quantum numbers for atomic states in (6.5) is assumed: the principal quantum number n, the electron orbital momentum l, the electron total angular momentum j, the atomic angular momentum F and its projection M_F. After summing over the projections of the total momentum in the final state and averaging over the projections of the initial state [84], the

cross section has the form:

$$\frac{d\sigma_{fi}}{d\boldsymbol{n}_{k_3}} = \frac{e^6}{2F_i+1}\left[\frac{f_{fi}^{(2\gamma)}(a,a)}{(\omega_0-2\omega)^2+\frac{\Gamma_a^2}{4}} + \frac{2f_{fi}^{(2\gamma)}(a,a')(\omega_0-2\omega)}{\left((\omega_0-2\omega)^2+\frac{\Gamma_a^2}{4}\right)(\omega_0-2\omega+\Delta)}\right], \quad (6.6)$$

where $\Delta = E_{a'} - E_a$ and

$$f_{fi}^{(2\gamma)}(a,a') = \sum_{M_{F_i}M_{F_f}} T_{fai}\left(\frac{\omega_0}{2}\right)T^*_{fa'i}\left(\frac{\omega_0}{2}\right), \quad (6.7)$$

$$T_{fni}(\omega) = \omega^3(E_i - E_f + 2\omega)^{3/2}\sum_{M_{F_n}}\langle f|\boldsymbol{e}_3^*\boldsymbol{r}|n\rangle \times \quad (6.8)$$

$$\sum_k\left[\frac{\langle n|\boldsymbol{e}_2\boldsymbol{r}|k\rangle\langle k|\boldsymbol{e}_1\boldsymbol{r}|i\rangle}{E_a - E_i - \omega} + \frac{\langle n|\boldsymbol{e}_1\boldsymbol{r}|k\rangle\langle k|\boldsymbol{e}_2\boldsymbol{r}|i\rangle}{E_a - E_n + \omega}\right].$$

The coefficients (6.7), as before, determine the angular dependences. In the nonrelativistic limit, the matrix elements in (6.6) do not depend explicitly on the photon directions $\boldsymbol{n}_{\boldsymbol{k}_3}$, $\boldsymbol{n}_{\boldsymbol{k}_2}$ and $\boldsymbol{n}_{\boldsymbol{k}_1}$. The dependence on these arises through the transversality conditions for photons. To completely eliminate the first-order Doppler effect, two opposing Gaussian laser beams are used to excite the ns/nd states [202, 203]. Thus, without restriction of generality, one can assume that in the experiment the incident photons propagate in opposite directions with fixed polarisation vectors $\boldsymbol{e}_1$ and $\boldsymbol{e}_2$, and the emitted photon has polarisation $\boldsymbol{e}_3$ and fixed direction $\boldsymbol{n}_{\boldsymbol{k}_3}$. Then, denoting the angles between any pair of two vectors as θ_{ij} (i, $j = 1$, 2, 3), the interference contribution to (6.6) corresponds to a situation similar to experiments based on the one-photon scattering process (the angle between incident photons can be set equal to π or zero) [145, 146].

In the resonance approximation (i.e., keeping only the first term in Eq. (6.6)), it immediately follows from the extremum condition $\omega_{\rm res} = \omega_{\rm max} = \omega_{ai}/2 = (E_{n_a l_a j_a F_a} - E_{n_i l_i j_i F_i})/2$. However, retaining the interference term in (6.6), from the extremum condition for the cross section as a function of ω, $\omega_{\rm max}$ is obtained

equal to

$$\omega_{\rm max} = (\omega_{ai} - \delta_{\rm NR})/2, \tag{6.9}$$
$$\delta_{\rm NR} = \frac{\sum\limits_f f_{fi}^{(2\gamma)}(a,a')}{\sum\limits_f f_{fi}^{(2\gamma)}(a,a)} \frac{\Gamma_a^2}{4\Delta}.$$

In a similar way to the one-photon scattering case discussed in 5.2, the NR correction (6.9) is represented as a dominant contribution following from the series expansion of Γ_a/Δ when this parameter is small. Angular correlations are obtained from the relation $f_{fi}^{(2\gamma)}(a,a')/f_{fi}^{(2\gamma)}(a,a)$ and represent the dependence on the angles between each pair of vectors $\boldsymbol{n}_{k_1}$, $\boldsymbol{e}_2$ and $\boldsymbol{e}_3$.

6.2. Two-photon spectroscopy of hydrogen

In this section, specific examples of NR corrections to the frequencies of two-photon $2s - ns/nd$ $(n = 4, 6, 8, 12)$ transitions in the hydrogen atom are discussed. Considering first the interference of $2s_{1/2}^{F_i=0} \to ns_{1/2}^{F_a=0}$ and $2s_{1/2}^{F_i=1} \to ns_{1/2}^{F_a=1}$ transitions it is assumed that the hyperfine structure of the initial $2s$ state is resolvable in experiments [32, 134, 204, 206, 207]. According to two-photon selection rules, electric dipole two-photon transitions with spin flip $2s_{1/2}^{F_i=0} \to ns_{1/2}^{F_a=1}$ or $2s_{1/2}^{F_i=1} \to ns_{1/2}^{F_a=0}$ are strongly suppressed by [122, 124, 125]. Therefore, interference with close nd states is only possible for the transitions $2s_{1/2}^{F_i=1} \to ns_{1/2}^{F_a=1}$ and $2s_{1/2}^{F_i=1} \to nd_{3/2}^{F_{a'}=1}$, $2s_{1/2}^{F_i=1} \to nd_{3/2}^{F_{a'}=2}$, $2s_{1/2}^{F_i=1} \to nd_{5/2}^{F_{a'}=2}$, $2s_{1/2}^{F_i=1} \to nd_{5/2}^{F_{a'}=3}$ [22]. Then for the resonance $2s_{1/2}^{F_i=1} \to ns_{1/2}^{F_a=1}$ one can set $n_i l_i = 2s$, $j_i = 1/2$, $F_i = 1$, $n_a l_a = ns$, $n_{a'} l_{a'} = nd$ $(n_a = n_{a'} = 4, 6, 8, 12)$, $j_a = 1/2$, $F_a = 1$.

In experiments [145, 146], the polarisations of laser photons $\boldsymbol{e}_1$ and $\boldsymbol{e}_2$ were fixed parallel to each other. Then the NR correction (6.9), depends on only one angle between the polarisation of the emitted photon $\boldsymbol{e}_3$ and one of the two parallel vectors $\boldsymbol{e}_1$ or $\boldsymbol{e}_2$. Summing over the polarisation $\boldsymbol{e}_3$ leads to a dependence on the propagation direction vector $\boldsymbol{n}_{k_3}$. Denoting the angle between the vectors $\boldsymbol{e}_1$ (or $\boldsymbol{e}_2$) and $\boldsymbol{n}_{k_3}$ by θ, after the necessary calculations (for details see

Eq. in [53]) one can find that for the frequency $2s^{F_i=1}_{1/2} \to ns^{F_a=1}_{1/2}$ transition, the correction (6.9) is proportional to $(1 + 3\cos\theta)$. The corresponding numerical results are presented in Fig. 6.2. As in the case of NR corrections to the frequencies of the one-photon transition, there are "magic angles" at which the correction (6.9) is zero: $\theta = 54.7°$ и $\theta = 125.3°$.

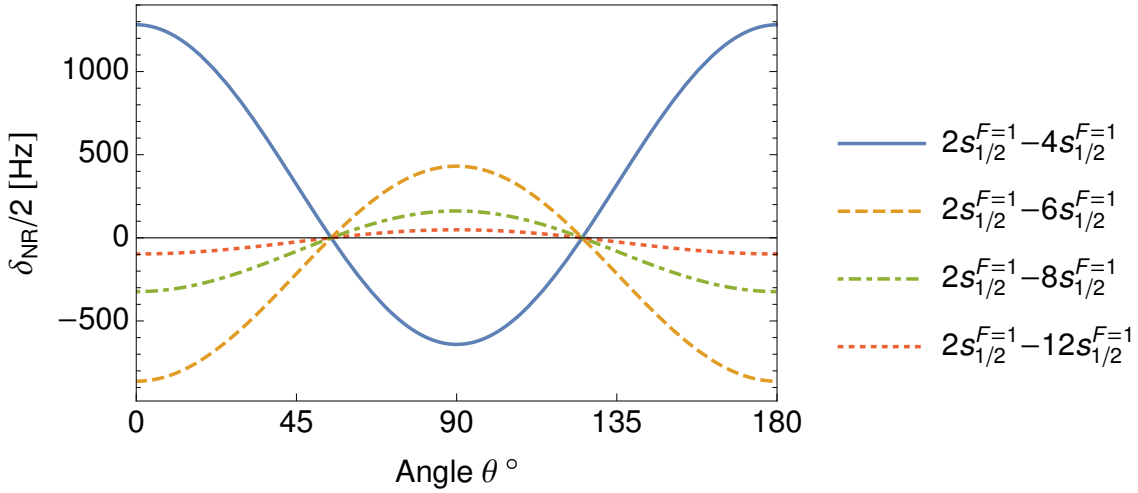

Figure 6.2. NR corrections $\delta_{\rm NR}/2$ (in Hz) to measure the frequencies of $2s^{F_i=1}_{1/2} - ns^{F_a=1}_{1/2}$ $(n = 4, 6, 8, 12)$ transitions in hydrogen as a function of the angle between the polarisation vector $\boldsymbol{e}_1$ of the absorbed photon (or $\boldsymbol{e}_2$, since in experiments $\boldsymbol{e}_1 ||| \boldsymbol{e}_2$) and the propagation vector $\boldsymbol{n}_{\boldsymbol{k}_3}$ of the emitted photon.

Recently, similar interference effects for measuring the frequency of the two-photon $1s - 3s$ transition were studied in [146]. It was found that for the two-photon laser-induced transition $1s^{F_i=1}_{1/2} \to 3s^{F_a=1}_{1/2}$ NR correction due to interference with four neighbouring transitions $1s^{F_a=1}_{1/2} \to 3d^{F_{a'}=1}_{3/2}$, $1s^{F_i=1}_{1/2} \to 3d^{F_{a'}=2}_{3/2}$, $1s^{F_i=1}_{1/2} \to 3d^{F_{a'}=2}_{5/2}$ and $1s^{F_i=1}_{1/2} \to 3d^{F_{a'}=3}_{5/2}$ is smaller than the experimental uncertainty. The expression (6.9) can be easily extended to the case of $1s^{F_i=1}_{1/2} \to 3s^{F_{a'}=1}_{1/2}$ by substituting $2s^{F_i=1}_{1/2} \leftrightarrow 1s^{F_i=1}_{1/2}$ and $n_a = n_{a'} = 3$. Then the correction can be found in the form:

$$\delta_{\rm NR}(1s^{F_i=1}_{1/2} - 3s^{F_a=1}_{1/2}) = -225.61(1 + 3\cos 2\theta)\ \text{Hz}. \tag{6.10}$$

The corresponding angular correlation is shown in Fig. 6.3.

For other transitions $2s^{F_i=0}_{1/2} \to ns^{F_a=0}_{1/2}$ there is interference with $2s^{F_i=0}_{1/2} \to nd^{F_{a'}=2}_{3/2}$ and $2s^{F_i=0}_{1/2} \to nd^{F_{a'}=2}_{5/2}$. The estimation results are presented in Fig. 6.4.

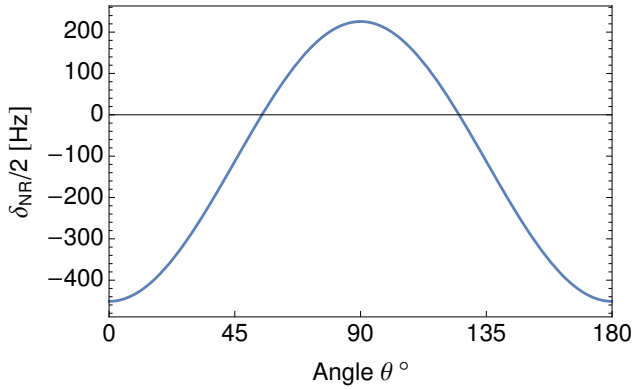

Figure 6.3. NR correction $\delta_{\rm NR}/2$ to the transition frequency $1s^{F_i=1}_{1/2} \to 3s^{F_a=1}_{1/2}$ in hydrogen (in Hz). The notations are the same as for Fig. 6.2.

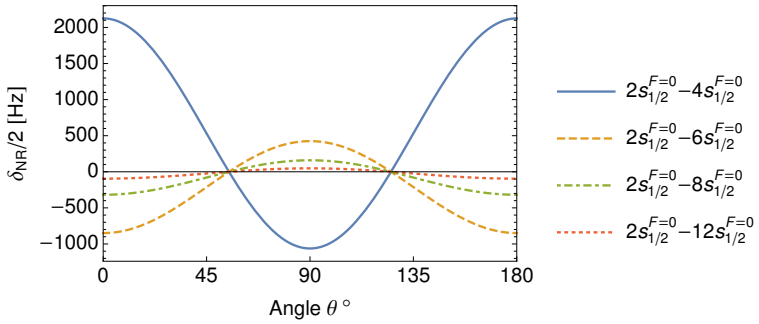

Figure 6.4. NR correction $\delta_{\rm NR}/2$ to $2s^{F_i=0}_{1/2} \to ns^{F_a=0}_{1/2}$ $(n = 4, 6, 8, 12)$ in Hz. The same notations as in the previous graphs are used.

Estimates of NR corrections to the frequencies of $2s^{F_i=1}_{1/2} \to nd^{F_a=2}_{3/2}$ $(n = 4, 6, 8, 12)$ two-photon transitions taking into account the neighbouring $nd^{F_{a'}=2}_{5/2}$ level can be carried out similarly. For this purpose in all expressions one should set $n_i l_i = 2s$, $j_i = 1/2$, $F_i = 1$, $n_a l_a = n_{a'} l_{a'} = nd$ $(n_a = 4, 6, 8, 12)$, $j_a = 3/2$, $F_a = 2$, $j_{a'} = 5/2$,$F_{a'} = 2$. Unlike the previous cases, it turned out that the NR corrections do not depend on the angle between the vectors $\boldsymbol{n}_{k_1}$, $\boldsymbol{e}_2$ and $\boldsymbol{e}_3$:

$$\delta_{\rm NR}(2s^{F=1}_{1/2} - 4d^{F=2}_{3/2}) = 967.75\,{\rm Hz}, \tag{6.11}$$

$$\delta_{\rm NR}(2s^{F=1}_{1/2} - 6d^{F=2}_{3/2}) = 296.48\,{\rm Hz}, \tag{6.12}$$

$$\delta_{\rm NR}(2s^{F=1}_{1/2} - 8d^{F=2}_{3/2}) = 127.31\,{\rm Hz}, \tag{6.13}$$

$$\delta_{\rm NR}(2s^{F=1}_{1/2} - 12d^{F=2}_{3/2}) = 38.38\,{\rm Hz}. \tag{6.14}$$

In addition to the corrections (6.11)-(6.14) arising from the neighbouring $nd_{3/2}^{F_a=2}$ and $nd_{5/2}^{F_{a'}=2}$ states, it is necessary to consider the interference with the transitions $2s_{1/2}^{F_i=1} \to nd_{3/2}^{F_a=2}$ and $2s_{1/2}^{F_i=1} - ns_{1/2}^{F_{a'}=1}$ [53]. According to the expression (6.9), one can write

$$\delta_{\rm NR}(2s_{1/2}^{F_i=1} - nd_{3/2}^{F_a=2}) = \frac{\sum\limits_{j_f F_f} f_{\rm nr}(nd_{3/2}^{F_a=2}, ns_{1/2}^{F_{a'}=1})}{\sum\limits_{j_f F_f} f_{\rm res}(nd_{3/2}^{F_a=2}, nd_{3/2}^{F_a=2})} \frac{\Gamma_{nd_{3/2}}^2}{4\Delta'''}, \tag{6.15}$$

where $\Delta''' = E_{nd_{3/2}^{F_a=2}} - E_{ns_{1/2}^{F_{a'}=1}}$. Then,

$$\delta_{\rm NR}(2s_{1/2}^{F_i=1} - 4d_{3/2}^{F_a=2}) = -232.602 \frac{1+3\cos 2\theta}{5+3\cos 2\theta}\,{\rm Hz}, \tag{6.16}$$

$$\delta_{\rm NR}(2s_{1/2}^{F_i=1} - 6d_{3/2}^{F_a=2}) = 107.937 \frac{1+3\cos 2\theta}{5+3\cos 2\theta}\,{\rm Hz}, \tag{6.17}$$

$$\delta_{\rm NR}(2s_{1/2}^{F_i=1} - 8d_{3/2}^{F_a=2}) = 68.697 \frac{1+3\cos 2\theta}{5+3\cos 2\theta}\,{\rm Hz}, \tag{6.18}$$

$$\delta_{\rm NR}(2s_{1/2}^{F_i=1} - 12d_{3/2}^{F_a=2}) = 25.582 \frac{1+3\cos 2\theta}{5+3\cos 2\theta}\,{\rm Hz}. \tag{6.19}$$

The total correction to the transition frequencies $2s_{1/2}^{F_i=1} \to nd_{3/2}^{F_a=2}$ is determined by the sum of the respective contributions: angle independent (6.11)-(6.14) and angle dependent (6.16)-(6.19). The total frequency shifts $\delta_{\rm NR}/2$ are shown in Fig. 6.5. The denominator in the expressions (6.11)-(6.14) is always non-zero and positive, while the numerator still converts these corrections to zero when θ equals the "magic angle".

In conclusion, the NR corrections arising from the differential cross section disappear after integration over the angles, i.e., for the total cross section (when the radiation is registered in the whole solid angle 4π). However, this is true only when the corrections depend on the angle. For example, integrating the expression $1+3\cos 2\theta$ with $\sin\theta$ from the Jacobian over the angle immediately yields zero, while contributions like (6.11)-(6.14) are preserved. Integration over the angle θ should be performed for the cross section and not the NR correction, which leads, therefore, to the disappearance of the interference contribution (if it is not constant) and a non-vanishing resonance term. The latter can be clearly

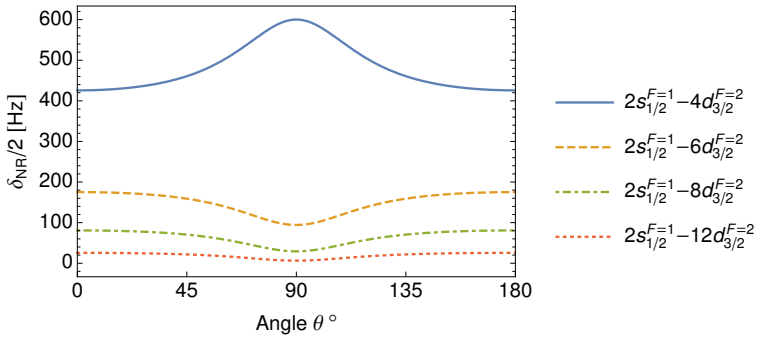

Figure 6.5. The total frequency shift $\delta_{\rm NR}/2$ (in Hz) for the frequencies $2s^{F_i=1}_{1/2} - nd^{F_a=2}_{3/2}$ ($n = 4, 6, 8, 12$) transitions in hydrogen, see expressions (6.11)-(6.14) and (6.16)-(6.19). All notations are similar to Fig. 6.4.

seen from the expressions (6.16)-(6.19), where the denominator represents the non-zero contribution of the resonance term. In addition, it is worth noting that in the experiments there is no strictly defined direction of photon departure; the radiation is registered in some solid angle. This circumstance can be taken into account by integrating the corresponding expressions (in the case of the formulas (6.16)-(6.19), separately the numerator and separately the denominator with subsequent dividing) according to the experimental conditions, which eventually leads to a non-zero result for the NR corrections.

6.3. Experiments registering a decrease in the population density of the $2s$ state

There is another type of spectroscopic experiments using the two-photon absorption process and based on the quenching rate of the $2s$ state [107, 204–207]. For such experiments, the initially prepared metastable state of hydrogen atoms is excited to ns/nd states ($n = 4, 6, 8, 12$) by absorbing two laser photons. In this case, only a part of the atoms populated in the $2s$ state is excited in the atomic beam. When an external homogeneous static electric field is applied behind the excitation region, the levels of opposite parity $2s$ and $2p$ mix, after which the Ly_α line luminescence appears. The dependence of the intensity of this line on the frequency of absorbed photons can be observed experimentally. The Ly_α line is absent if two-photon resonance is achieved.

In experiments of this type it is sufficient to consider only the two-photon excitation process itself and not to take into account the subsequent emission process, in contrast to the method of recording the fluorescence signal. Following [107], the process amplitude can be considered only as the part corresponding to absorption in the scattering amplitude (6.5):

$$U_{ni}^{(\mathrm{abs})} = \frac{e^2 2\pi\omega}{E_i + 2\omega - E_n} \sum_k \left(\frac{\langle n|\boldsymbol{e}_1\boldsymbol{r}|k\rangle\langle k|\boldsymbol{e}_2\boldsymbol{r}|i\rangle}{E_n - E_k - \omega} + \frac{\langle n|\boldsymbol{e}_2\boldsymbol{r}|k\rangle\langle k|\boldsymbol{e}_1\boldsymbol{r}|i\rangle}{E_i - E_k + \omega} \right), \quad (6.20)$$

where the equality of the absorbed frequencies is already taken into account, $\omega_1 = \omega_2 = \omega$. The formula (6.20) is written in a general form, but with a discarded factor corresponding to the radiation process. In the framework of the resonance approximation, this is warranted since the corresponding matrix element enters the amplitude (6.20) by a common factor [8].

Omitting for brevity the intermediate calculations involving integration over angles and summation over projections [107], each term in (6.20) can be reduced to the expression

$$\sum_k \frac{\langle a|\boldsymbol{e}_2\boldsymbol{r}|k\rangle\langle k|\boldsymbol{e}_1\boldsymbol{r}|i\rangle}{E_i + \omega - E_k(1 - \mathrm{i}0)} = (-1)^{l_k+l_i+j_a+2j_k+F_a+j_i+F_k} \Pi_{l_i}\Pi_{l_k}\Pi_{j_i}\Pi_{j_a}\Pi_{j_k} \times (6.21)$$
$$\left\{ \begin{array}{ccc} l_k & s & j_k \\ j_a & 1 & l_a \end{array} \right\} \left\{ \begin{array}{ccc} l_i & s & j_i \\ j_k & 1 & l_k \end{array} \right\} \left\{ \begin{array}{ccc} j_k & I & F_k \\ F_a & 1 & j_a \end{array} \right\} \left\{ \begin{array}{ccc} j_i & I & F_i \\ F_k & 1 & j_k \end{array} \right\} \times$$
$$\Pi_{F_k}\Pi_{F_i} C^{l_a 0}_{l_k 0 1 0} C^{l_k 0}_{l_i 0 1 0} \sum_{q_1,q_2} (-1)^{q_1+q_2} C^{F_a M_a}_{F_k M_k 1 -q_1} C^{F_k M_k}_{F_i M_i 1 -q_2} e_{1_{q_1}} e_{2_{q_2}} g_{l_k}(E_i + \omega).$$

Here the summation over k in the left-hand side means all necessary summations over quantum numbers not included in the right-hand side, e_{1_q}, e_{2_q} are the spherical components of the polarisation vectors, and $g_{l_k}(E_i + \omega)$ represents the corresponding integrals with the radial part of the Coulomb Green's function, see section 3.2.

The absorption profile can be obtained from the differential cross section $d\sigma_{ai}^{(\mathrm{abs})} = \frac{d^3k_1}{(2\pi)^3}\frac{d^3k_2}{(2\pi)^3}\left|U_{ai}^{(\mathrm{abs})}\right|^2$. According to [43], the most significant nonresonant contribution arises when the fine structure of the excited levels is taken into account. Then the amplitude (6.20) should include states with the same orbital

momentum but different total angular momenta (e.g., levels $nd_{3/2}$ and $nd_{5/2}$ in hydrogen). Leaving only these terms [107] in the amplitude, the absorption profile can be written as follows:

$$\frac{d\sigma_{ai}^{(\mathrm{abs})}}{d\omega d\Omega_1 d\Omega_2} \sim \frac{C_a}{(2\omega-\omega_0)^2+\frac{1}{4}\Gamma_a^2} + \frac{C_{aa'}}{(2\omega-\omega_0)^2+\frac{1}{4}\Gamma_a^2}\frac{2(2\omega-\omega_0)}{2\omega-\omega_0-\Delta_{\mathrm{fs}}}. \quad (6.22)$$

Here Ω_i, $i=1,2$ are solid angles in the phase spaces of the absorbed photons, Γ_a is the natural line width of the resonance state, Δ_{fs} denotes the energy interval of the fine structure, and $\omega_0 = E_a - E_i$. The factor C_a corresponds to the resonance transition $i \to a$ interfering with $i \to a'$ and leading to the factor $C_{aa'}$. The factors C_a, $C_{aa'}$ are calculated using the expressions (6.20), (6.21).

Considering the interfering $2s_{1/2}^{F_i=1} \to nd_{3/2}^{F_a=2}$, $2s_{1/2}^{F_i=1} \to nd_{5/2}^{F_{a'}=2}$ transitions for $n=4,6,8,12$, $\Delta_{\mathrm{fs}} = E_{nd_{3/2}^{F_a=2}} - E_{nd_{5/2}^{F_{a'}=2}}$ and denoting the level width as Γ_{nd}, the results of the calculated NR corrections are shown in Table 6.1.

Table 6.1. Nonresonant corrections (fourth column) in Hz for the interfering transitions $2s_{1/2}^{F_i=1} \to nd_{3/2}^{F_a=2}$ and $2s_{1/2}^{F_i=1} \to nd_{5/2}^{F_{a'}=2}$ for $n=4$, 6, 8, 12. The splitting energies of the fine structure in Hz are given in the second column, the natural widths of the lines in Hz are given in the third column. The last column shows the frequency determination uncertainties for the corresponding transitions.

Statw	Δ_{fs}, Hz	Γ_{nd}, Hz	δ_{NR}, Hz	Unc., Hz
$4d$	4.557026×10^8	4.40503×10^6	-8691.82	$24. \times 10^3$
$6d$	1.350231×10^8	1.33682×10^6	-2701.67	$10. \times 10^3$
$8d$	5.69628×10^7	5.72382×10^5	-1174.02	6.4×10^3
$12d$	1.68779×10^7	1.72261×10^5	-358.88	7.0×10^3

As can be seen from Table 6.1, the NR correction contributions are of the order of the experimental error, see [11] and decrease with increasing principal quantum number n. One can also conclude from the results of the previous section that the corrections for this type of experiments are larger than for the same transitions in experiments where the fluorescence signal $nd-2p$ is recorded, see Fig. 6.4-6.5. It is important to note that a recent new experi-

mental measurement of the $2s_{1/2} - 8d_{5/2}$ transition frequency is based on the type of experiments discussed in 6.2. As indicated in [143], the nonresonant contributions due to QIE are negligible. However, the NR correction for this transition was found to be -1174.02 Hz, which corresponds to an experimental error of the order of 2 kHz.

6.4. Two-photon spectroscopy of helium

Significant progress in the spectroscopy of one-electron systems has stimulated the study of nonresonant corrections to transition energies in many-electron systems [46–48, 50]. Although helium has been studied theoretically and experimentally for many years, nonresonant effects and QIE, as their dominant part [43], have not been taken into account in spectroscopic measurements of transition frequencies until recently [47, 50].

The energies of atomic levels in helium are usually expressed as a sum of nonrelativistic energies, leading-order relativistic corrections, Lamb shift, etc., including quantum electrodynamics corrections and higher-order relativistic contributions. Recent calculations of QED effects at the $\alpha^7 m$ level have improved the theoretical predictions of the energy levels of helium atoms, leading to strong agreement with the measured transition frequency of the 2^3S-2^3P [208]. However, as was found in [208], such calculations do not eliminate the discrepancy between the theoretical predictions and the experimental result for the $2^3S_1 - 3^3D_1$ transition [55].

Using the results of the previous sections, this section presents an analysis of the QIE arising for neighbouring sublevels of the fine structure when measuring the $2^3S_1-3^3D_1$ transition energy in a helium atom. In the experiment described in [56], the helium atoms in the beam are in the 2^3S_1 metastable state and then excited to the 3^3D_1 state by absorbing two photons with equal frequencies, $\omega_1 = \omega_2$, having parallel polarisations $\mathbf{e}_1$ and $\mathbf{e}_2$ and propagating in opposite [207] directions. Detection of the excited fraction of 3^3D_1 atoms is observed by fluorescence (i.e., decay into 2^3P states) with emission of a photon with frequency ω_3, polarisation $\mathbf{e}_3^*$ in the $\boldsymbol{n}_{k_3}$ direction. Accordingly, interference should occur between the 3^3D_1, 3^3D_2, and 3^3D_3 sublevels of the fine structure.

This experimental situation is similar to that previously discussed in 6.2, see also [53]. Following the setting of the experiment [56], it is necessary to analyse the nonresonant corrections due to interference between different fine sublevels, $3^3D_{J_n}$, for the scattering process $2^3S_1 + 2\gamma(E1) \to 3^3D_{J_n} \to 2^3P_{J_f} + \gamma(\mathrm{E1})$, where $J_n = 1, 2, 3$ and the frequency of absorbed photons $\omega_1 = \omega_2 = (E_{3^3D_{J_n}} - E_{2^3S_1})/2$.

Repeating the calculations given in the previous sections, we can find similar expressions for the nonresonant correction. Then, substituting the values of the natural line width $\Gamma_{3^3D_1} = 11.35(6)$ MHz [209] corresponding to the energy difference $\Delta_{12} = 1325.025(33)$ MHz, $\Delta_{13} = 1400.290(33)$ MHz [55] into the expression (6.9), the correction to the transition frequency $2^3S_1 - 3^3D_1$ is equal to

$$\delta_{\mathrm{NR}} = 0.0124(4) \text{ MHz}. \tag{6.23}$$

Calculations of the expressions (6.6)-(6.9) show that similar to the NR correction to the frequency of the $2s^{F_i=1}_{1/2} \to nd^{F_a=2}_{3/2(5/2)}$ (cf. (6.11)-(6.14)) transition in hydrogen [53, 107], the effect considered is also independent of the angle between any pair of vectors $\boldsymbol{n}_{k_3}$, $\boldsymbol{e}_1$ and $\boldsymbol{e}_2$. An important result of these calculations, which include the natural level width, is that the magnitude of the effect is at the 0.056 MHz experimental error level [56]. However, the experimentally observed Γ^{exp} width of the spectral line profile differs significantly from the natural Γ^{nat} due to different broadening mechanisms [210]. In fact, the level width in (6.9) should be related to the experimental value of [205]. In [56], the main effect of line broadening is due to pressure and transit time. Denoting the latter two contributions as Γ^{pb} and Γ^{tt}, respectively, the full-width-half-maximum can be expressed as the sum of the three contributions:

$$\Gamma^{\mathrm{exp}} = \Gamma^{\mathrm{nat}} + \Gamma^{\mathrm{pb}} + \Gamma^{\mathrm{tt}}. \tag{6.24}$$

According to [56], the pressure-dependent broadening is parameterised as $\Gamma^{\mathrm{pb}}/p = 35.7(1.7)$ [MHz/Torr], where p is the pressure in Torr. Typically, the absorption signal is measured at various values of p and the result is then ex-

trapolated to zero pressure (values of p were used in the range $0.05 - 0.5$ Torr in [56]). The value of the broadening, $\Gamma^{\rm tt}$, due to the atomic beam transit time is not presented in the experiment of [56]. However, it can be roughly estimated as the difference between the experimental width extrapolated to zero pressure $\Gamma^{\rm exp} = 11.33(19)$ MHz and the natural width $\Gamma^{\rm nat} = 11.26$ MHz calculated theoretically in [211]: $\Gamma^{\rm tt} = 0.07(19)$ MHz. Finally, for p pressures between 0.05 and 0.5 Torr, the experimental width in (6.24) corresponds to the interval $\Gamma^{\rm exp} \in [13.2(4), 29.2(4)]$ MHz. Substituting these values into the expression (6.9) results in an NR correction in the range $\delta_{\rm NR} \in [0.016(1), 0.082(19)]$ MHz. The latter value partially eliminates the present discrepancy between the theoretical and experimental value of the frequency of the $2^3S_1 - 3^3D_1$ transition, which is about 0.5 MHz [208].

The observed fluorescence signal was recorded at $p = 0.151$ Torr (see Figure 1 in [56]). The NR correction corresponding to $p = 0.151$ Torr is $\delta_{\rm NR} = 0.027$ MHz. This value still does not eliminate the discrepancy between theoretical calculations and experiment found in [208], but reaches the experimental error level $E^{\rm exp}(2^3S_1 - 3^3D_1) = 786\,823\,850.002(56)$ MHz [56]. Since the resulting experimental value of the frequency of the $2^3S_1 - 3^3D_1$ transition in [56] is obtained by extrapolating the line position to zero pressure, it is necessary to "reconstruct" the centre of the line taking into account the NR correction at each pressure value. The result can be expected to be different (see Fig. 2b in [56]) and at least partially eliminate the present discrepancy with the theory [108].

Similar NR correction calculations can be performed for the $2^3S_1 - 4^3D_1$ and $2^3S_1 - 5^3D_1$ transition frequencies measured in [212]. These experiments were performed using the same technique as the [56], resulting in values of $\Delta E^{\rm exp}(2^3S_1 - 4^3D_1) = 947\,000\,197.11(1.8)$ MHz and $\Delta E^{\rm exp}(2^3S_1 - 5^3D_1) = 102\,112\,869\,7.31(2.4)$ MHz. The broadening of the $2^3S_1 - 4^3D_1$ and $2^3S_1 - 5^3D_1$ lines were determined as $\Gamma^{\rm pb}/p = 68.1(2.7)$[MHz/Torr] and $\Gamma^{\rm pb}/p = 78.5(2.7)$[MHz/Torr], respectively (see Table III in [212]), while the broadening due to transit time can still be considered negligible. Using the values of the corresponding fine structure intervals $\Delta_{12} = E_{4^3D_1} - E_{4^3D_2} = 555.231(7)$ MHz, $\Delta_{13} = E_{4^3D_1} - E_{4^3D_3} = 591.253(6)$ MHz [199], and for the natural level width

$\Gamma^{\rm nat}_{4^3D_1} = 4.96274$ MHz [213], one finds NR corrections to the transition frequency $2^3S_1 - 4^3D_1$ ranging from 0.350(23) to 2.65(2) MHz for pressures $p = 0.5 - 1.5$ Torr. The indicated corrections are at or above the experimental error for the transition frequency $2^3S_1 - 4^3D_1$, which is 1.8 MHz. Similarly, the correction values for the transition frequency $2^3S_1 - 5^3D_1$ start at 0.79(5) and end at 6.6(4) MHz given the energy intervals $\Delta_{12} = E_{5^3D_1} - E_{5^3D_2} = 283.560(8)$ MHz, $\Delta_{13} = E_{5^3D_1} - E_{5^3D_3} = 302.781(8)$ MHz [199] and natural width $\Gamma^{\rm nat}_{5^3D_1} = 2.61381$ MHz [213]. The results for all considered examples are summarised in Table 6.2.

Table 6.2. The range of nonresonant corrections to the transition frequencies $2^3S_1 - n^3D_1$ $(n = 3, 4, 5)$ $(n = 3, 4, 5)$ (5th column). The experimental transition frequency values are given in the second column, the theoretical values in the third column, and the range of experimental level width values in the fourth column. All values are given in MHz. The uncertainties are given in parentheses.

Transition	Experiment, MHz [56, 212]	Theory, MHz [55, 208]	Width $\Gamma^{\rm exp}$, MHz	$\delta_{\rm NR}$, MHz
$2^3S_1 - 3^3D_1$	786 823 850.002(56)	786 823 849.540(57)	13.2(4) – 29.2(4)	0.016(1) – 0.082(19)
$2^3S_1 - 4^3D_1$	947 000 197.11(1.8)	947 000 194.44(5)	39(1.4) – 107(4)	0.350(23) – 2.65(2)
$2^3S_1 - 5^3D_1$	102 112 869 7.31(2.4)	102 112 869 8.36(5)	41.9(1.4) – 120(4)	0.79(5) – 6.6(4)

Although the presented analysis cannot completely eliminate the current discrepancies between experimental and theoretical values for the transition frequencies, nonresonant corrections in experiments of the type [56, 212] should be accurately taken into account. One can expect that the agreement between experiment and theory is likely to be related to the issue of more careful measurement and appropriate extrapolation (taking into account nonresonant contributions) of experimental results.

6.5. Thermal broadening effect

In view of the discussion presented in the previous section 6.4, the observed linewidth plays a crucial role in determining the transition frequency. This conclusion follows directly from the expression for the nonresonant correction (6.9).

The proportionality of the $\sim \Gamma^2$ correction makes it sensitive to the width of the spectral line observed in the experiment. There are a number of factors that lead to spectral line broadening, such as transit time, pressure, residual electric and magnetic fields, and many others. In principle, all these effects require the use of a specific line profile, but in the simplest way such consideration can be reduced to a parameter characterising the width of the line contour defined by the sum of the respective contributions, see (6.24). Reducing the role of these effects allows a more accurate determination of transition frequencies by narrowing the observed spectral bands to lines of natural width, but is accompanied by a significant complication of the experiment. Another obvious way to avoid the corresponding error is to carry out appropriate theoretical calculations of these "subtle" effects.

In this section, attention is drawn to another effect of line broadening, which is also well known and has been considered by many authors, namely thermal broadening. The theoretical description of these effects is reduced to the calculation of probabilities of transitions induced by blackbody radiation (BBR). The latter can be realised in the nonrelativistic limit and in the dipole approximation by means of the following expression (see, for instance, [214–216]):

$$\Gamma_a^\beta = \frac{4}{3}e^2 \sum_n \left|\langle a|\boldsymbol{r}|n\rangle\right|^2 n_\beta(\omega_{an})\omega_{an}^3, \tag{6.25}$$

where $\omega_{ab} = E_a - E_b$ is the energy difference between the states of atom a and b (resonance transition frequency), k_B is the Boltzmann constant, T is the temperature in kelvin, $n_\beta(\omega)$ is the Planck distribution function,

$$n_\beta(\omega) = \frac{1}{e^{\frac{\omega}{k_B T}} - 1}. \tag{6.26}$$

The summation in (6.25) runs over the whole spectrum of the Schr?dinger equation and includes higher states. At low temperatures, the partial contributions from the continuum energy spectrum are negligible. At room temperature, the numerical values of the BBR radiation-induced widths for the ns/nd levels ($n = 4$, 6, 8, 12) in hydrogen are given in Table 6.3, where the natural widths are also given for comparison. The effect of thermal line broadening on NR

Table 6.3. Natural and induced by radiation BBR line widths for ns/nd states in the hydrogen atom at $T = 300$ K. All values are given in Hz. The summation over n in (6.25) is restricted to the discrete spectrum and $n = 300$ only, which is justified by the rather small coefficient $k_B T \approx 9.5 \times 10^{-4}$ in atomic units. The values are given in Hz. The fraction of the contribution to the nonresonant correction, x (dimensionless value), is also given.

n	ns				nd			
	Γ^{β}_{ns}, [214]	Γ^{β}_{ns}	$\Gamma^{\rm nat}_{ns}$	$x = 2\Gamma^{\beta}_{ns}/\Gamma^{\rm nat}_{ns}$	Γ^{β}_{nd}, [214]	Γ^{β}_{nd}	$\Gamma^{\rm nat}_{nd}$	$x = 2\Gamma^{\beta}_{nd}/\Gamma^{\rm nat}_{nd}$
4	2.54966	2.53778	7.03×10^5	7.22×10^{-6}	4.30037	4.2809	4.41×10^6	1.94×10^{-6}
6	1120.13	1119.48	2.98×10^5	0.075	1530.75	1529.73	1.34×10^6	0.0023
8	4036.17	4036.93	1.44×10^5	0.056	5026.11	5027.23	5.72×10^5	0.018
12	5718.44	5721.15	4.77×10^4	0.24	6434.63	6437.68	1.72×10^5	0.075

corrections can be accounted for by substituting the full widths of the atomic levels $\Gamma^{\rm tot}_a \equiv \Gamma^{\beta}_a + \Gamma^{\rm nat}_a$, into the expression (6.9) for the resonance state a. Since Γ^{β}_a is smaller than $\Gamma^{\rm nat}_a$, the order of magnitude of the thermally induced nonresonant correction can be estimated as the ratio $x = 2\Gamma^{\beta}_a/\Gamma^{\rm nat}_a$ relative to the value given by the natural level width. The values of x are given in Table 6.3 and can be used by multiplying the results of the previous sections by this factor. In particular, it follows from the values of x that the thermally induced broadening becomes significant for highly excited ns states, leading to an additional contribution of the order of a quarter of the "natural" one.

6.6. Conclusion on the NR corrections

In conclusion, spectroscopic measurements of transition frequencies in various atomic systems form a significant part of modern physics. They allow one to test fundamental interactions, determine physical constants and study fundamental symmetries found in nature with unprecedented accuracy. Studies based on two-photon spectroscopy of simple atoms represent some of the most precise experiments to date. The verification of precision experimental results is largely supported by theoretical analyses, which are most rigorous for light nonrelativistic atoms and ions. In the last decade much attention in the scientific literature has been paid to the study of the effect of quantum interference in

hydrogen and hydrogen-like atomic systems. This has allowed us to significantly reduce the experimental error in determining the corresponding transition frequencies. The theoretical description of QIE refers to the consideration of interfering transitions arising for states close to the resonance level. Thus, studies of the influence of nonresonant processes, including the need to take into account the emission process on the formation of the absorption profile, are an integral part of spectroscopic measurements. More recently, calculations have been performed showing the need to account for the QIE in cascade emission (similar to the results of the section 5.5) to accurately determine the frequency of the absorption transition to highly excited states in two-photon spectroscopic experiments [190].

Finally, for the [32] experiment, the effect of line profile asymmetry can be schematically illustrated by the plots shown in Fig. 6.6.

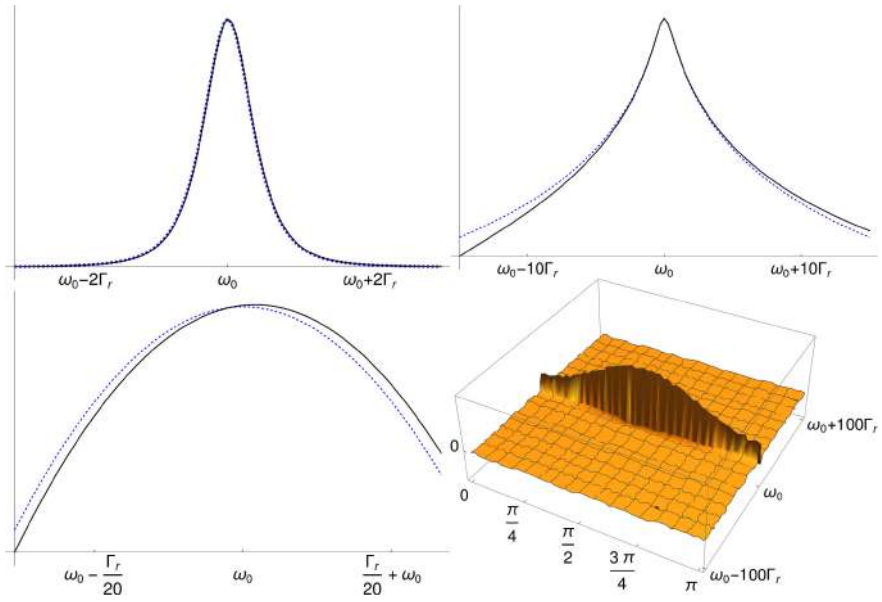

Figure 6.6. Schematic illustration of the line profile asymmetry arising beyond the resonance approximation for the experiment [32].

The graphs are given in arbitrary units on the ordinate axis, while the abscissa axis shows the frequency in units of the natural width of the resonance state. The upper left panel shows the symmetric (dashed curve) and asymmetric (solid curve) profiles, indistinguishable to the naked eye. The same is shown in logarithmic scale in the upper right panel. The part of the line profile close to the region of the line maximum is shown in logarithmic scale in the lower left panel.

The difference between symmetric and asymmetric profiles depending on the angle between the polarisation of the incident photon and the direction of the emitted photon is shown in the lower right panel. The scale of profile values is set so that the effect is visible (normalisation factor is used), the same with the choice of frequency scale.

6.7. Adapted method of moments for determining the transition frequency

This section is devoted to the search for alternative possibilities of determining spectroscopic standards of atomic frequency. Leaving aside the discussion of nonresonant effects, the search for alternative ways to compare theoretical results with experimental results becomes one of the significant tasks of precision atomic spectroscopy. For example, if the profile of the observed line can be measured in detail, a thorough comparison of the theoretical and experimental spectral distributions can be proposed as one of the methods for such a determination. Then, having estimated the dispersion of the two spectral functions, it is possible to determine the transition frequency, width, amplitude, etc. by the minimum of their deviation:

$$\overline{\left(S^{\mathrm{exp}}(\omega_i) - S^{\mathrm{theor}}(\omega_i)\right)^2} - \left(\overline{S^{\mathrm{exp}}(\omega_i) - S^{\mathrm{theor}}(\omega_i)}\right)^2 . \tag{6.27}$$

Here $S^{\mathrm{exp}}(\omega_i)$ is the value of the observed spectral distribution at point ω_i, and $S^{\mathrm{theor}}(\omega_i)$ is the theoretically estimated spectral distribution at the same point ω_i.

The ordinary procedure for determining the transition frequency in atomic and molecular spectroscopy is to fit the observed spectral line with a Lorentz, Gauss, Voigt, or other profile. The Lorentz line profile describes the process of one-photon emission (absorption) taking into account the natural width of levels due to radiative decay of the excited state. However, in more general cases, the experimentally observed linewidth is much larger than the natural linewidth. The broadening of spectral lines is due, for example, to Doppler and

collision effects, to the influence of external fields, etc. The Gaussian profile can be used to extrapolate experimental data in case of significant distortion of the spectral line. In turn, the combined natural and "external" (e.g., collisional and Doppler) broadening is described by the Voigt profile. As a consequence, the maximum (or frequency value at half-height) of the observed line shape is interpreted as the transition frequency.

The choice of fitting contour corresponds to different physical conditions and is not limited to these three [217] profiles. Each of the profiles serves its purpose and should be used to describe in detail the physical processes occurring in the experiment. The most problematic case arises when describing experimental data with a poor signal-to-noise ratio. Assuming that the effects described in, for example, [217] are minimised by routine theoretical calculations inextricably linked to the experimental simulations of [218], the theoretical description presented below is limited to Lorentz, Gauss and Voigt profiles. The main purpose of this section is to demonstrate various possibilities for carefully extracting the transition frequency from the observed asymmetric profile (see [109] for details).

An experimentally observed spectral line can be described by one of three different profiles:

$$\begin{aligned} L(\omega) &= \frac{f^2}{(\omega-\omega_0)^2+\alpha_L^2}, \quad G(\omega) = f^2 e^{-\frac{(\omega-\omega_0)^2}{2\alpha_D^2}}, \\ V(\omega) &= \int\limits_{-\infty}^{\infty} G(\omega')L(\omega-\omega')d\omega' = \int\limits_{-\infty}^{\infty} \frac{f^2 e^{-\frac{\omega'^2}{2\alpha_D^2}} d\omega'}{(\omega-\omega_0-\omega')^2+\alpha_L^2}. \end{aligned} \tag{6.28}$$

Here $\alpha_L \equiv \Gamma/2$, Γ is the natural width of the atomic level, α_D is the Gaussian half-width at half-maximum, ω_0 is the theoretical value of the energy difference between atomic levels, and f represents the transition amplitude depending on all possible quantities (in particular, quantum numbers and angles). Such notations are introduced for convenience and do not affect the generality of the calculations. The first line form is the Lorentz profile, the second is the Gaussian function, and the third line form is called the Voigt line profile. These distribu-

tion functions should be normalised to unity: $\int\limits_{-\infty}^{\infty} [L(\omega), G(\omega), V(\omega)]\, d\omega = 1$.

The functions (6.28) can be used to define well-known moments: the zero moment is the overall probability, the first moment is the mean, the second central moment is the variance, the third moment is the skewness (a numerical characteristic of the symmetry of the distribution), and the fourth moment is the kurtosis (how heavy the tails of the distribution are). The zero moment gives the normalisation constant, and the first moment reproduces the mean frequency, which coincides with the theoretical value ω_0:

$$\overline{\omega} \equiv \mu_1 = \frac{\int\limits_{-\infty}^{\infty} d\omega\, \omega\, [L(\omega), G(\omega), V(\omega)]}{\int\limits_{-\infty}^{\infty} d\omega\, [L(\omega), G(\omega), V(\omega)]} = \omega_0. \tag{6.29}$$

The evaluation of any moments for the Gaussian distribution is not difficult, and the result (6.29) for Lorentz or Voigt profiles deserves a separate discussion. Calculations for both can be performed using the principal value of the integrals when the upper and lower limits of integration equally tend to infinity. For higher moments, however, this procedure is violated. The characteristic function of the corresponding distribution can be used to solve this problem.

The result (6.29) can be easily adapted to the processing of experimental data, i.e. using a data table with values of frequencies and spectral functions. Then the average frequency value (first moment) is equal to

$$\overline{\omega}^{\mathrm{exp}} = \frac{\sum\limits_{i} \omega_i\, [L(\omega_i), G(\omega_i), V(\omega_i)]}{\sum\limits_{j} [L(\omega_j), G(\omega_j), V(\omega_j)]}, \tag{6.30}$$

where the summation is performed over all available values. Then the mean frequency $\overline{\omega}^{\mathrm{exp}}$ should coincide with the theoretical value ω_0 and be close to the frequency found as the maximum of the observed line shape (symmetric profile).

The expression (6.30) can be compared to a fitting procedure: (i) it is based on experimental data only; (ii) the expression (**??**) is independent of the theo-

retical line shape model, i.e., Lorentz, Gauss or Voigt profiles lead to the same result; (iii) the accuracy of the determination of $\overline{\omega}^{\exp}$ is limited by the uncertainty of the measured values of ω_i and $L(\omega_i)$, $G(\omega_i)$, or $V(\omega_i)$. Some results of the adaptation of this method for several close smooth (non-noisy) lines, which are of most interest in precision spectroscopy, are shown below.

Applying the "Lorentz model" for two neighbouring lines gives the

$$\begin{gathered} N_L = \int\limits_{-\infty}^{\infty} d\omega L(\omega) = \pi \left[\frac{f_1^2}{\alpha_{L1}} + \frac{f_2^2}{\alpha_{L2}} \right], \\ \int\limits_{-\infty}^{\infty} d\omega \, \omega L(\omega) = \pi \frac{\delta f_2^2 \alpha_{L1} + f_1^2 \alpha_{L2} \omega_0 + f_2^2 \alpha_{L1} \omega_0}{\alpha_{L1} \alpha_{L2}}, \\ \overline{\omega}_L^{\exp} \equiv \mu_1^L = \omega_0 + \delta \frac{f_2^2 \alpha_{L1}}{f_1^2 \alpha_{L2} + f_2^2 \alpha_{L1}}, \end{gathered} \tag{6.31}$$

where δ is the shift of the second maximum relative to the first (in the case of the experiment [32] is the splitting energy of the fine structure), $\alpha_{L1(2)}$ and $f_{1(2)}$ are the widths and amplitudes of the levels for the $1, 2$ resonance lines, respectively. The spectral function $L(\omega)$ has the form:

$$L(\omega) = \left| \frac{f_1}{\omega - \omega_0 - \mathrm{i}\alpha_{L1}} + \frac{f_2}{\omega - \omega_0 - \delta - \mathrm{i}\alpha_{L2}} \right|^2, \tag{6.32}$$

i.e., takes into account the interference and "quadratic" contributions of the two resonant lines. Finding the following moments, it is possible to compose a system of independent equations for all unknowns in (6.31).

There is another possibility to determine the frequency of ω_0 from experimental data (not only for two peaks). It can be expressed by the formula:

$$\overline{\omega}^{\exp} \approx \omega_0 = \frac{\sum\limits_i \omega_i \left[L(\omega_i), G(\omega_i), V(\omega_i) \right]^n}{\sum\limits_j \left[L(\omega_j), G(\omega_j), V(\omega_j) \right]^n}, \tag{6.33}$$

where $n \to \infty$. In this case, the factor in the summand proportional to δ (see (6.31)) tends to zero at $f_1 \neq f_2$. In practice, this means that the distribution of

the highest peak tends to a delta function and hence this procedure corresponds to the definition of maximum. This definition can be used with the desired accuracy; larger values of n should be used to achieve greater accuracy.

A detailed analysis of the different profile models, as well as a validation of the method for some transitions in different atomic systems based on the *NIST Atomic Spectra Database*, was presented in [109]. Omitting further details of the calculations, the application of the method of moments can be illustrated on "real" (unprocessed) experimental data.

The isolated Raman scattering line of polycrystalline silicon was considered as the first test system. The silicon optical phonon band at 520.7 cm^{-1} serves as a standard in vibrational spectroscopy. Therefore, it is of interest to precisely determine its position [219–221]. Experimental data for this band are shown in Fig. 6.7 for four spectra recorded with different signal-to-noise ratios.

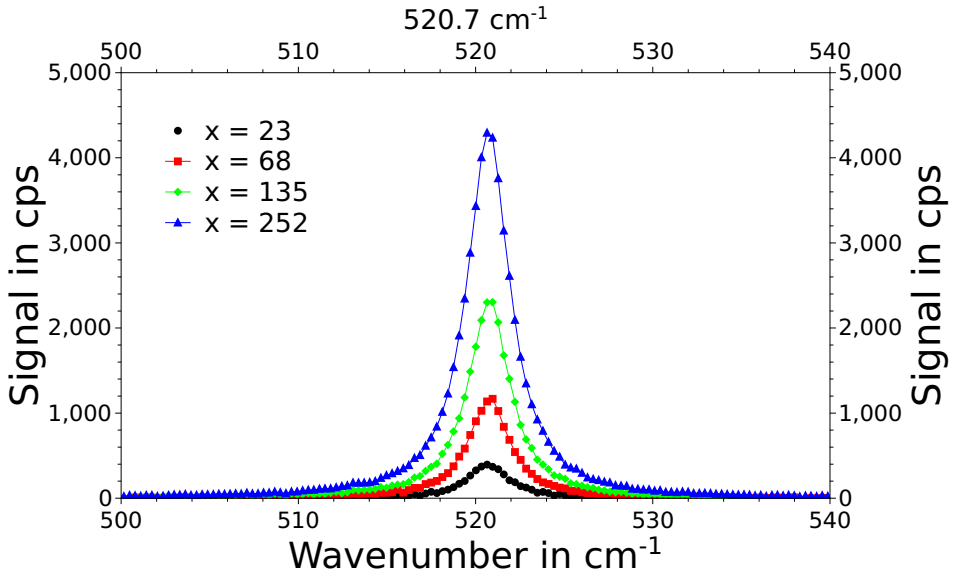

Figure 6.7. Experimental profile of the optical phonon band for Raman scattering of polycrystalline silicon. The x values show the signal-to-noise ratio. Here and below, spectra were measured on a LabRam HR-800 spectrometer with 632.8 nm laser line excitation from a He-Ne source, 100 micron confocal aperture, and 1800 deg/mm diffraction grating. The measurement error is 0.35 cm^{-1}. The signal-to-noise ratio was varied by using neutral density filters in the laser path.

Using the table of experimental data, the frequency values corresponding to the peak (maximum) were found: 520.63 ± 0.35 cm^{-1} and 520.74 calculated

Table 6.4. Maximum of the Raman bandwidth of silicon obtained from calculations and fitting (wave numbers, ν, in cm^{-1}). The first column shows the signal-to-noise ratio x, while the second column shows the experimental error. The values obtained using the Gaussian, $\nu^G_{\max}$, and Lorentz approximations, $\nu^L_{\max}$, are given in the third and fourth columns, respectively. The results of the calculations by the method of moments are given in the fifth column. Finally, the last column shows the values calculated in the approximation (6.33) with the difference between $n = 20$ and $n = 40$ in parentheses.

x	Ubc., cm^{-1}	$\nu^G_{\max}$, cm^{-1}	$\nu^L_{\max}$, cm^{-1}	$\bar{\nu}$, cm^{-1}	$\bar{\nu}^{(n)}$, cm^{-1}
23	±0.35	520.70	520.69	520.47	520.65(1)
68	±0.35	520.75	520.76	520.55	520.84(4)
135	±0.35	520.75	520.76	520.59	520.80(1)
252	±0.35	520.72	520.72	520.63	520.74(1)

according to (6.29) and in approximation (6.33) for the signal-to-noise ratio parameter $x = 252$. The result is in excellent agreement with the [221]. To verify the effectiveness of the method for different signal-to-noise ratios x, Table 6.4 is presented showing the wavelength values calculated for different x, as well as the values obtained by the profile fitting procedure.

First of all, it should be noted that the values found by approximation by Gaussian or Lorentz contours gave the same results for the data presented in Fig. 6.7. The results for the Voigt profile approximation are not given in Table 6.4, assuming its apparent validity, since $\lambda^G_{\max} = \lambda^L_{\max}$. In turn, the results corresponding to the calculations by the method of moments agree with them within the experimental uncertainty. As expected, as the parameter x increases, the values determined by the method of moments tend towards the tabulated value (520.70 cm^{-1} [221]), but even at $x = 23$ an acceptable agreement within the measurement error can be found. Furthermore, the estimated full width at half height (FWHM) is 2.64 cm^{-1} at $x = 252$, and the fitting procedure gives 2.89 cm^{-1}, which are in agreement with each other given the accuracy of the numerical calculations, estimated by a frequency step of about 0.3 cm^{-1}.

As another example, consider a double line around 219 cm^{-1} for sulphur, which is also used as a reference sample in Raman spectroscopy. The rele-

vant data are shown in Fig. 6.8, including the results of the approximation by two Lorentz profiles. As for the single silicon line discussed above, the

Figure 6.8. Experimental α band profile for double-structured sulfur at about 219 cm^{-1}, fitted according to the Lorentzian model. The measurement error is ± 0.35 cm^{-1}.

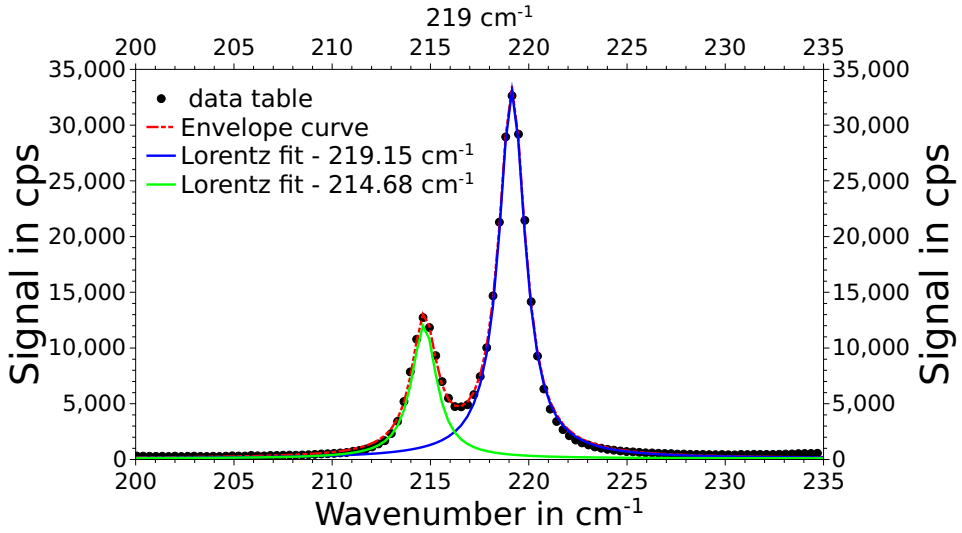

measurement error is 0.35 cm^{-1}. The values of the two observed maxima found by fitting are 219.15 and 214.68 cm^{-1}. The wave number of the higher peak agrees well with the database results https://www.chem.ualberta.ca/ mccreery/ramanmaterials.html, i.e., 219.1 cm^{-1} with a standard deviation of 0.57 cm^{-1}, see also [222]. In turn, applying the method of moments, the values turn out to be 219.15 and 214.63 cm^{-1}, respectively. The calculated FWHM values of 1.59 and 1.55 cm^{-1} are in agreement with the fitting results of 1.63 and 1.54 cm^{-1}.

Finally, Fig. 6.9 illustrates the results of another double sulphur band around 473 cm^{-1}, characterised by a more blurred structure. The tabular value of this frequency is 473.2 ± 0.49 cm^{-1} (see https://www.chem.ualberta.ca/ mccreery/ramanmaterials.html), and the values obtained by approximating the experimental data are 473.08 ± 0.35 and 467.59 ± 0.35 cm^{-1} for the high and low peaks, respectively. This case is of particular interest because there is a strong overlap between the two bands. The method of moments gives values of 473.10 and 467.67 cm^{-1}, which agree with the fitting result within the experimental error. In turn, the widths correlate as 4.52 and 4.92 for the higher peak,

Figure 6.9. Observed band profile for sulfur with blurred double structure at 473 cm^{-1}. A Lorentz model was used to approximate the experimental data. The measurement error is equal to ± 0.35 cm^{-1}.

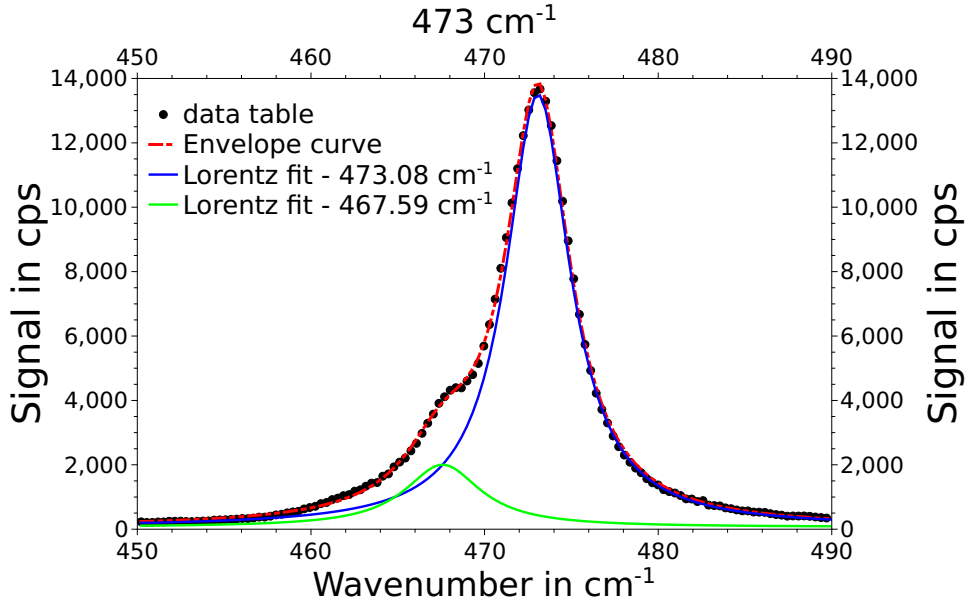

5.31 and 5.61 for the lower peak, found by fitting and numerically in cm^{-1}, respectively.

The results demonstrate the possibility of using the method of moments to determine the characteristics of spectral lines, such as transition frequency, amplitudes, widths, etc. This can be achieved by calculating the corresponding moments in the data table with the experimental values of the observed spectral distribution.The method of moments can be compared to the ingrained fitting procedure. It is important to note that, firstly, the frequency value is independent of the choice of model, i.e. it is the same for Lorentz, Gaussian or Voigt line shapes. Second, the method of moments also uses only experimental data: calculations are performed only within the experimentally obtained table of values, based on the above theory. Third, the method has shown good accuracy for overlapping resonances. Fourth, it does not matter whether the lines are due to radiation or other processes. Finally, the presented results are limited to the presence of two resonances, but can be extended to a larger number of spectral lines.

However, the method of moments has its drawbacks. The first (and most problematic) is that the system of equations is completely nonlinear. As a re-

sult, the method of finding solutions or selecting approximations becomes more complicated. Nevertheless, one may find that all the nonlinearity arises from considering the widths of the levels. Then, assuming that the level widths are small compared to the transition frequencies and the energy splitting of the lines, the solution can be found in the approximation of equivalent widths (or, in a simpler case, corresponds to zero widths), see details in [109]. It can also be a problem to choose a solution. But again, using experimental data, one can determine the corresponding values of the maxima as a zero approximation. It can be expected that there should not be a large discrepancy between this method and the search for maxima (the line centre).

Thus, the presented analysis establishes the fundamental possibility of using the method of moments for processing experimental spectral data and determining transition frequencies. At least, the method of moments can be used to control the accuracy of the required parameters by comparing the corresponding moments estimated from the table of experimental data and from the data obtained by fitting according to (6.27).

Experimental data were provided by E. Solovyeva (co-author of the paper [109]).

Chapter 7.

Spectroscopy of the anti-hydrogen atom

Advances in the production of anti-hydrogen atoms have enabled spectroscopic studies of their properties [66,70,72,223–226]. A detailed comparison of the spectroscopic properties of anti-hydrogen ($\bar{\mathrm{H}}$) with the precisely measured properties of hydrogen atom spectrum (H) can provide information on the possible violation of the CPT and Lorentz invariance [227]. According to the CPT-theorem, the spectra of matter and antimatter atoms should be identical. Nevertheless, it has been shown that violations of CPT and Lorentz symmetries on the Planck scale could be observed in the framework of hydrogen and anti-hydrogen spectroscopy [227]. Effects of this type can appear in the spectra of H and $\bar{\mathrm{H}}$ at zero order on the fine structure constant and can be detected not only in the $1s-2s$ line but also in the hyperfine transition with spin flip. Moreover, extra-accurate measurements of the transition frequency in hydrogen (see, e.g., [20, 137, 228]) have stimulated the development of spectroscopic experiments with anti-matter atoms. To date, the accuracy of the latter is at the level of 10^{-8} relative magnitude [73–75].

The spectra of hydrogen and anti-hydrogen atoms in an external electric field differ because of the presence of terms linear in the electric field in the expressions for the transition probabilities [103–105]. Such terms are absent in the energy due to the conservation of spatial (P) and time (T) parities. However, they can enter the expression for the line profile, since the latter is proportional

to the transition probability. The Lorentz line profile at resonant scattering of a photon on an atomic electron in the presence of an external electric field remains symmetric with respect to the resonant frequency ω_0. This symmetry is broken when nonresonant corrections are taken into account. NR corrections have been discussed in the sections above. In contrast to the "standard" energy corrections, it has been shown that they can depend linearly on the electric field and thus differ for hydrogen and anti-hydrogen atoms. Such effects reveal a specific difference in the spectra of H and $\bar{\text{H}}$ atoms in the presence of an external electric field.

This chapter is devoted to theoretical aspects related to the consideration of external fields in the comparative analysis of the spectra of atoms H and $\bar{\text{H}}$. In particular, estimates of the corrections affecting the determination of the transition frequency and arising from the asymmetry of the observed line profile are first given, and then a comparative analysis of the distinctive features of the emission (absorption) lines in the presence of an external magnetic field is presented. The latter is addressed to the possibility of searching for $\bar{\text{H}}$ atoms in the interstellar medium. The importance of the presented analysis can be emphasised by the recent experiments [66,73,74] aimed at a detailed comparison of hydrogen and anti-hydrogen spectra. It can be expected that the results obtained can serve to further experimentally improve such measurements.

7.1. Estimates of the NR correction in the external electric field to the frequency of the Ly_α line in $\bar{\text{H}}$

In this section it is shown that nonresonant corrections to the transition frequency can contain terms linear in the electric field. In particular, the process of elastic resonant scattering of photons on the ground state of a hydrogen or anti-hydrogen atom placed in a weak electric field is considered. The frequency of the incident photons is close to the transition energy Ly_α. It is assumed that a natural profile of the $1s-2p$ transition line can be observed, as first reported in [137]. The external electric field is assumed to be "weak". It will be shown

that the existence of linear field terms does not violate PT-parity and leads to a difference in the resonance spectroscopic measurements of hydrogen and anti-hydrogen atoms in an external electric field.

Adapting the expression (6.6) and the formalism used in section 4.1 as an estimate of the NR correction, the cross section for one-photon scattering for the Ly_α transition in the hydrogen atom can be reduced to the form (see [126]):

$$\sigma \sim \frac{W_{2p'_{1/2}}(\boldsymbol{k}')W_{2p'_{1/2}}(\boldsymbol{k})}{x^2+\frac{1}{4}\Gamma^2_{2p'_{1/2}}} + 2\Re\frac{W_{2p'_{1/2};2p'_{3/2}}(\boldsymbol{k}')W_{2p'_{1/2};2p'_{3/2}}(\boldsymbol{k})}{\left(x-\frac{\mathrm{i}}{2}\Gamma_{2p'_{1/2}}\right)(x+\Delta_{\mathrm{fs}})}, \tag{7.1}$$

where $x \equiv \omega-\omega_0$, $\boldsymbol{k}'$, $\boldsymbol{k}'$ denote the absorbed and emitted photons, respectively. $W_{2p'_{1/2}}$ is the differential probability of the $1s-2p$ transition, and $W_{2p'_{1/2};2p'_{3/2}}$ is the "mixed" (due to interference for the $2p_{1/2}$ and $2p_{3/2}$ states) transition probability, see [43]. The character strokes indicate the states for which the admixture of a state of opposite parity arising in the external electric field is taken into account [103–105].

In the following it is considered that the influence of the external electric field on the energies is negligible and only the $2p_{1/2}$ and $2s$ states are effectively mixed. According to (4.14), it follows directly that

$$\begin{aligned}\psi_{2p'_{1/2}} &= \psi_{2p_{1/2}} - \xi_{\mathrm{S}}\psi_{2s},\\ \psi_{2s'} &= \psi_{2s} + \xi_{\mathrm{S}}\psi_{2p_{1/2}},\end{aligned} \tag{7.2}$$

where the states are defined by the Stark parameter ξ_{S}. As before for a small electric field $\xi_{\mathrm{S}} = \langle 2s|\boldsymbol{d}\boldsymbol{\mathcal{E}}|2p\rangle/\Delta E_L \ll 1$. For the $2p_{3/2}$ state, the Lamb shift ΔE_L should be replaced by the corresponding fine structure interval, which is much larger than ΔE_L. Then it is assumed that $2p'_{3/2} \equiv 2p_{3/2}$. Also an important circumstance is the existence of differential transition probabilities $W_{2p'_{1/2}}$, since the total probability (integrated over all possible directions), which coincides in this case with the level width, depends on the field only quadratically. This result will be obtained explicitly in the following sections.

Using for simplicity the extremum condition, the nonresonant correction

can be found in the form:

$$x_{\rm NR} = \frac{1}{4}\frac{\Gamma_{2p}^2}{\Delta_{\rm fs}}\frac{W_{2p'_{1/2};2p_{3/2}}(\boldsymbol{k}')W_{2p'_{1/2};2p_{3/2}}(\boldsymbol{k})}{W_{2p'_{1/2}}(\boldsymbol{k}')W_{2p'_{1/2}}(\boldsymbol{k})} \tag{7.3}$$

Passing to a completely nonrelativistic description, the angular momenta in (7.3) can be totally omitted. It is also taken into account that the admixture of $2s$ states weakly changes the natural width of the level $2p$ and, hence, $\Gamma_{2p'_{1/2}} \approx \Gamma_{2p'} \approx \Gamma_{2p}$.

A linear dependence on the external field can be obtained by taking into account the results obtained in [103–105], where, in particular, the differential probability of emission was reduced to the form:

$$W_{2s'} = W_{2s} - \sqrt{3}\frac{e\Gamma_{2p}}{\Delta E_L^2}\,(\boldsymbol{k}\boldsymbol{\mathcal{E}})\,\sqrt{W_{2p}W_{2s}}. \tag{7.4}$$

Here the electron charge, e, is explicitly written out, and W_{2p} and W_{2s} are independent of $\boldsymbol{k}$ and represent the emission probabilities of the corresponding states in the absence of field. Also in (7.4) the quadratic field contribution is neglected. Accordingly, one can obtain (see details in [126])

$$W_{2p'} = W_{2s} + \sqrt{3}\frac{e\Gamma_{2p}}{\Delta E_L^2}\,(\boldsymbol{k}\boldsymbol{\mathcal{E}})\,\sqrt{W_{2p}W_{2s}}, \tag{7.5}$$

$$W_{2p';2p} = W_{2p} + \frac{\sqrt{3}}{2}\frac{e\Gamma_{2p}}{\Delta E_L^2}\,(\boldsymbol{k}\boldsymbol{\mathcal{E}})\,\sqrt{W_{2p}W_{2s}}. \tag{7.6}$$

When the correlation $(\boldsymbol{k}\boldsymbol{\mathcal{E}})$ is of interest, i.e., the dependence on the angle between the direction vector of the emitted photon and the field, one can consider the following $W_{2p'}(\boldsymbol{k}') = W_{2p';2p}(\boldsymbol{k}') = W_{2p}$. Then, according to (7.5), (7.6), the series expansion of the denominator in (7.3) gives

$$\begin{aligned} x_{\rm NR} = \frac{1}{4}\frac{\Gamma_{2p}^2}{\Delta_{\rm fs}}\left[1 - e\frac{\sqrt{3}}{2}\frac{\Gamma_{2p}}{\Delta E_L^2}\sqrt{\frac{\Gamma_{2s}}{\Gamma_{2p}}}\,(\boldsymbol{k}\boldsymbol{\mathcal{E}})\right] \\ = x_{\rm NR}^{(0)} + \delta x_{\rm NR}. \end{aligned} \tag{7.7}$$

Here $x^{(0)}_{\rm NR}$ is exactly the same as the result of [43], and $\delta x_{\rm NR}$ represents the field-dependent contributions.

The linear dependence of the NR correction on the electric field does not imply the existence of a linear Stark effect. It should be remembered that such corrections are not shifts of the energy of atomic levels in the literal sense; they represent corrections to be made to compare the results of frequency measurements with theoretical calculations of energy levels [35, 43].

The formal T-invariance of the factor $(\boldsymbol{k}\boldsymbol{\mathcal{E}})$ ($\boldsymbol{k}$, $\boldsymbol{\mathcal{E}}$ are T odd and T odd vectors, respectively) is compensated by a linear dependence on Γ_{2p} in (7.7). Such a simulation of T-noninvariance in unstable systems was predicted by Zeldovich [229]. The above T-noninvariance is contained already in the expression (7.4) and can be explained as follows [103, 104]. The expression (7.4) describes the emission of a photon with momentum $\boldsymbol{k}$. In the time-reversed process, i.e., the absorption of a photon with momentum $-\boldsymbol{k}$, it is also necessary to change the sign of Γ in the energy denominators of the amplitude, which depend on the boundary conditions determining the pole position in the electron propagator of the electrons (2.3). Then, the expressions (7.4) and (7.7) are invariant with respect to time reversal.

Considering a weak electric field when $\xi_{\rm S} = 0.1$ (the corresponding value of field strength $\mathcal{E} = 47.5$ V/cm), consider that $\Delta_{\rm fs} = 0.03m(\alpha Z)^4$, $\Delta E_L = 0.4m\alpha(\alpha Z)^4$ and $\Gamma_{2p} = 0.04m\alpha(\alpha Z)^4$, $\Gamma_{2s} = 10^{-3}m\alpha(\alpha Z)^{10}$ (the expression (7.7) includes one-photon probabilities/amplitudes). Then $\delta x_{\rm NR} \simeq -e10^{-4}\,(\boldsymbol{k}\boldsymbol{\varepsilon})$ Hz ($\boldsymbol{\varepsilon} \equiv \boldsymbol{\mathcal{E}}/\mathcal{E}$ is the unit field direction vector). The proportionality of the electron charge, written out explicitly for clarity, demonstrates the difference for atoms H and $\bar{\rm H}$.

The estimate (7.7), while being rough (indicating only an order of magnitude) and assuming that the effect may be larger, demonstrates the fundamental importance of monitoring the external electric field in experiments related to the analysis of the spectral characteristics of the atom $\bar{\rm H}$. The order of magnitude of this effect shows that it is hardly to be observed in resonant photon scattering at the $1s - 2p$ transition in the near future: the frequency measurement error in this process is about MHz [74, 137].

7.2. Linear in the field "quadratic" NR correction to the frequency of Ly_α line

Considering that in an external electric field due to mixing of $2s$, $2p$ levels (see (7.2)) one-photon absorption can effectively pass to the $2s'$ state (e.g., the Stark coefficient $\xi_{\mathrm{S}} = 1$ indicates complete mixing of the closely adjacent $2s$, $2p$ states [103, 104]). The Ly_α scattering cross section of a photon can be represented as quadratic contributions (see [38, 39]):

$$\sigma \sim \frac{W_{2p'_{1/2}}(\vec{k}')W_{2p'_{1/2}}(\vec{k})}{x^2 + \frac{1}{4}\Gamma^2_{2p'_{1/2}}} + \frac{W_{2s'_{1/2}}(\vec{k}')W_{2s'_{1/2}}(\vec{k})}{(x + \Delta E_L)^2}. \tag{7.8}$$

Here, as before, $W_{2p'_{1/2}}(\boldsymbol{k}')$ and $W_{2s'_{1/2}}(\boldsymbol{k}')$ denote the differential absorption probabilities (corresponding to the "hatched" photon), and $W_{2p'_{1/2}}(\boldsymbol{k})$, $W^e_{2s'_{1/2}}(\boldsymbol{k})$ are the differential emission probabilities (corresponding to the " non-hatched" photon) for the transitions $2p'_{1/2} \leftrightarrow 1s$ and $2s'_{1/2} \leftrightarrow 1s$, respectively. Similarly, one can set $\Gamma_{2p'_{1/2}} \equiv \Gamma_{2p}$, since even for $\xi_{\mathrm{S}} = 1$ the width of $\Gamma_{2p'}$ is weakly susceptible to modification (due to the smallness of the $2s$ level width). The first term in (7.8) represents the resonant contribution (the Lorentz line profile), while the second term provides a nonresonant correction.

Accounting for the NR contribution to (7.8) in leading order gives

$$x_{\mathrm{NR}} = -\frac{1}{16}\frac{\Gamma^4_{2p}}{\Delta E^3_L}\frac{W_{2s'}(\boldsymbol{k}')W_{2s'}(\boldsymbol{k})}{W_{2p'}(\boldsymbol{k}')W_{2p'}(\boldsymbol{k})}. \tag{7.9}$$

In the absence of electric field ($\xi = 0$) for the total cross section, the nonresonant correction (7.9) is vanishingly small. In this case, $\Gamma_{2p} = 0.04\alpha^3$, $\Delta E_L = 0.4\alpha^3$, $W_{2p} \approx \Gamma_{2p}$ and $W_{2s} \approx \Gamma_{2s} = 10^{-3}\alpha^9$ (in atomic units). This then yields $x_{\mathrm{NR}} \approx -10^{-22}$ Hz. The main contribution to the shift of the x_{NR} maximum in the absence of field comes from the interference terms between the $1s - 2p_{1/2}$ and $1s - np_{1/2}$ transitions and from the quadratic $1s - 2p_{3/2}$ contribution (see previous sections). However, in the presence of an electric field $\xi_{\mathrm{S}} = 1$, the correction (7.9) becomes the largest: $x_{\mathrm{NR}} \approx -6.4$ kHz.

Being interested in the linear field contribution, one can make calculations

similar to the previous section (see also [38]). The series expansion of the denominator in (7.9) gives

$$x_{\mathrm{NR}} = -\frac{1}{16}\frac{\Gamma_{2p}^4}{\Delta E_L^3}\xi_{\mathrm{S}}^4\left[1 - e\left(\xi_{\mathrm{S}} + \frac{1}{\xi_{\mathrm{S}}}\right)\frac{\Gamma_{2p}}{\Delta E_L}\left(\frac{W_{2s}}{W_{2p}}\right)^{1/2}(\boldsymbol{k}\boldsymbol{\mathcal{E}})\right]. \tag{7.10}$$

Here the charge of the bound particle is again written out explicitly for clarity.

For $\xi_{\mathrm{S}} = 1$ NR correction linear in the field is defined by the formula:

$$\delta x_{\mathrm{NR}} = -e\frac{1}{8}\frac{\Gamma_{2p}^5}{\Delta E_L^4}\left(\frac{W_{2s}}{W_{2p}}\right)^{1/2}(\boldsymbol{k}\boldsymbol{\mathcal{E}}) \tag{7.11}$$

The numerical result reduces to the estimation of $|\delta x_{\mathrm{NR}}| \approx 10^{-4}$ Hz.

Thus, a direct observation of this difference also seems very improbable at present. Note, however, that the part of the correction x_{NR} independent of the field direction and therefore equal for atoms H and $\bar{\mathrm{H}}$ is only three orders of magnitude smaller than the experimental error [137].

7.3. Two-photon $1s - 2s$ resonance: H and $\bar{\mathrm{H}}$ atoms in an external electric field

In this section, the NR correction to the transition frequency for the $1s - 2s$ two-photon resonance in H and $\bar{\mathrm{H}}$ atoms is calculated. Measurements made in the hydrogen atom with an accuracy of about 46 Hz are considered as an experimental basis for this kind of study [134, 182].

In [182], a simplified quantum mechanical approach based on the density matrix formalism was used to describe the shape of the resonance line of the $1s - 2s$ two-photon excitation process with delayed fluorescence registration due to the application of an electric field. In [37], an estimate of x_{NR} based on purely phenomenological considerations was presented (see section 4 of the thesis). In this part of the thesis a description of the opposite process to the one considered in the [43]: two-photon $1s - 2s$ excitation and decay in an external electric field is presented. The case considered here will correspond to $\xi_{\mathrm{S}} = 1$,

and the case of [43] corresponds to $\xi_S = 0$.

It should be emphasised that the process considered here also differs from the real experiment [134, 182], where the electric field is present only in the region of fluorescence registration, not in the "excitation part". The process with the constant presence of the electric field, of course, loses much of the advantages of the experimental approach developed in the [134, 182], and should provide much lower precision. However, it is this approach that is more realistic in experiments aimed at finding the difference between the spectral characteristics of H and $\bar{\text{H}}$ atoms [73, 74].

Using the previous approximations, including the neglect of Stark shifts of atomic levels, the cross section of the process was represented in [38] as follows:

$$\sigma \sim \frac{W_{2s',2\gamma}(\boldsymbol{k}')W_{2s',1\gamma}(\boldsymbol{k})}{x^2 + \frac{1}{4}\Gamma_{2s'}^2} + \frac{W_{2p',2\gamma}(\boldsymbol{k}')W_{2p',1\gamma}(\boldsymbol{k})}{(x + \Delta E_L)^2}. \tag{7.12}$$

Indeces 2γ, 1γ denote two- and one-photon absorption and emission processes $2s' \leftrightarrow 1s+2\gamma$, $2p' \leftrightarrow 1s+2\gamma$, $2s' \leftrightarrow 1s+\gamma$, $2p' \leftrightarrow 1s+\gamma$, and $x = E_{2s'} - E_{1s} - \omega$ (as before).

Repeating the calculations outlined in section 7.1, the following expression arises for the nonresonant correction:

$$x_{\text{NR}} = -\frac{1}{16}\frac{\Gamma_{2s'}^4}{\Delta E_L^3}\frac{W_{2p',2\gamma}(\boldsymbol{k}')W_{2p',1\gamma}(\boldsymbol{k})}{W_{2s',2\gamma}(\boldsymbol{k}')W_{2s',1\gamma}(\boldsymbol{k})} \tag{7.13}$$

The maximum nonresonant contribution corresponds to the case $\xi_S = 1$. Then, by considering $\Gamma_{2s'} = \Gamma_{2p}$ and $W_{2p',2\gamma}(\boldsymbol{k}') \approx W_{2s',2\gamma}(\boldsymbol{k}')$, $W_{2p',1\gamma}(\boldsymbol{k}) \approx W_{2s',1\gamma}(\boldsymbol{k}) \approx \Gamma_{2p}$, the same result as for the one-photon $1s-2p$ transition can be obtained: the field direction-independent correction is $x_{\text{NR}} \approx -6.4$ kHz. The same result is obtained for the correction that depends on the field direction: $|\delta x_{\text{NR}}| \approx 10^{-4}$ Hz.

Thus, it is shown that the resonance spectra in an external electric field are different for H and $\bar{\text{H}}$ atoms. Estimates show that the positions of the maxima of the line profiles for the Ly_α resonances in H and $\bar{\text{H}}$ atoms are shifted relative to each other by $\sim 2 \times 10^{-4}$ Hz. The same applies to the two-photon transitions in the $1s+2\gamma \to 2s$ absorption processes occurring in an external electric field.

Moreover, in an electric field with $\xi_{\rm S} = 1$, the nonresonant corrections independent of the field direction appear to be several orders of magnitude larger than the nonresonant corrections in the absence of the field. This enhancement is due to the overlap of resonances with the same quantum numbers. The latter has been theoretically studied for highly charged ions in [133]. In the case of hydrogen and anti-hydrogen atoms the levels $2p'$, $2s'$ in the field $\xi_{\rm S} = 1$ do not actually overlap, but in contrast to the levels $2p$, $2s$ they have the same quantum numbers. Since these levels are still close to each other, their mutual influence leads to large NR corrections.

It is also worth mentioning another effect that looks different in atoms H and $\bar{\rm H}$ placed in an external electric field. This is the effect of quantum beats in Ly_α radiation. It has been investigated theoretically and experimentally by many authors, see, for example, [230–232] and the corresponding references in these papers. In the case of hydrogen and anti-hydrogen atoms, the effect of quantum beats was considered in Refs. [233, 234].

In conclusion on the NR corrections in the external electric field, it is worth noting that the above estimates are rather rough and indicate only an order of magnitude of the spectral line asymmetry. The presence of an external electric field in experiments related to the measurement of frequencies in the anti-hydrogen atom [73, 74] is rather insignificant at this stage [73]. Moreover, measurements of transition frequencies in $\bar{\rm H}$ have an error on the order of a few MHz [74] for the Ly_α line and fractions of MHz for the hyperfine splitting of the ground state [73]. This circumstance makes the results presented above rather unobservable at present. However, a detailed comparison of the spectra of H and $\bar{\rm H}$ atoms is extremely important for the verification of, e.g., CPT symmetry, and hence improving the experimental accuracy is a priority. Thus, on the basis of the fact that the field-linear effects of spectral line asymmetry lead to opposite profile distortions, one can conclude the importance of these results.

7.4. Atoms H and $\bar{\text{H}}$ in an external magnetic field

This section deals with the atoms H and $\bar{\text{H}}$ in an external field. The main goal here is to investigate possible spectroscopic differences between hydrogen and anti-hydrogen atoms. Electric and magnetic fields are actually applied in all experiments on the synthesis of anti-hydrogen atoms [66,70,72,223]. Therefore, it is necessary to study all spectroscopic properties of the $\bar{\text{H}}$ atom to search for contributions in expressions for energy level splittings, shifts, or transition probabilities that may provide a distinction between H and $\bar{\text{H}}$ atoms.

The Hamiltonian of a hydrogen atom (anti-hydrogen) in homogeneous electric and magnetic external fields has the form:

$$\hat{H} = \hat{H}_0 - \hat{\boldsymbol{d}}\boldsymbol{\mathcal{E}} - \hat{\boldsymbol{\mu}}\boldsymbol{\mathcal{H}}, \tag{7.14}$$

where $\hat{H}_0$ is the Hamiltonian in the absence of external fields, $\hat{\boldsymbol{d}} = \mp|e|\boldsymbol{r}$ is the electric dipole moment operator of the electron (positron), $\boldsymbol{r}$ is the radius-vector of the light particle, $|e|$ is the absolute value of the electron charge, $\hat{\boldsymbol{\mu}} = -\mu_0(\hat{\boldsymbol{L}} + 2\hat{\boldsymbol{S}})$ is the magnetic dipole moment operator, $\hat{\boldsymbol{L}}$ and $\hat{\boldsymbol{S}}$ are the orbital and spin operators of the electron (positron) momentum, $\mu_0 = \mp|e|\hbar/2mc$ is the Bohr magneton, m is the mass of the light particle, and finally, $\boldsymbol{\mathcal{E}}$ and $\boldsymbol{\mathcal{H}}$ are the strengths of the external electric and magnetic fields. In expression (7.14), the quadratic contributions in the magnetic field are neglected. The Hamiltonian $\hat{H}_0$ is invariant with respect to charge conjugation, but the full Hamiltonian $\hat{H}$ breaks this symmetry. This circumstance can lead to differences in the spectra of atoms H and $\bar{\text{H}}$. Of interest are the contributions that depend linearly on the field strength, since they are proportional to the charge of light particles and, therefore, of opposite sign for hydrogen and anti-hydrogen atoms.

The linear Stark effect $\Delta E = -\boldsymbol{\mathcal{E}}\langle\hat{\boldsymbol{d}}\rangle$, where $\langle\hat{\boldsymbol{d}}\rangle$ is the averaged dipole moment operator, is forbidden due to symmetry in the combined charge-space parity (CP) transformation, or time reversal (T) transformation if there is no CPT violation. If $\langle\hat{\boldsymbol{d}}\rangle \neq 0$, then the proportionality $\langle\hat{\boldsymbol{d}}\rangle \sim \hat{\boldsymbol{S}}$ should exist, but then it violates P and T invariance. The linear Stark effect in the hydrogen atom is actually pseudo-linear, because the splitting between the $2s$ and $2p$

states in an external electric field is proportional to $\langle 2s|\hat{\boldsymbol{d}}\boldsymbol{\mathcal{E}}|2p\rangle = \sqrt{3}ea_0\mathcal{E}$ (Stark coefficient), where a_0 is the Bohr radius. This effect occurs when the formula for the energy shift $\Delta E = \sqrt{\langle 2s|\hat{\boldsymbol{d}}\boldsymbol{\mathcal{E}}|2p\rangle^2 + \Delta E_L^2}$ neglects the Lamb shift ΔE_L. So ΔE is the same for atoms H and $\bar{\text{H}}$.

A comparison of the spectra of hydrogen and anti-hydrogen atoms based on the Zeeman effect for the Ly_α transition was carried out in [39], see also [235]. Zeeman splitting is proportional to μ_0, which has opposite signs for electrons and positrons, respectively. Thus, the splitting pattern is the same for atoms H and $\bar{\text{H}}$, but the upper and lower Zeeman components correspond to different values of the electron angular momentum projections. This is the simplest spectroscopic difference between hydrogen and anti-hydrogen atoms in external fields. The experimental observation of this effect requires only an analysis of the polarisation of the radiation and depends on the number of available atoms $\bar{\text{H}}$. If the direction of photon emission coincides with the direction of the magnetic field, the high-frequency component of the Zeeman doublet has a left circular polarisation and the low-frequency component has a right circular polarisation. The picture is opposite for H atom [39, 235].

A more complicated situation arises in the presence of external electric and magnetic fields. Referring to the works of [39, 103, 235] this analysis is not carried out further. It should be emphasised, however, that the case of parallel fields (electric and magnetic) makes it possible to distinguish spectroscopically between hydrogen and anti-hydrogen atoms. As a consequence, in [127] it was proposed to use this phenomenon to search for anti-matter in the Universe.

In particular, the 21 cm absorption line (HFS of the ground state) in the hydrogen atom, which is of particular importance in the study of the factors and mechanisms responsible for the formation of gas-dust clouds in the interstellar medium (ISM), their role in stellar evolution, etc., can serve this purpose. [236]. The precision of the observations achieved gives a detailed picture of the 21 cm absorption line profile, see, e.g., [237]. In this case, the most important fact is that the Zeeman splitting can be resolved in such observations [238].

The analysis of the polarisation of the 21 cm line radiation is reduced to the calculation of the matrix element corresponding to the transition between the hyperfine components of the ground state in the hydrogen atom. Assuming the

registration of radiation along the field direction (see details in [127]), it was found that

$$\langle n\,1\,M_F|\boldsymbol{e}[\boldsymbol{k}\times\boldsymbol{\mu}]|n\,0\,0\rangle = -\mathrm{i}\sqrt{\frac{2}{3}}(-1)^{M_F}\sum_r C^{1-M_F}_{1r\;00}e_r\,k_0\,\langle n\frac{1}{2}||\mu_1||n\frac{1}{2}\rangle. \quad (7.15)$$

Here the matrix element from the magnetodipole radiation operator [6] is obtained for an arbitrary value of the principal quantum number n and corresponds to the transition from the upper sublevel of the hyperfine structure (with total atomic momentum $F = 1$ and projection M_F) of the one-electron state of the atom with orbital momentum equal to zero to the sublevel with $F' = 0$ and, therefore, $M_{F'} = 0$. For the ground state of the hydrogen atom, this transition is shown in Fig. 7.1 and corresponds to the 21 cm line.

The reduced matrix element (see [179]) in (7.15), as well as the common factor, are not important for further analysis. What is important is that the Clebsch-Gordan coefficient, $C^{1-M_F}_{1r\;00}$, is different from zero at $r = -M_F \neq 0$. Circular polarisation with $r = \pm 1$ (clockwise and anticlockwise) occurs at the transition between the lower ($M_F = -1$) or upper ($M_F = +1$) Zeeman components of the excited ($F = 1$) and ground ($F' = 0$) hyperfine sublevels. Linear polarisation corresponds to the transition $n10 \to n00$ ($F = 1\,M_F = 0 \to F' = 0\,M_{F'} = 0$) [5].

Considering that the lowest-order splitting in the magnetic field is defined according to $\mu_0\,g\,M_F\mathcal{H}$, where g is the Landé factor, M_F is the magnetic quantum number of the corresponding state, the values of M_F for the lower and upper components of the Zeeman splitting for atoms H and $\bar{\mathrm{H}}$ have opposite signs at a fixed field direction. Therefore, the blue and red wings of the line profile have different polarisation for hydrogen and anti-hydrogen atoms with the same field direction, see Fig. 7.1. The maximum of the effect corresponds to the case of completely separated Zeeman sublevels (non-overlapping Zeeman absorption/emission lines).

For typical magnetic fields of the order of 10^{-5} Gs, the distance between hyperfine sublevels is much smaller than the 21 cm linewidth. The corresponding Zeeman splitting in a field of 10^{-5} Gs is about 14 Hz, and the line width ex-

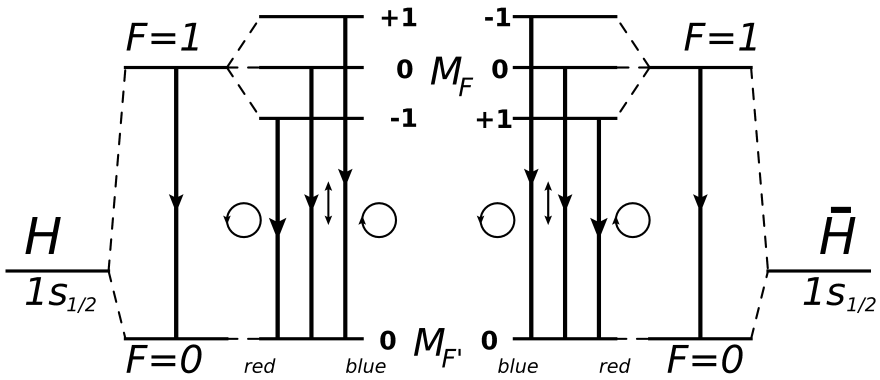

Figure 7.1. Level scheme of the ground $1s_{1/2}$ state in hydrogen (H) and antihydrogen ($\bar{\text{H}}$) atoms. The levels are depicted taking into account the spin of the nucleus (the total momentum F) and the Zeeman splitting corresponding to the splitting of degenerate sublevels with different magnetic quantum numbers M_F. The linear polarisation corresponding to the transition $F\,M_F = 1\,0 \to F'\,M_{F'} = 0\,0$, is shown by the up-down arrow. The left and right circular polarisations are indicated by circles with arrows.

ceeds kHz at a temperature of 100 K because of the large Doppler broadening. Therefore, absorption lines are usually chosen to detect the Zeeman effect; absorption lines occur in colder gas and hence have smaller widths. The weakness of the Zeeman splitting in the interstellar medium allows it to be observed only in regions where the interstellar fields are stronger and the gas temperature is lower than average, i.e., in sufficiently dense clouds. Thus, the observation of two separate peaks of the line profile is generally speaking difficult. At the same time, there are situations when the Zeeman effect is detected in the 21 cm [239] line. The polarisation of hyperfine sublevels is potentially measurable if the magnetic field strength is such that the magnitude of the difference between the left and right polarisations exceeds the detector noise [240]. Thus, in principle, it is not necessary to observe Zeeman splitting to find an anti-hydrogen atom; it would be sufficient to detect different polarisations in the blue and red wings of the 21 cm line profile.

Another effect that also allows one to distinguish between hydrogen and anti-hydrogen atoms in a magnetic field is the Faraday rotation, that is, the rotation of the plane of linear polarisation around the direction of propagation of light. The central component of the 21 cm line profile corresponding to the transition $M_F = 0 \to M_{F'} = 0$ (see Fig. 7.1) is linearly polarised, and the

plane of this polarisation rotates around the direction of light propagation in opposite directions for atoms H and $\bar{\text{H}}$. Thus, the Faraday effect on this central line can also be used to distinguish between atoms H and $\bar{\text{H}}$, provided that the direction of the external magnetic field is known. Faraday rotation is often used to observe the polarisation and emission geometry of pulsars, see, e.g., [241].

Chapter 8.

One- and two-photon transition rates

This chapter is mainly devoted to the calculation of one- and two-photon transitions both in the absence (spontaneous emission) and in the presence of an external electric field. The chapter starts with general statements and refers to the material presented in the book [242]. Nevertheless, in view of the use of the latter to verify the results, a summary of these basics seems appropriate. Furthermore, in contrast to the previous sections, a different and also well known representation for the multipole expansion of the photon wave function will be used here, namely the multipole operators for the photon will be represented in terms of the polarisation and wave vector of the photon [243]. This representation is convenient for revealing the influence of the external electric field on the transition probabilities and the corresponding comparative analysis of the spectra of atoms H and $\bar{\mathrm{H}}$. In addition to the calculation of one- and two-photon transition probabilities as applied to H and $\bar{\mathrm{H}}$ atoms, problems related to astrophysical studies of cosmic microwave background radiation (CMB) are considered.

8.1. Transition probabilities in different forms and gauges

This section describes different calibrations combined with different "forms" for the one-photon transition probability [242]; the atomic system of units $\hbar = e = m = 1$ is used.

The probability of emission of a photon with a certain angular momentum and parity in an arbitrary gauge can be described in the first order of perturbation theory as follows:

$$W_{A\,A'} = \sum_{kq} \left[\left| \langle A' | \left(\boldsymbol{\alpha}\, {}_{\mathrm{e}}\boldsymbol{A}_{\omega kq}(\boldsymbol{r}) \right) + \Phi_{\omega kq}(\boldsymbol{r}) | A \rangle \right|^2 + \left| \langle A' | \boldsymbol{\alpha}\, {}_{\mathrm{m}}\boldsymbol{A}_{\omega kq}(\boldsymbol{r}) | A \rangle \right|^2 \right], \quad (8.1)$$

where ${}_{\mathrm{e}}\boldsymbol{A}_{\omega kq}$ and ${}_{\mathrm{m}}\boldsymbol{A}_{\omega kq}$ denote the electric and magnetic vector potentials, and $\Phi_{\omega kq}$ corresponds to the scalar potential; ω is the photon frequency, k, q are the momentum and projection of the emitted photon. The states $|A\rangle$ and $\langle A'|$ are stationary solutions of the Dirac equation (wave functions) with energies E_A and $E_{A'}$, and $\boldsymbol{\alpha}$ denote the Dirac matrices.

In the momentum representation these potentials take the form:

$$ {}_{\mathrm{e}}\boldsymbol{A}_{\omega kq}(\boldsymbol{k}) = \frac{4\pi^2 c^{3/2}}{\omega^{3/2}} \delta\left(k - \frac{\omega}{c}\right) \left({}_{\mathrm{e}}\boldsymbol{Y}_{kq}(\boldsymbol{n_k}) + \mathcal{K} \boldsymbol{n_k} Y_{kq}(\mathbf{n_k}) \right) , \quad (8.2)$$

$$ {}_{\mathrm{m}}\boldsymbol{A}_{\omega kq}(\boldsymbol{k}) = \frac{4\pi^2 c^{3/2}}{\omega^{3/2}} \delta\left(k - \frac{\omega}{c}\right) {}_{\mathrm{m}}\boldsymbol{Y}_{kq}(\boldsymbol{n_k}) , \quad (8.3)$$

$$ \Phi_{\omega kq}(\boldsymbol{k}) = \frac{4\pi^2 c^{3/2}}{\omega^{3/2}} \delta\left(k - \frac{\omega}{c}\right) \mathcal{K} Y_{kq}(\boldsymbol{n_k}) . \quad (8.4)$$

Here $\boldsymbol{k}$ denotes the variable in the momentum representation, the speed of light c is written out for clarity. The functions ${}_{\mathrm{e}}\boldsymbol{Y}_{kq}$ and ${}_{\mathrm{m}}\boldsymbol{Y}_{kq}$ are vector spherical harmonics of electric and magnetic type, respectively, Y_{kq} is the ordinary spherical harmonic, and $\mathcal{K}$ is the gauge constant. The potentials ${}_{\mathrm{e}}\boldsymbol{A}_{\omega kq}(\boldsymbol{k})$, ${}_{\mathrm{m}}\boldsymbol{A}_{\omega kq}(\boldsymbol{k})$ in the momentum representation are related to the expressions (2.12)-(2.14). Using the Fourier transform, they can be defined in the coordinate representation according to (2.9)-(2.11), see e.g. [244] (here and below $k = j_\gamma$).

Two gauges are commonly used: the so-called Coulomb gauge, corresponding

to the conditions $\nabla \cdot \mathbf{A} = \nabla \cdot {}_{\mathrm{e}}\mathbf{A} = 0$ and characterised by the choice of the gauge parameter $\mathcal{K} = 0$; another convenient gauge is determined by the value of the parameter $\mathcal{K} = -\sqrt{\frac{k+1}{k}k}$. The calculations are usually carried out in several gauges: "length", $\mathcal{K} = 0$, and "velocity", $\mathcal{K} = -\sqrt{\frac{k+1}{k}k}$), which serves as an independent test of the correctness of the result (the final answer has to be gauge invariant).

However, using the integral relation for the wave functions of the Dirac equation [2],

$$\mathrm{i}\int \psi^*_{A'}\,(\boldsymbol{\alpha}\boldsymbol{\nabla}\chi)\,\psi_A\,d^3\tau = \frac{\omega}{c}\int \psi^*_{A'}\chi\psi_A\,d^3\tau, \tag{8.5}$$

where χ is an arbitrary function, two expressions can be obtained for the emission probability of the Ek-photon (see details in [242] as well as [114]):

$$W^{\mathrm{E}k}_{A\,A'} = \frac{2(k+1)\omega^3}{k(2k+1)c}\left|\langle A'|{}_rO^{(k)}_{-q} + \mathcal{K}\sqrt{\frac{k}{k+1}}\left[\frac{1}{\omega}{}_vO^{(k)}_{-q} - {}_rO^{(k)}_{-q}\right]|A\rangle\right|^2, \tag{8.6}$$

$$W^{\mathrm{E}k}_{A\,A'} = \frac{2(k+1)\omega}{k(2k+1)c}\left|\langle A'|{}_vO^{(k)}_{-q} + \mathcal{K}\sqrt{\frac{k}{k+1}}\left[{}_vO^{(k)}_{-q} - \omega\,{}_rO^{(k)}_{-q}\right]|A\rangle\right|^2, \tag{8.7}$$

where the relativistic radiation operators are defined according to

$$\begin{aligned}{}_vO^{(k)}_{-q} = -\mathrm{i}\Bigg[&k\sqrt{\frac{2k+3}{k+1}}g_{k+1}(\omega r)\left[C^{(k+1)}\times\alpha^{(1)}\right]^{(k)}_{-q} \\ &+\sqrt{k(2k-1)}g_{k-1}(\omega r)\left[C^{(k-1)}\times\alpha^{(1)}\right]^{(k)}_{-q}\Bigg],\end{aligned} \tag{8.8}$$

$${}_rO^{(k)}_{-q} = -\frac{2k+1}{\omega}\left[g_k(\omega r)C^{(k)}_{-q} + \mathrm{i}\sqrt{\frac{2k+3}{k+1}}\left[C^{(k+1)}\times\alpha^{(1)}\right]^{(k)}_{-q}g_{k+1}(\omega r)\right]. \tag{8.9}$$

The notations used here are: $C^{(k)}_{-q} =$
$sqrt\frac{4\pi}{2k+1}Y_{k\,-q}$, $[a^{(s_1)}\times b^{(s_2)}]^{(s)}_q$ is the tensor product of two irreducible spherical tensors of rank s_1 and s_2, related to a spherical tensor of rank s with components q (notation is preserved according to [242]). The second expression, (8.7), was obtained using (8.5), and the relativistic radiation operators (8.8), (8.9) in the

nonrelativistic limit reduce to the well-known expressions for the multipole decomposition of the photon wave function [244].

Thus, there are two different (equivalent) forms of the Ek-transition probability (expressions (8.6) and (8.7)) together with an arbitrary choice of the gauge constant $\mathcal{K}$. Choosing $\mathcal{K} = 0$, the operator in (8.6) corresponds to a transition operator in the "velocity" form, and when $\mathcal{K} = -\sqrt{\frac{k+1}{k}}$ it is related to a transition operator in the "length" form. However, the consistency of a certain choice of gauge with a certain type of transition operator is not unique. Taking into account the expression (8.7), one can specify that the choice of $K = 0$ transforms the emission operator into "length" and $K = -\sqrt{\frac{k+1}{k}}$ into the form of "velocity". Finally, as the main conclusion of this section, it can be deduced that the transformation (8.5) for the wave function can be used along with the gradient transformation of the radiation operator to verify the result. Nevertheless, in the following, the commonly accepted treatment of this issue is used: the gradient transformation of the radiation operator to verify the results of calculations of transition probabilities.

8.2. Probability of one-photon radiation in the Pauli approximation

In this section we consider the process of one-photon radiation in a one-electron atom. The Pauli approximation [243] is used for the radiation operator. Using the "standard" fully relativistic S-matrix formalism, the radiation amplitude can be obtained as follows. According to [2], the process of one-photon radiation can be described by the S-matrix element

$$S_{A\,A'} = e\sqrt{\frac{4\pi}{2\omega}} \int d^4x \overline{\psi}_{A'}(x) \hat{e}^{(\lambda)*}_{\mu} \gamma^{\mu} e^{-\mathrm{i}(\boldsymbol{kr}-\omega t)} \psi_A(x), \tag{8.10}$$

where the relativistic system of units and notations corresponding to the previous sections are used. After integration on the time variable, the amplitude

of the transverse photon emission is reduced to (see [106])

$$A_{A\,A'}(\boldsymbol{k},\boldsymbol{e}) = \left(\sqrt{2\pi\omega}/e\right) U_{A\,A'} = \langle A'|\boldsymbol{e}\boldsymbol{\alpha}e^{-\mathrm{i}\boldsymbol{k}\boldsymbol{r}}|A\rangle. \tag{8.11}$$

The expression for the transition probability integrated over the emission angles of photons $\boldsymbol{\nu} = \boldsymbol{k}/\omega$ and summed over polarisations $\boldsymbol{e}$ is given by the expression:

$$W^{(1\gamma)}_{A\,A'} = \frac{e^2\omega_{A\,A'}}{2\pi}\sum_{\boldsymbol{e}}\int d\boldsymbol{\nu}\,|A_{A\,A'}(\boldsymbol{k},\boldsymbol{e})|^2\,. \tag{8.12}$$

Here, the integration over frequency is removed due to the δ-function arising after integration over the time variables. As a consequence, $\omega = |\boldsymbol{k}| = \omega_{A\,A'} = E_A - E_{A'}$ (it is assumed that the final state A' is located below the initial state A, hence $\omega_{A\,A'} > 0$). The energies $E_{A'}$ and E_A are the Dirac energies of the atomic levels A' and A, respectively. The integral over $d\boldsymbol{\nu}$ comes from the phase volume $d\boldsymbol{k} = \omega^2 d\omega d\boldsymbol{\nu}$. For summation on polarisations of the photon $\boldsymbol{e}$ the following relation can be employed:

$$\sum_{\boldsymbol{e}} e_i e_k = \delta_{ik} - \nu_i\nu_k, \tag{8.13}$$

and the integral $\int d\boldsymbol{\nu}$ can be calculated using

$$\begin{aligned}
\int d\boldsymbol{\nu} &= 4\pi, \\
\int d\boldsymbol{\nu}\nu_i = \int d\boldsymbol{\nu}\nu_i\nu_k\nu_k &= \int d\boldsymbol{\nu}\mathrm{odd} = 0, \\
\int d\boldsymbol{\nu}\nu_i\nu_k &= \frac{4\pi}{3}\delta_{ik}, \\
\int d\boldsymbol{\nu}\nu_i\nu_k\nu_j\nu_l &= \frac{4\pi}{15}(\delta_{ik}\delta_{jl} + \delta_{ij}\delta_{kl} + \delta_{il}\delta_{kj}).
\end{aligned} \tag{8.14}$$

Calculation of photon absorption (emission) amplitudes in the Pauli approximation (denoted hereafter by the upper index P) transforms the formula

(8.12) to

$$W^{(1\gamma)}_{A\,A'} = \frac{e^2\omega_{A\,A'}}{2\pi}\sum_{\boldsymbol{e}}\int d\boldsymbol{\nu}\left|A^P_{A\,A'}(\boldsymbol{k},\boldsymbol{e})\right|^2, \tag{8.15}$$

где амплитуда $A^P_{A\,A'}(\boldsymbol{k},\boldsymbol{e})$ (см. [243]) определена следующим выражением:

$$A_{A\,A'}(\boldsymbol{k},\boldsymbol{e}) = \left([(\boldsymbol{e}\boldsymbol{p}) + \mathrm{i}[\boldsymbol{k}\times\boldsymbol{s}]]\,e^{-\mathrm{i}\boldsymbol{k}\boldsymbol{r}}\right)_{A\,A'}. \tag{8.16}$$

Here $\boldsymbol{p} = -\mathrm{i}\boldsymbol{\nabla}$ is the non-relativistic momentum operator, $\boldsymbol{s} = \boldsymbol{\sigma}/2$ is the electron spin operator, and $\boldsymbol{\sigma}$ is the Pauli matrices. The brackets $(\dots)_{A\,A'}$ mean that the matrix element is calculated using nonrelativistic wave functions. In the case of the dipole approximation $exp(-\mathrm{i}\boldsymbol{k}\boldsymbol{r}) \approx 1$, the first summand of the matrix element (8.16) describes the emission of the E1 photon (electric dipole photon), and the second summand corresponds to the magnetic M1 transition (magnetic dipole photon). Possible transitions between atomic levels are defined according to the selection rules [6].

Higher multipoles can be obtained by considering the exponent decomposition in (8.16). In particular, it can be obtained (see [112, 114])

$$A^P(\boldsymbol{e},\boldsymbol{k}) = ((\boldsymbol{e}^*\boldsymbol{p}) + i(\boldsymbol{e}^*[\boldsymbol{k}\times\boldsymbol{s}]))e^{-i\boldsymbol{k}\boldsymbol{r}} \tag{8.17}$$
$$\approx \frac{im}{\hbar}[H,\boldsymbol{e}^*\boldsymbol{r}] + \frac{m}{2\hbar}[H,(\boldsymbol{e}^*\boldsymbol{r})(\boldsymbol{k}\boldsymbol{r})] + \frac{i}{2}\left(\boldsymbol{e}^*[\boldsymbol{k}\times([\boldsymbol{r}\times\boldsymbol{p}]+2\boldsymbol{s})]\right).$$

The first term in this expression represents the electric dipole moment of the emitted photon, the second term is the electric quadrupole moment, and the last term in (8.17) represents the magnetic dipole moment of the emitted photon, proportional to the magnetic moment operator $\sim \boldsymbol{l} + 2\boldsymbol{s}$, $\boldsymbol{l} \equiv [\boldsymbol{r}\times\boldsymbol{p}]$. For brevity, the details of the transformations are omitted, as well as the following contributions.

The order of magnitude of the corresponding multipole radiation contributions can be estimated in the standard way. For instance, for the atomic electron, the following relation holds: $r \sim a_0 = 1/m\alpha Z$ (a_0 is the Bohr radius, m is the electron mass, $\alpha \approx 1/137$ is the fine structure constant), the characteristic transition frequency $\omega \approx m(\alpha Z)^2$ and hence $kr \sim \alpha Z$. Averaging (8.17)

on the wave functions according to (8.16), the action of the Hamilton operator H (hats omitted for brevity) reduces to the energy difference or (which is the same as well) to the transition frequency $\omega_{A\,A'}$.

As an example, one can calculate the one-photon $2s-1s$ transition in the hydrogen atom (see [106, 243] and related references). This electron transition is accompanied by the emission of a M1 photon. For the calculation one should use, respectively, the third summand in (8.17) and the wave function in the Pauli approximation in the form:

$$\psi_{njlm}(\boldsymbol{r}) = \sum_{m_l,m_s} C^{jm}_{lm_l\ sm_s} R_{nl}(r) Y_{lm_l}(\boldsymbol{n}_{\boldsymbol{r}}) \chi_{m_s}. \tag{8.18}$$

Here the atomic state is given by the following set of quantum numbers: n is the principal quantum number, jm is the total angular momentum of the electron and its projections (respectively) and the orbital momentum l. Since one-electron states will be considered, the electron spin is always equal to 1/2. The spin part of the wave function of the electron is given by χ_{m_s}, and the summation is carried out by the projections of the orbital momentum m_l and spin m_s. The amplitude of the transition is

$$A^P_{2s_{1/2}m,1s_{1/2}m'} = -\mathrm{i}k^2 \langle m|\boldsymbol{e}[\boldsymbol{k}\times\boldsymbol{\sigma}]|m'\rangle R_{2s,1s}, \tag{8.19}$$

$$R_{2s,1s} = \int\limits_0^\infty dr\, r^4 R_{2s}(r) R_{1s}(r).$$

The integral $R_{2s,1s}$ arises taking into account the relativistic correction to the wave function (see [243] for details). Taking into account the estimates above, the final result is

$$W^{(1\gamma)}_{2s,1s} = \frac{1}{972} m\alpha(\alpha Z)^{10} = 2.8\times 10^{-6}\ \mathrm{c}^{-1}. \tag{8.20}$$

To conclude the section, it is worth noting that the representation of the radiation operator in the form (8.17) turns out to be convenient when the external field is taken into account, since it allows one to determine quite simply the correlation of the direction of the emitted photon ($\boldsymbol{k} = \omega\boldsymbol{\nu}$) with the field

direction. The latter is expressed by the scalar product $(\boldsymbol{k}\boldsymbol{\mathcal{E}})$.

8.3. Two-photon decay probabilities of $2s$ and $2p$ states in the hydrogen atom

An important continuation of the previous section is the calculation of probabilities of two-photon emission processes. In particular, it is well known that the dominant decay channel of the $2s$ state in the hydrogen atom (hydrogen-like atomic systems) is $E1E1$ two-photon radiation (emitting two electric dipole photons, see (8.17)). A careful calculation in the framework of the nonrelativistic theory was presented in [245] (see also relevant references to earlier papers). $E1E1$ two-photon emission has played an essential role in many studies, including the astrophysics (see, for example, [77, 79]) and laboratory problems (see, for example, [134, 182]). Calculations of two-photon multipole transitions based on the results of sections 3.2, 8.1 were carried out in [111], and a careful fully relativistic calculation was presented in [110], where the probabilities of two-photon $E1E1$, $E1E2$, and $E1M1$ transitions were calculated.

In the nonrelativistic approximation, using the expansion of the Coulomb Green's function through the eigenfunctions (3.14), (3.15), the probability of the two-photon decay process for arbitrary electric photons Ek and Ek' takes the form:

$$dW^{EkEk'}_{A\,A'} = \frac{2\pi}{2l_A+1}\sum_{qq'm_Am_{A'}}\Bigg|\sum_{lm_l}\int\int d\boldsymbol{r}_1 d\boldsymbol{r}_2\, R_{n_{A'}l_{A'}}(r_1)Y^*_{l_{A'}m_{A'}}(\boldsymbol{n}_{\boldsymbol{r}_1})\times \tag{8.21}$$

$$V^{\mathrm{E}k}(\boldsymbol{r}_1)g_l(\nu;r_1,r_2)Y_{lm_l}(\boldsymbol{n}_{\boldsymbol{r}_1})Y^*_{lm_l}(\boldsymbol{n}_{\boldsymbol{r}_2})V^{\mathrm{E}k'}(\boldsymbol{r}_2)R_{n_Al_A}(r_2)Y_{l_Am_A}(\boldsymbol{n}_{\boldsymbol{r}_2})+$$

$$\sum_{lm_l}\int\int d\boldsymbol{r}_1 d\boldsymbol{r}_2\, R_{n_{A'}l_{A'}}(r_1)Y^*_{l_{A'}m_{A'}}(\boldsymbol{n}_{\boldsymbol{r}_1})V^{\mathrm{E}k'}(\boldsymbol{r}_1)g_l(\nu';r_1,r_2)Y_{lm_l}(\boldsymbol{n}_{\boldsymbol{r}_1})$$

$$\times Y^*_{lm_l}(\boldsymbol{n}_{\boldsymbol{r}_2})V^{\mathrm{E}k}(\boldsymbol{r}_2)R_{n_Al_A}(r_2)Y_{l_Am_A}(\boldsymbol{n}_{\boldsymbol{r}_2})\Big|^2 d\omega,$$

where $V^{Ek}(\boldsymbol{r}) = \sqrt{(k+1)/k}(2\omega^{k+1/2}/(2k+1)!!)r^kY_{k\,-q}$ represents the corresponding photon multipole written in the gauge $\mathcal{K} = -\sqrt{(k+1)/k}$, $\nu = Z/\sqrt{-2(E_A-\omega)}$, $\nu' = Z/\sqrt{-2(E_A-\omega')}$, and photon frequencies are related

according to the energy conservation law by the relation $\omega' = E_A - E_{A'} - \omega$ [111, 112, 114].

For the case of $E1E1$ two-photon radiation, all calculations can be performed analytically, except for the finite integration over the ω frequency. The final result can be represented in the form:

$$W^{E1E1}_{2s,1s} = \frac{1}{2}\int_0^{\omega_0} dW^{E1E1}_{2s,1s}(\omega) = 0.00131823\,(\alpha Z)^6\ \text{a.u.}, \tag{8.22}$$

$$W^{E1E1}_{2s,1s} = 8.22932\ \text{c}^{-1}\ (Z=1),$$

where $\omega_0 = E_{2s} - E_{1s}$. The expression (8.22) specifies the Z-dependence of the transition probability $W^{E1E1}_{2s,1s}$. The numerical value of (8.22) coincides perfectly with the most accurate result [246].

8.3.1. Two-photon $E1E2$ decay for the state $2p$

The expression (8.21) is general for arbitrary two-photon transitions. The result for the $E1E2$ (dipole-quadrupole two-photon emission) transition can be obtained as follows. By setting the states $A = 2p$, $A' = 1s$ and considering that in this case the angular momentum of the photon can take values $k = 1, 2$, four different summands arise due to photon permutations in the radiation amplitude. After angular integration and summation over projections, see [114], it turns out

$$dW^{E1E2}_{2p,1s}(\omega) = \frac{2^2\omega^3\omega'^3}{3^3 5^2 \pi}\left[\omega'^2\left|I_1(\omega') + I_2(\omega)\right|^2 + \omega^2\left|I_1(\omega) + I_2(\omega')\right|^2\right] d\omega, \tag{8.23}$$

where

$$I_1(\omega) = \frac{1}{\sqrt{6}}\int_0^\infty\int_0^\infty dr_1 dr_2\, r_1^3 r_2^5\, e^{-r_1-\frac{r_2}{2}}\, g_1(E_A - \omega; r_1, r_2), \tag{8.24}$$

$$I_2(\omega) = \frac{1}{\sqrt{6}}\int_0^\infty\int_0^\infty dr_1 dr_2\, r_1^4 r_2^4\, e^{-r_1-\frac{r_2}{2}}\, g_2(E_A - \omega; r_1, r_2), \tag{8.25}$$

Substituting again the expression for the radial part of the Coulomb Green's function (3.15), the radial integrals in (8.24) and (8.25) can be calculated analytically.

As a result, the final output is

$$W^{E1E2}_{2p,1s} = \frac{1}{2}\int_0^{\omega_0} dW^{E1E2}_{2p,1s} = 1.98896 \times 10^{-5}\,(\alpha Z)^8\,\text{a.u.}, \qquad (8.26)$$

$$W^{E1E2}_{2p,1s} = 6.61197 \times 10^{-6}\ \text{c}^{-1}\,(Z=1),$$

where $\omega_0 = E_{2p} - E_{1s}$ and the dependence on the nuclear charge Z is given. Comparison with the fully relativistic calculation gives a relative deviation in the "length" gauge at the level of 0.1% [110].

The calculation of the two-photon $E1E2$ decay in the nonrelativistic "velocity" form, is more complicated. Now the gauge constant should be chosen either $K = -\sqrt{\frac{k+1}{k}}$ for the form (8.7), or $K = 0$ for the form (8.6) [242].

Choosing $K = 0$ for (8.7) and substituting the corresponding potential into (8.21), after integration over angular variables and summation over projections, it can be found that

$$dW^{E1E2}_{2p,1s}(\omega) = \frac{2^4 d\omega}{3^3 5^2 \pi}\omega'\omega\left[\omega^2\left|I_1(\omega) + I_2(\omega')\right|^2 + \omega'^2\left|I_1(\omega') + I_2(\omega)\right|^2\right], \qquad (8.27)$$

$$I_1(\omega) = \frac{1}{\sqrt{6}}\int_0^\infty\int_0^\infty dr dr'\, r^2 r'^3\, e^{-r-\frac{r'}{2}}\left[1 - \frac{9i}{2} - \frac{r'}{2}\right]\left[\frac{\partial}{\partial r} - \frac{2i}{r}\right] g_1(\nu; r, r'), \qquad (8.28)$$

$$I_2(\omega) = \frac{1}{\sqrt{6}}\int_0^\infty\int_0^\infty dr dr'\, r^3 r'^2\, e^{-r-\frac{r'}{2}}\left[1 - 5i - \frac{r'}{2}\right]\left[\frac{\partial}{\partial r} - \frac{3i}{r}\right] g_2(\nu; r, r'). \qquad (8.29)$$

Here $\nu = Z/\sqrt{-2(E_{2p} - \omega)}$, $\nu' = Z/\sqrt{-2(E_{2p} - \omega')}$, and $\omega + \omega' = E_A - E_{A'}$. Integration over r and r' leads to a rather long analytic expressions. Finally,

the final integration over frequency gives

$$W_{2p,1s}^{E1E2} = \frac{1}{2}\int_0^{\omega_0} dW_{2p,1s}^{E1E2}(\omega) = 3.6896 \times 10^{-6}\,(\alpha Z)^8\,\text{a.u.} \qquad (8.30)$$

$$W_{2p1s}^{E1E2} \simeq 1.227 \times 10^{-6}\ \text{c}^{-1}\,(Z=1),$$

The value (8.30) differs from the result obtained in the framework of the fully relativistic calculation in the "velocity" gauge, [110] by about 0.5%. This discrepancy exceeds the relativistic corrections (of the relative order of α^2) and can be explained by purely numerical uncertainties. The most important conclusion, however, is the comparison of the values of (8.30) and (8.26). The gauge invariance of the result is restored only by taking into account the negative energy spectrum when summing over the intermediate states in (8.21). In contrast to the "length" form, the negative energy contribution is no longer negligible when using the "velocity" form. The contribution (8.30) does not coincide with equation (8.26) and represents only the positive energy contribution to $W_{2p,1s}^{E1E2}$ in the "velocity" gauge. Therefore, the value of 1.227×10^{-6} should be compared with the positive energy contribution calculated in the [110]. In the nonrelativistic limit, the contribution of the negative energy in the "velocity" gauge, for small values of Z was estimated analytically in [110].

8.3.2. The negative energy contribution to the $E1M1$ and $E1E2$ probabilities of $2p-1s$ transitions in the "velocity" gauge, for small values of Z

In this section an explicit expression for the negative-energy contribution to the $E1M1$ and $E1E2$ probabilities of $2p-1s$ transitions in the "velocity" gauge, for small values of Z, is obtained. This conclusion can be used to test the validity of numerical nonrelativistic calculations. The derivation is carried out with a different set of photon characteristics, namely the photon momentum $\boldsymbol{k}$ and the polarisation vector $\boldsymbol{e}$. Without distinguishing between $E1M1$ and $E1E2$ transitions the following estimate can be considered as a correction to

the dominant dipole transition.

As an initial formula one can use (2.1) with the corresponding replacement of the absorbed photon by the emitted one (conjugate from the mathematical point of view). All analytical calculations are repeated in complete analogy with the scattering amplitude. An important consequence in this case is the presence of summation over intermediate states in the amplitude (2.6), including the negative energy spectrum (see the expressions for the propagator of the atomic electron (2.3). Then, keeping only the sum only on the negative energy states in the expression for the process amplitude, the corresponding energy denominators in the nonrelativistic limit can be replaced by $-2m$, neglecting also the photon frequencies limited by the value $\omega_{if} = E_A - E_{A'}$ (equal in the case of (8.30) to the energy difference $E_{2p} - E_{1s}$) [2]. Also, consider a series expansion of the exponents included in the wave function of the photon (2.5), replacing one of them by one and leaving only the next term of the expansion in the other. After summing over the polarisations and integrating over the directions of the emitted photons, a leading-order correction will arise. The contribution of the negative spectrum to the emission probability can be represented by the following expressions(in relativistic units $e^4 = \alpha^2$):

$$W_{if}^{(-)} = \frac{\alpha^2}{(2\pi)^3} \sum_{\boldsymbol{e},\boldsymbol{e}'} \int d\boldsymbol{\nu} \int d\boldsymbol{\nu}' \left| U_{if}^{(-)} \right|^2, \tag{8.31}$$

$$U_{if}^{(-)} \approx -\frac{\mathrm{i}}{2m} \sum_{n^{(-)}} \Big[\langle i|(\boldsymbol{e}\boldsymbol{\sigma})(\boldsymbol{k}\boldsymbol{r})|n^{(-)}\rangle\langle n^{(-)}|(\boldsymbol{e}'\boldsymbol{\sigma})|f\rangle +$$

$$\langle i|(\boldsymbol{e}\boldsymbol{\sigma})|n^{(-)}\rangle\langle n^{(-)}|(\boldsymbol{e}'\boldsymbol{\sigma})(\boldsymbol{k}'\boldsymbol{r})|f\rangle + [\boldsymbol{e},\boldsymbol{k} \leftrightarrow \boldsymbol{e}',\boldsymbol{k}'] \Big].$$

The expression (8.31) corresponds to the "velocity" gauge. Here $\boldsymbol{\sigma}$ are Pauli matrices, and the summation is carried out over the set of Dirac equation solutions for an electron in the field of a nucleus with negative energy. In the nonrelativistic limit this set becomes a complete set of the Schr?dinger equation for the positron in the field of the nucleus. Then using the completeness condition

$$U_{if}^{(-)} = -\mathrm{i}\frac{(\boldsymbol{e}\boldsymbol{e}')}{m}\langle i|(\boldsymbol{k}\boldsymbol{r}) + (\boldsymbol{k}'\boldsymbol{r})|f\rangle. \tag{8.32}$$

Summing over polarisations and integration over directions of photon emission is carried out according to (8.13), (8.14).

As a result, the following can be arrived at:

$$W_{if}^{(-)} = \frac{4\alpha^2}{9\pi m^2} \left|\langle i|\boldsymbol{r}|f\rangle\right|^2 \int_0^{\omega_{if}} d\omega\, \omega(\omega_{if} - \omega\left(\omega^2 + (\omega_{if} - \omega)^2\right)) \qquad (8.33)$$

$$= \frac{2\alpha^2\omega_{if}^5}{45\pi m^2} \left|\langle i|\boldsymbol{r}|f\rangle\right|^2 .$$

The order of magnitude and scaling factor for the $2p-1s$ two-photon transition in the "velocity" gauge are given by the relation

$$W_{2p,1s}^{E1M1(-)} + W_{2p,1s}^{E1E2(-)} = 5.625 \times 10^{-5}\,(\alpha Z)^8 \text{ a.u.} \qquad (8.34)$$

This result can be compared with the value obtained in the framework of the fully relativistic approach [110] (also in the "velocity" gauge):

$$W_{2p,1s}^{E1M1(-)} + W_{2p,1s}^{E1E2(-)} = 5.806 \times 10^{-5}\,(\alpha Z)^8 \text{ a.u.} \qquad (8.35)$$

The discrepancy (3.1%) exceeds the expected due to relativistic corrections ($\sim \alpha^2$ for $Z = 1$). However, as an estimate, the value (8.34) is quite satisfactory, showing the necessity to take into account the negative energy spectrum in the "velocity" gauge in calculations of two-photon probabilities of transitions involving "higher" multipoles. For $E1E1$ transitions, the contribution of the negative energy spectrum remains negligibly small both in the "length" and "velocity" gauges, see [110].

8.3.3. Two-photon $E1M1$ decay for the state $2p$

For the two-photon $E1M1$ transition, the emission probability can be expressed as follows:

$$dW^{E1M1}_{A\,A'} = \sum_{M_E M_M m_A m_{A'}} \left| \sum_n \frac{\langle A'|V^{E1}(\omega)|n\rangle\langle n|V^{M1}(\omega')|A\rangle}{E_n - E_A + \omega} + \right. \tag{8.36}$$
$$\frac{\langle A'|V^{M1}(\omega')|n\rangle\langle n|V^{E1}(\omega)|A\rangle}{E_n - E_A + \omega'} + \frac{\langle A'|V^{E1}(\omega')|n\rangle\langle n|V^{M1}(\omega)|A\rangle}{E_n - E_A + \omega'} +$$
$$\left. \frac{\langle A'|V^{M1}(\omega)|n\rangle\langle n|V^{E1}(\omega')|A\rangle}{E_n - E_A + \omega} \right|^2 d\omega.$$

Here $V^{E1}(\omega) = \frac{4}{3}\omega^{3/2} r Y_{1M_E}$, $V^{M1}(\omega) = \sqrt{\frac{4}{3}}\mu_0\omega^{3/2}\left(j_{1M_V} + s_{1M_M}\right)$, Y_{1M} is a spherical function with unit momentum and projection M, $\mu_0 = \frac{\alpha}{2}$ is the Bohr magneton, j_{1M_M} and s_{1M_M} are the spherical components of the total angular momentum and spin momentum of the electron, respectively. These potentials belong to the non-relativistic limit obtained in the "length" gauge. Since the magnetic photon potential includes the total angular momentum and the spin operator, one should use wave functions with the set of quantum numbers $nlsjm$, see (8.18).

It is worth noting that the matrix elements of the magnetic moment "cut out" from the summation over intermediate states only $n = A$ or A' by the condition of orthogonality of the radial parts of the wave functions [179]. After angular integration and summation over all projections,

$$dW^{E1M1}_{2p,1s}(\omega) = \frac{2^8\mu_0^2}{\pi}\left(\frac{2}{3}\right)^{12}\omega\omega'^3 d\omega \tag{8.37}$$

and, therefore,

$$W^{E1M1}_{2p,1s} = \frac{1}{2}\int_0^{3/8} dW^{E1M1}_{2p,1s}(\omega) = \frac{2^5}{\pi}\left(\frac{2}{3}\right)^{12}\alpha^8\int_0^{3/8}\omega\left(\frac{3}{8}-\omega\right)^3 d\omega. \tag{8.38}$$

Finally, the final result is

$$W^{E1M1}_{2p,1s} = \frac{2^5}{\pi}\left(\frac{2}{3}\right)^{12}\frac{243}{655360}(\alpha Z)^8\,\text{a.u.} = 9.6769\times10^{-6}\ \text{c}^{-1}\,(Z=1). \quad (8.39)$$

The Z-dependence of the transition probability $W^{E1M1}_{2p,1s}$ is again indicated. Comparison with the result of the fully relativistic calculation [110] reveals a discrepancy about 0.1%.

The calculations of the probabilities of two-photon transitions are directly related to the calculation, for example, of the NR corrections (see the previous sections). The theory and corresponding numerical calculations in the framework of the fully relativistic approach for the probabilities of three-photon emission were presented in [123] (omitted for brevity). Multiphoton emission (absorption) processes can also serve to test the fundamental properties of bosons. For example, two electric dipole photons do not carry a momentum equal to unity (Landau-Yang theorem), see [122–125]. Separately, it is worth noting the result of the [117], which can also be used to verify the numerical results. Omitting the details of calculations, mainly related to the angular algebra, the connection between the probabilities of multiphoton transitions and the partial decay channels of fine (hyperfine) sublevels of a given state was established. Expressions analogous to one-photon transitions were derived, see, e.g., [6]. The theory presented here will be further used to elucidate a number of questions related to astrophysical studies of CMB and to compare the spectral characteristics of hydrogen and anti-hydrogen atoms.

8.3.4. Two-photon decay of highly excited states in H

Recent advances in observations of the temperature anisotropy of the cosmic microwave background (CMB) and its polarisation, see [247, 248], have led to a revision of the details of the theoretical description of the cosmological history of hydrogen recombination. In turn, the corresponding analyses necessitatively require correct knowledge of the two-photon decay processes of hydrogen (see, e.g., [77, 79, 164] and many others). For example, the $E1E1$ two-photon decay of the metastable $2s$ level in the hydrogen atom of [77, 79] is of fundamental

importance, since this is the dominant decay channel. Two-photon emission is characterised by the fact that the frequency of a single photon (out of the available two) is not sufficient to excite a neighbouring atom (absorption in the wing of the absorption profile is suppressed) and thus the radiation "escapes" from the substance, leading to the final recombination of atoms.

Within the framework of the study of one- and two-photon radiation processes in the astrophysical context, several questions are considered in this thesis. The first will be discussed in the next section and relates to the possibility of separating two-photon radiation of highly excited states into "pure", leading to direct radiation "escape", and cascade radiation. The cascade (resonant) radiation is effectively reabsorbed, and the esape mechanism of such radiation is described in detail, for example, in [165, 167, 168].The careful separation of "pure" radiation from cascade radiation is of fundamental importance and requires the use of various mechanisms of radiation "escape".

Another question can be formulated as follows. In the works [76, 99] for an accurate description of the cosmological recombination epoch of the early Universe, the importance of taking into account, if possible, the whole spectrum of atomic states was emphasised. In view of the obvious difficulties of using the full set of atomic states in the theory of radiative transfer, it becomes necessary to define an admissible restriction on their number. This concerns not only one-photon transitions, but also other possible (two-, three-, etc.) decay channels. It should be emphasised that, despite the rather small probability, the two-photon decays of the $2p$ level considered in the previous sections can be attributed to "pure" radiation. Thus, a study of the behaviour of "pure" radiation with increasing principal quantum number of the excited state can provide an appropriate answer. The study was presented in [83], where it was determined that effectively any two-photon transitions ($E1E1$, $E1E2$, $E1M1$, as well as $E2E2$, $M1M1$, $E1M2$) for ns, np states decrease as $1/n^3$. It is worth noting that, as for one-photon transitions, this asymptotic behaviour for some transitions has been obtained analytically. Thus, it is possible to determine with high accuracy the number of states required for accounting.

Another goal of the work [83] was to search for effects beyond the dipole approximation (cases when the usually used dipole approximation is insufficient)

in the astrophysical context. For this purpose fully relativistic calculations were carried out. The gauge invariance served as a test of calculations. Nonrelativistic calculations were carried out in the "length" gauge and directly compared with the results of relativistic calculations obtained in the "length" and "velocity" gauges (gauge invariant).

The dipole approximation can be characterised by taking into account only the first term in the expansion of the photon wave function when the argument is small (see above). However, for highly excited states the argument of the photon wave function grows with increasing principal quantum number, since $\omega_{nl,1s}\langle r\rangle \sim n^2$ ($\langle r\rangle$ the mean value of the orbital radius in the n state). The search for effects beyond the nonrelativistic dipole approximation consisted in comparing the contributions of the nonrelativistic and relativistic dipole photon emission operator. It was also supposed that at large values of the argument of the Bessel function the subsequent terms of the expansion, beyond the dipole approximation, can be comparable to the first one. The $E2E2$ and $M1M1$ transition probabilities represent the next order of such an approximation for two-photon $ns/nd-1s$ radiation processes. To avoid the issue of cascade emission, the calculations were performed at a frequency equal to half of the energy interval. The result of the study is that the dipole approximation works quite well for the $ns/np/nd \to 1s+2\gamma$ transitions in the hydrogen atom. For obvious reasons this fact is violated with increasing of the charge number of the nucleus, see [110, 123].

8.4. Two-photon decay of excited levels in hydrogen: ambiguity of separation into cascade and "pure" two-photon emission

There is a fundamental difference between the decay of highly excited ns levels (similarly to nd, $n > 2$) and $2s$ levels, which consists in the presence of cascade transitions as dominating decay channels. For the $2s$ level there are no cascade transitions. Since cascade photons can be effectively re-absorbed, the problem of separating the "pure" two-photon contribution from the cascade contribution

arises. The interference between the two decay channels, i.e., the product of the amplitudes of the "pure" and the cascade two-photon decay, should also be taken into account.

A similar problem arose much earlier in the framework of the theory of two-electron HCI, see [249] and related references. Typically, the "pure" two-photon contribution is isolated by subtracting the Lorentz contour as a cascade contribution from the total two-photon decay frequency distribution, see for example the works of [250,251]. The existence of interference terms was recognised in [250, 251], but only approximately included in the Lorentz approximation as an asymmetric deviation of the line contour. A rigorous QED approach to estimate the two-photon decay width with the presence of cascades for HCI was performed in [249] (see also [8]). This approach was based on the standard estimation of the width as the sum of the transition probabilities to lower levels. In the case of cascades, the integral over the frequency distribution of emitted photons becomes divergent due to singular terms corresponding to cascade resonances. To avoid such singularity, a regularisation was performed in [249] according to the theory in [85]. In [250, 251] the level widths in the singular energy denominators were also taken into account, albeit purely phenomenologically. In a similar way, i.e., by introducing the level widths into the singular energy denominators, the two-photon decay of the excited levels ns and nd in hydrogen was recently estimated in the astrophysical works of [164, 252].

In [249], the ambiguity of the separation between "pure" two-photon decay and cascades for HCI was revealed for the first time. In particular, it was shown that interference terms can contribute significantly to the total decay probability. In [164, 252], the ambiguity of the separation of "pure" two-photon decay was neither emphasised nor demonstrated explicitly. This will be addressed in this section, which focuses on the $3s - 1s$ two-photon decay, see [82], and also [118]. The numerical results for the $3s$-level in hydrogen are in agreement with recent calculations performed in [164]. However, they strongly disagree with the value obtained in [253]. The [253] result follows from an "alternative" approach to the two-photon decay estimation developed in [254–256]. This "alternative" approach is based on the estimation of the imaginary part of the two-loop contribution to the Lamb shift for the $3s$-level, see the reasons for

this approach in [88, 257]. In [254–256] it was argued that there is no singularity in the integration over the photon frequency distribution for two-photon decay and thus the finite integral represents directly the probability of "pure" two-photon decay. Further it will be shown that, in fact, the value calculated in the [253] has a completely different interpretation and should have the meaning of a radiative correction to the full width of the excited level [121].

Also, to verify the correctness of the conclusion about the inseparability of two-photon emission in the presence of cascades, an analysis of the derivation of the two-photon decay width through the imaginary part of the second-order Lamb shift will be presented below. A consequence of the "optical theorem" for the adiabatic S-matrix will be used [89]. The results of the analysis show that the estimation of the two-photon decay width through the imaginary part of the Lamb shift gives the same expressions as the standard description of QED by summing the transition probabilities (see above, and e.g. [117]). The integration over the frequency of emitted photons for two-photon decay with cascades remains divergent and requires the introduction of level widths in the singular energy denominators [85]. Calculations using both methods (summation of transition probabilities and estimation of the imaginary part of the Lamb shift) are presented. The results clearly demonstrate the ambiguity of the separation of the "pure" two-photon and cascade contributions with a precision higher than that required for modern astrophysical studies (the last $\sim 1\%$).

8.4.1. Two-photon decay involving cascade: $3s - 2p - 1s$

The expression for the two-photon $E1E1$ decay of the $2s$ state is well known and can be easily found in the academic literature, see, e.g., [101, 244]. Since the derivation of the expression in the framework of the S-matrix formalism for ns ($n > 2$) is completely identical, for the sake of brevity it can be written

immediately as follows

$$dW_{ns,1s}(\omega) = \frac{8\omega^3(\omega_0-\omega)^3}{27\pi}e^4\left|S_{1s,ns}(\omega)+S_{1s,ns}(\omega_0-\omega)\right|^2 d\omega, \quad (8.40)$$

$$S_{1s,ns}(\omega) = \sum_{n'p}\frac{\langle R_{1s}|r|R_{n'p}\rangle\langle R_{n'p}|r|R_{ns}\rangle}{E_{n'p}-E_{ns}+\omega}, \quad (8.41)$$

$$\langle R_{n'l'}|r|R_{nl}\rangle = \int_0^\infty r^3 R_{n'l'}(r)R_{nl}(r)dr, \quad (8.42)$$

where $\omega_0 = E_{ns} - E_{1s}$, $R_{nl}(r)$ is the radial part of the nonrelativistic wave function of hydrogen, and E_{nl} is the corresponding energy of the nl level. The expression (8.40) is written in the nonrelativistic limit in the "length" gauge.

The total probability of a two-photon transition can be obtained by integration in the frequency interval

$$W_{ns,1s} = \frac{1}{2}\int_0^{\omega_0} dW_{ns,1s}(\omega). \quad (8.43)$$

The limit of integration over frequency is determined by the energy conservation law. In the case $n = 2$, there are no cascade transitions, the frequency distribution (8.40) is not singular, and the integral (8.43) converges.

In the presence of cascade transitions ($n > 2$), some terms in (8.41) become singular and the integral (8.43) diverges. For example, fixing $n = 3$ in (8.40) there is a divergence at $n' = 2$. For the summand written as (8.41), the divergence corresponds to the transition $3s \to 2p$, for the second summand in (8.40) the transition $2p \to 1s$. This divergence has a physical origin: the emitted photon corresponds to a resonance. So the divergence can only be avoided by introducing the width of this resonance. This situation was studied in [249] for HCI. The same recipe can be used in the case of the hydrogen atom. Following the prescriptions given in the previous sections, one should extract the resonance terms (corresponding to the cascades) in the sum over the intermediate states of the expression (8.40) and then apply the regularization procedure [85]. Practically, this leads to the appearance of energy level widths in the energy de-

nominators. Then Lorentz profiles for the resonance terms in the expression for the probability arise. However, the Lorentz profile is valid only near resonance and cannot be extended too far from the resonance frequency value. As for any multichannel processes, this separation is an approximate procedure because of the existence of interference terms.

According to this, the integration over the frequency interval $[0, \omega_0]$ in (8.43) should be divided into several subintervals. In the case of the frequency distribution for the two-photon decay of the $3s$ level, it is convenient to introduce 5 subintervals, see Fig. 8.1. The first interval (**I**) extends from $\omega = 0$ to the

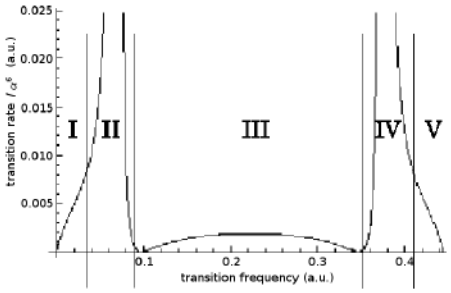

Figure 8.1. Frequency distribution $dW^{(2\gamma)}_{3s;1s}/d\omega$ for the full $3s \to 1s{+}2\gamma$ two-photon transition, including cascade and "pure" two-photon transitions as a function of frequency (in atomic units). The values $dW^{(2\gamma)}_{3s;1s}/d\omega$ divided by α^6 (α is the fine structure constant) are presented as a function of frequency in the interval $[0, \omega_0]$, $\omega_0 = E_{3s} - E_{1s}$. The boundaries of the frequency intervals **I**-**V** are indicated by vertical lines.

lower boundary of the second interval (**II**). The latter contains the value of the resonance frequency $\omega_1 = E_{3s} - E_{2p}$. In the interval (**II**), the resonance term $n = 2$ in (8.41) should be subtracted from the sum over the intermediate states and replaced by a term with a modified energy denominator. This modified denominator is $E_{2p} - E_{3s} + \omega - \frac{\mathrm{i}}{2}\Gamma$, where $\Gamma = \Gamma_{2p} + \Gamma_{3s}$. The third interval (**III**) extends from the upper boundary of the interval (**II**) to the lower boundary of the interval (**IV**), the latter containing one more value of the resonant frequency $\omega_2 = E_{2p} - E_{1s}$. Inside the interval (**IV**), again the resonance term $n = 2$ in (8.41) should be replaced by a term with a modified denominator $E_{2p} - E_{1s} - \omega - \frac{\mathrm{i}}{2}\Gamma_{2p}$. Finally, the fifth interval (**V**) extends from the upper boundary of the interval (**IV**) to the maximum frequency value ω_0. It

is worth noting that the frequency distribution $dW_{3s,1s}(\omega)$ is symmetric about $\omega = \omega_0/2$ with an accuracy of 1% (the asymmetry is due to the difference between $\Gamma = \Gamma_{2p} + \Gamma_{2s}$ and Γ_{2p}, respectively). The choice of the size of the intervals (**II**) and (**IV**), which determines the sizes of the other intervals, as well as further approximations, is discussed below.

Keeping in (8.41) only the resonance term in the second and fourth frequency intervals, it is possible to calculate the cascade contribution to the total two-photon decay rate of the $3s$ level according to an expression similar to (8.43). Taking the ratio to the total width of the $3s$ level Γ_{3s}, the absolute probability or branching ratio $W^{(\mathrm{cas})}_{3s,1s}/\Gamma_{3s} \equiv b^{(\mathrm{cas})}_{3s-2p-1s}$ is obtained for the cascade transition. The contributions to $b^{(\mathrm{cas})}_{3s-2p-1s}$ from intervals (**I**), (**III**), (**V**) are assumed to be zero. Then

$$W^{(\mathrm{cas}\,1\gamma)}_{3s,1s} = \frac{4}{27\pi}\int\limits_{(\mathbf{II})} \omega^3\omega'^3 \left|\frac{\langle R_{3s}(r)|r|R_{2p}(r)\rangle\langle R_{2p}(r')|r'|R_{1s}(r')\rangle}{E_{2p}-E_{3s}+\omega-\frac{\mathrm{i}}{2}\Gamma}\right|^2 d\omega \quad (8.44)$$
$$+\frac{4}{27\pi}\int\limits_{(\mathbf{IV})} \omega^3\omega'^3 \left|\frac{\langle R_{3s}(r)|r|R_{2p}(r)\rangle\langle R_{2p}(r')|r'|R_{1s}(r')\rangle}{E_{2p}-E_{1s}-\omega-\frac{\mathrm{i}}{2}\Gamma_{2p}}\right|^2 d\omega,$$

$\omega_0 - \omega \equiv \omega'$.

Accordingly, the "pure" two-photon decay probabilities within each interval, Fig. 8.1, are as follows:

$$dW^{(\mathrm{pure}2\gamma)}_{3s,1s} = \frac{4}{27\pi}\omega^3\omega'^3\left|S^{(2p)}_{1s;3s}(\omega)+S_{1s;3s}(\omega')\right|^2 d\omega,\ \omega\in\mathbf{II} \quad (8.45)$$
$$dW^{(\mathrm{pure}2\gamma)}_{3s,1s} = \frac{4}{27\pi}\omega^3\omega'^3\left|S_{1s;3s}(\omega)+S^{(2p)}_{1s;3s}(\omega')\right|^2 d\omega,\ \omega\in\mathbf{IV} \quad (8.46)$$
$$dW^{(\mathrm{pure}2\gamma)}_{3s;1s} = \frac{4}{27\pi}\omega^3\omega'^3\left|S_{1s;3s}(\omega)+S_{1s;3s}(\omega')\right|^2 d\omega,\ \omega\in\mathbf{I},\mathbf{III},\mathbf{V}. \quad (8.47)$$

Here $S^{(2p)}_{1s,3s}(\omega)$ is an expression (8.41) with excluded term $n = 2$.

In contrast to the cascade, all intervals contribute to the "pure" two-photon emission. The branching coefficient for the $3s \to 2\gamma{+}1s$ transition is determined

as follows

$$b^{(\mathrm{pure2}\gamma)}_{3s-1s} = \frac{1}{2}\frac{1}{\Gamma_{3s}}\int_0^{\omega_0} dW^{(\mathrm{pure2}\gamma)}_{3s;1s}(\omega). \tag{8.48}$$

It remains to introduce the interference contribution. This contribution occurs only for the 2nd and 4th intervals. The corresponding distribution functions have the form:

$$dW^{(\mathrm{inter})1}_{3s;1s} = \frac{4\omega^3(\omega_0-\omega)^3}{27\pi}\Re\left[\frac{\langle R_{3s}(r)|r|R_{2p}(2r)\rangle\langle R_{2p}(r')|r'|R_{1s}(r')\rangle}{E_{2p}-E_{3s}+\omega-\frac{\mathrm{i}}{2}\Gamma_{2p}}\right] \times\left[S^{(2p)}_{1s;3s}(\omega)+S_{1s;3s}(\omega_0-\omega)\right]d\omega, \tag{8.49}$$

$$dW^{(\mathrm{inter})2}_{3s;1s} = \frac{4\omega^3(\omega_0-\omega)^3}{27\pi}\Re\left[\frac{\langle R_{3s}(r)|r|R_{2p}(2r)\rangle\langle R_{2p}(r')|r'|R_{1s}(r')\rangle}{E_{2p}-E_{1s}-\omega-\frac{\mathrm{i}}{2}\Gamma_{2p}}\right] \times\left[S_{1s;3s}(\omega)+S^{(2p)}_{1s;3s}(\omega_0-\omega)\right]d\omega, \tag{8.50}$$

($\Re$ means the real part of the expression in brackets), and the branching coefficient is equal to

$$b^{(\mathrm{inter})}_{3s;1s} = \frac{1}{2\Gamma_{3s}}\int_{(\mathbf{II})} dW^{(\mathrm{inter})1}_{3s;1s} + \frac{1}{2\Gamma_{3s}}\int_{(\mathbf{IV})} dW^{(\mathrm{inter})2}_{3s;1s}. \tag{8.51}$$

The results are presented in Table 8.1. The size $\Delta\omega$ of the second interval is conveniently defined as l-fold the total width $\Gamma = \Gamma_{2p} + \Gamma_{3s}$, i.e., $\Delta\omega = 2l\Gamma$ and similarly for the fourth interval as $\Delta\omega = 2l\Gamma_{2p}$.

Table 8.1 summarizes the results for various values of l ranging from $l \simeq 10^5$ to $l \simeq 10^7$. The upper limit of the interval (**II**) is $\omega_1 + l\Gamma = \frac{5}{72} + l\Gamma$ (in atomic units), and the lower limit of the interval (**IV**) is $\omega_2 - l\Gamma_{2p} = \frac{3}{8} - l\Gamma_{2p}$. The different rows in Table 8.1 present the branching ratios and probabilities of the "pure" two-photon, and "interference" channels, respectively. For a more detailed analysis, the contributions of the "pure" two-photon transition rate for each frequency interval are also summarized. The branching ratio and transition probability of the cascade contribution can be obtained from the relation

Table 8.1. Branching ratios and transition probabilities (in s^{-1}) for different decay channels of the $3s$ level of the hydrogen atom with different frequency intervals (l).

l	10^4	10^5	2.5×10^5	5×10^5	10^6	1.5×10^6	4.53×10^6	1.00256×10^7
$b^{(\mathrm{pure2}\gamma)}$	3.2003×10^{-5}	3.5091×10^{-6}	1.6270×10^{-6}	1.0239×10^{-6}	7.6765×10^{-7}	7.2201×10^{-7}	9.1487×10^{-6}	1.2567×10^{-6}
$W_{\mathbf{I}}^{(\mathrm{pure2}\gamma)}$	53.054	7.0547	3.5743	2.1898	1.27737	0.85130	2.4979×10^{-6}	0
$W_{\mathbf{II}}^{(\mathrm{pure2}\gamma)}$	0.006247	0.06247	0.15614	0.31201	0.62183	0.92718	2.4666	3.9810
$W_{\mathbf{III}}^{(\mathrm{pure2}\gamma)}$	95.536	7.8778	2.7928	1.4517	1.0457	1.0031	0.86005	0
$W_{\mathbf{IV}}^{(\mathrm{pure2}\gamma)}$	0.006185	0.061847	0.15458	0.30890	0.61569	0.91813	2.4523	3.9575
$W_{\mathbf{V}}^{(\mathrm{pure2}\gamma)}$	53.561	7.1101	3.5999	2.2056	1.2886	0.861254	3.1665×10^{-4}	0
$W^{(\mathrm{pure2}\gamma)}$	202.16	22.167	10.278	6.4680	4.8492	4.5609	5.7792	7.9385
$b^{(\mathrm{inter})}$	-1.4342×10^{-9}	-1.4343×10^{-8}	-3.5852×10^{-8}	-7.1665×10^{-8}	-1.4302×10^{-7}	-2.1376×10^{-7}	-6.0829×10^{-7}	-1.0459×10^{-6}
$W^{(\mathrm{inter})}$	−0.0090599	−0.090602	−0.22647	−0.45270	−0.90346	−1.3503	−3.8426	−6.6067

$b_{3s-2p-1s}^{(\mathrm{cas})} + b_{2s,1s}^{(\mathrm{pure2}\gamma)} + b_{3s,1s}^{(\mathrm{inter})} = 1$. This relation is satisfied with high accuracy, since the only neglected decay channel is the very weak direct one-photon $M1$-transition $3s \to 1s + \gamma$. The following conclusions can be drawn from Table 8.1: as in the case of HCI [249], the "pure" two-photon, and cascade contributions to the total decay probability are inseparable. Varying the size of the $\Delta\omega$ interval yields quite different values for $dW_{3s,1s}^{(\mathrm{pure2}\gamma)}$ ranging from 202.16 s^{-1} (for $l = 10^4$) to 7.9385 s^{-1} (for $l = 1.00256 \times 10^7$).

Moreover, according to the calculations, depending on the interval size, the interference contribution can also become very large, comparable in magnitude to the "pure" two-photon contribution. Thus, even the order of magnitude of the "pure" two-photon decay probability of the $3s$-state in hydrogen cannot be reliably predicted.

For the "non-resonant" contribution calculated in the [164], a value of 10.556 s^{-1} was given, which plays the role of the "pure" two-photon decay probability in astrophysical applications. This value is within the range of the results given in Table 8.1. However, the value of 2.08 s^{-1} obtained for the "pure" two-photon decay probability in the [253] is in strong contradiction with the present analysis.

Finally, both the standard QED approach based on the line profile theory [249–251] and an "alternative" approach based on the two-loop theory [254–256] were presented in [258]. A reasonable agreement between the two methods was found. However, it is clear from the analysis that using the imaginary part of the Lamb shift gives exactly the same results as the standard QED approach. A more detailed comparison between this approach and the "alternative" ap-

proach is presented in a later section.

8.4.2. Two-photon decay $4s - 1s$

The calculations of the two-photon $4s - 1s$ transition in [118] were carried out in a similar way. The integration over the frequency on the interval $[0, \omega_0]$ in this case should be divided into 9 subintervals. The first interval starts from 0 to the lower boundary of the second interval. The latter covers the vicinity of the first resonance corresponding to the frequency $\omega^{res\,1}_{4s-3p} = 7/288$ (in atomic units). Within the interval (**II**), the resonance term $n = 3$ in (8.41) should be separated from the sum over all intermediate states and replaced by an expression with a regularized energy denominator. Such denominator is $E_{3p} - E_{4s} + \omega - \frac{\mathrm{i}}{2}\Gamma$, where $\Gamma = \Gamma_{3p} + \Gamma_{4s}$. The third interval (**III**) extends from the upper boundary of the interval (**II**) to the lower boundary of the interval (IV), which, in its turn, corresponds to another resonance with frequency $\omega^{res\,2}_{4s-2p} = 3/32$. Inside the interval (**IV**), the resonance term in (8.41) should again be replaced by a similar one with a modified denominator $E_{2p} - E_{4s} + \omega - \frac{\mathrm{i}}{2}\Gamma$, where $\Gamma = \Gamma_{2p} + \Gamma_{4s}$. Further, the interval (**V**) extends from the upper boundary of the interval (**IV**) to the lower boundary of the interval (**VI**), which defines the vicinity of the second "link" $\omega^{res\,3}_{2p-1s} = 3/8$ of the second cascade. Inside this interval, the energy singular denominator should be replaced by $E_{2p} - E_{1s} - \omega - \frac{i}{2}\Gamma_{2p}$. The next interval (**VII**) is defined from the upper boundary of the interval (**VI**) to the lower boundary of the interval (**VIII**). The interval (**VIII**) defines the vicinity of the second "link" for the first cascade and corresponds to the frequency $\omega^{res\,4}_{3p-1s} = 4/9$. Inside this interval, the singular energy denominator is $E_{3p} - E_{1s} - \omega - \frac{\mathrm{i}}{2}\Gamma_{3p}$. Finally, the last interval (**IX**) is bounded by the upper limit of the interval (**VIII**) and the maximum frequency $\omega_0 = 15/32$ in the case of two-photon decay of the $4s$ level in the hydrogen atom. The frequency distribution function is symmetric with respect to the frequency $\omega = \omega_0/2$ with 1% accuracy (due to the difference in the denominator widths).

The contribution of cascade radiation, as before at $n = 3$, arises, leaving only the resonance terms in the second, fourth, sixth, and eighth frequency intervals (see Fig. 8.2).

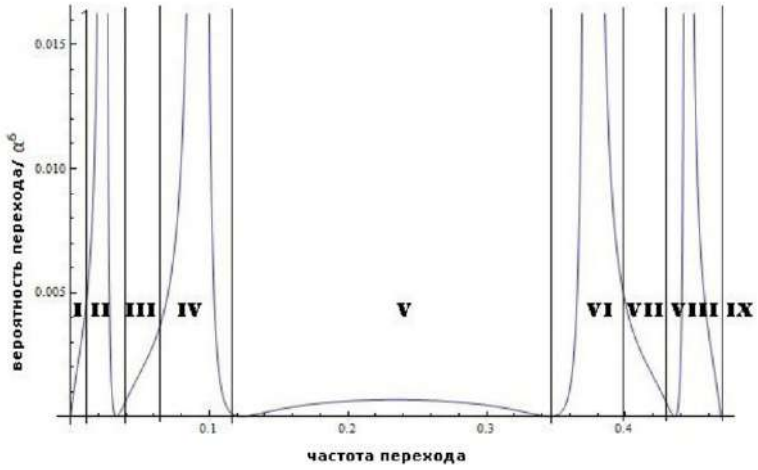

Figure 8.2. The frequency distribution function $dW^{(2\gamma)}_{4s,1s}/d\omega$ for the total two-photon $4s \to 1s + 2\gamma$ transition, including resonant and nonresonant transitions. $dW^{(2\gamma)}_{4s,1s}/d\omega$ is plotted in atomic units as a function of frequency in the interval $[0, \omega_0]$, $\omega_0 = E_{4s} - E_{1s}$; the probability values are divided by α^6 (α is the fine structure constant) for clarity. The boundaries of the subintervals (**I**)-(**IX**) are marked by vertical lines.

Omitting for brevity the corresponding expressions for the cascade, "pure" and interference contributions, the results of numerical calculations are presented in Table 8.2.

It is convenient to define the size $\Delta\omega$ of the second interval as the product of some integer l and the width $\Gamma = \Gamma_{3p} + \Gamma_{4s}$, i.e., $\Delta\omega = 2l\Gamma$. Also, the fourth, sixth, and eighth intervals are defined as $\Delta\omega = 2l\Gamma$, $\Delta\omega = 2l\Gamma_{2p}$, and $\Delta\omega = 2l\Gamma_{3p}$, respectively. In Table 8.2, the numbers are given for different values of l from $l = 10^4$ to $l \approx 10^7$. The upper bound of the interval (**II**) is $\omega^{res\,1} + l\Gamma = 7/288 + l\Gamma$ (in atomic units), and the lower bound of the interval (**IV**) is $\omega^{res\,1} - l\Gamma = 7/288 - l\Gamma$. The remaining (fourth, sixth, and eighth) intervals are defined similarly. The rows in Table 8.2 correspond to the relative (b) (branching factor) and absolute (W) transition probabilities of the "pure" and interference channels, respectively. For a more detailed analysis, the contributions of the probabilities of the "pure" two-photon transitions are also given for each frequency interval. The branching ratio and transition probability for the cascade can be obtained from the relation: $b^{(\mathrm{cas})}_{4s-3p-1s} + b^{(\mathrm{cas})}_{4s-2p-1s} + b^{(\mathrm{pure}2\gamma)}_{4s,1s} + b^{(\mathrm{inter})}_{4s,1s} = 1$. This relation is fulfilled with high

Table 8.2. The transition probabilities in s^{-1}, as well as their relative magnitudes, for different two-photon decay channels of the $4s$ level in the subintervals (**I**)-(**IX**) as a function of the interval sizes (l-fold of the corresponding width, see in the text). The last column of the table refers to the limiting case where the intervals **II**,**IV**,**VI** and **VIII** are closed to each other using two parameters $l_1 = 3.48\times10^6, l_2 = 3.52\times10^6$. This case corresponds to the calculation method in [164, 252].

l	10^4	10^5	5×10^5	10^6	2×10^6	3.47×10^6	l_1, l_2
$b^{(\mathrm{pure2}\gamma)}$	3.0233×10^{-5}	3.1750×10^{-6}	8.0662×10^{-7}	5.5264×10^{-7}	4.9533×10^{-7}	5.6681×10^{-7}	7.2829×10^{-7}
$W_{\mathbf{I}}^{(\mathrm{pure2}\gamma)}$	13.35220	1.73703	0.52511	0.30539	0.14332	0.04029	0
$W_{\mathbf{II}}^{(\mathrm{pure2}\gamma)}$	0.00145	0.01449	0.07243	0.14468	0.28785	0.49154	0.52825
$W_{\mathbf{III}}^{(\mathrm{pure2}\gamma)}$	33.47500	3.61406	0.82795	0.41625	0.14812	0.00036	0
$W_{\mathbf{IV}}^{(\mathrm{pure2}\gamma)}$	0.00184	0.01842	0.09193	0.18293	0.35780	0.57374	1.08139
$W_{\mathbf{V}}^{(\mathrm{pure2}\gamma)}$	39.08470	3.17576	0.51206	0.33606	0.31441	0.29873	0
$W_{\mathbf{VI}}^{(\mathrm{pure2}\gamma)}$	0.00183	0.01829	0.09129	0.18167	0.35545	0.57088	1.08164
$W_{\mathbf{VII}}^{(\mathrm{pure2}\gamma)}$	33.91020	3.65639	0.83566	0.42000	0.15043	0.00204	0
$W_{\mathbf{VIII}}^{(\mathrm{pure2}\gamma)}$	0.00142	0.01416	0.07078	0.14140	0.28140	0.48093	0.52414
$W_{\mathbf{IX}}^{(\mathrm{pure2}\gamma)}$	13.64800	1.76918	0.53400	0.31152	0.14813	0.04396	0
$W^{(\mathrm{pure2}\gamma)}$	133.47664	14.01778	3.56123	2.43989	2.18690	2.50247	3.21542
$b^{(\mathrm{inter})}$	-1.08815×10^{-9}	-1.08822×10^{-8}	-5.43989×10^{-8}	-1.08722×10^{-7}	-2.16848×10^{-7}	-3.73758×10^{-7}	-5.87950×10^{-7}
$W^{(\mathrm{inter})}$	−0.00480	−0.04804	−0.24017	−0.48001	−0.95738	−1.65014	−2.59248

accuracy because only the very weak one-photon $M1$ transition $4s \to 1s + \gamma$ is neglected. The following conclusions can be drawn from Table 8.2: as in the case of HCI [249] and in the case of the $3s \to 1s + 2\gamma$ two-photon transition, the contributions of "pure" two-photon (nonresonant), and cascade (resonant) radiation to the decay probability are inseparable. By varying the size of the $\Delta\omega$ intervals, significantly different values of $dW_{4s,1s}$ are obtained, ranging from 133.47664 s^{-1} (for $l = 10^4$) to 2.50247 s^{-1} (for $l = 3.47 \times 10^6$). Moreover, in the calculations that depend on the interval size, the interference contribution is also quite significant with respect to the "pure" two-photon decay. Thus, the value of the "pure" two-photon decay for the $4s$ state of the hydrogen atom cannot be strictly determined. In [253], a value of 11.951 s^{-1} was obtained for the nonresonant contribution to the $4s \to 1s + 2\gamma$ transition. This value is within the range of the data values in Table 8.2, but, as shown above, cannot serve as an unambiguous determination of the magnitude of the "pure" two-photon decay.

8.4.3. Decay width via the S-matrix adiabatic formalism

In this section, the adiabatic S-matrix formalism ($\hat{S}_\eta$) and the formula for the energy shift ΔE_A [89] of the excited atomic state are used A:

$$\Delta E_A = \lim_{\eta\to 0} \frac{\mathrm{i}\eta}{2} \frac{e\frac{\partial}{\partial e}\langle A|\hat{S}_\eta|A\rangle}{\langle A|\hat{S}_\eta|A\rangle}. \tag{8.52}$$

The adiabatic $\hat{S}_\eta$-matrix differs from the "ordinary" matrix by the presence of an adiabatic (exponential) factor $e^{-\eta|t|}$ at each vertex (for each interaction). This refers to the concept of adiabatic on/off interaction, formally introduced by the substitution $\hat{H}_{\rm int}(t) \to \hat{H}^\eta_{\rm int}(t) = e^{-\eta|t|}\,\hat{H}_{\rm int}(t)$. A symmetrized version of the adiabatic formula containing $S_\eta(\infty,-\infty)$, more convenient for QED calculations, was proposed in [87]. The first application of the formula (8.52) to QED calculations for bound states was made in [259]. In particular, it was shown how to handle the adiabatic exponential multiplier when evaluating the real part of the corrections to the energy levels (8.52), see also [3]. The imaginary part (8.52) can be calculated by the same methods. It is worth noting that the first application of the adiabatic S-matrix theory to the estimation of level widths was given in [88], albeit in a slightly different way than in [82] (see below).

For a free atom (or ion) in the $|A\rangle$ state interacting with the photon vacuum $|0_\gamma\rangle$ (i.e., $|A,0_\gamma\rangle = |A\rangle|0_\gamma\rangle$ in the absence of external fields), the complex energy correction (8.52) contains only diagonal elements of the S-matrix of even order, since $\langle 0_\gamma|\hat{S}^{(1)}_\eta|0_\gamma\rangle = \langle 0_\gamma|\hat{S}^{(3)}_\eta|0_\gamma\rangle = 0$, etc. To extract the imaginary part of the energy shift $\Delta E^{(2i)}_A$ of a given order $2i$, it is more convenient to visualize the expression (8.52) as a series of perturbations of the form (with exactness up to terms e^4) [3]:

$$\Delta E_A = \lim_{\eta\to 0} \mathrm{i}\eta \left[\langle A|\hat{S}^{(2)}_\eta|A\rangle + \left(2\langle A|\hat{S}^{(4)}_\eta|A\rangle - \langle A|\hat{S}^{(2)}_\eta|A\rangle^2\right) + \dots\right]. \tag{8.53}$$

For the adiabatic matrix $\hat{S}_\eta$ the standard decomposition by powers of the in-

teraction constant e is used

$$\hat{S}_\eta(\infty,-\infty) = 1 + \sum_{i=1}^{\infty} \hat{S}_\eta^{(i)}(\infty,-\infty), \tag{8.54}$$

which permits to separate real and imaginary parts of matrix elements in any given order of perturbation theory, i.e.

$$\langle A|\hat{S}_\eta^{(i)}|A\rangle = \Re\langle A|\hat{S}_\eta^{(i)}|A\rangle + \mathrm{i}\Im\langle A|\hat{S}_\eta^{(i)}|A\rangle. \tag{8.55}$$

Here $\Re$, $\Im$ means the real and imaginary parts of the corresponding expression.

The second summand in (8.55) gives the width of the one-photon decay:

$$\Im\Delta E_A^{(2)} = \lim_{\eta\to 0} \eta Re\langle A|\hat{S}_\eta^{(2)}|A\rangle. \tag{8.56}$$

Comparing all fourth-order terms that describe the two-photon decay width, as well as the part representing radiative corrections (one-loop) to the one-photon width, one obtains

$$\Im\Delta E_A^{(4)} = \lim_{\eta\to 0} \eta \left[2\Re\langle A|\hat{S}_\eta^{(4)}|A\rangle + \left|\langle A|\hat{S}_\eta^{(2)}|A\rangle\right|^2 - 2\left(\Re\langle A|\hat{S}_\eta^{(2)}|A\rangle\right)^2\right], \tag{8.57}$$

where the last two summands come from $\langle A|\hat{S}_\eta^{(2)}|A\rangle^2$.

The total width Γ_A of the excited state A (specifying the initial state as $|A,0_\gamma\rangle \equiv |A\rangle$) has to follow (by definition) from the imaginary part of the total shift according to

$$\Gamma_A = -2\Im\Delta E_A. \tag{8.58}$$

Accordingly, after decomposition of ΔE_A up to e^4

$$\begin{aligned}\Gamma_A = \lim_{\eta\to 0}(-2\eta) \Big[&\Re\langle A|\hat{S}_\eta^{(2)}|A\rangle + 2\Re\langle A|\hat{S}_\eta^{(4)}|A\rangle \\ &+ \left|\langle A|\hat{S}_\eta^{(2)}|A\rangle\right|^2 - 2\left(\Re\langle A|\hat{S}_\eta^{(2)}|A\rangle\right)^2\Big].\end{aligned} \tag{8.59}$$

The formulas (8.56), (8.57), and (8.59) give definitions for the one-photon and

two-photon widths, $\Gamma_A^{(1\gamma)}$ and $\Gamma_A^{(2\gamma)}$, within the adiabatic $\hat{S}_\eta$ matrix formalism.

Further results are based on the "optical theorem". Omitting the details (see [82]), it can be formulated using the relations $\hat{S} = 1 + \mathrm{i}\hat{T}$ [260] and, as a consequence, $\Re\langle I|\hat{S}^{(i)}|I\rangle = -\Im\langle I|\hat{T}^{(i)}|I\rangle$:

$$-2\Re\langle I|\hat{S}^{(2i)}|I\rangle = \sum_F \left|\langle F|\hat{S}^{(i)}|I\rangle\right|^2 + \sum_{F,j<i} 2\Re\langle I|\hat{S}^{(j)\,\dagger}|F\rangle\langle F|\hat{S}^{(2i-j)}|I\rangle\,. \quad (8.60)$$

Then, collecting the second order terms, there appears the relation

$$-2\Re\langle I|\hat{S}^{(2)}|I\rangle = \sum_{F\neq I} \left|\langle F|\hat{S}^{(1)}|I\rangle\right|^2, \quad (8.61)$$

where only non-diagonal such as $\langle F||\hat{S}^{(1)}|I\rangle$ matrix elements contribute. For the fourth-order term

$$-2\Re\langle I|\hat{S}^{(4)}|I\rangle = \left|\langle I|\hat{S}_\eta^{(2)}|I\rangle\right|^2 + \sum_{F\neq I}\left|\langle F|\hat{S}^{(2)}|I\rangle\right|^2 + \sum_{F\neq I} 2\Re\langle I|\hat{S}_\eta^{(1)}|F\rangle\langle F|\hat{S}^{(3)}|I\rangle. \quad (8.62)$$

The last summand in (8.62) obviously represents radiative corrections to the one-photon width. These corrections were estimated by directly calculating the corresponding imaginary part of the two-loop diagram (Lamb shift) in [88]. It is worth noting that the $F = I$ term in the sum over F is absent in this contribution, since $\langle I|\hat{S}^{(1)}|I\rangle = \langle I|\hat{S}^{(3)}|I\rangle = 0$.

As indicated above, the adiabatic S-matrix, $\hat{S}_\eta$, arises after the introduction of the adiabatic factor $e^{-\eta|t|}$. Assuming that no dynamical excitations of the system occur when the interaction is switched on and off, the adiabatic S-matrix remains unitary [1, 184]. Thus all observables calculated on the basis of the adiabatic approach should not depend on a particular kind of adiabatic factor in the limit $\eta \to 0$. Therefore, the relations of the "optical theorem" (8.61) and (8.62) can be applied to the adiabatic formulas (8.56), (8.57) and (8.59). In the future it will also be necessary to fix not only the state of the electron in the atom, but also the number of photons.

Then it follows from (8.56), (8.57) and (8.59) that for the initial state $I = A, 0_\gamma$ (photons are absent) the one-photon width is defined by the following expression:

$$\Gamma_A^{(1\gamma)} = \lim_{\eta\to 0} \eta \sum_{F\neq A,0_\gamma} \left|\langle F|\hat{S}_\eta^{(1)}|A,0_\gamma\rangle\right|^2, \tag{8.63}$$

and the two-photon width

$$\Gamma_A^{(2\gamma)} = \lim_{\eta\to 0} \eta \left[2\sum_{F\neq A,0_\gamma} \left|\langle F|\hat{S}_\eta^{(2)}|A,0_\gamma\rangle\right|^2 + 4\left(\Re\langle A,0_\gamma|\hat{S}_\eta^{(2)}|A,0_\gamma\rangle\right)^2\right]. \tag{8.64}$$

Hereinafter the remaining fourth-order summand ($\sim e^4$)

$$\Gamma_A^{\mathrm{rad}} = \lim_{\eta\to 0} \eta \sum_{F\neq A,0_\gamma} 2\Re\langle A,0_\gamma|\hat{S}_\eta^{(1)}|F\rangle\langle F|\hat{S}_\eta^{(3)}|A,0_\gamma\rangle \tag{8.65}$$

is discarded since it represents corrections to the single-photon width.

Using (8.61), $\Gamma_A^{(2\gamma)}$ reduces to the form:

$$\Gamma_A^{(2\gamma)} = \lim_{\eta\to 0} \eta \left[2\sum_{F\neq A,0_\gamma} \left|\langle F|\hat{S}_\eta^{(2)}|A,0_\gamma\rangle\right|^2 + 2\sum_{2_\gamma} \left|\langle A,2_\gamma|\hat{S}_\eta^{(2)}|A,0_\gamma\rangle\right|^2 + \left(\sum_{F'\neq A,0_\gamma} \left|\langle F'|\hat{S}_\eta^{(1)}|A,0_\gamma\rangle\right|^2\right)^2\right]. \tag{8.66}$$

In the expression (8.66) it is necessary to distinguish between the final states (F) and (F') for two-photon and one-photon transitions. Importantly, the contribution $\left|\langle A,0_\gamma|\hat{S}_\eta^{(2)}|A,0_\gamma\rangle\right|^2$ available in (8.64) is reduced. The penultimate term in (8.66), represents the clearly unphysical transition $A \to A + 2\gamma$, but is formally present in the sum over the F states. It will be necessary for further calculations and will be reduced in the final expression (see below). The notation $\sum_{2_\gamma}$ means here integration over the frequencies of the two photons. In the following, the basic expressions for the widths of one- and two-photon decays

will be presented using the expressions (8.63) and (8.66).

8.4.4. Width of one-photon decay according to the optical theorem

The one-photon width $\Gamma_A^{(1\gamma)}$, (8.63), can be obtained from the adiabatic S_η-matrix:

$$\langle A', \boldsymbol{k}, \boldsymbol{e}|\hat{S}_\eta^{(1)}|A, 0_\gamma\rangle = e\int d^4x\bar{\psi}_{A'}(x)\gamma_\mu A_\mu^*(x)\psi_A(x)e^{-\eta|t|}. \tag{8.67}$$

Now integration over the time variable gives essentially a representation of the δ-function:

$$\int\limits_{-\infty}^{\infty} dte^{i(E_A-E_{A'}-\omega)t-\eta|t|} = \frac{2\eta}{(\omega_{AA'}-\omega)^2+\eta^2} \equiv 2\pi\,\delta_\eta(\omega_{AA'}-\omega), \tag{8.68}$$

where $\lim\limits_{\eta\to 0}\delta_\eta(x) = \delta(x)$. The next step is to perform integration over the photon frequency. For the square of the modulus (8.68) multiplied by ω, the result is

$$4\eta^2\int\limits_0^{\infty}\frac{\omega d\omega}{\left[(\omega_{AA'}-\omega)^2+\eta^2\right]^2} = 4\eta^2\left[\frac{\pi\omega_{AA'}}{4\eta^3}+\frac{1}{2\eta^2}+\frac{\omega_{AA'}}{2\eta^3}\mathrm{arctg}\left(\frac{\omega_{AA'}}{\eta}\right)\right]. \tag{8.69}$$

Then, in the limit $\eta\to 0$,

$$4\eta^2\int\limits_0^{\infty}\frac{\omega d\omega}{\left[(\omega_{AA'}-\omega)^2+\eta^2\right]^2} = \frac{2\pi\omega_{AA'}}{\eta}. \tag{8.70}$$

Taking into account the normalization factor of the photon wave function, as well as the factor from the phase volume, and multiplying by η (see (8.63), the final expression for the level width A is given by

$$\Gamma_A^{(1)} = \frac{e^2}{2\pi}\sum_{A'\,(E_{A'}<E_A)}\omega_{AA'}\sum_{\boldsymbol{e}}\int d\boldsymbol{\nu}\left|\left((\boldsymbol{e}^*\boldsymbol{\alpha})e^{-\mathrm{i}\boldsymbol{kr}}\right)_{A'A}\right|^2. \tag{8.71}$$

In the above derivation, operations with δ-functions have been excluded. Multiplication by the adiabatic parameter η in (8.63) plays the same role as dividing the result by time T (see, e.g., (4.10)): the adiabatic factor η has dimension s^{-1}. It is worth noting that this approach does not automatically exclude (see [244]) transitions to states higher than A when summing over F, and to avoid them we have to refer to the energy conservation law.

8.4.5. Width of two-photon cascade-free decay according to the optical theorem

Omitting for brevity the analytical calculations for the two-photon amlitude case, see details in [82], the following expression can be obtained:

$$\langle A', \boldsymbol{k}', \boldsymbol{e}'; \boldsymbol{k}, \boldsymbol{e}|\hat{S}_\eta^{(2)}|A, 0_\gamma\rangle = -\frac{4\eta}{[(\omega_0-\omega-\omega')^2+4\eta^2]} \times \sum_n \frac{\langle A'|\vec{\alpha}\boldsymbol{A}^*_{\boldsymbol{k}',\boldsymbol{e}'}|n\rangle\langle n|\boldsymbol{\alpha}\boldsymbol{A}^*_{\boldsymbol{k},\boldsymbol{e}}|A\rangle}{E_n - E_A + \omega}, \tag{8.72}$$

and, taking into account the permutation symmetry of photons,

$$\langle A'|\hat{S}_\eta^{(2)}|A, 0_\gamma\rangle = -\frac{4\eta}{[(\omega_0-\omega-\omega')^2+4\eta^2]} \times \left[\sum_n \frac{\langle A'|\boldsymbol{\alpha}\boldsymbol{A}^*_{\boldsymbol{k}',\boldsymbol{e}'}|n\rangle\langle n|\boldsymbol{\alpha}\boldsymbol{A}^*_{\boldsymbol{k},\boldsymbol{e}}|A\rangle}{E_n - E_A + \omega} + \sum_n \frac{\langle A'|\boldsymbol{\alpha}\boldsymbol{A}^*_{\boldsymbol{k},\boldsymbol{e}}|n\rangle\langle n|\boldsymbol{\alpha}\boldsymbol{A}^*_{\boldsymbol{k}',\boldsymbol{e}'}|A\rangle}{E_n - E_{A'} - \omega}\right]. \tag{8.73}$$

In matrix elements of photon emission operators, in contrast to S-matrix elements, the abbreviations $|A\rangle$ are introduced instead of $|A, 0_\gamma\rangle$, since in this case it is difficult to expect misunderstandings in the notations.

Substitution (8.73) into the first term in the right-hand side of the expression (8.66) in the nonrelativistic limit leads to

$$\Gamma_A^{(2\gamma),1} = \lim_{\eta\to 0} 2\eta\,(\sqrt{2\pi})^4 \frac{e^4}{(2\pi)^6} \sum_{\boldsymbol{e},\boldsymbol{e}'} \int\cdots\int \frac{d\boldsymbol{\nu}d\boldsymbol{\nu}'d\omega d\omega'\omega\omega'(4\eta)^2}{[(\omega_0-\omega-\omega')^2+4\eta^2]^2} \times \left|\sum_n \frac{\langle A'|\boldsymbol{\alpha}\boldsymbol{A}^*_{\boldsymbol{k}',\boldsymbol{e}'}|n\rangle\langle n|\boldsymbol{\alpha}\boldsymbol{A}^*_{\boldsymbol{k},\boldsymbol{e}}|A\rangle}{E_n - E_A + \omega} + \sum_n \frac{\langle A'|\boldsymbol{\alpha}\boldsymbol{A}^*_{\boldsymbol{k},\boldsymbol{e}}|n\rangle\langle n|\boldsymbol{\alpha}\boldsymbol{A}^*_{\boldsymbol{k}',\boldsymbol{e}'}|A\rangle}{E_n - E_{A'} - \omega}\right|^2. \tag{8.74}$$

Integration over ω, ω' in (8.74) can be performed using a similar method as in the previous section. One can first integrate over ω', i.e., on the interval $(\infty, 0)$ or even on $(-\infty, \infty)$, which in this case is actually equivalent. The second integration over ω should be carried out in the interval $[0, \omega_0]$ (according to the energy conservation law).

Thus, for the integral over ω' the following relation (in the limit $\eta \to 0$) can be used:

$$(4\eta)^2 \int_0^\infty \frac{\omega' d\omega'}{\left[(\omega_0 - \omega - \omega')^2 + 4\eta^2\right]^2} = \frac{\pi(\omega_0 - \omega)}{\eta}. \tag{8.75}$$

Then integration over directions of emitted photons and summation over polarizations give in the nonrelativistic limit (in the "velocity" gauge):

$$\Gamma_A^{(2\gamma),1} = \frac{4e^4}{9\pi} \int_0^{\omega_0} \omega(\omega_0 - \omega) d\omega \sum_{i,k=1}^{3} \left| \left(U_{ik}(\omega)\right)_{A'A} \right|^2, \tag{8.76}$$

$$\left(U_{ik}\right)_{A'A} = \sum_n \frac{\langle A'|p_i|n\rangle\langle n|p_k|A\rangle}{E_n - E_A + \omega} + \sum_n \frac{\langle A'|p_k|n\rangle\langle n|p_i|A\rangle}{E_n - E_{A'} - \omega},$$

where $p_i \equiv (\boldsymbol{p})_i$. For $A = 2s$, $A' = 1s$, going to the "length" gauge (using the relation $\omega_{A'A}(\boldsymbol{r})_{A'A} = \frac{\mathrm{i}}{m}(\boldsymbol{p})_{A'A}$) the expression exactly the same as (8.40) appears.

8.4.6. Reducing divergences

In contrast to the expression (8.63) for the one-photon width, in (8.66) there are two more summands diverging in the limit $\eta \to 0$. It is further shown, they are exactly reducible. Thus for the last summand in (8.66) it can be seen that in the case of no cascades (intermediate state between A and A') the only contribution to the sum over F' is $F' = A', 1_\gamma$. Then, omitting all necessary

calculations, one can come to

$$\lim_{\eta\to 0}\,\eta\left(\sum_{F'\neq A,0}\left|\langle F'|\hat{S}^{(1)}|A,0_\gamma\rangle\right|^2\right)^2=\lim_{\eta\to 0}\frac{1}{\eta}\left(\Gamma_A^{(1)}\right)^2. \tag{8.77}$$

This divergent contribution can only be eliminated by the "non-physical" (second in (8.66)) $2\sum\limits_{2\gamma}\left|\langle A,2_\gamma|\hat{S}_\eta^{(2)}|A,0_\gamma\rangle\right|^2$. The latter looks exactly like (8.74), with A' replaced by A. Assuming $n=A'$ to sum over n in $2\langle A,2_\gamma|\hat{S}_\eta^{(2)}|A,0_\gamma\rangle$, one obtains the same set of matrix elements as in (8.77). This contribution also turns out to be divergent, $\sim\eta^{-1}$, and eliminates the divergence (8.77).

The latter can be demonstrated as follows.

$$\sum_{2\gamma}\left|\langle A,2_\gamma|\hat{S}_\eta^{(2)}|A,0_\gamma\rangle\right|^2=\frac{e^4}{(2\pi)^4}\sum_{\boldsymbol{e},\boldsymbol{e}'}\int\cdots\int\frac{(4\eta)^2\omega\omega' d\boldsymbol{\nu}d\boldsymbol{\nu}'d\omega d\omega'}{\left[(\omega_0-\omega-\omega')^2+4\eta^2\right]^2} \tag{8.78}$$
$$\times\left|\frac{\langle A|\boldsymbol{\alpha}\boldsymbol{A}^*_{\boldsymbol{k}',\boldsymbol{e}'}|A'\rangle\langle A'|\boldsymbol{\alpha}\boldsymbol{A}^*_{\boldsymbol{k},\boldsymbol{e}}|A\rangle}{E_{A'}-E_A+\omega+\mathrm{i}\eta}+\frac{\langle A|\boldsymbol{\alpha}\boldsymbol{A}^*_{\boldsymbol{k},\boldsymbol{e}}|A'\rangle\langle A'|\boldsymbol{\alpha}\boldsymbol{A}^*_{\boldsymbol{k}',\boldsymbol{e}'}|A\rangle}{E_{A'}-E_A-\omega+\mathrm{i}\eta}\right|^2.$$

In this expression, it is necessary to keep $\mathrm{i}\eta$ in the energy denominators to keep track of all divergences. In summary

$$2\eta\sum_{2\gamma}\left|\langle A,2_\gamma|\hat{S}_\eta^{(2)}|A,0_\gamma\rangle\right|^2=\frac{2\eta e^4}{(2\pi)^4}\sum_{\boldsymbol{e},\boldsymbol{e}'}\int d\boldsymbol{\nu}d\boldsymbol{\nu}'\left|\langle A|\boldsymbol{\alpha}\boldsymbol{A}^*_{\boldsymbol{k},\boldsymbol{e}}|A'\rangle\right|^4\times$$
$$\left(-\frac{\pi}{\eta}\right)\int\omega^2 d\omega\left|\frac{1}{E_{A'}-E_A+\omega+\mathrm{i}\eta}+\frac{1}{E_{A'}-E_A-\omega+\mathrm{i}\eta}\right|^2. \tag{8.79}$$

Finally, the expression (8.79) can be written in the form:

$$\lim_{\eta\to 0}2\eta\sum_{2\gamma}\left|\langle A,2_\gamma|\hat{S}_\eta^{(2)}|A,0_\gamma\rangle\right|^2=-\lim_{\eta\to 0}\frac{1}{2\pi}\left(\Gamma_A^{(1)}\right)^2F(\eta), \tag{8.80}$$

where

$$F(\eta)=4\omega_0^2\int\frac{d\omega}{(\omega_0^2-\eta^2-\omega^2)^2+4\eta^2\omega_0^2}. \tag{8.81}$$

By performing the necessary calculations (see details in [82]), it can be found that

$$F(\eta) = \frac{4\pi i}{2i\eta} = \frac{2\pi}{\eta}. \tag{8.82}$$

Substituting the obtained result into (8.80), the contribution of the second summand to (8.66) is exactly equal and opposite in sign to (8.77) (the last summand in (8.66)). The remaining n summands with $n \neq A'$ in the expression for $2\langle A, 2_\gamma|\hat{S}_\eta^{(2)}|A, 0_\gamma\rangle$, can be ignored because they do not satisfy the energy conservation law.

Thus, the second and third terms in (8.66) in the absence of cascades compensate each other, and the two-photon width is determined entirely by the first term, $\Gamma_A^{(2\gamma),1} = \Gamma_A^{(2\gamma)}$. Then, (8.76) coincides exactly with the standard QED expression for the two-photon decay width in the absence of cascades, see, e.g., (8.40) for the case of $2s$.

8.4.7. Two-photon decay width in the presence of cascade radiation

The derivation of the expression for the two-photon decay width in the presence of cascades does not differ in principle from the previous one. The expression (8.74) is valid in this case as well. Considering that there is only one cascade channel (e.g., $3s - 2p - 1s$ in the case of decay of the $3s$ level in hydrogen), the only difference is the existence of an additional divergence at $n = r$ in the sum over n in (8.74): $\omega = E_A - E_r$ (r is the resonance state). In view of the energy conservation, this also implies the existence of another resonance (the lower branch of the cascade): $\omega' = E_r - E_{A'}$. Now (8.76) contains two divergences as η^{-1}: for $F' = A', 1_\gamma$ (this divergence is analogous to the case of no cascades) and $F' = r, 1_\gamma$ (additional divergence due to the existence of a cascade). The first one is compensated by the term $n = A'$ in the "unphysical contribution" $\langle A, 2_\gamma|\hat{S}_\eta^{(2)}|A, 0_\gamma\rangle$, and the latter is similarly compensated by the $n = r$ summand in the expression for $\langle A, 2_\gamma|\hat{S}_\eta^{(2)}|A, 0_\gamma\rangle$. However, in the presence of a cascade, a third divergence arises directly when summing over n

(when $n = r$) in expression (8.79). This divergence cannot be eliminated by any counter term because it is proportional to the special product of the elements: $|\langle A'|p_i|r\rangle\langle r|p_k|A\rangle|^2$, there is no counter term containing such a product in the expression (8.66). One can eliminate this remaining divergence only by taking into account (at a given order of perturbation theory) radiative corrections to the level width. Equivalently, one can introduce a level width, as was done in [85]. Thus, evaluating the two-photon decay width in the presence of cascades reveals the same expressions with the same problems discussed above (see section 8.4.1).

8.4.8. Two-photon decay width as an imaginary part of the two-loop radiative correction

The separation of "pure" radiation for two-photon decays of highly excited states (with $n > 2$), required in astrophysical studies, led to the appearance of the so-called "alternative" approach, see, for example, [256]. This approach is based on calculating the imaginary part of the two-loop diagram to the self-energy of the electron. Thus, in [256] it was shown that the divergence arising in this case can be eliminated by means of the integral

$$I_1 = \int_0^1 \left|\frac{1}{a-\omega+i\epsilon}\right|^2 d\omega = \frac{\pi}{\epsilon} + \frac{1}{a(a-1)} + O(\epsilon^2) \tag{8.83}$$

where $0 < a < 1$ and the result is written out in lowest order by $\epsilon \to 0$ (and, of course, $\epsilon \ll a$). The convergent second summand in (8.83) was used to obtain a finite number that was interpreted as the width of the "pure" two-photon emission. Omitting for brevity the details of the evidence for the ineligibility of this interpretation presented in [82], this section present another reason for this. It fully utilizes the theory presented in the [253–256], but leads to different conclusions on the results obtained.

It should be pointed out that the determination of the excited level width through the imaginary part of the one-loop correction to the self-energy of the bound electron can be proved completely analytically [244]. The calculation

reduces to the so-called cutting of the diagram. The result can be obtained in the form:

$$\Gamma_A = -2\Im\Delta E_A. \tag{8.84}$$

These widths are contributed by the sum of the probabilities of one-photon transitions to lower levels (one-photon width $\Gamma_A^{(1\gamma)}$). One would expect that the imaginary part of the two-loop contributions, see Fig. 8.3, should contain two-photon widths. In case Γ_A also coincides with the sum of two-photon decay

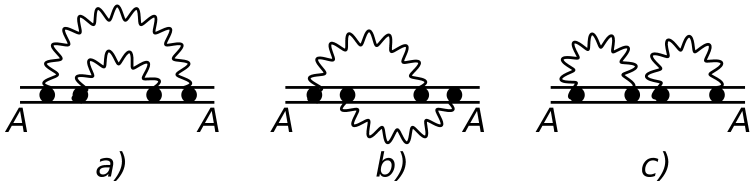

Figure 8.3. A set of two-loop Feynman diagrams used to calculate the "two-photon width". Depending on how the diagram is "cut", corrections to the one- and two-photon decay widths arise (a detailed description is given in [121]). The standard notations are used here: the state for which the correction is needed is denoted by A, the wavy line denotes the photon propagator, the double solid line denotes the electron propagator. Diagrams a), b) are irreducible, while c) is reducible. The latter requires the use of the adiabatic theory of the S-matrix to eliminate additionally arising divergences due to "reference" states.

probabilities (including cascades), see, e.g., (8.40), the perturbation theory for the imaginary part of the radiative shift of energy levels would not exist: the cascade contributions are always of the same order (parametrically) as the one-photon widths. The present analysis shows that this is not the case. In the case of two loops, the expression (8.40) does not arise. Instead of the square of the modulus, the real part appears, as obtained in [256]. Details of the calculations can be found in [84, 121].

The imaginary part of the two-photon radiative corrections to the self-energy of the electron arises from the corresponding "cutting" of the diagrams in Fig. 8.3. Not all possible such procedures will lead to two-photon contributions: corrections to one-photon widths will also appear. It should be noted that one should not "cut" the vacuum loops, since the corrections to the vacuum polarization do not give a contribution to the imaginary part of the energy. The

result for the case of the two-photon contribution is

$$\tilde{\Gamma}^{(2\gamma)}_{3s,1s} = e^4 \lim_{\eta\to 0} \Re \sum_{\boldsymbol{e},\boldsymbol{e}'} \int d\boldsymbol{\nu} \int d\boldsymbol{\nu}' \int_0^{\omega_0} d\omega \frac{\omega(\omega_0-\omega)}{2^4\pi^3} \times \tag{8.85}$$

$$\left[\sum_{n_1} \frac{\langle A'|\boldsymbol{\alpha}\boldsymbol{A}^*_{\boldsymbol{k}',\boldsymbol{e}'}|n_1\rangle\langle n_1|\boldsymbol{\alpha}\boldsymbol{A}^*_{\boldsymbol{k},\boldsymbol{e}}|A\rangle}{E_{n_1}-E_A+\omega} + \sum_{n_2} \frac{\langle A'|\boldsymbol{\alpha}\boldsymbol{A}^*_{\boldsymbol{k},\boldsymbol{e}}|n_2\rangle\langle n_2|\boldsymbol{\alpha}\boldsymbol{A}^*_{\boldsymbol{k}',\boldsymbol{e}'}|A\rangle}{E_{n_2}-E_{A'}-\omega}\right] \times$$

$$\left[\sum_{n_3} \frac{\langle A'|\boldsymbol{\alpha}\boldsymbol{A}^*_{\boldsymbol{k}',\boldsymbol{e}'}|n_3\rangle\langle n_3|\boldsymbol{\alpha}\boldsymbol{A}^*_{\boldsymbol{k},\boldsymbol{e}}|A\rangle}{E_{n_3}-E_A+\omega} + \sum_{n_3} \frac{\langle A'|\boldsymbol{\alpha}\boldsymbol{A}^*_{\boldsymbol{k},\boldsymbol{e}}|n_3\rangle\langle n_3|\boldsymbol{\alpha}\boldsymbol{A}^*_{\boldsymbol{k}',\boldsymbol{e}'}|A\rangle}{E_{n_3}-E_{A'}-\omega}\right]^* .$$

As mentioned above, (8.85) has a real part, which immediately shows the difference with the standard expression (8.40), which has the square of the modulus of the radiation amplitude. "Dangerous" denominators do not require regularization and reduce to finite terms, so that the two-photon contribution $\tilde{\Gamma}^{(2\gamma)}_{AA'}$ does not violate perturbation theory. In turn, the two-photon transition probability contains a singularity corresponding to the cascade and requires regularization. Thus, the value $\tilde{\Gamma}^{(2\gamma)}_{3s,1s}$ is no longer the two-photon level width (the sum of probabilities of transitions to lower states). Numerical results for $\tilde{\Gamma}^{(2\gamma)}_{3s,1s}$ are presented in Table 8.3.

The main conclusion from Table 8.3 is that the $\tilde{\Gamma}^{(2\gamma)}_{AA'}$ widths cannot be regarded as "pure" two-photon emission widths (or probabilities of "pure" two-photon transitions to a particular final state), but are two-photon corrections to the total level width. This claim is supported by the fact that some values of $\tilde{\Gamma}^{(2\gamma)}_{AA'}$ turn out to be negative: $4d-2s$ and $5s-3d$ transitions, see Table 8.3. This makes it impossible to consider $\tilde{\Gamma}^{(2\gamma)}_{AA'}$ as transition probabilities and hence to use them in radiative transfer theory [76, 99].

In the analysis it is necessary to point out the weighty contribution of T. Zalialiutdinov.

Table 8.3. Two-photon contributions $\tilde{\Gamma}^{(2\gamma)}_{AA'}$, (8.85), to the total atomic level width for the hydrogen atom. The values are given in s^{-1}.

State		n'				
nl	$n'l$	1	1, [256]	2	3	4
$2s$	$n's$	8.229355	8.229352	-	-	-
$3s$	$n's$	2.083086	2.082853	0.064531	-	-
$3d$	$n's$	1.042708	1.042896	0.000776	-	-
$4s$	$n's$	0.699717	0.698897	0.016843	0.002925	-
$4s$	$n'd$	-	-	-	9.69×10^{-6}	-
$4p$	$n'p$	-	-	0.015623	0.002503	-
$4d$	$n's$	0.598406	0.598798	-0.007319	0.000030	-
$4d$	$n'd$	-	-	-	0.001685	-
$4f$	np	-	-	0.031754	0.000044	-
$5s$	$n's$	0.288117	0.287110	0.081741	0.000704	0.000298
$5s$	$n'd$	-	-	-	-0.000028	1.82×10^{-6}

8.5. Two-photon approximation in multiphoton decay processes

Within the framework of the study of multiphoton radiation processes, the question of the inseparability of cascade and "pure" radiation from full probability has led to the following problem. It can be seen that in multiphoton processes involving cascade radiation there are transitions belonging to the "two-photon link". For example, one can point to the decay of the $3p$ state in the hydrogen atom. In addition to the dominant one-photon decay directly to the ground state, there is a three-photon process. Such transitions ($E1E1E1$) are allowed according to the selection rules, although they are small. The order of magnitude of the probabilities of $E1E1E1$ transitions is determined by the estimate $c_{3\gamma}\alpha(\alpha Z)^8$ (in atomic units). Calculations (see, e.g., [114]) show that the numerical coefficient $c_{3\gamma}$ is also found to be small, for $2p \to 1s + 3\gamma$ $c_{3\gamma} \approx 0.263 \times 10^{-4}$ atomic units [114]. A more detailed study of three-photon (cascade-free) emission processes was presented in [123], where calculations in hydrogen-like ions were performed for a wide set of values of the nuclear charge

Z. Cascade-free processes may be interesting due to the fact that they cannot be effectively reabsorbed, and thus should lead to direct radiation escape from matter. The probability of cascade processes (see the previous section) is of the same order as the one-photon decay directly to the ground state, $\sim \alpha^3 Z^4$ atomic units. Consequently, one can ask what is the probability of detecting a "pure" two-photon emission process in a cascade decay with the presence of a two-photon link in it.

It should be noted that in the context of studying only the radiation process one can inquire about the dependence of the initial state on the process of its formation (see the previous sections). In principle, the QED treatment of any process is absolutely certain only when this process begins with a stable state and ends also with a stable (metastable) state. Then the question about the preparation process of an excited state does not arise. In this context, all atomic states can be considered as metastable, since the widths of energy levels are always smaller than the intervals between levels. Of course, the formulation of the problem of the transition probability from some initial excited state is always an idealization. Such a formulation is possible provided that in the process of creation of the initial state the nonresonant corrections can be considered negligible. The NR corrections depend on the excitation process; however, it can be stated with high accuracy that they are relatively small for all types of excitation processes. Consequently, one can safely assume that the creation history of the initial state has no influence on the estimates of cascade transitions. The presence of interference should also be noted. According to previous discussions (see on the inseparability of cascade and "pure" radiation), this phenomenon is quite insignificant, since interference should be considered for an equal number of photons, i.e., with "pure" three-photon radiation $\sim 10^{-4}\alpha(\alpha Z)^8$ at $Z = 1$. The above circumstances refer to the basic approximations used to determine the probability of transition from level A to the ground state by cascade decay. By registering a frequency with energy related to a two-photon link (e.g. $3p-2p$ or $2s-1s$ for the decay of the $3p$ state), the decay rate may not coincide with the natural width of the A level.

As a first example, consider the three-photon transition from the $3p$ state to the $1s$ ground level of the hydrogen atom. It has several cascade channels:

$3p \to 2p + 2\gamma \to 1s + \gamma$ and $3p \to 2s + \gamma \to 1s + 2\gamma$. Both involve "pure" two-photon emission ("two-photon link") associated with the $3p \to 2p + 2\gamma$ and $2s \to 1s + 2\gamma$ transitions. The decay process of the $3p$ state, including three-photon cascade emission, is schematically depicted in Fig. 8.4.

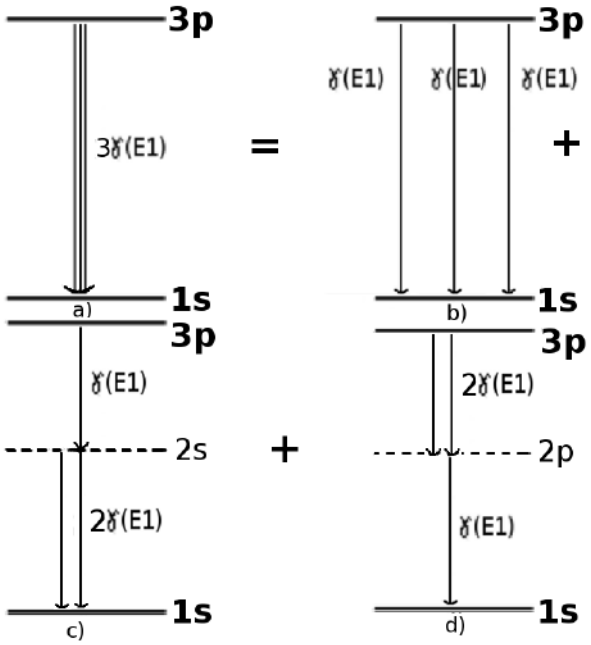

Figure 8.4. Schematic representation of the $3p \to 1s + 3\gamma(E1)$ transition. The triple vertical line with arrow (a)) denotes the total three-photon contribution consisting of a "pure" three-photon decay to the $1s$ state (b), a one-photon transition to the $2s$ state followed by a two-photon link (c), and a two-photon $3p - 2p$ link followed by a one-photon decay d).

Using the standard S-matrix formalism to describe the three-photon emission process (see details in [115]), in the framework of the resonance approximation (see above), the contribution to the $2s$ and $2p$ states, Fig. 8.4 (c), (d), respectively, should be distinguished in the emission amplitude. Using the regularization of the resonance contributions according to the procedure described in [8,85], as well as carrying out all the necessary intermediate calculations, the following expression can be obtained:

$$W_{3p,1s}^{(\mathrm{total})} = W_{3p,1s}^{(1\gamma)} + W_{3p,1s}^{(3\gamma)} = W_{3p,1s}^{(1\gamma)} + \frac{W_{2p,1s}^{(1\gamma)}}{\Gamma_{2p}} W_{3p,2p}^{(2\gamma)} + \frac{W_{3p,2s}^{(1\gamma)}}{\Gamma_{3p}} W_{2s,1s}^{(2\gamma)}, \quad (8.86)$$

where the integration over the frequency of the one-photon link in the cascade

radiation was also performed. The result of integration of the corresponding Lorentz contour is the appearance of the branching ratio in front of the two-photon emission probabilities in (8.86). The coefficient in the second summand is equal to one in the highest order, but is retained to demonstrate its emergence from the three-photon process. It is worth noting that the 3/4 coefficient obtained in [115] is incorrect and must be replaced by one as in (8.86). The latter was noted in [121]. The numerical values for the last two summands in (8.86) give

$$\frac{W^{(1\gamma)}_{2p,1s}}{\Gamma_{2p}} W^{(2\gamma)}_{3p,2p} = 0.0475 \text{ s}^{-1}, \qquad (8.87)$$
$$\frac{W^{(1\gamma)}_{3p,2s}}{\Gamma_{3p}} W^{(2\gamma)}_{2s,1s} = 0.9738 \text{ s}^{-1},$$

which turns out to be significant compared to the order of magnitude of the 10 s^{-1} two-photon contribution to the 2γ-decay probability of the $3s$ level [164, 252].

The calculations for the four-photon emission probability $4s \to 1s + 4\gamma$ were carried out in a similar way. The decay process with the presence of two-photon links is schematically depicted in Fig. 8.5. Within the same approximations, given the correct coefficient, the final result can be represented as

$$W^{(\text{total})}_{4s,1s} = W^{(2\gamma)}_{4s,1s} + W^{(4\gamma)}_{4s,1s} = W^{(2\gamma)}_{4s,1s} + \qquad (8.88)$$
$$\frac{W^{(1\gamma)}_{3s,2p}}{\Gamma_{3s}} \frac{W^{(1\gamma)}_{2p,1s}}{\Gamma_{2p}} W^{(2\gamma)}_{4s,3s} + \frac{W^{(1\gamma)}_{4s,3p}}{\Gamma_{4s}} \frac{W^{(1\gamma)}_{2p,1s}}{\Gamma_{2p}} W^{(2\gamma)}_{3p,2p} + \frac{W^{(1\gamma)}_{4s,3p}}{\Gamma_{4s}} \frac{W^{(1\gamma)}_{43p,2s}}{\Gamma_{3p}} W^{(2\gamma)}_{2s,1s}.$$

The corresponding numerical result:

$$\frac{W^{(1\gamma)}_{2p,1s}}{\Gamma_{2p}} \frac{W^{(1\gamma)}_{3s,2p}}{\Gamma_{3s}} W^{(2\gamma)}_{4s,3s} = 0.0029 \text{ s}^{-1}, \qquad (8.89)$$
$$\frac{W^{(1\gamma)}_{4s,3p}}{\Gamma_{4s}} \frac{W^{(1\gamma)}_{2p,1s}}{\Gamma_{2p}} W^{(2\gamma)}_{3p,2p} = 0.0199 \text{ s}^{-1},$$
$$\frac{W^{(1\gamma)}_{4s,3p}}{\Gamma_{4s}} \frac{W^{(1\gamma)}_{3p,2s}}{\Gamma_{3p}} W^{(2\gamma)}_{2s,1s} = 0.4076 \text{ s}^{-1}.$$

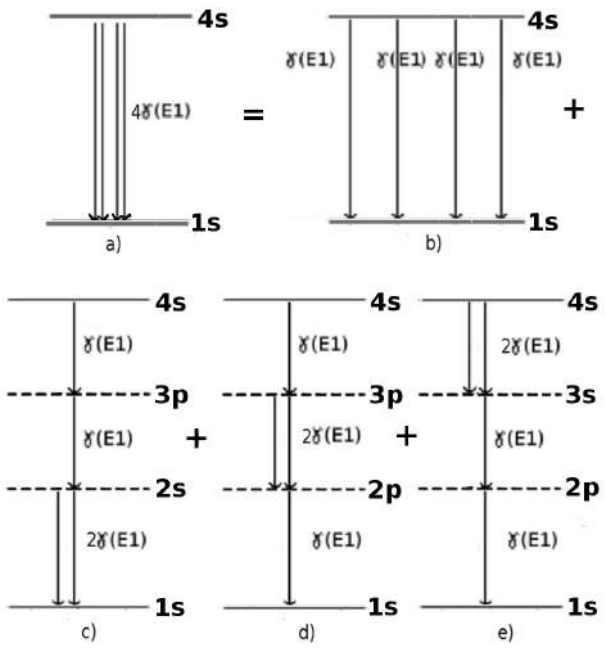

Figure 8.5. Schematic representation of the $4s \to 1s + 4\gamma(E1)$ transition with the presence of two-photon links. The notations are similar to Fig. 8.4.

Finally, in [116], the case of four-photon decay of the decay of the $4d$ state was considered with result

$$W^{(\mathrm{total})}_{4d,1s} = W^{(2\gamma)}_{4d,1s} + \frac{W^{(1\gamma)}_{3s,2p}}{\Gamma_{3s}} \frac{W^{(1\gamma)}_{2p,1s}}{\Gamma_{2p}} W^{(2\gamma)}_{4d,3s} + \frac{W^{(1\gamma)}_{3d,2p}}{\Gamma_{3d}} \frac{W^{(1\gamma)}_{2p,1s}}{\Gamma_{2p}} W^{(2\gamma)}_{4d,3d} \quad (8.90)$$
$$+ \frac{W^{(1\gamma)}_{4d,3p}}{\Gamma_{4d}} \frac{W^{(1\gamma)}_{2p,1s}}{\Gamma_{2p}} W^{(2\gamma)}_{3p,2p} + \frac{W^{(1\gamma)}_{4d,3p}}{\Gamma_{4d}} \frac{W^{(1\gamma)}_{3p,2s}}{\Gamma_{3p}} W^{(2\gamma)}_{2s,1s},$$

$$\frac{W^{(1\gamma)}_{3s,2p}}{\Gamma_{3s}} \frac{W^{(1\gamma)}_{2p,1s}}{\Gamma_{2p}} W^{(2\gamma)}_{4d,3s} = 6.045 \times 10^{-6}\ \mathrm{s}^{-1}, \quad \frac{W^{(1\gamma)}_{3d,2p}}{\Gamma_{3d}} \frac{W^{(1\gamma)}_{2p,1s}}{\Gamma_{2p}} W^{(2\gamma)}_{4d,3d} = 0.0017\ \mathrm{s}^{-1},$$
$$\frac{W^{(1\gamma)}_{4d,3p}}{\Gamma_{4d}} \frac{W^{(1\gamma)}_{2p,1s}}{\Gamma_{2p}} W^{(2\gamma)}_{3p,2p} = 0.0121\ \mathrm{s}^{-1}, \quad \frac{W^{(1\gamma)}_{4d,3p}}{\Gamma_{4d}} \frac{W^{(1\gamma)}_{3p,2s}}{\Gamma_{3p}} W^{(2\gamma)}_{2s,1s} = 0.2477\ \mathrm{s}^{-1}.$$

The paper [120], where a detailed calculation of the scattering process of $1s + \gamma \to 3p \to 1s + 3\gamma$ (from stable to stable state) was performed, should be emphasized. As before, a cascade with the presence of two-photon links in the radiation process was considered. The aim of the study was, first, to investigate the influence of the state preparation on the emission process (in the framework of the resonance approximation, as expected, no such influence was found) and, second, to compare in detail the QM and QED approaches to regularize the

resonance contributions. It was shown that the QM approach also produces a sum of widths for the cascade (resonance) state. The result for the scattering process was obtained in the form:

$$b^{(3\gamma)}_{3p-1s}(3p-2s-1s) = \frac{W^{(1\gamma)}_{3p-2s} W^{(2\gamma)}_{2s-1s}}{\Gamma_{3p}\Gamma_{2s}}, \tag{8.91}$$

where $b^{3\gamma}_{3p-1s}(3p-2s-1s-1s)$ represents the branching ratio.

Several remarks should be made at once. The first one refers to the fact that in the case of the description of the scattering process instead of simply radiation there appears a dimensionless branching ratio b. This is the result of integration over the frequency of the absorbed photon and the corresponding resonance profile (the latter appears as an additional absorption amplitude and energy denominator), see [120] for details. The second remark refers to the fact that the width Γ_{2s} is highly determined by the probability $W^{(2\gamma)}_{2s-1s}$ in the hydrogen atom, and hence in the expression (8.91) their ratio could be put equal to one. The exclusion of this coefficient leads, it would seem, to a contradiction with the previous results. However, it should be pointed out that the dimensionless coefficient b makes it possible to determine the probability of a two-photon transition in a cascade radiation process as follows.

The value b should determine the probability of the $3p \to 1s + 3\gamma$ transition through the $3p \to 2s + \gamma \to 1s + 2\gamma$ channel, which is much smaller than the main decay channel of the $3p$ state, i.e., $W^{(1\gamma)}_{3p-1s}$. Considering that the value $b^{3\gamma}_{3p-1s}(3p-2s-1s)$ is the branching ratio for the three-photon transition probability $W^{(3\gamma)}_{3p,1s}(3p-2s-1s)$ to the two-photon transition width Γ_{2s}, from (8.91) follows

$$W^{(3\gamma)}_{3p,1s}(3p-2s-1s) = \frac{W^{(1\gamma)}_{3p-2s}}{\Gamma_{3p}} W^{(2\gamma)}_{2s-1s}. \tag{8.92}$$

Similarly for the cascade $3p \to 2p + 2\gamma \to 1s + 3\gamma$:

$$b^{(3\gamma)}_{3p-1s}(3p-2p-1s) = \frac{W^{(1\gamma)}_{2p,1s} W^{(2\gamma)}_{3p,2p}}{\Gamma_{2p}\Gamma_{3p}}. \tag{8.93}$$

In contrast to $b^{3gamma}_{3p,1s}(3p-2s-1s)$, the value (8.93) should be viewed as the branching ratio for the transition probability over a $3p \to 2p + 2\gamma \to 1s + \gamma$ channel to the total $3p$ width of the level, i.e., Γ_{3p}. Then

$$W^{(3\gamma)}_{3p,1s}(3p-2p-1s) = \frac{W^{(1\gamma)}_{2p,1s}}{\Gamma_{2p}} W^{(2\gamma)}_{3p,2p}, \tag{8.94}$$

leading to the same result as (8.86).

Thus, we can formulate a two-photon approximation that permits to distinguish cascade radiation with two-photon links. This type of cascade contributes to two-photon transitions (i.e., to the radiation escape) comparable to the contribution of "direct" two-photon transitions. The calculations of two-photon transition probabilities were performed within the framework of these studies in the nonrelativistic approximation by the Coulomb Green's function method and are in good agreement with the corresponding fully relativistic values (at the level $\leq 0.01\%$). The basic formulas for such calculations were presented in [111, 117], where the method of calculating the multiphoton emission probabilities for the sublevels corresponding to the fine structure of the atomic state is also presented.

Chapter 9.

Emission probabilities in an external electric field

9.1. Probability of $2s$ level decay in a hydrogen atom in an external electric field

According to the theory presented in section 8.2, it is quite simple to calculate the probability of one-photon decay of the $2s$ state in a hydrogen atom placed in an external electric field. The corresponding probability was studied in detail in [103] in order to reveal effects imitating violating spatial parity (see also another application of the phenomenon in [104, 105]).

To address this issue, within the framework of analytical calculations, see, e.g., [106], the wave function can be represented as:

$$|\overline{2s}, m_s\rangle = |2s, m_s\rangle + \eta \sum_{m'_s} \langle 2p_{1/2}, m'_s | e(\boldsymbol{\mathcal{E}}\boldsymbol{r}) | 2s_{1/2}, m_s\rangle |2p_{1/2}, m'_s\rangle. \qquad (9.1)$$

The matrix element due to the dipole interaction with the external electric field $\boldsymbol{\mathcal{E}}$ refers, as before, to the Stark coefficient (see previous sections of the thesis). However, a more accurate notation for the η coefficient is used in the following calculations: $\eta = (\Delta E_L + \mathrm{i}\Gamma_{2p}/2)^{-1}$. The result of the calculations [106, 112–114]

is

$$dW_{\overline{2s},1s} = W_0 \left[1 \mp \beta(\mathcal{E})(\boldsymbol{\nu}\boldsymbol{\mathcal{E}})/\mathcal{E}\right] d\boldsymbol{\nu}, \tag{9.2}$$

where the notations are introduced (see [103]):

$$W_0 = dW^{(1\gamma)}_{2s,1s} + \frac{e^2\mathcal{E}^2}{(\Delta E_L)^2 + \frac{1}{4}\Gamma^2_{2p}} dW^{(1\gamma)}_{2p_{1/2},1s}, \tag{9.3}$$

$$\beta(\mathcal{E}) = |e|\mathcal{E}\frac{\Gamma_{2p}\sqrt{W^{(1\gamma)}_{2s,1s}W^{(1\gamma)}_{2p_{1/2},1s}}}{W^{(1\gamma)}_{2s,1s}\left(\Delta E_L^2 + \frac{1}{4}\Gamma^2_{2p}\right) + e^2\mathcal{E}^2 W^{(1\gamma)}_{2p_{1/2},1s}}.$$

The $\mp$ sign in the formula (9.2) corresponds to hydrogen $(-)$ and anti-hydrogen $(+)$ atoms. Hence, the function $\beta(\mathcal{E})$ determines the difference between H and $\bar{\text{H}}$ in the probability of a $2s-1s$ transition in an external electric field. The maximum value of $\beta(\mathcal{E})$, see [103], is reached in the field with the strength of

$$\mathcal{E}_{\max} = \frac{1}{|e|}\sqrt{\frac{W^{(1\gamma)}_{2s,1s}}{W^{(1\gamma)}_{2p_{1/2},1s}}\left(\Delta E_L^2 + \frac{1}{4}\Gamma^2_{2p}\right)} \approx 0.3 \times 10^{-4}\ \text{V/cm} \tag{9.4}$$

and, then, $\beta_{\max} \equiv \beta(\mathcal{E}_{\max}) = \Gamma_{2p}\sqrt{\Delta E_L^2 + \Gamma^2_{2p}/4} \approx 1/20$. The relative difference of one-photon $2s-1s$ transition probabilities of atoms H and $\bar{\text{H}}$ in an external electric field $\mathcal{E}_{\max}$ is equal to

$$\frac{\Delta\left(dW_{\overline{2s},1s}\right)}{dW_{2s,1s}} = \frac{2W_0\beta_{\max}}{dW_{2s,1s}} = \frac{1}{5}\cos\phi, \tag{9.5}$$

where ϕ is the angle between the vectors $\boldsymbol{\mathcal{E}}$ and $\boldsymbol{\nu}$. Thus, only in very weak fields (9.4) this difference is close to 20% and it can be detected in experiments like [134, 182].

9.2. Two-photon decay of $2s$ and $2p$ hydrogen states in an external electric field

In this part of the thesis, the probabilities of two-photon $2s-1s$ and $2p-1s$ transitions for the hydrogen atom in the presence of an external electric field are considered. As in the previous chapter 7 and section 9.1, only the mixing of $2s$ and $2p$ states is considered here. This level mixing leads to additional two-photon decays $E1E2$ and $E1M1$ in addition to the dominant two-photon $E1E1$ transition. As shown in the previous sections, the probabilities of the two-photon $E1E2$ or $E1M1$ transition are about $(\alpha Z)^2$ times smaller than the probability of the $E1E1$ transition. However, given the rapidly increasing precision of spectroscopic experiments, the probabilities of two-photon $E1E2$ or $E1M1$ transitions can be considered as a correction to the $E1E1$ decay. Moreover, as was shown in [112,114], in the presence of an external electric field, contributions linear in the field are added to the $E1E1$ transition probability due to interference. The description of two-photon decays in an external electric field can be addressed to experiments of the type [182], which use the influence of an external electric field to register the absorption process.

Omitting for brevity the analytical calculations presented in [112, 114] and based on the theory outlined above, the final result can be represented as:

$$\begin{aligned}\frac{dW^{(2\gamma)}_{\overline{2s},1s}}{d\boldsymbol{\nu}d\boldsymbol{\nu}'} = W_0 \big[1 \pm \beta_1(\mathcal{E})\left[\boldsymbol{\nu}_{\boldsymbol{\mathcal{E}}}\boldsymbol{\nu} + \boldsymbol{\nu}_{\boldsymbol{\mathcal{E}}}\boldsymbol{\nu}'\right](1+(\boldsymbol{\nu}\boldsymbol{\nu}')^2) \\ \pm\beta_2(\mathcal{E})\left[\boldsymbol{\nu}_{\boldsymbol{\mathcal{E}}}\boldsymbol{\nu} + \boldsymbol{\nu}_{\boldsymbol{\mathcal{E}}}\boldsymbol{\nu}'\right](1+\boldsymbol{\nu}\boldsymbol{\nu}_{\mathbf{k}'})\big],\end{aligned} \tag{9.6}$$

where $W_0 = W^{(2\gamma)}_{2s} + \widetilde{W}^{(2\gamma)}_{2p} e^2\mathcal{E}^2/\Delta^2$, $\widetilde{W}^{(2\gamma)}_{2p}$ is the sum of $E1E2$ and $E1M1$ transition probabilities, $\boldsymbol{\nu}_{\boldsymbol{\mathcal{E}}} = \boldsymbol{\mathcal{E}}/\mathcal{E}$ and $\Delta = \sqrt{\Delta E_L^2 + \Gamma^2_{2p}/4}$. The functions $\beta_1(\mathcal{E})$ and $\beta_2(\mathcal{E})$ are defined as follows

$$\begin{aligned}\beta_1(\mathcal{E}) &= \frac{0.000230135(\alpha Z)^7}{W_0\pi^3}\frac{|e|\mathcal{E}\Gamma_{2p}}{\Delta^2}, \\ \beta_2(\mathcal{E}) &= \frac{0.0000340919(\alpha Z)^7}{W_0\pi^3}\frac{|e|\mathcal{E}\Gamma_{2p}}{\Delta^2}.\end{aligned} \tag{9.7}$$

The maximum values of β_1 (or β_2) are reached at the value of field strength

$$\mathcal{E}_{\max} = \frac{w^{2\gamma}\Delta}{|e|} \approx \pm 0.000018\,\text{a.u.} \approx \pm 57\,\text{kV/cm}. \tag{9.8}$$

Here $w^{2\gamma} = W_{2p}^{(2\gamma)}/W_{2s}^{(2\gamma)}$, and the signs $(-)$ and $(+)$ refer to the atoms H and $\bar{\text{H}}$, respectively.

Then the maximum value of $dW_{\overline{2s}\,1s}^{(2\gamma)}$ is expressed as

$$\begin{aligned}\frac{dW_{\overline{2s},1s}^{(2\gamma)}}{d\boldsymbol{\nu}d\boldsymbol{\nu}'} = W_0(\mathcal{E}_{\max})\,\big[1 \pm 0.00024397\,[\boldsymbol{\nu}_{\boldsymbol{\mathcal{E}}}\boldsymbol{\nu} + \boldsymbol{\nu}_{\boldsymbol{\mathcal{E}}}\boldsymbol{\nu}']\,(1 + (\boldsymbol{\nu}\boldsymbol{\nu}')^2) \\ \pm 0.00003614\,[\boldsymbol{\nu}_{\boldsymbol{\mathcal{E}}}\boldsymbol{\nu} + \boldsymbol{\nu}_{\boldsymbol{\mathcal{E}}}\boldsymbol{\nu}']\,(1 + \boldsymbol{\nu}\boldsymbol{\nu}')\big]\,.\end{aligned} \tag{9.9}$$

Integration over the directions of emitted photons $\boldsymbol{\nu}$ and $\boldsymbol{\nu}'$ leads to a value for the two-photon $E1E1$ decay probability of the $2s$ state, since the interference terms give zero. But for the differential transition probability, the interference terms clearly show a linear dependence on the external electric field $\boldsymbol{\mathcal{E}}$. Thus, the total two-photon transition probability $W_{\overline{2s},1s}^{(2\gamma)}$, integrated over the photon directions, is equal to

$$\begin{aligned}W_{\overline{2s}\,1s}^{(2\gamma)}(\mathcal{E}_{\max}) = W_0(\mathcal{E}_{\max}) = W_{2s}^{(2\gamma)} + \frac{\widetilde{W}_{2p}^{(2\gamma)} e^2 \mathcal{E}_{\max}^2}{\Delta^2} \\ \approx 3.98116 \times 10^{-16}\,\text{a.u.} \approx 16.4585\,\text{s}^{-1},\end{aligned} \tag{9.10}$$

i.e. twice as much as in the absence of the field.

In principle, the dependence on the external electric field in the transition probability $W_{\overline{2s}\,1s}^{(2\gamma)}$ can be regarded as a correction that does not vanish after integration over the photon emission directions. If we refer to the radiative correction considered in [246], it is easy to see that the radiative correction (expression (36) in [246]) $\delta\Gamma_{2s}/\Gamma_{2s} = -2.020536\frac{\alpha}{\pi}(\alpha Z)^2 \ln\left[(\alpha Z)^{-2}\right] = -2.4594\times 10^{-6}$ corresponds to a field value of $|\boldsymbol{\mathcal{E}}_{\text{r}}| \approx \mathcal{E}_{\max}\sqrt{\delta\Gamma_{2s}/\Gamma_{2s}} \approx 2.8 \times 10^{-8}\,\text{a.u.} \approx 90$ V/cm. Such fields are often used in spectroscopic experiments, so this effect should also be taken into account.

The relative difference in the two-photon decay probabilities of hydrogen

and anti-hydrogen atoms at the maximum value of $\mathcal{E}_{\max}$ is equal to

$$\frac{dW^{(2\gamma)}_{\overline{2s},1s}(\mathrm{H})}{W_0(\mathcal{E}_{\max})d\boldsymbol{\nu}d\boldsymbol{\nu}'} - \frac{dW^{(2\gamma)}_{\overline{2s},1s}(\bar{\mathrm{H}})}{W_0(\mathcal{E}_{\max})d\boldsymbol{\nu}d\boldsymbol{\nu}'} = \tag{9.11}$$
$$2\beta_1(\mathcal{E}_{\max})(\boldsymbol{\nu_\mathcal{E}\nu}+\boldsymbol{\nu_\mathcal{E}\nu}')(1+(\boldsymbol{\nu\nu}')^2)+2\beta_2(\mathcal{E}_{\max})(\boldsymbol{\nu_\mathcal{E}\nu}+\boldsymbol{\nu_\mathcal{E}\nu}')(1+\boldsymbol{\nu\nu}) =$$
$$(\boldsymbol{\nu_\mathcal{E}\nu}+\boldsymbol{\nu_\mathcal{E}\nu}')(0.000280111+0.00024397(\boldsymbol{\nu\nu}')+0.0000361414(\boldsymbol{\nu\nu}')).$$

This ratio is close to 0.028% and is a small effect, reflecting the difference between matter and antimatter even at maximum field strengths $\mathcal{E}_{\max}$.

Finally, it is possible to perform similar calculations for the case $\overline{2\mathrm{p}} \to 1\mathrm{s}+2\gamma$. The mixing of states is expressed as follows

$$|\overline{2p},\mu''\rangle = |2p,\mu''\rangle - \eta\sum_{\mu}\langle 2s,\mu''|e\boldsymbol{\mathcal{E}}\mathbf{r}|2p,\mu\rangle|2s,\mu''\rangle. \tag{9.12}$$

In this case, the two-photon transition without an external electric field will be provided by the sum of the decays $E1E2$ and $E1M1$, and the interference terms will be the same. The result reduces to

$$dW^{(2\gamma)}_{\overline{2p},1s} = \Bigg[dW^{(E1E2)}_{2p,1s}+dW^{(E1M1)}_{2p,1s}+\frac{9e^2\mathcal{E}^2}{\Delta^2}dW^{(E1E1)}_{2s,1s}+ \tag{9.13}$$
$$\frac{0.000230135}{\pi^3}\frac{\Gamma_{2p}}{\Delta^2}[e\boldsymbol{\mathcal{E}\nu}+e\boldsymbol{\mathcal{E}\nu}']\left(1+(\boldsymbol{\nu\nu}')^2\right)(\alpha Z)^7+$$
$$\frac{0.0000340919}{\pi^3}\frac{\Gamma_{2p}}{\Delta^2}[e\boldsymbol{\mathcal{E}\nu}+e\boldsymbol{\mathcal{E}\nu}'](1+\boldsymbol{\nu\nu}')(\alpha Z)^7\Bigg]\,d\boldsymbol{\nu}d\boldsymbol{\nu}',$$

$$\frac{dW^{(2\gamma)}_{\overline{2p},1s}}{d\boldsymbol{\nu}d\boldsymbol{\nu}'} = W_0\left[1\mp\beta_1(\mathcal{E})\left[\boldsymbol{\nu_\mathcal{E}\nu}+\boldsymbol{\nu_\mathcal{E}\nu}'\right](1+(\boldsymbol{\nu\nu}')^2)\right. \tag{9.14}$$
$$\left.\mp\beta_2(\mathcal{E})\left[\boldsymbol{\nu_\mathcal{E}\nu}+\boldsymbol{\nu_\mathcal{E}\nu}'\right](1+\boldsymbol{\nu\nu}')\right],$$

where $W_0 = W^{(E1E2)}_{2p,1s}+W^{(E1M1)}_{2p,1s}+9e^2D^2W^{(E1E1)}_{2s\,1s}/\Delta^2$,and the functions $\beta_1(D)$, $\beta_2(D)$ are defined as before (9.10). The signs $(+)$ and $(-)$ refer to hydrogen and anti-hydrogen atoms, respectively.

The maximum values of β_1 (or β_2) are achieved for

$$\mathcal{E}_{\max} = \frac{\Delta}{3|e|w^{2\gamma}} \approx 7.1 \times 10^{-11}\,\text{a.u.} \approx 0.23\,\text{V/cm}. \tag{9.15}$$

The corresponding maximum value of $dW^{(2\gamma)}_{\overline{2p},1s}$ is equal to

$$\begin{aligned}\frac{dW^{(2\gamma)}_{\overline{2p},1s}}{d\boldsymbol{\nu}d\boldsymbol{\nu}'} = W_0(\mathcal{E}_{\max})\,\big[1 \mp 0.00048613\,[\boldsymbol{\nu}_{\boldsymbol{\mathcal{E}}}\boldsymbol{\nu} + \boldsymbol{\nu}_{\boldsymbol{\mathcal{E}}}\boldsymbol{\nu}']\,(1 + (\boldsymbol{\nu}\boldsymbol{\nu}')^2) \\ \mp 0.000720147\,[\boldsymbol{\nu}_{\boldsymbol{\mathcal{E}}}\boldsymbol{\nu} + \boldsymbol{\nu}_{\boldsymbol{\mathcal{E}}}\boldsymbol{\nu}']\,(1 + \boldsymbol{\nu}\boldsymbol{\nu}')\big]\,.\end{aligned} \tag{9.16}$$

After integration over the photon emission directions, the field quadratic contribution is equal to

$$\begin{aligned}W^{(2\gamma)}_{\overline{2p},1s}(\mathcal{E}_{\max}) = W^{(E1E2)}_{2p,1s} + W^{(E1M1)}_{2p,1s} + \frac{9e^2\mathcal{E}^2_{\max}W^{(E1E1)}_{2s,1s}}{\Delta^2} \\ \approx 4.09 \times 10^{-22}\,\text{a.u.} \approx 1.69 \times 10^{-5}\,\text{s}^{-1}.\end{aligned} \tag{9.17}$$

The maximum relative probability difference (in the field $\mathcal{E}_{\max}$) is equal to

$$\begin{aligned}\frac{dW^{(2\gamma)}_{\overline{2p},1s}}{W_0(\mathcal{E}_{\max})d\boldsymbol{\nu}d\boldsymbol{\nu}'}(\mathrm{H}) - \frac{dW^{(2\gamma)}_{\overline{2p},1s}}{W_0(\mathcal{E}_{\max})d\boldsymbol{\nu}d\boldsymbol{\nu}'}(\bar{\mathrm{H}}) = \\ 2\beta_1(\mathcal{E}_{\max})(\boldsymbol{\nu}_{\boldsymbol{\mathcal{E}}}\boldsymbol{\nu} + \boldsymbol{\nu}_{\boldsymbol{\mathcal{E}}}\boldsymbol{\nu}')(1 + (\boldsymbol{\nu}\boldsymbol{\nu}')^2) + 2\beta_2(\mathcal{E}_{\max})(\boldsymbol{\nu}_{\boldsymbol{\mathcal{E}}}\boldsymbol{\nu} + \boldsymbol{\nu}_{\boldsymbol{\mathcal{E}}}\boldsymbol{\nu}')(1 + \boldsymbol{\nu}\boldsymbol{\nu}') \\ = (\boldsymbol{\nu}_{\boldsymbol{\mathcal{E}}}\boldsymbol{\nu}) + \boldsymbol{\nu}_{\boldsymbol{\mathcal{E}}}\boldsymbol{\nu}')(0.0111629 + 0.0097226(\boldsymbol{\nu}\boldsymbol{\nu}')^2 + 0.00144029(\boldsymbol{\nu}\boldsymbol{\nu}').\end{aligned} \tag{9.18}$$

This ratio turns out to be close to 1%. However, any direct observation of this difference should be difficult because of the prevailing background from the one-photon transition $2p \to 1s + \gamma$.

9.3. Decay of highly excited states in an external electric field

In the previous sections of the thesis, see 9.1, 9.2, it was shown that the linear field contribution arising in the differential transition probability leads to a sig-

nificant difference between the spectra of H and $\bar{\text{H}}$. This deviation disappears after integration over the photon emission directions, i.e., in the total transition probability. Nevertheless, the difference arising in the electric field can be observed in experiments when the photon emission is registered in a given direction. According to [66], the formation of anti-hydrogen atoms in low-lying states is very difficult, and, therefore, theoretical analysis of highly excited state decays can be used to identify possible differences in H and $\bar{\text{H}}$ atoms.

Using the technique [106, 112–114], in this section the estimates of decay probabilities of highly excited states are given. In particular, a comparison of the differential transition probabilities of hydrogen and anti-hydrogen atoms is illustrated using the example of mixing states ns, np. Then the total decay probabilities (the same for atoms H and $\bar{\text{H}}$) of mixed states $\overline{ns}$ for arbitrary principal quantum numbers of the initial and final states are calculated. The choice of ns and np states is mainly due to the fact that the mixing is stronger for close states of opposite parity. In this case, the Lamb shift acts as a parameter that allows the ns and np states to be completely mixed in very weak fields, which can be associated with "residual" fields. The main goal is to demonstrate the difference in the spectra of hydrogen and anti-hydrogen atoms for Rydberg states, which can mimic the effects of CPT-symmetry breaking.

According to perturbation theory, the wave function of an atomic level subjected to an external electric field [103, 104] can be written as

$$|\overline{ns}m_{j_s}\rangle = |nsm_{j_s}\rangle + \eta_n \sum_{m_{j_p}} \langle npm_{j_p}|e\boldsymbol{\mathcal{E}}\boldsymbol{r}|nsm_{j_s}\rangle |npm_{j_p}\rangle,$$
$$\eta_n = \frac{1}{\Delta E^{(n)}_{L(f)} + \mathrm{i}\Gamma_{np}/2}, \tag{9.19}$$

where $m_{j_{s(p)}}$ corresponds to the projection of the total angular momentum of the electron ($j_{s(p)}$) of the $ns(p)$ state, n is the principal quantum number of the hydrogen state, $\Delta E^{(n)}_{L(f)}$ is the Lamb shift (L-index) or fine structure splitting (f) of the n-th atomic state, Γ_{np} is the np-level width, e is the electron charge. The matrix element $\langle npm_{j_p}|e\boldsymbol{\mathcal{E}}\boldsymbol{r}|nsm_{j_s}\rangle$ represents the dipole interaction of an atomic electron with an external electric field with strength $\boldsymbol{\mathcal{E}}$, $\boldsymbol{r}$ is the radius-

vector of the atomic electron.

Carrying out the corresponding analytical calculations, it can be found

$$\langle npm_{j_p}|e\boldsymbol{\mathcal{E}}\boldsymbol{r}|nsm_{j_s}\rangle = \frac{\sqrt{3}}{2}n\sqrt{n^2-1}\sum_q(-1)^{q+j_s+j_p}e\mathcal{E}_q C^{j_p\,m_{j_p}}_{j_s\,m_{j_s}\;\;1\,-q}, \quad (9.20)$$

where $C^{j\,m}_{j_1\,m_1\;\;j_2\,m_2}$ is the Clebsch-Gordan coefficient with the total angular momentum j and its projection m determined by the summing rule of the angular momenta j_1, j_2 and their projections m_1, m_2 [179], $\mathcal{E}_q$ - spherical component q of the electric field strength vector $\boldsymbol{\mathcal{E}}$.

Restricting ourselves to the consideration of one-photon transitions in an external electric field (see section 9.1), the mixing of low-lying states has to be taken into account as well. The total amplitude of the one-photon emission process should include $\overline{ns} \to \overline{ks} + 1\gamma$ and $\overline{ns} \to \overline{kp} + 1\gamma(E1)$ decay channels:

$$\begin{aligned} U^P_{\overline{ns}m,\overline{ks}m'} &= U^P_{nsm,\,ksm'} \;\; + \\ \eta_n\sum_{m_{j_p}}\langle nsm|e\boldsymbol{\mathcal{E}}\boldsymbol{r}|npm_{j_p}\rangle U^P_{npm_{j_p},\,ksm'} &\;\; + \;\; \eta_k\sum_{m_{j_p}}\langle kpm_{j_p}|e\boldsymbol{\mathcal{E}}\boldsymbol{r}|ksm'\rangle U^P_{nsm,\,kpm_{j_p}}, \end{aligned} \quad (9.21)$$

where the ks state admixture to the kp level is discarded due to its insignificance (the corresponding magnetic transition leads to an essential smallness, see (8.20)), and the index P, as before, stands for the Pauli approximation. The projections m and m' refer to the angular momenta of the initial ns and final ks states, respectively. Carrying out the necessary calculations, the transition probability is reduced to the form:

$$\begin{aligned} \frac{dW^{(1\gamma)}_{\overline{ns},\overline{ks}}}{d\boldsymbol{\nu}} = \frac{3}{8\pi}\frac{dW^{(1\gamma)}_{ns,ks}}{d\boldsymbol{\nu}}\Bigg[1 - (-1)^{j_s+j_p}e\mathcal{E}(\boldsymbol{\nu}_{\boldsymbol{\mathcal{E}}}\boldsymbol{\nu})\frac{n\sqrt{n^2-1}}{2\sqrt{3}}\frac{\Gamma_{np}}{w_1\Delta_1^2} - \\ (-1)^{j_s+j_p}e\mathcal{E}(\boldsymbol{\nu}_{\boldsymbol{\mathcal{E}}}\boldsymbol{\nu})\frac{k\sqrt{k^2-1}}{6}\frac{\Gamma_{kp}}{w_2\Delta_2^2} + \frac{e^2\mathcal{E}^2}{w_1^2\Delta_1^2}\frac{n^2(n^2-1)}{12} + \frac{e^2\mathcal{E}^2}{w_2^2\Delta_2^2}\frac{k^2(k^2-1)}{36}\Bigg]. \end{aligned} \quad (9.22)$$

Here $\boldsymbol{\nu}_{\boldsymbol{\mathcal{E}}}$ - unit vector of field direction ($\boldsymbol{\nu}_{\boldsymbol{\mathcal{E}}} \equiv \boldsymbol{\mathcal{E}}/\mathcal{E}$, $\mathcal{E}$ - field amplitude), and

parameters Δ_i and w_i $(i = 1, 2)$ are defined as

$$\Delta_1 = \sqrt{\left(\Delta E^{(n)}_{L(f)}\right)^2 + \frac{1}{4}\Gamma^2_{np}}, \quad \Delta_2 = \sqrt{\left(\Delta E^{(k)}_{L(f)}\right)^2 + \frac{1}{4}\Gamma^2_{kp}}, \tag{9.23}$$

$$w_1 = \sqrt{\frac{W^{(1\gamma)}_{ns,ks}}{W^{(1\gamma)}_{np,ks}}} \quad \text{и} \quad w_2 = \sqrt{\frac{W^{(1\gamma)}_{ns,ks}}{W^{(1\gamma)}_{ns,kp}}}.$$

Here it is taken into account that the state width np $\Gamma_{np} = \Gamma_{np_{1/2}} = \Gamma_{np_{3/2}}$ [117]. The notations $W^{(1\gamma)}_{ns,ks}$, $W^{(1\gamma)}_{np,ks}$, and $W^{(1\gamma)}_{ns,kp}$ represent the one-photon transition probabilities for the corresponding ns and np levels. The sign $(-1)^{j_s+j_p}$ in the expression (9.22) shows the opposite contribution of the $np_{1/2}$ and $np_{3/2}$ states. This difference arises because the ns state is between $np_{3/2}$ and $np_{1/2}$ for the hydrogen atom.

In expression (9.22), the last two terms do not depend on the direction of the emitted photon or the direction of the electric field. In contrast to the linear field contributions, the quadratic field contributions are retained after averaging over the photon emission directions. It should be noted that the formal T-noninvariance of the factor $(\boldsymbol{\nu_\mathcal{E}\nu})$ in (9.22) ($\boldsymbol{\nu_\mathcal{E}}$ - T-even and $\boldsymbol{\nu_\mathcal{E}}$ - T-odd vectors) is compensated by the dependence on $\Gamma_{n(k)p}$ [229].

According to the expression (9.22), the differential transition probability $dW^{(1\gamma)}_{\overline{ns},\overline{ks}}(\boldsymbol{\nu})$ is lined up as follows: the first term corresponds to the unperturbed decay $ns \to ks + 1\gamma(M1)$, the additional terms (linear and quadratic in the electric field $\mathcal{E}$) represent the interference $M1$, $E1$ photons and emission probabilities for the decays $ns \to ks + 1\gamma(M1)$ and $ns \to kp + 1\gamma(E1)$, $np \to ks + 1\gamma(E1)$. The linear terms are proportional to the electron charge, so they have opposite signs for hydrogen and anti-hydrogen atoms. All other terms in (9.22) are identical for hydrogen and anti-hydrogen. The observation of contrast in the spectra of hydrogen and anti-hydrogen becomes sharper when the emission of photons is registered at an angle in (opposite to) the field direction. Accordingly, in the perpendicular direction the effect is nullified.

It is more convenient to compare differential transition probabilities by

rewriting the expression (9.22) in the form:

$$dW^{(1\gamma)}_{\overline{ns},\overline{ks}} = \frac{3}{8\pi} dW^{(1\gamma)}_{ns,ks} \left(1 + e^2\mathcal{E}_0^2 a^2\right) \left[1 \pm (-1)^{1+j_s+j_p} \frac{e\mathcal{E}(\boldsymbol{\nu}_{\boldsymbol{\mathcal{E}}}\boldsymbol{\nu}) b}{1 + e^2\mathcal{E}_0^2 a^2}\right] d\boldsymbol{\nu}, \quad (9.24)$$

where the sign $\pm$ in (9.24) corresponds to hydrogen (+) and anti-hydrogen (−), and the electron charge e enters in modulus. The coefficients a and b are determined by the relations:

$$a = \sqrt{\frac{n^2(n^2-1)}{12 w_1^2 \Delta_1^2} + \frac{k^2(k^2-1)}{36 w_2^2 \Delta_2^2}}, \quad (9.25)$$

$$b = \frac{n\sqrt{n^2-1}}{2\sqrt{3}} \frac{\Gamma_{np}}{w_1 \Delta_1^2} + \frac{k\sqrt{k^2-1}}{6} \frac{\Gamma_{kp}}{w_2 \Delta_2^2}.$$

The second summand in square brackets of the expression (9.24) represents the expected difference in the spectra of atoms H and $\bar{\text{H}}$ in an external field (when the signal is registered at a certain angle). Acting similarly to the previous sections, it is possible to determine the field value at which the maximum difference will be achieved:

$$e\mathcal{E}^{\max} = \frac{1}{a}. \quad (9.26)$$

The relative difference $dW^{(1\gamma)}_{\overline{ns},\overline{ks}}(\text{H})$ and $dW^{(1\gamma)}_{\overline{ns},\overline{ks}}(\bar{\text{H}})$ for the H и $\bar{\text{H}}$ atoms in the field (9.26) is

$$\delta(\mathcal{E}^{\max}) = \frac{dW^{(1\gamma)}_{\overline{ns},\overline{ks}}(\text{H}) - dW^{(1\gamma)}_{\overline{ns},\overline{ks}}(\bar{\text{H}})}{\frac{3}{8\pi} W^{(1\gamma)}_{ns,ks} \left(1 + e^2\mathcal{E}^2 a\right)} \quad (9.27)$$

$$= (-1)^{1+j_s+j_p}(\boldsymbol{\nu}_{\boldsymbol{\mathcal{E}}}\boldsymbol{\nu}) \frac{b}{a} = (-1)^{1+j_s+j_p}(\boldsymbol{\nu}_{\boldsymbol{\mathcal{E}}}\boldsymbol{\nu}) \frac{\frac{n\sqrt{n^2-1}\Gamma_{np}}{2\sqrt{3} w_1 \Delta_1^2} + \frac{k\sqrt{k^2-1}\Gamma_{kp}}{6 w_2 \Delta_2^2}}{\sqrt{\frac{n^2(n^2-1)}{12 w_1^2 \Delta_1^2} + \frac{k^2(k^2-1)}{36 w_2^2 \Delta_2^2}}}.$$

The case $n = 2$ and $k = 1$ (the case of mixing $2s$ and $2p$ states) leads to the result [114], see the previous section. Note that the admixture of states $np_{1/2}$ and $np_{3/2}$ gives a contribution to $\delta(\mathcal{E}^{\max})$ with opposite sign. However, the impurity of the $np_{3/2}$ state is smaller because $\Delta E_L^{(n)} \ll \Delta E_f^{(n)}$. Thus, the splitting of the

fine structure with respect to the Lamb shift can be neglected. Moreover, the expression (9.27) can be significantly simplified by series expansion over powers of $1/n$. The dominant contribution in both cases $k \ll n$ and $k \sim n$ is equal to

$$\delta(\mathcal{E}^{\max}) \approx (\boldsymbol{\nu}_{\boldsymbol{\mathcal{E}}}\boldsymbol{\nu})\frac{\Gamma_{np}}{\Delta_1} \approx (\boldsymbol{\nu}_{\boldsymbol{\mathcal{E}}}\boldsymbol{\nu})\frac{\Gamma_{np}}{\Delta E_L^{(n)}}, \tag{9.28}$$

assuming $\Gamma_{np} \ll E_L^{(n)}$.

The results (9.27), (9.28) enable the spectral difference between H and $\bar{\text{H}}$ atoms to be determined as a function of the principal quantum numbers n, k of the initial and final states, respectively. Table 9.1 summarizes the values of the dimensionless function $\delta(\mathcal{E})$ defined according to (9.27) as a function of the principal quantum numbers n and k for the electric field $\mathcal{E}^{\max}$ (9.26) and 500 V/m. In the last column of Table 9.1, the electric field strength is related to the experimental value. It should be noted that the $\mathcal{E}^{\max}$ values in Table 9.1 are rather values that can be attributed to "stray" fields.

Table 9.1. The numerical values of $\delta(\mathcal{E})$ for different values of the principal quantum numbers of the initial, n, and final, k, states are presented. The third column presents the value of $\mathcal{E}^{\max}$ in V/m as a function of the principal quantum numbers n and k. The fourth and fifth columns show the values of $\delta(\mathcal{E}^{\max})$ and $\delta(\mathcal{E})$ at $\mathcal{E} = 500$ V/m in the case $(\boldsymbol{\nu}_{\boldsymbol{\mathcal{E}}}\boldsymbol{\nu}_{\boldsymbol{\mathcal{E}}}) = 1$, i.e. when photon detection occurs in the field direction.

n	k	$\mathcal{E}^{\max}$, V/m	$\delta(\mathcal{E}^{\max})$	$\delta(\mathcal{E})$ at $D_0 = 500$ V/m
2	1	0.005	0.094	$1.97 \cdot 10^{-6}$
3	1	0.0009	0.087	$3.14 \cdot 10^{-7}$
3	2	0.0001	0.094	$3.77 \cdot 10^{-8}$
4	1	0.0002	0.097	$7.94 \cdot 10^{-8}$
4	2	0.00003	0.098	$1.18 \cdot 10^{-7}$
4	3	$5.9 \cdot 10^{-6}$	0.11	$2.60 \cdot 10^{-9}$
100	1	$1.6 \cdot 10^{-11}$	0.099	$6.33 \cdot 10^{-15}$
100	2	$4.2 \cdot 10^{-11}$	0.099	$1.65 \cdot 10^{-14}$
100	3	$7.2 \cdot 10^{-11}$	0.099	$2.85 \cdot 10^{-14}$

Thus, it is shown that a significant difference ($\sim 0.1\%$) arises for the differential transition probabilities in very weak electric fields. This difference vanishes after integration over the photon emission directions, i.e., in the total decay probability. There are also field quadratic terms that contribute to the total decay rate. This leads to a strong modification of the corresponding level width. According to the selection rules, the one-photon $ns \to 1s$ decay is determined by the emission of a magnetic dipole photon of an isolated atom. However, the impurity of the np state allows the emission of an electric dipole (E1) photon directly into the ground state. In the case when the $2s$, $2p$ states are mixed, this channel gives the main contribution to the level width [103–105]. At critical field strength $\mathcal{E}_c = 475$ V/cm, the state width $\overline{2s}$ is equal to the level width $2p$. For highly excited states, the field strength should be significantly smaller than $\mathcal{E}_c$, since the Lamb shift decreases with increasing principal quantum number. Thus, one can expect a significant reduction of the lifetimes of the Rydberg states in a weak electric field.

There are two ways to determine the level widths: a) calculation of the imaginary part of the self-energy correction [8, 121], and b) summation of all partial transition probabilities to the underlying levels. In the following, the second one is used. Namely, it follows from the expression (9.22) that the additional damping rate due to electric dipole radiation is given as follows:

$$\frac{W^{(E1)}_{\overline{ns},\overline{ks}}}{e^2\mathcal{E}^2} = \frac{n^2(n^2-1)}{12\Delta_1^2} W^{(E1)}_{np,ks} + \frac{k^2(k^2-1)}{36\Delta_2^2} W^{(E1)}_{ns,kp}. \tag{9.29}$$

The determination of the level widths of highly excited states requires the consideration of cascade transitions, which can be approximated by one-photon decays into intermediate atomic levels [82, 120]. In this case, a sum over all partial transition probabilities $W^{(1\gamma)}_{ns,kp}$ arises for an isolated atom. Therefore, in the presence of an electric field one should write

$$\Gamma_{\rm tot} = \Gamma_{ns} + \Gamma_{\overline{ns}} = \sum_{k=1}^{n-1} W^{(1\gamma)}_{ns\,kp} + \sum_{k=1}^{n-1} W^{(1\gamma)}_{ns\,ks} + \sum_{k=1}^{n-1} W^{(E1)}_{\overline{ns}\,\overline{ks}}, \tag{9.30}$$

where Γ_{ns} is the natural width of the ns level, i.e., the sum of partial transition

probabilities from the initial state ns to all underlying atomic levels kp, and $\Gamma_{\overline{ns}}$ in (9.30) represents the contribution of additional decay channels arising in the electric field. The transition probability $W^{(1\gamma)}_{ns,ks}$ corresponds to the $M1$ transition and leads to a negligible contribution to the $\Gamma_{\rm tot}$ level width (see, e.g., Table 9.2).

In principle, the summation over k in expression (9.30) can be performed using Gordon's formula for the transition probabilities $W^{1\gamma}_{ns,kp}$, $W^{(1\gamma)}_{np,ks}$ [5]. However, the dependence on the principal quantum number k should be taken into account in the factor Δ_2. In addition, the applicability of the formula (9.19) to calculate transition probabilities requires analyzing the magnitude of the field strength $\mathcal{E}$. Perturbation theory is valid when

$$\left| \frac{\langle np|e\boldsymbol{\mathcal{E}}\boldsymbol{r}|ns\rangle}{\Delta E^{(n)}_L + i\Gamma_{np}/2} \right| < 1 \tag{9.31}$$

and, therefore, $|\langle np|e\boldsymbol{\mathcal{E}}\boldsymbol{r}|ns\rangle| < \Delta E^{(n)}_L$. Taking into account that $\Delta E^{(n)}_L \sim 1/n^3$ [5], one can find

$$\mathcal{E}^{(n)}_c \sim \frac{1}{n^5}\mathcal{E}_c, \tag{9.32}$$

where $\mathcal{E}_c$ defines the field strength when 100% mixing of the $2s$ and $2p$ states in the hydrogen atom occurs, i.e., $\mathcal{E}_c = 475$ V/cm. The scaling of the field strength according to (9.32) is known as the Inglis-Teller limit [261]. Thus, the complete mixing of the states ns and np should arise in a very weak electric field.

Estimating the electric field strength using the formula (9.32) for each nth initial state, numerical results for partial probabilities, natural widths, and values induced by the external electric field are given in Tables 9.2, 9.3. Table 9.2 shows the contribution of the field-quadratic summands (9.29) as functions of the principal quantum numbers n and k. The one-photon transition probabilities $W^{(1\gamma)}_{ns,ks}$, $W^{(1\gamma)}_{ns,kp}$, $W^{(1\gamma)}_{np,ks}$ and $W_1 \equiv \frac{n^2}{12}(n^2-1)e^2{D^{(n)}_c}^2 W^{(1\gamma)}_{np,ks}/\Delta_1^2$, $W_2 \equiv \frac{k^2}{36}(k^2-1)e^2{D^{(n)}_c}^2 W^{(1\gamma)}_{ns,kp}/\Delta_2^2$ are given in inverse seconds. The calculations of the probabilities of spontaneous one-photon decay are carried out in the framework of standard quantum electrodynamics and their values can be

found, for example, in [262–264].

In particular, it follows from Table 9.2 that the transition probabilities W_1 and W_2 arising in the field contribute at the level of partial probabilities of one-photon decay of np states. Thus, the width of the mixed $\overline{ns}$ state becomes comparable to the natural width of Γ_{np} in a very weak field $\mathcal{E}_c^{(n)}$ and exceeds the natural width of the ns state of an isolated atom. For example, the field strength for the $n = 100$ state is estimated to be $4 \cdot 10^{-7}$ V/cm, and the corresponding $\Gamma_{\overline{100s}}$ level width is approximately 8.5×10^3 c^{-1}. Consequently, the width of the mixed atomic level $\overline{100s}$ is an order of magnitude larger than the natural width of Γ_{100s}, and the lifetime is shorter in the presence of a very weak field, which may be due to "residual" ("stray") fields.

The contribution of quadratic in-field terms, as a function of the principal quantum number k, for the initial state $\overline{55s}$ at a field strength of $\mathcal{E}_c^{(55)} \approx 3 \times 10^{-5}$ V/cm is examined in more detail. The results in Table 9.3 show that the mixing of the lower states becomes significant for transitions between the nearest atomic levels, while the main contribution follows from the first summand in the right-hand side of the expression (9.29). Summing all the partial transition probabilities in Table 9.3, it can be found that $\Gamma_{55s} \approx 6.5 \times 10^3$ s^{-1}, $\Gamma_{55p} \approx 3.2 \times 10^4$ s^{-1}, and the width induced by the electric field is $\Gamma_{\overline{55s}} \approx 1.4 \times 10^4$ s^{-1}.

The values in Tables 9.2, 9.3 should be compared to the level widths estimated in [265–267]. The main result of the [265–267] calculations is that the value of the corresponding widths can exceed the value of the largest Lyman-α transition probability $\sim 6 \cdot 10^8$ s^{-1} in fields violating the relation (9.32), see, e.g., [268]. However, the field strengths considered in our paper correspond rather to very weak fields. Using the electric field in the form (9.32) in the semiempirical expression for the ionization probability $\Gamma_{nn_1n_2m}$ [269], one can obtain quite insignificant values.

Table 9.2. Numerical values of $W_1 \equiv \frac{n^2(n^2-1)}{12} e^2\mathcal{E}^2 W^{(1\gamma)}_{np,ks}/\Delta^2$ and $W_2 \equiv \frac{k^2(k^2-1)}{36}\frac{e^2\mathcal{E}^2 W^{(1\gamma)}_{ns,kp}}{\Delta_2^2}$ for different values of the principal quantum numbers of the initial n and final k states (in inverse seconds). The first and second columns contain the values of the principal quantum numbers n and k. The third column corresponds to the values of the transition probabilities $W^{(1\gamma)}_{ns,ks}$, and the values of $W^{(1\gamma)}_{np,ks}$ in s^{-1} are given in the fourth column [262–264]. The fifth column presents the$W^{(1\gamma)}_{np,ks}$ values of the transition probability. The used values of the Lamb shift ΔE_L in MHz are given in the sixth column. The natural level widths Γ_{np} and Γ_{ns} are given in the seventh and eighth columns, respectively. Γ_{np} and Γ_{ns} are obtained as the sum of all partial $E1$ transition probabilities to lower states. The ninth and tenth columns represent the contributions of the quadratic terms in (9.29). The field strength used is $\mathcal{E}_c^{(n)}$, which approximates the complete mixing of ns and np states. All values are given in inverse seconds (except for the Lamb shift).

n	k	$W^{(1\gamma)}_{ns\,ks}$	$W^{(1\gamma)}_{ns\,kp}$	$W^{(1\gamma)}_{np\,ks}$	$\Delta E_L^{(n)}$	Γ_{np}	Γ_{ns}	W_1	W_2
2	1	$2.495 \cdot 10^{-6}$	—	$6.265 \cdot 10^{8}$	1057.911	$6.265 \cdot 10^{8}$	8.229	$2.063 \cdot 10^{8}$	0
3	1	$1.109 \cdot 10^{-6}$	—	$1.672 \cdot 10^{8}$	344.896	$1.897 \cdot 10^{8}$	$6.314 \cdot 10^{6}$	$5.394 \cdot 10^{6}$	0
3	2	$1.877 \cdot 10^{-9}$	$6.314 \cdot 10^{6}$	$2.245 \cdot 10^{7}$	344.896	—	—	$7.2398 \cdot 10^{6}$	$1.2021 \cdot 10^{5}$
4	1	$5.303 \cdot 10^{-7}$	—	$6.819 \cdot 10^{7}$	133.084	$8.092 \cdot 10^{7}$	$4.414 \cdot 10^{6}$	$2.771 \cdot 10^{7}$	0
4	2	$1.617 \cdot 10^{-9}$	$2.578 \cdot 10^{6}$	$9.668 \cdot 10^{6}$	133.084	—	—	$3.929 \cdot 10^{6}$	276.37
4	3	$2.047 \cdot 10^{-11}$	$1.836 \cdot 10^{6}$	$3.065 \cdot 10^{6}$	133.084	—	—	$1.246 \cdot 10^{6}$	$1.111 \cdot 10^{4}$
100	1	$3.949 \cdot 10^{-11}$	—	$4.185 \cdot 10^{3}$	$1.058 \cdot 10^{-3}$	$\approx 5.25 \cdot 10^{3}$	$\approx 0.476 \cdot 10^{3}$	$6.371 \cdot 10^{3}$	0
100	2	$2.033 \cdot 10^{-13}$	153.31	613.19	$1.058 \cdot 10^{-3}$	—	—	933.7	$1.077 \cdot 10^{-17}$
100	3	$9.195 \cdot 10^{-15}$	101.105	206.37	$1.058 \cdot 10^{-3}$	—	—	314.2	$4.011 \cdot 10^{-16}$
100	4	—	66.866	96.728	$1.058 \cdot 10^{-3}$	—	—	147.	$5.937 \cdot 10^{-15}$
100	5	—	46.506	54.171	$1.058 \cdot 10^{-3}$	—	—	82.48	$3.989 \cdot 10^{-14}$
100	6	—	33.856	33.896	$1.058 \cdot 10^{-3}$	—	—	51.61	$1.821 \cdot 10^{-13}$
100	7	—	25.580	22.877	$1.058 \cdot 10^{-3}$	—	—	34.84	$6.474 \cdot 10^{-13}$
100	8	—	19.916	16.311	$1.058 \cdot 10^{-3}$	—	—	24.84	$1.925 \cdot 10^{-12}$
100	9	—	15.890	12.123	$1.058 \cdot 10^{-3}$	—	—	18.46	$5.005 \cdot 10^{-12}$
100	10	—	12.938	9.3092	$1.058 \cdot 10^{-3}$	—	—	14.17	$6.225 \cdot 10^{-12}$

Table 9.3. The designations are the same as in Table 9.2, the value $D_c^{(55)} \approx 3 \cdot 10^{-5}$ V/cm is used.

n	k	$W^{(1\gamma)}_{ns\,ks}$	$W^{(1\gamma)}_{ns\,kp}$	$W^{(1\gamma)}_{np\,ks}$	W_1	W_2
55	1	$2.372 \cdot 10^{-10}$	—	$2.516 \cdot 10^{4}$	$1.104 \cdot 10^{4}$	—
55	2	$1.219 \cdot 10^{-12}$	921.77	$3.686 \cdot 10^{3}$	$1.617 \cdot 10^{3}$	$4.09 \cdot 10^{-13}$
55	3	$5.499 \cdot 10^{-14}$	608.11	$1.241 \cdot 10^{3}$	544.3	$1.52 \cdot 10^{-11}$
55	4	—	402.39	581.47	255.2	$2.26 \cdot 10^{-10}$
55	5	—	280.06	325.7	142.9	$1.52 \cdot 10^{-9}$
55	6	—	204.06	203.86	89.46	$6.93 \cdot 10^{-9}$
55	7	—	154.33	137.64	60.41	$2.47 \cdot 10^{-8}$
55	8	—	120.3	98.19	43.09	$7.35 \cdot 10^{-8}$
55	9	—	96.111	73.028	32.05	$1.91 \cdot 10^{-7}$
55	10	—	78.372	56.12	24.63	$4.48 \cdot 10^{-7}$
55	15	—	35.0001	20.657	9.066	$1.16 \cdot 10^{-5}$
55	30	—	8.7556	4.05	1.777	$2.98 \cdot 10^{-3}$
55	40	—	5.2734	2.2317	0.979	0.032
55	45	—	4.5069	1.8316	0.804	0.089
55	50	—	4.2245	1.6413	0.721	0.238
55	54	—	4.4807	1.6496	0.724	0.546

9.4. Conclusions on one- and two-photon decays in an external electric field

Thus, this section shows the difference in the emission of the Rydberg atoms H and $\bar{\text{H}}$. The field-linear terms vanish in the total transition probability after integration over the photon emission directions, which corresponds to the detection of photons in all directions simultaneously. However, spectral measurements are mainly concerned with the detection of photon emission at a given angle or at a given solid angle. The latter can be accounted for by integrating the cosine corresponding to the product $(\boldsymbol{\nu}_{\boldsymbol{\mathcal{E}}}\boldsymbol{\nu})$ in expression (9.22), and will lead to a nonzero result.

A discussion of experiments on the detection of radiation asymmetry in the electric field of metastable hydrogen and deuterium atoms can be found, for example, in [270]. The main purpose of such experiments is to determine the Lamb shift. Later, the author of [104] extended these ideas to experiments

to measure the Lamb shift for ions with large Z. Linear (asymmetric) terms give field strength-dependent contributions of opposite sign to the intensity in directions parallel and antiparallel to the electric field. In contrast, at a fixed field direction, the contributions linear in the field have opposite sign for the H and $\bar{\text{H}}$ atoms, i.e., an increase in the relative emission intensity of the hydrogen atom should be accompanied by a proportional decrease in the relative emission intensity of the anti-H atom. The recent development of the fly-through spectroscopy experiment of antihydrogen atoms [271] makes it possible to compare the spectra of H and $\bar{\text{H}}$ in an electric field.

It should be emphasized that the [66] experiments do not measure the spectrum of the anti-hydrogen atoms, but determine the quenching of the luminescence, thus estimating the lifetimes of the Rydberg states. As reported in [66], the retention time of anti-hydrogen is about 1000 s, which is an important step towards precision spectroscopy of anti-atoms [271]. The high-resolution comparison of both systems provides sensitive tests of CPT symmetry. Any measured difference would indicate a violation of the CPT [271]. Thus, a theoretical study of the effects that can mimic such a violation is extremely important. The difference appearing in the spectra of atoms H and $\bar{\text{H}}$ in the presence of an external electric field can mimic the effects of CPT symmetry breaking. The difference in the spectra depends on the direction of photon emission registration: (a) the maximum difference occurs when photon emission is registered in the along (opposite) field direction $(\boldsymbol{\nu}_{\boldsymbol{\mathcal{E}}}\boldsymbol{\nu}) = \pm 1$ and (b) the difference disappears when photon emission is registered in the direction perpendicular to the field $(\boldsymbol{\nu}_{\boldsymbol{\mathcal{E}}}\boldsymbol{\nu}) = 0$. The electric field strength $\mathcal{E}^{\max}$, when this effect has a maximum for the Rydberg states, can be related to the "residual" fields.

Values of the maximum difference of decay probabilities $\delta(\mathcal{E}^{\max})$ leads to a discrepancy of up to 10% in the Rydberg spectra of H and $\bar{\text{H}}$ atoms. Two competing contributions lead to the same effect: 1) mixing of the initial states ns, np and 2) mixing of the final states ks, kp. Mixing of the lower atomic levels should lead to more significant deviations in the spectra of hydrogen and anti-hydrogen atoms in the case of stronger fields. Taking into account the experiments of [271], the example of the decay of the $55s$ state has been considered in more detail. The calculation of the total transition probabilities for

the different decay channels of highly excited states permits the determination of the corresponding level widths as a sum over all partial channels. The most interesting conclusion that follows from the above estimates is that even in the presence of a very weak uniform electric field the ns and np states become indistinguishable in spectroscopic experiments. This is primarily because $ns \to 1s + 1\gamma(E1)$ decay is strongly suppressed by the selection rules, but emission of an electric dipole photon is allowed in the presence of an external electric field. "Additional" $E1$ decay channels into the ground and intermediate atomic levels are described by summands that are quadratic in the field. They are comparable to the partial decay probabilities of the $np \to ks + 1\gamma(E1)$ or $ns \to kp + 1\gamma(E1)$ transitions for an isolated atom. For example, 100% mixing of the $100s$ and $100p$ states occurs in a field of the order of 4×10^{-7} V/cm, making the decays of these states identical in rate. The presence of an external electric field should be taken into account for both the initial and final (intermediate) states, leading to a significant change in the width of the levels.

In conclusion, it should be noted that even very weak fields can lead to significant changes in the emission spectra of hydrogen and anti-hydrogen atoms in the Rydberg states. First, the maximum asymmetry (the same for any ns-states) in the spectra of hydrogen and anti-hydrogen occurs in fields of order $\mathcal{E}^{\max}$, see Table 9.1. Second, the results in Tables 9.2, 9.3 show that the 100%-mixing of ns and np states occurring in a field of order $\mathcal{E}_c$ significantly increases the decay rate of the Rydberg ns-states. To estimate the maximum contribution of both effects, the field strengths $\mathcal{E}^{\max}$ and $\mathcal{E}_c$ were calculated for each ns state, which can vary significantly. Thus, the results impose significant constraints on the experimental conditions. Effective control of external electric fields or photon emission angles is required. Registering photon emission in the perpendicular to the field direction will nullify the asymmetry of the spectra of H and $\bar{\text{H}}$. The results of these studies were published in the author's work [119].

Chapter 10.

Line profile distortion in multiphoton processes: astrophysical applications

In view of the significant advances in experimental observations of the cosmic microwave background (CMB), close attention has been paid to the theoretical description of the processes occurring in the cosmological recombination epoch of the early Universe. In order to accurately describe CMB, it is necessary to take into account the various processes of photon emission and absorption, photon-electron scattering, etc. Special attention is paid to the spectral characteristics of atomic radiation. The polarizability and cross sections of the processes due to various phenomena are of special interest from the astrophysical point of view. As a rule, in standard calculations of such problems the quantum mechanical approach for an isolated atom is applied. However, taking into account the atom-field interaction may be important in the case of astrophysical experiments, in which, in particular, the observational accuracy is about 1% [247, 248] and is expected to be $\sim 0.1\%$. The interaction of an atom with external fields can lead to effects such as inversion of atomic populations, violation of "stability" stationary solutions, changes in line strengths, cross sections, susceptibility, polarizability, etc. [272, 273].

In this chapter of the thesis, the theory of the statistical operator (density

matrix) [96] is used to study the atom-field system. The application of the density matrix formalism in the three-level approximation seems to be simpler and more appropriate in this case. A description of the density matrix theory and its applications, such as spontaneous emission, line broadening (power-law broadening and saturation, line broadening due to collisions, Doppler broadening, etc.) can be found, for example, in [274].

The theory of radiative transfer, which is usually applied in the study of the cosmic microwave background, was proposed in the works of [77, 79]. In particular, within the framework of the three-level model, it was found that the $2s \leftrightarrow 1s$ transition can significantly control the dynamics of cosmological hydrogen recombination. Moreover, distortions of CMB of the order of 10^{-6} were predicted in [79]. Recently, the radiative transfer theory during the recombination epoch of the early Universe has been intensively reviewed in [76, 99] and by many other authors in subsequent papers (a review of the relevant literature is omitted for brevity). An important consequence of radiative transfer theory is the determination of the absorption coefficient calculated per atom. The influence of electromagnetic radiation on the absorption coefficient is widely investigated at present. As an example, one can refer to the work of [275], where the effect of powerful high-frequency electromagnetic radiation on the absorption coefficient in the low-frequency line in a three-level Λ-atom is considered. In this chapter, another kind of multiphoton process, namely the phenomenon of electromagnetic induced transparency (EIT), is considered. The nature of the EIT phenomenon can be investigated by evaluating the response of a multilevel system to the presence of an external radiation field. Electromagnetic induced transparency leads to a significant modification of the absorption profile of the atom. A description of the EIT effect for a three-level "ladder" (Ξ) level scheme of an atomic system interacting with two near-resonant monochromatic fields can be found, for example, in [93, 95]. A detailed study of the three-level ladder atom, the absorption and emission spectra, and the response of the Ξ-atom was presented in [276]. This chapter presents a study of the response of the hydrogen atom in the three-level approximation to the external field created by photons in the recombination epoch of the early Universe. Estimates of the line profile distortion leading to corrections to the absorption coefficient determined in the

framework of radiative transfer theory are given. The physics of the atom interacting with photon fields can be understood on the basis of the description of "interfering paths" which corresponds to a multiphoton process defined through a power series expansion in terms of field amplitudes (see, e.g., [93, 95, 276]). The question of the influence of radiation from powerful sources of radiation on the line profile of the HFS of the hydrogen atom is also discussed.

10.1. Effect EIT: Ξ-scheme of levels

BThis section considers a three-level ladder Ξ-level scheme to describe a hydrogen atom subjected to external electromagnetic fields. It is assumed that hydrogen atoms formed during the recombination epoch in the early Universe reach their ground states by emitting photons in all spectral lines corresponding to atomic free-bond and bond-bond transitions. All emitted photons generate an external field of the medium, which acts back on the hydrogen atom. The study of this "self-consistent" scenario under conditions of cosmic expansion is the main goal. The limitation of the problem also applies to the consideration of only spontaneous radiation probabilities. Collisional excitation and ionization can be excluded, since at appropriate temperatures and densities they are negligibly small for a three-level hydrogen atom [99].

To reveal the possible effect, an atom exposed to two external fields belonging to two neighboring spectral lines, namely the Ly_α and H_α lines, is considered with an initial condition corresponding to the full population of the ground state of the atom. Next, the standard density matrix formalism is applied, which can be found, e.g., in [95]. The details of this section were presented in [128] (the paper [128] was chosen by the editors of the Journal of Physics B: Atomic, Molecular and Optical Physics in compilation "Highlights of 2012").

A typical three-level ladder system is shown in Fig. 10.1.

Solving the density matrix equations using steady-state approximation and rotating-wave approximation, when neglecting fast oscillating contributions to the Hamiltonian and time dependence in the equations on the statistical operator, gives the following set of equations for the corresponding density matrix

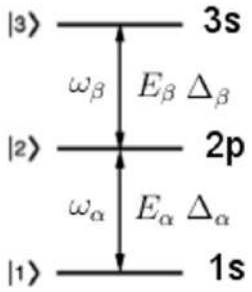

Figure 10.1. The considered scheme of the three-level atom is a ladder Ξ-scheme. The three levels correspond to the hydrogen states: $|1\rangle \to |1s\rangle$, $|2\rangle \to |2p\rangle$, and $|3\rangle \to |3s\rangle$, respectively. The frequencies ω_α, ω_β are the frequencies of the external fields corresponding to the "probe" (probe) and "controlled" (controlled) laser [95] fields. The fields E_α, E_β stimulate the $1s-2p$ and $2p-3s$ transitions (α-Lyman and Balmer lines). The possible detunings Δ_α and Δ_β for the field frequencies are also given.

elements [95]:

$$\begin{aligned}
\rho_{21} &= \frac{\mathrm{i}}{2}\frac{\Omega_\alpha(\rho_{22}-\rho_{11})-\Omega^*_\beta\rho_{31}}{\gamma_{21}-\mathrm{i}\Delta_\alpha},\\
\rho_{32} &= \frac{\mathrm{i}}{2}\frac{\Omega_\beta(\rho_{33}-\rho_{22})+\Omega^*_\alpha\rho_{31}}{\gamma_{32}-\mathrm{i}\Delta_\beta},\\
\rho_{31} &= \frac{\mathrm{i}}{2}\frac{\Omega_\alpha\rho_{32}-\Omega_\beta\rho_{21}}{\gamma_{31}-\mathrm{i}(\Delta_\alpha+\Delta_\beta)},\\
\rho_{22} &= \frac{\mathrm{i}}{2\Gamma_2}(\Omega^*_\alpha\rho_{21}-\Omega_\alpha\rho_{12}),\\
\rho_{33} &= \frac{\mathrm{i}}{2\Gamma_3}(\Omega^*_\beta\rho_{32}-\Omega_\beta\rho_{23}).
\end{aligned} \tag{10.1}$$

The levels of the system are given by the following hydrogen states $|1\rangle = |1s\rangle$, $|2\rangle = |2p\rangle$ and $|3\rangle = |3s\rangle$. The frequencies ω_{21} and ω_{32} belong to transitions $|1\rangle \to |2\rangle$ and $|2\rangle \to |3\rangle$, respectively. The system is driven by a probe field with amplitude E_α at frequency ω_α and a controlled field with amplitude E_β and frequency ω_β. $\Delta_\alpha = \omega_\alpha - \omega_{21}$, $\Delta_\beta = \omega_\beta - \omega_{32}$ determines the corresponding frequency detuning, $\Omega_\beta = 2d_{32}E_\beta$ and $\Omega_\alpha = 2d_{21}E_\alpha$ are the Rabi frequencies, which are determined by the atomic dipole matrix element d_{ij}. All these expressions are given in atomic units. Neglecting the effects of collisional dephasing, the decay probability is given by the expression $\gamma_{ij} = (\Gamma_i + \Gamma_j)/2$,

where Γ_i is the natural width of the level $|i>$.

In the limit of a weak probe field and $\rho_{11} \approx 1$, $\rho_{22} \approx \rho_{33} \approx 0$ (full occupancy of the ground state of the atom), the solution of the equations on ρ_{21} at first order for the probe field and at all orders for the controlled field was found in [93, 95]. However, the complete solution for ρ_{21} can be obtained in the form:

$$\rho_{21} = \frac{-\mathrm{i}\frac{\Omega_\alpha}{2}\left(\frac{\Omega_\alpha^2}{4} + A\right)}{\frac{\Omega_\beta^2}{4}\left(\frac{\Omega_\alpha^2}{4\Gamma_2} - B\right) - \left(-\frac{\Omega_\alpha^2}{4\Gamma_2} + \gamma_{21} - \mathrm{i}\Delta_1\right)\left(\frac{\Omega_\alpha^2}{4} + A\right)}, \tag{10.2}$$
$$A = B\left(\gamma_{31} - \mathrm{i}(\Delta_1 + \Delta_2)\right), \qquad B = \frac{\Omega_\beta^2}{4\Gamma_3} + \gamma_{32} - \mathrm{i}\Delta_2,$$

which is easily transformed in the weak field approximation to expression (2) in [95].

The physics of the system's response to external fields can be understood by decomposing the solution (10.2) into a power series on the variables Ω_α and Ω_β. The authors of [95] derived a series containing terms up to third order on Ω_α and Ω_β at zero detuning. For further purposes, however, it is important to keep the non-zero detuning and, as before, in the weak field approximation, to represent the expression (10.2) in the form of a power series over Ω_α and Ω_β.

The obtained expression for ρ_{21} is considerably simplified in the case of exact two-photon resonance, i.e., when the frequencies of the two external fields coincide exactly with the transition frequency $\omega_{31} = E_3 - E_1$. In this case, the equality $\Delta_\alpha + \Delta_\beta = 0$ is satisfied and the series expansion takes the form:

$$\rho_{21} = \frac{\mathrm{i}\Omega_\alpha/2}{\gamma_{21} - \mathrm{i}\Delta_\alpha}\left[1 - \frac{\Omega_\beta^2/4}{\gamma_{31}(\gamma_{21} - \mathrm{i}\Delta_\alpha)} + \frac{\Omega_\alpha^2/4}{\Gamma_2(\gamma_{21} - \mathrm{i}\Delta_\alpha)} + \right. \tag{10.3}$$
$$\left. \frac{\Omega_\alpha^2/4 \cdot \Omega_\beta^2/4}{(\gamma_{21} - \mathrm{i}\Delta_\alpha)^2(\gamma_{32} - \mathrm{i}\Delta_\beta)} \frac{(\Gamma_2 + \gamma_{31})(\gamma_{21} - \mathrm{i}\Delta_\alpha) - 2\gamma_{31}(\gamma_{32} - \mathrm{i}\Delta_\beta)}{\Gamma_2\gamma_{31}^2} + \ldots\right],$$

where $\ldots$ denote the higher order terms of Ω_α, Ω_β, and the product of $\Omega_\alpha \cdot \Omega_\beta$. The series expansion is performed under the conditions $\Omega_\beta/\gamma_{ij} \ll 1$ and $\Omega_\alpha/\gamma_{ij} \ll 1$.

As it was shown in [95], the common factor in (10.3) corresponds to the

one-photon absorption process, and the quadratic terms are related to the two-photon absorption and subsequent emission processes. The products $\Omega_\alpha^2 \cdot \Omega_\beta^2$ represent the terms of the "interfering paths", see Fig. 10.2. Thus, the matrix

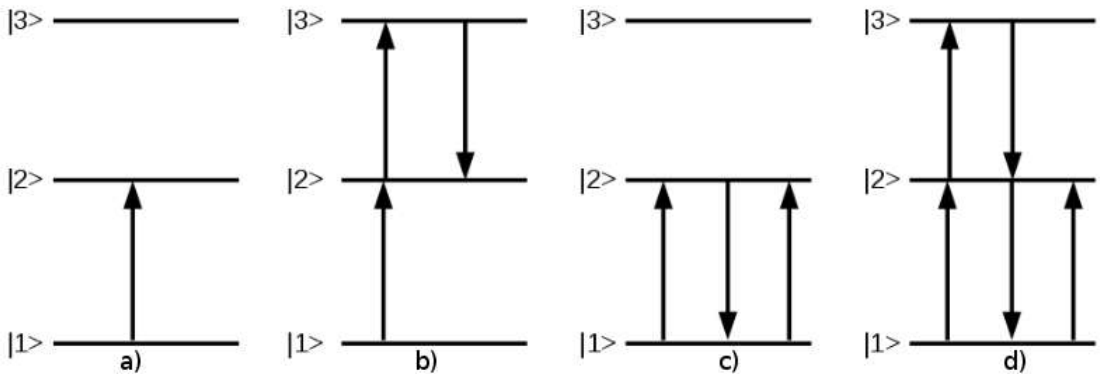

Figure 10.2. Schematic of the transitions occurring in the three-level ladder system corresponding to the expression (10.3): part (a) of the figure corresponds to one-photon absorption processes (the common factor in (10.3)); parts (b) and (c) represent the second and third summands, and part (d) describes the "interfering paths" (the fourth summand in (10.3)).

element ρ_{21} describes multiphoton processes of the atom-field interaction. A detailed analysis of the expression (10.3) is presented in Ref. [95].

It follows from (10.3) that the density matrix can be used to determine the line profile (in this case for the $1-2$ absorption line). The imaginary part, $\Im\{\rho_{21}\}$ of the first summand leads to the Lorentz contour. It may be noted at once that this is a purely quantum mechanical description and its QED extension was presented in section 2.3 by the expression (2.40). The remaining terms in (10.3) represent the effect of electromagnetic induced transparency (EIT). From an observational point of view, the added contributions can lead to a significant distortion of the line contour. Since studies of the EIT effect are widely presented in the scientific literature, the essence of the effect can be simplified to the following. The photon corresponding to the "probe" field is effectively absorbed in the $1-2$ transition. If the "controlled" field moves the system to the 3 state, see Fig. 10.2 b), then the next photon at the $1-2$ transition will "escape" - the system is transparent to the test field and there is an additional "output" (escape) of radiation. Other cases can be explained in a similar way. Further it will be shown how this effect can be taken into account

in astrophysical studies of CMB.

10.2. Absorption coefficient and photon escape probability in the Sobolev approximation

Radiation transfer theory for multilevel atoms is presented in the [99] as a direct application to the formation of CMB. This theory uses the concept of photon escape probability in the Sobolev approximation (local changes in the velocity gradient are negligible compared to those at longer lengths) [100]. Using the escape probability method, a simple solution to the radiative transfer problem for bound transitions can be found. The Sobolev escape probability p_{ij} (j refers to the upper level and i to the lower level of a multilevel atom) is the probability that the photons associated with this transition will "escape" without further scattering or absorption. If $p_{ij} = 1$, the photons originating at the transition can escape to infinity - they do not cause distortion of the radiation field. If $p_{ij} = 0$, the photons cannot go to infinity; they are all re-absorbed and the line becomes optically thick. In the general case, assuming a hydrogen atom in the ground state, $p_{ij} \ll 1$ for Lyman lines and $p_{ij} \approx 1$ for all other transitions. The Sobolev escape probability is included in the direct astrophysical equations of radiative transfer, see, e.g., expression (25) in [99].

According to Section 2.3.3 in [99], the photon escape probability can be represented as

$$p_{ij} = \frac{1 - exp(-\tau_S)}{\tau_S}, \tag{10.4}$$

where τ_S is the Sobolev optical thickness. Optical thickness is a measure of the damping or absorption coefficient up to a certain "depth". In other words, optical thickness expresses the amount of light removed from a beam as a result of scattering or absorption during its passage through a medium. It is defined according to the expression:

$$\tau_S = \frac{\lambda_{ij}\tilde{k}}{|v'|}. \tag{10.5}$$

Here $\tilde{k}$ is the integral absorption coefficient of the line, and λ_{ij} is the wavelength of the line center. The monochromatic absorption coefficient (opacity or attenuation coefficient) is $k = \tilde{k}\phi(\nu_{ij})$ (ν_{ij} is the frequency of a given transition, and $\phi(\nu_{ij})$ is the normalized line profile), v' is the velocity gradient determined by the Hubble expansion rate $H(z)$.

The absorption coefficient strongly depends on external conditions and requires special consideration in each case. In the presence of an external field, it can be related to the imaginary part of the elements of the density matrix ρ_{ij} as follows:

$$k = \frac{N d_{ij}^2 \omega_{ij}}{2\varepsilon_0 \Omega_{ij}} \Im\{\rho_{ij}\}, \tag{10.6}$$

where ε_0 is the dielectric permittivity of vacuum and N is the number of atoms.

Using the expression (10.3) to determine the imaginary part of ρ_{21}, it can be found that

$$\Im\{\rho_{21}\} = \frac{\gamma_{21}\Omega_\alpha/2}{\Delta_\alpha^2 + \gamma_{21}^2}\left[1 + f(\Omega_\alpha^2, \Omega_\beta^2, \Delta_\alpha, \Delta_\beta)\right] \tag{10.7}$$

together with the dimensionless function

$$\begin{aligned} f(\Omega_\alpha^2, \Omega_\beta^2, \Delta_\alpha, \Delta_\beta) = \frac{\Delta_\alpha^2 - \gamma_{21}^2}{\Delta_\alpha^2 + \gamma_{21}^2}\left[\frac{\Omega_\beta^2}{4\gamma_{21}\gamma_{31}} - \frac{\Omega_\alpha^2}{4\Gamma_2\gamma_{21}}\right] + \\ \frac{\left(\gamma_{21}^4\gamma_{32} - \gamma_{32}\Delta_\alpha^4 - 2\gamma_{21}^3\gamma_{32}^2 + 2\gamma_{21}\Delta_\alpha^2(3\gamma_{32}^2 + \Delta_\beta(3\Delta_\beta - \Delta_\alpha))\right)\Omega_\alpha^2\Omega_\beta^2}{16\Gamma_2\gamma_{21}\gamma_{31}(\Delta_\alpha^2 + \gamma_{21}^2)^2(\Delta_\beta^2 + \gamma_{32}^2)} + \\ \frac{\left(\gamma_{21}^2\gamma_{32} - \gamma_{32}\Delta_\alpha^2 - 2\gamma_{21}\Delta_\alpha\Delta_\beta\right)\Omega_\alpha^2\Omega_\beta^2}{16\gamma_{21}\gamma_{31}^2(\Delta_\alpha^2 + \gamma_{21}^2)(\Delta_\beta^2 + \gamma_{32}^2)} + \ldots \end{aligned} \tag{10.8}$$

To determine the integral absorption coefficient of the line in (10.7), the line profile is extracted as a common factor, which corresponds to the monochromatic absorption coefficient, see expression (31) in [99], and the function f depends on the fixed parameters Δ_α and Δ_β, $\Delta_\alpha = \omega_\alpha - \omega_{21}$.

Thus, the integral absorption coefficient of the line can be represented as:

$$\tilde{k}_{21} = \frac{\pi d_{21}^2 N \omega_{21}}{4\varepsilon_0} \left[1 + f(\Omega_\alpha^2, \Omega_\beta^2, \Delta_\alpha, \Delta_\beta)\right] \tag{10.9}$$

with line profile $\phi(\nu_{21}) = \gamma_{21} / \left[(\omega_\alpha - \omega_{21})^2 + \gamma_{21}^2\right]$. According to the theory in [99], the line profile should be normalized in the interval $[0, \infty]$, this accounts for the π coefficient. Thus, the probability of photon escape in the $2-1$ line is given by the expression:

$$p_{12} = \frac{1 - exp\left(-\tau_S[1 + f(\Omega_\alpha^2, \Omega_\beta^2, \Delta_\alpha, \Delta_\beta)]\right)}{\tau_S[1 + f(\Omega_\alpha^2, \Omega_\beta^2, \Delta_\alpha, \Delta_\beta)]}, \tag{10.10}$$

where τ_S can be taken in the form (10.5). For rough estimates, it is sufficient to restrict ourselves to considering the function $f(\Omega_\alpha^2, \Omega_\beta^2, \Delta_\alpha, \Delta_\beta)$. Decomposing the expression (10.10) into a series over the small additive f, one can obtain the approximate equality $p_{12} \approx p_{12}^{(0)}(1 - f(\Omega_\alpha^2, \Omega_\beta^2, \Delta_\alpha, \Delta_\beta))$, where $p_{12}^{(0)}$ corresponds to the "standard" approach used in [99]. The function f depends strongly on the parameters $\Omega_\alpha^2, \Omega_\beta^2, \Delta_\alpha, \Delta_\beta$. Estimates of the field amplitudes can be derived from the distribution of cosmic microwave radiation corresponding to the hydrogen recombination epoch in the early Universe.

10.3. Numerical results: Ξ-scheme of levels

As the Universe continued to expand and cool, electrons and protons tended to form hydrogen atoms. The temperature at this epoch is very well known from laboratory physics: $T \approx 3000 - 4500$ K. After recombination, the released photons could travel through the Universe relatively undisturbed and formed the primary background radiation. However, this photon environment (background) should have affected the hydrogen atom. The field amplitudes for a circularly polarized wave can be obtained from the spectral energy density

$$\frac{c\varepsilon_0 |E|^2}{4\pi} = \frac{2h\nu_{ij}^3 \Delta\nu_{ij}}{c^2} \frac{1}{e^{\frac{h\nu_{ij}}{k_B T_e}} - 1}, \tag{10.11}$$

where c is the speed of light, k_B is Boltzmann's constant, h is Planck's constant and for further evaluations the temperature value $T_e = 3000$ K is used. The right-hand side of the above equation corresponds to the blackbody distribution of CMB, and the left-hand side defines the (electric) energy density.

To avoid the problem of unphasing, it should be selected $\Delta\nu_{ij} \sim \Gamma_i$. Hence, for spectral lines $\nu_{21} = \nu_\alpha$ (Ly_α line) and $\nu_{32} = \nu_\beta$ (H_α line) it can be found that

$$\begin{aligned} E_\alpha &\approx 0.000068802 \text{ V/m} = 1.33799 \times 10^{-16} \text{ a.u.}, \\ E_\beta &\approx 52.8636 \text{ V/m} = 1.02803 \times 10^{-10} \text{ a.u.} \end{aligned} \tag{10.12}$$

The field magnitudes (10.12) are small; one should compare the Rabi frequencies with the corresponding level widths. The probabilities of one-photon transitions, which give the main contribution to the level widths, are well known. For the hydrogen atom, the dominant transition probability is Ly_α, $\Gamma_{2p} \sim 10^{-8}$ in atomic units, and hence a power series (10.3) can be used. Moreover, the estimates given in (10.12) show that all terms of order Ω_α^2 and higher can be neglected.

Then the function $f(\Omega_\alpha^2, \Omega_\beta^2, \Delta_\alpha, \Delta_\beta)$ can be evaluated numerically. In the case when the detunings are defined by $\Delta_\alpha \equiv \Gamma_{2p}$ and $\Delta_\beta \equiv \Gamma_{2p} + \Gamma_{3s}$, the function f is given in the form:

$$\begin{aligned} f(\Omega_\alpha^2, \Omega_\beta^2, \Delta_\alpha, \Delta_\beta) \approx &-1.30494 \cdot 10^{15}\Omega_\alpha^2 - 2.08127 \cdot 10^{30}\Omega_\alpha^4 \\ &+8.67218 \cdot 10^{14}\Omega_\beta^2 + 5.15573 \cdot 10^{29}\Omega_\beta^4 + 2.42665 \cdot 10^{44}\Omega_\beta^6 \\ &+3.22916 \cdot 10^{29}\Omega_\alpha^2 - 1.08979 \cdot 10^{47}\Omega_\alpha^2\Omega_\beta^4 - 6.18661 \cdot 10^{44}\Omega_\alpha^4\Omega_\beta^2 \\ &-1.63588 \cdot 10^{62}\Omega_\alpha^4\Omega_\beta^4 + 2.92629 \cdot 10^{63}\Omega_\alpha^2\Omega_\beta^6 - 4.88545 \cdot 10^{78}\Omega_\alpha^4\Omega_\beta^6. \end{aligned} \tag{10.13}$$

Taking into account the estimates(10.12)

$$\begin{aligned} \Omega_\alpha &\approx 1.99343 \cdot 10^{-16} \text{ a.u.}, \\ \Omega_\beta &\approx 1.92942 \cdot 10^{-10} \text{ a.u.}, \\ f &\approx 0.0000322844. \end{aligned} \tag{10.14}$$

For the case of exact resonances ($\Delta_\alpha = 0$ and $\Delta_\beta = 0$)

$$f \approx -0.015814. \tag{10.15}$$

Finally, in the case of exact two-photon resonance, when $\Delta_\alpha + \Delta_\beta = 0$ in combination with $\Delta_\alpha = \Gamma_{2p}$, the function f takes a value:

$$\Delta_\alpha = \Gamma_{2p} = -\Delta_\beta \sim 10^{-8}\,\text{a.u.},$$
$$f \approx 0.00952743. \tag{10.16}$$

Thus, the value of the function $f(\Omega_\alpha^2, \Omega_\beta^2, \Delta_\alpha, \Delta_\beta)$ is about 1%; in the case of exact one-photon resonances about 1.5%, respectively about 0.95% if the detunings are non-zero but of opposite sign. In quantum optics this effect is well known in the study of electromagnetic induced transparency for different kinds of systems (two-, three-, or four-level systems with Λ-, V-, or Ξ-scheme of levels). The calculation results for different detuning values are summarized in Table 10.1 and graphically represented in Figs. 10.3 and 10.4.

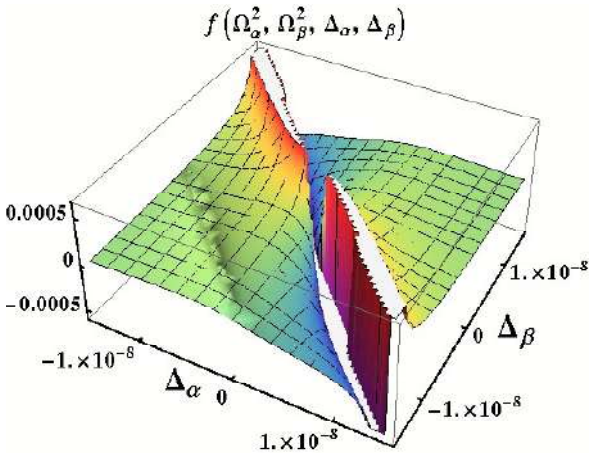

Figure 10.3. Dependence of the function $f(\Omega_\alpha^2, \Omega_\alpha^2, \Delta_\alpha, \Delta_\alpha, \Delta_\beta)$ on the detunings Δ_α and Δ_β at fixed values of the external fields (??), $\Omega_\beta/\gamma_{ij} \ll 1$, and $\Omega_\alpha/\gamma_{ij} \ll 1$. Detunings Δ_α and Δ_β vary within the range of $[-\Gamma_{2p}, \Gamma_{2p}]$.

In astrophysical studies of the processes of cosmic microwave background

Table 10.1. Numerical values of the function $f(\Omega_\alpha, \Omega_\beta, \Delta_\alpha, \Delta_\beta)$ at different detunings. The first column shows the different values of $f(\Omega_\alpha, \Omega_\beta, \Delta_\alpha, \Delta_\beta)$, in the second and third columns - detunings and corresponding field magnitudes.

$f\,(\Omega_\alpha, \Omega_\beta, \Delta_\alpha, \Delta_\beta)$	Δ_α, s^{-1} Δ_β, s^{-1} $\Delta\nu_{ij} = \lvert\Delta_\alpha\rvert$, $\lvert\Delta_\beta\rvert$ in (10.11)	$\lvert E_\alpha\rvert$, V/m $\lvert E_\beta\rvert$, V/m
$6.48635 \cdot 10^{-7}$	$W_{21} = 6.26826 \cdot 10^8$ $W_{32} = 6.31696 \cdot 10^6$	$6.8802 \cdot 10^{-5}$ 5.30686
0.0000326097	$W_{21} = 6.26826 \cdot 10^8$ $W_{21} + W_{32} = 6.33143 \cdot 10^8$	$6.8802 \cdot 10^{-5}$ 53.1293
0.00952743	$W_{21} = 6.26826 \cdot 10^8$ $-W_{21} = -6.26826 \cdot 10^8$	$6.8802 \cdot 10^{-5}$ 52.8636
0.00952743	$-W_{21} = -6.26826 \cdot 10^8$ $W_{21} = 6.26826 \cdot 10^8$	$6.8802 \cdot 10^{-5}$ 52.8636
0.0000324474	$-W_{21} = -6.26826 \cdot 10^8$ $-W_{21} = -6.26826 \cdot 10^8$	$6.8802 \cdot 10^{-5}$ 52.8636
0.0000326097	$-W_{21} = -6.26826 \cdot 10^8$ $-W_{21} - W_{32} = 6.33143 \cdot 10^8$	$6.8802 \cdot 10^{-5}$ 53.1293
$4.06852 \cdot 10^{-6}$	$10W_{21} = -6.26826 \cdot 10^9$ $10(W_{21} + W_{32}) = 6.33143 \cdot 10^9$	$2.1757 \cdot 10^{-4}$ 168.01

formation, the Lorentz line profile is used to determine the absorption coefficient. This line profile is the dominant contribution to $\Im\{\rho_{21}\}$, and is identified by the common factor in (10.7). From Table 10.1 and the results of (10.15), (10.6), it follows that the function $f(\Omega_\alpha^2, \Omega_\beta^2, \Delta_\alpha, \Delta_\beta)$ should be included in astrophysical calculations according to the expression (10.10). In reality, the escape probability dependence $p_{ij}(\tau_S)$ for a photon in the wing of the line due to the expanding Universe may have a more complicated form. The Sobolev approximation works for a certain phase, which is well known. In more complicated cases one has to apply the diffusion approximation [277]. However, the description of the EIT effect presented above can serve as estimates of the EIT influence on radiative transfer.

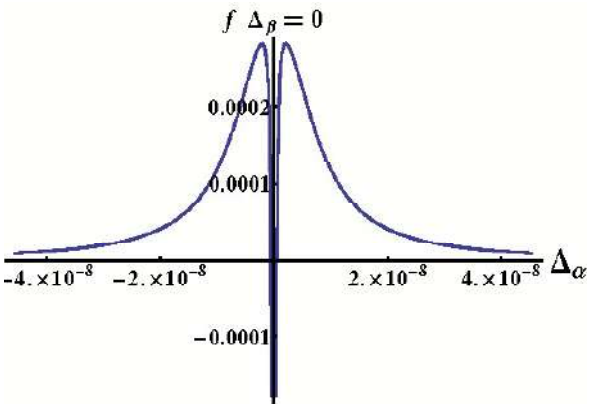

Figure 10.4. Two-dimensional graph section for the function $f(\Omega_\alpha^2, \Omega_\beta^2, \Delta_\alpha, \Delta_\beta)$ (see 10.3) when $\Delta_\beta = 0$. The remaining tuning parameter Δ_α varies within the range of $[-3\Gamma_{2p}, 3\Gamma_{2p}]$.

10.4. Numerical results: Ξ-scheme of levels taking into account fine structure

In this section, the function $f(\Omega_\alpha, \Omega_\beta, \Delta_\alpha, \Delta_\beta)$ is calculated numerically. The physical meaning of f can be found using Fig. 10.2. The processes corresponding to the function f are illustrated in Fig. 10.2 (b), (c) and (d). Namely, graph a) corresponds to the "standard" Sobolev escape probability. However, the "controlled" field leads to a delay of the electron on the excited states and prevents the final recombination due to additional processes, see plots b)-d). The function f is dimensionless, it represents the contribution of the multiphoton processes b)-d) with respect to the one-photon absorption process a). The $1s - 2p - 3s$ cascade scheme for the hydrogen atom was considered in [128]. It is shown that in the case of exact resonances (when both the Δ_α and Δ_β detunings are zero) the maximum value of f is about 1.5% and reaches 0.95% for the exact two-photon resonance.

Similar to the [128], a cascade scheme is considered here, but taking into account the fine structure of the hydrogen atom. Taking into account the Lamb

shift, the three-level ladder scheme can be defined as follows: $|1>\equiv|1s>$, $|2>\equiv|2p_{1/2}>$ and $|3>\equiv|2s>$. Substituting the corresponding widths and frequencies $\Gamma_{2s}=8.229$ s^{-1}, $\Gamma_{2p}=6.26826\times10^{8}$ s^{-1} and $\nu_{31}=2.4674\times10^{15}$ Hz, $\nu_{23}=1.057911\times10^{9}$ Hz, at $\Delta\nu_{ij}=\Gamma_{2p}$, see [129], the following estimates can be obtained:

$$\begin{aligned} E_\alpha &\approx 0.000068802 \text{ V/m} = 1.33799\times10^{-16}\,\text{a.u.}, \\ E_\beta &\approx 0.0017496 \text{ V/m} = 3.40242\times10^{-15}\,\text{a.u.}, \\ \Omega_\alpha &\approx 9.96713\times10^{-17}\,\text{a.u.}, \\ \Omega_\beta &\approx 1.02073\times10^{-14}\,\text{a.u.}. \end{aligned} \tag{10.17}$$

Numerical results of the f function for different detuning values are collected in Table 10.2.

Table 10.2. Numerical values of the function $f(\Omega_\alpha,\Omega_\beta,\Delta_\alpha,\Delta_\beta)$ for different values of detunings. The first column shows $f(\Omega_\alpha,\Omega_\beta,\Delta_\alpha,\Delta_\beta)$, the second and third columns show the detunings.

$f(\Omega_\alpha,\Omega_\beta,\Delta_\alpha,\Delta_\beta)$	Δ_α, s^{-1}	Δ_β, s^{-1}
-1.38066×10^{-4}	0	0
-1.38066×10^{-4}	$\Gamma_{2s}=8.229$	$-\Gamma_{2s}=-8.229$
8.28426×10^{-5}	$\Gamma_{2p}=6.26826\times10^{8}$	$-\Gamma_{2p}=-6.26826\times10^{8}$
-8.12364×10^{-6}	$\Gamma_{2s}=8.229$	$\Gamma_{2s}=8.229$
7.25115×10^{-13}	$\Gamma_{2p}=6.26826\times10^{8}$	$\Gamma_{2s}=8.229$
3.62557×10^{-13}	$\Gamma_{2p}=6.26826\times10^{8}$	$\Gamma_{2p}=6.26826\times10^{8}$

In particular, in the case of exact resonances, the maximum value of f is -1.38066×10^{-4}, i.e., 0.01%. In the case of the exact two-photon resonance $\Delta_\alpha+\Delta_\beta=0$, when the field frequencies are close but insignificantly different from the corresponding resonances, $f\approx0.0083\%$. Thus, in contrast to the results of [128], the maximum value of the f function is beyond the required accuracy of the CMB calculations. It should also be noted that if $\Delta\nu_{ij}=\Gamma_{2s}$, then the maximum value of f is of the order of 10^{-12}. Thus, it can be concluded

that the EIT phenomenon does not require the consideration of a fine structure for the Ξ-scheme.

10.5. Λ-scheme of levels

To describe the Λ-scheme of levels it is necessary to make the substitution $\Delta_\beta \to -\Delta_\beta$ and set $|1>\equiv|1s>$, $|3>\equiv|2s>$, $|2>\equiv|3p>$ in conjunction with $\nu_{21} = 2.4674 \times 10^{15}$ Hz, $\nu_{31} = 2.9243 \times 10^{15}$ Hz, $\Gamma_3 \equiv \Gamma_{2s} = 8.229$ c^{-1} and $\Gamma_2 \equiv \Gamma_{3p} = 1.89802 \times 10^8$ c^{-1}, assuming also $\Delta\nu_{31} \approx \Gamma_{2s}$ and $\Delta\nu_{32} \approx \Gamma_{3p}$. Then,

$$\begin{aligned} E_\alpha &\approx 2.45765 \times 10^{-18}\,\text{a.u.}, \\ E_\beta &\approx 1.17805 \times 10^{-14}\,\text{a.u.}, \\ \Omega_\alpha &\approx 7.33142 \times 10^{-19}\,\text{a.u.}, \\ \Omega_\beta &\approx 2.08452 \times 10^{-14}\,\text{a.u.} \end{aligned} \tag{10.18}$$

The numerical values of $f\,(\Omega_p, \Omega_c, \Delta_p, \Delta_c)$ are given in Table 10.3 for different detunings of transition frequencies (see [129] for details).

Table 10.3. Numerical values of the function $f(\Omega_\alpha, \Omega_\beta, \Delta_\alpha, \Delta_\beta)$ for different values of detunings. The first column shows $f(\Omega_\alpha, \Omega_\beta, \Delta_\alpha, \Delta_\beta)$, the second and third columns show the detunings.

$f\,(\Omega_\alpha, \Omega_\beta, \Delta_\alpha, \Delta_\beta)$	Δ_α, s^{-1}	Δ_β, s^{-1}
-0.00189829	0	0
-0.00189829	$\Gamma_{2s} = 8.229$	$\Gamma_{2s} = 8.229$
0.00113955	$\Gamma_{3p} = 1.89802 \times 10^8$	$\Gamma_{3p} = 1.89802 \times 10^8$
-0.000112064	$\Gamma_{2s} = 8.229$	$-\Gamma_{2s} = -8.229$
3.29832×10^{-11}	$\Gamma_{3p} = 1.89802 \times 10^8$	$\Gamma_{2s} = 8.229$
1.64916×10^{-11}	$\Gamma_{3p} = 1.89802 \times 10^8$	$-\Gamma_{3p} = -1.89802 \times 10^8$

According to estimates in [129], assuming $\Delta\nu_{31} \approx \Gamma_{2s}$ and $\Delta\nu_{32} \approx \Gamma_{2s}$, one can get $\Omega_\alpha \approx 1.52655 \times 10^{-22}$ and $\Omega_\beta \approx 2.08452 \times 10^{-14}$ (in atomic units). The

final numerical values are similar to Table 10.3, since Ω_α can still be neglected.

In the case of $\Delta\nu_{31} \approx \Gamma_{3p}$ and $\Delta\nu_{32} \approx \Gamma_{3p}$, it can be found that

$$\Omega_\alpha \approx 7.33142 \times 10^{-19}\,\text{a.u.}, \qquad (10.19)$$
$$\Omega_\beta \approx 1.00111 \times 10^{-10}\,\text{a.u.}$$

These estimates show that one can neglect the higher order terms of Ω_α. However, the approximation is satisfied under the condition $\Omega_i/\gamma_{ij} \ll 1$, which is violated for Ω_β/γ_{13}. Then the solution of the equations on the density matrix should be used without series expansion. For the matrix element ρ_{21} it can be written as

$$\rho_{21} \approx -\frac{i\Omega_\alpha}{\gamma_{23} + \mathrm{i}\Delta_\alpha + \frac{\Omega_\beta^2}{\gamma_{13}+\mathrm{i}\delta}}. \qquad (10.20)$$

The corresponding values of f are given in Table 10.4.

Table 10.4. The notations are the same as in Table 10.2.

$f\,(\Omega_\alpha, \Omega_\beta, \Delta_\alpha, \Delta_\beta)$	Δ_α, c^{-1}	Δ_β, c^{-1}
0.000761156	$\Gamma_{3p} = 1.89802 \times 10^8$	$\Gamma_{2s} = 8.229$
0.000380479	$\Gamma_{3p} = 1.89802 \times 10^8$	$-\Gamma_{3p} = -1.89802 \times 10^8$
-9.04486×10^{-7}	$\Gamma_{2s} = 8.229$	$\Gamma_{3p} = 1.89802 \times 10^8$

According to the results of Tables 10.3, 10.4, the maximum value of f can be found close to 0.2%. The contribution of this order is comparable to the present-day accuracy of the observations of CMB.

Taking into account the fine structure of the levels for the Λ scheme, one can set $|1> \equiv |1s>$, $|2> \equiv |2p_{3/2}>$, $|3> \equiv |2s>$ and hence $\nu_{31} \approx 2.46741 \times 10^{15}$ Hz, $\nu_{32} \approx 9.96903 \times 10^9$ Hz, $\Gamma_2 \equiv \Gamma_{2p} = 6.26826 \times 10^8\ \mathrm{s}^{-1}$ and $\Gamma_3 \equiv \Gamma_{2s} = 8.229\ \mathrm{s}^{-1}$. To evaluate the field amplitudes, $\Delta\nu_{21} \sim \Gamma_{2p}$, $\Delta\nu_{31} \sim \Gamma_{2s}$ are used. Then,

$$\Omega_\alpha \approx 9.96632 \times 10^{-17}\,\text{a.u.}, \qquad (10.21)$$
$$\Omega_\beta \approx 1.10204 \times 10^{-10}\,\text{a.u.}$$

Numerical values of f are small and for the sake of brevity are not given (similarly for the $\Delta\nu_{21} \sim \Gamma_{2s}$ and $\Delta\nu_{31} \sim \Gamma_{2s}$ [129]).

However, for $\Delta\nu_{21} \sim \Gamma_{2p}$ and $\Delta\nu_{31} \sim \Gamma_{2p}$ it is possible to find

$$\Omega_\alpha \approx 9.96632 \times 10^{-17}\,\text{a.u.}, \qquad (10.22)$$
$$\Omega_\beta \approx 9.61828 \times 10^{-14}\,\text{a.u.}$$

The numerical values for the function f are collected in Table 10.5.

Table 10.5. The notations are the same as in Table 10.2.

$f\,(\Omega_\alpha, \Omega_\beta, \Delta_\alpha, \Delta_\beta)$	Δ_α, c^{-1}	Δ_β, c^{-1}
-0.0121124	0	0
-0.0121124	$\Gamma_{2s} = 8.229$	$\Gamma_{2s} = 8.229$
0.00729051	$\Gamma_{2p} = 6.26826 \times 10^8$	$\Gamma_{2p} = 6.26826 \times 10^8$
-0.000729015	$\Gamma_{2s} = 8.229$	$-\Gamma_{2s} = -8.229$
6.43847×10^{-11}	$\Gamma_{2p} = 6.26826 \times 10^8$	$\Gamma_{2s} = 8.229$
3.21924×10^{-11}	$\Gamma_{2p} = 6.26826 \times 10^8$	$-\Gamma_{2p} = -6.26826 \times 10^8$

As follows from Table 10.5, the maximum value of the function f reaches the level of 1%. The contribution of this order is sufficiently large and should therefore be taken into account in the theoretical description of the cosmic microwave background.

10.6. V-scheme of hydrogen levels

For the V-scheme of levels, see [129], the states are defined as follows: $|1> \equiv |3p>$, $|2> \equiv |2p>$ and $|3> \equiv |1s>$. Then, $\nu_{23} = 2.4674 \times 10^{15}$ Hz, $\nu_{13} = 2.9243 \times 10^{15}$ Hz, $\Gamma_2 \equiv \Gamma_{2p} = 6.26826 \times 10^8$ s^{-1} and $\Gamma_1 \equiv \Gamma_{3p} = 1.89802 \times 10^8$ s^{-1}. Setting $\Delta\nu_{23} \approx \Gamma_{2p}$ and $\Delta\nu_{13} \approx \Gamma_{3p}$,

$$\Omega_\alpha \approx 7.33142 \times 10^{-19}\,\text{a.u.}, \qquad (10.23)$$
$$\Omega_\beta \approx 9.96713 \times 10^{-17}\,\text{a.u.}$$

The corresponding numerical values for the function f are presented in Table 10.6.

Table 10.6. The notations are the same as in Table 10.2.

$f\,(\Omega_\alpha, \Omega_\beta, \Delta_\alpha, \Delta_\beta)$	Δ_α, s^{-1}	Δ_β, s^{-1}
-5.70837×10^{-16}	0	0
4.8248×10^{-16}	$\Gamma_{3p} = 1.89802 \times 10^8$	$\Gamma_{3p} = 1.89802 \times 10^8$
4.52944×10^{-16}	$\Gamma_{3p} = 1.89802 \times 10^8$	$-\Gamma_{3p} = -1.89802 \times 10^8$
4.14603×10^{-16}	$\Gamma_{2p} = 6.26826 \times 10^8$	$\Gamma_{2p} = 6.26826 \times 10^8$
-1.14167×10^{-16}	$\Gamma_{3p} = 1.89802 \times 10^8$	$\Gamma_{2p} = 6.26826 \times 10^8$
1.76641×10^{-17}	$\Gamma_{2p} = 6.26826 \times 10^8$	$-\Gamma_{2p} = -6.26826 \times 10^8$

Finally, taking into account the fine structure, assuming $|1> \equiv |2p_{3/2}>$, $|2> \equiv |2p_{1/2}>$, and $|3> \equiv |1s>$, there are $\nu_{23} = 2.4674 \times 10^{15}$ Hz, $\nu_{13} = 2.46741 \times 10^{15}$ Hz, $\Gamma_2 \equiv \Gamma_{2p_{1/2}} = 6.26826 \times 10^8$ s^{-1} and $\Gamma_1 \equiv \Gamma_{2p_{3/2}} = 6.26826 \times 10^8$ s^{-1}. In [129], the corresponding numerical values of f were found to be negligibly small. In the case of $\Delta\nu_{13} \approx \Gamma_{2p}$ and $\Delta\nu_{23} \approx \Gamma_{2p}$, $f \sim 10^{-16}$. Thus, in the context of the processes of CMB formation the phenomenon of electromagnetic induced transparency does not matter for the V-scheme of levels.

10.7. Full occupancy of $2s$ states

The process of two-photon $2s \to 1s$ decay can significantly control the dynamics of cosmological recombination of hydrogen, allowing about 57% of all hydrogen atoms in the Universe to recombine through this channel [77, 79]. Taking into account the complete occupation of the $2s$ state in hydrogen, it is worth considering the influence of the EIT phenomenon on the processes of CMB radiation formation. Then the conditions (see section 10.1) should be replaced by $\rho_{2s}(0) = 1$, and the others are zero. For the cascade scheme, it was obtained that for the full population of the $2s$ state, the maximum value of f is about 0.03%, see Table 10.7.

Table 10.7. The notations are the same as in Table 10.2.

$f\left(\Omega_\alpha, \Omega_\beta, \Delta_\alpha, \Delta_\beta\right)$	Δ_α, s^{-1}	Δ_β, s^{-1}
-0.000276132	0	0
-0.000276132	$\Gamma_{2s} = 8.229$	$\Gamma_{2s} = -8.229$
-0.0000552386	$\Gamma_{2p} = 6.26826 \times 10^8$	$-\Gamma_{2p} = -6.26826 \times 10^8$
0.00003314	$-\Gamma_{2p} = -6.26826 \times 10^8$	$\Gamma_{2p} - \Gamma_{2s} = 6.26826 \times 10^8$
-0.0000162473	$\Gamma_{2s} = 8.229$	$\Gamma_{2s} = 8.229$
7.25115×10^{-13}	$\Gamma_{2p} = 6.26826 \times 10^8$	$\Gamma_{2p} = 6.26826 \times 10^8$

For the Λ-scheme, the maximum value of $f\left(\Omega_\alpha, \Omega_\beta, \Delta_\alpha, \Delta_\beta\right)$ is of the order of 10^{-12} [129]. Taking into account the fine structure of the levels it is possible to obtain the maximum value of the function f at the level of 10^{-8}. It should be emphasized that in the case of full population of the $2s$ state, the matrix element ρ_{31} is suppressed by the factor $\Omega_\alpha \Omega_\beta^2$ and, therefore, the effect remains negligible for the Ly_α line.

To conclude this section, it is worth noting that despite rather detailed and accurate calculations that take into account various "subtle" effects (see, for example, [164,252]), the influence of the external field on the characteristics of the environment has not yet been taken into account in the framework of radiation transfer theory. As a demonstration of the importance of the relevant effects, estimates of the electromagnetic induced transparency phenomenon have been presented. It is shown that EIT manifests itself under the conditions of CMB formation and can reach the 1% level. Even though rough estimates of the EIT effect strongly depend on the "field parameters" and temperature in particular. All the estimates presented above correspond to an equilibrium temperature of 3000 K, when recombination has already effectively ended. Thus, the effect can be expected to be stronger for higher temperatures.

10.8. Analysis of the absorption line profile at 21 cm wavelength of hydrogen atom in the interstellar medium

According to the theory presented in section 10.1, the consideration of adjacent transitions in determining any transition frequency can be decisive. Based on the results of the previous sections, it may be pointed out that the most significant modification of the line profile under astrophysical conditions is found for the Ξ-scheme of levels. In this section, the absorption line profile at wavelength 21 cm of a hydrogen atom in the interstellar medium (ISM) is analyzed. The hydrogen atom is considered as a three-level system illuminated by a powerful light source at neighboring resonances corresponding to the hyperfine splitting of the ground state and the Ly_α transition. The field acting on the resonances induces physical processes that can be explained as interfering paths between the different transitions. The section considers special cases where the 21 cm line profile is significantly modified by the Ly_α transition. A correction for the optical depth is presented. It is shown that the correction can be significant and should be taken into account when determining the column density of hydrogen atoms in ISM. The effects of the non-Doppler broadening and frequency shift are also discussed.

The Ξ-scheme of levels of the hydrogen atom (three-level ladder (cascade) system), where the states $|1\rangle$ and $|2\rangle$ are two hyperfine sublevels of the ground state, and $|3\rangle$ is the excited state $2p$, is presented in Fig. 10.5.

10.8.1. Correction to the optical depth for the three-level Ξ-scheme

As before, it is assumed that the hydrogen atom is subject to probe and controlled fields with corresponding frequencies $\omega_p \to \omega_{21} = |1\rangle \leftrightarrow |2\rangle$ for the 21 cm line and Ly_α transition $\omega_c \to \omega_{32} = |2\rangle \leftrightarrow |3\rangle$. The set of equations of the

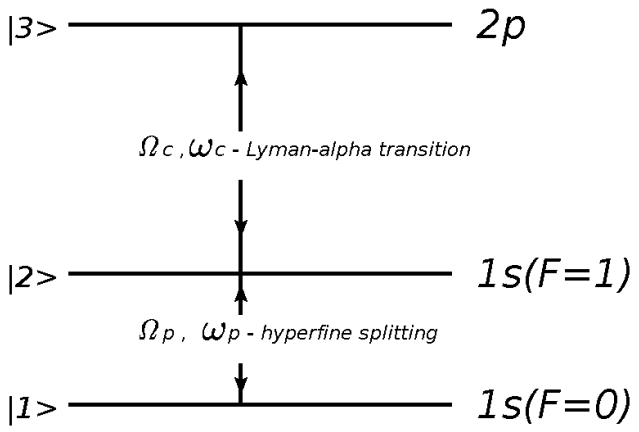

Figure 10.5. Schematic representation of energy levels in the hydrogen atom. The lower states correspond to the ground state with hyperfine sublevels for the total angular momenta of the atom $F = 1$ and $F = 0$. The wavelength of the resonance transition between the hyperfine sublevels is 21 cm. The upper state is represented by an excited $2p$ state corresponding to the Lyman-α transition. The Ω_p and Ω_c denote the corresponding Rabi frequencies for the probe and controlled fields (Ω_α and Ω_β in the previous notations) from an external source.

ladder scheme has the form:

$$\begin{aligned}
\rho_{21} &= \frac{\mathrm{i}}{2}\frac{(\Omega_p(\rho_{22}-\rho_{11})-\Omega_c^*\rho_{31})}{\gamma_{21}-\mathrm{i}\delta_p}, \\
\rho_{32} &= \frac{\mathrm{i}}{2}\frac{\left(\Omega_c(\rho_{33}-\rho_{22})+\Omega_p^*\rho_{31}\right)}{\gamma_{32}-\mathrm{i}\delta_c}, \\
\rho_{31} &= \frac{\mathrm{i}}{2}\frac{(\Omega_p\rho_{32}-\Omega_c\rho_{21})}{\gamma_{31}-\mathrm{i}(\delta_p+\delta_c)}, \\
\rho_{22} &= \frac{\mathrm{i}}{2\Gamma_2}(\Omega_p^*\rho_{21}-\Omega_p\rho_{12}), \\
\rho_{33} &= \frac{\mathrm{i}}{2\Gamma_3}(\Omega_c^*\rho_{32}-\Omega_c\rho_{23}),
\end{aligned} \tag{10.24}$$

where the detunings for the probing and controlling fields are $\delta_p = \omega_p - \omega_{21}$, $\delta_c = \omega_c - \omega_{32}$, respectively, and ω_{21}, ω_{32} represent the resonance values of the transition frequencies. The Rabi frequencies are denoted by $\Omega_c = 2d_{32}E_c/\hbar$ and $\Omega_p = 2\mu_{21}B_p/\hbar$. Since the transition between hyperfine sublevels corresponds to the emission (absorption) of the magnetic dipole $M1$, the Rabi frequency Ω_p is written through the magnetic field strength B_p and magnetic moment μ_{ij}. E_c represents the electric field strength for the Ly_α transition, and d_{ij} is the

dipole matrix element. The wave functions for the $|3\rangle$, $|2\rangle$, and $|1\rangle$ states can be taken as the solution of the Schr?dinger equation. In the absence of collisions, $\gamma_{ij} = (\Gamma_i + \Gamma_j)/2$, where Γ_i is the natural width of the ith level. The set of equations (10.24) is written in the same approximations as before.

Using the definition for the absorption coefficient (10.6), the line profile can be found in the form (10.7). Taking into account the relation $k = \tilde{k}\phi(\omega)$, the monochromatic optical depth is defined according to

$$d\tau(\omega_{ij}) = -\tilde{k}\phi(\omega_{ij})dl = -\tau\phi(\omega_{ij})\frac{dl}{L}, \tag{10.25}$$

where l is the distance along the beam ($L = v_{\text{th}}/v'$, v_{th} is the thermal velocity, and v' is the gradient of v_{th}) [99, 100].

In the usual case, the monochromatic optical depth corresponds to a one-photon resonance process, which reduces to the evaluation of a two-level atomic system. Then the one-photon absorption process is described by the Lorentz line profile:

$$\Im\{\rho_{21}^{(0)}\} = -\frac{\gamma_{21}\Omega_p/2}{\delta_p^2 + \gamma_{21}^2}, \tag{10.26}$$

where δ_p can be considered as a variable. A more precise solution of the equations (10.24) corresponds to taking into account the second field acting on the neighboring resonance. Then, in the limit of a weak "probe" field [93], the matrix element ρ_{21} in the first order on it and in all orders on the "controlled" field is equal to

$$\rho_{21} = \frac{\mathrm{i}\Omega_p/2}{\mathrm{i}\delta_p - \gamma_{21} + \frac{\Omega_c^2/4}{i(\delta_p+\delta_c)-\gamma_{31}}}. \tag{10.27}$$

The expression (10.27) depends on the field parameters Ω_c and δ_c and reduces to (10.26) in the limit $\Omega_c \to 0$, i.e., when the influence of the field on the neighboring resonance is negligible. In this case, corrections to the "usual" definition (10.27) can be found by series expansion of $\Omega_{p(c)}$ at zero detunings $\delta_{p(c)}$. Then the transition amplitudes associated with the paths $|1\rangle \to |2\rangle$ and $|2\rangle \to |3\rangle$ lead to destructive interference and decrease the total probability

that the trial ("probe") photon will be absorbed [95].

However, a series expansion in Rabi frequencies cannot be used in this case because of the smallness of the level width $\Gamma_2 \approx 2.85 \times 10^{-15}$ s^{-1}. Nevertheless, see [130], the imaginary part of ρ_{21} can be extracted

$$-\Im\{\rho_{21}\} \equiv -\Im\{\rho_{21}^{(1)}\} - \Im\{\rho_{21}^{(2)}\} = \frac{\gamma_{21}\Omega_p/2}{\left(\delta_p - \frac{(\delta_p+\delta_c)\Omega_c^2/4}{(\delta_p+\delta_c)^2+\gamma_{31}^2}\right)^2 + \left(\gamma_{21} + \frac{\gamma_{31}\Omega_c^2/4}{(\delta_p+\delta_c)^2+\gamma_{31}^2}\right)^2} + \frac{\gamma_{31}\Omega_p\Omega_c^2/8}{\left[\left(\delta_p - \frac{(\delta_p+\delta_c)\Omega_c^2/4}{(\delta_p+\delta_c)^2+\gamma_{31}^2}\right)^2 + \left(\gamma_{21} + \frac{\gamma_{31}\Omega_c^2/4}{(\delta_p+\delta_c)^2+\gamma_{31}^2}\right)^2\right]((\delta_p+\delta_c)^2+\gamma_{31}^2)}. \tag{10.28}$$

The first summand here is a one-photon process $|1\rangle \to |2\rangle$ (21 cm), the second summand can be associated with an additional process $|1\rangle \to |2\rangle \to |3\rangle \to |2\rangle$. In the absence of the second field $\Omega_c = 0$, the second summand in (10.28) vanishes and the usual definition of (10.26) can be found. The effect of (10.28) can be represented as in Fig. 10.3.

Thus, the absorption coefficient and the optical depth, respectively, cannot be described by a single Lorentz contour (10.26) with the subsequent transformation into the Voigt profile. One can also note that the first term corresponding to the absorption in the 21 cm line has a broadening and a *a priori* line profile shift.

The dimensionless correction to the optical depth (10.25) arising in the context of expression (10.28) can be defined as follows:

$$\tau = \tau_0(1 + \delta\tau), \tag{10.29}$$

where τ_0 refers to the profile $\Im\{\rho_{21}^{(1)}\}$, and the correction $\delta\tau$ is equal to

$$\delta\tau = \frac{\Im\{\rho_{21}\} - \Im\{\rho_{21}^{(1)}\}}{\Im\{\rho_{21}^{(1)}\}} \equiv \frac{\Im\{\rho_{21}^{(2)}\}}{\Im\{\rho_{21}^{(1)}\}}. \tag{10.30}$$

The expression (10.30) reduces to

$$\delta\tau = \frac{\gamma_{31}}{\gamma_{21}} \frac{\Omega_c^2}{4((\delta_p + \delta_c)^2 + \gamma_{31}^2)}. \tag{10.31}$$

The expression (10.31) is resonant but independent of the probe field Ω_p acting in the line 21 cm.

10.8.2. Non-Doppler broadening and frequency shift

According to (10.28) one can determine the broadening and frequency shift due to the presence of multiphoton processes at neighboring resonances, i.e., having a purely non-Doppler origin. The non-Doppler line broadening for the $|1\rangle \to |2\rangle$ transition follows from the denominator in the first summand and is proportional to Ω_c. This broadening can be expressed as an additional term to the natural width γ_{21}:

$$\gamma = \gamma_{21} + \frac{\gamma_{31}\Omega_c^2/4}{(\delta_p + \delta_c)^2 + \gamma_{31}^2} = \gamma_{21} + \gamma_{\text{broad}}. \tag{10.32}$$

The maximum value of γ_{broad} is achieved for the exact two-photon resonance $\delta_p + \delta_c = 0$:

$$\gamma_{\text{broad}} = \frac{\Omega_c^2}{4\gamma_{31}}. \tag{10.33}$$

For a very powerful light source and small distances between the absorber and the source, the γ_{broad} value can be expected to exceed the natural level width γ_{21}.

Taking into account the motion of the interstellar gas cloud, the resonant frequency is expected to be shifted. This Doppler shift results in $\delta_c \to \delta_c + \frac{v}{c}\omega_c$, where c is the speed of light. The velocity of hydrogen clouds can be on the order of several hundred km/s, and in some cases can reach thousands of kilometers per second. Then the sum of the detunings $\delta_p + \delta_c$ can be estimated as $(10^{-3} - 10^{-2})\omega_c \sim (10^4 - 10^5)\gamma_{31}$, where $\gamma_{31} = \frac{1}{2}\Gamma_{2p} = \frac{1}{2}6.265 \times 10^8$ s^{-1} and the Ly$_\alpha$ transition frequency is $\omega_c = 2.466 \times 10^{15}$ s^{-1}. Thus, the Doppler shift

results in a suppression of γ_{broad}. Nevertheless, since the emission spectrum of the source has a continuum character, it is always possible to isolate the case of an exact two-photon resonance. It should be emphasized that this discussion is consistent with γ_{broad} and does not invalidate the Doppler broadening [130].

The expression (10.28) also permits the frequency shift for the transition $|1\rangle \to |2\rangle$ to be found. For this purpose, the detuning δ_p can be considered as a "scanning" parameter (variable). Then the resonance condition will be

$$\delta_p - \frac{(\delta_p + \delta_c)\Omega_c^2/4}{(\delta_p + \delta_c)^2 + \gamma_{31}^2} = 0. \tag{10.34}$$

Now the frequency shift is zero for the exact two-photon resonance, $\delta_p + \delta_c = 0$. In the case when the two-photon resonance is detuned $\delta_p + \delta_c = \gamma_{31}/2$, the frequency shift can be found as follows

$$\delta_{\text{shift}} = \frac{\Omega_c^2}{4\gamma_{31}}. \tag{10.35}$$

Here the γ_{31} level width acts as a natural parameter of the resonant excitation of the atom.

Another result arises under the assumption that $\delta_p \sim \gamma_{21} \ll \delta_c \sim \gamma_{31}$ (one-photon resonances). Then, neglecting δ_p in the second term of the expression (10.34), the frequency shift is equal to

$$\delta_{\text{shift}} = \frac{\delta_c \Omega_c^2}{4\delta_c^2 + 4\gamma_{31}^2}. \tag{10.36}$$

The motion of the hydrogen cloud can be accounted for by utilizing the parameter β: $\delta_c = \upsilon/c \cdot \omega_c \equiv \beta\gamma_{31}$. Therefore,

$$\delta_{\text{shift}}^{\beta} = \frac{\Omega_c^2}{4\gamma_{31}} \frac{\beta}{1+\beta^2} \approx \frac{\Omega_c^2}{4\gamma_{31}} \frac{1}{\beta}. \tag{10.37}$$

The shift is negligibly small and the maximum shift can be achieved for two-photon resonance with detuning $\delta_p + \delta_c = \gamma_{31}/2$, (10.35).

10.8.3. Numerical results

To estimate the contribution of the non-Doppler broadening, frequency shift, and optical depth correction, the Rabi frequency Ω_c needs to be found. This can be done using the flux density or brightness of the light sources and the distance between the source and absorber. For this purpose data from observations of damped Lyman-α systems at 1216 Å the line in hydrogen [237, 278] and many others have been used (see references in [130]).

$$r = \frac{c}{H_0}(z_{\text{em}} - z_{\text{abs}}), \tag{10.38}$$
$$I_{\text{abs}} = \frac{L_*}{4\pi(1 + z_{\text{em}} - z_{\text{abs}})^4 r^2},$$

where L_* is the luminosity of the star (measured in units of W/Hz), independent of distance, $H_0 = 2.3 \times 10^{-18}$ s^{-1} is the Hubble constant, z_{em}, z_{abs} are the redshifts of the source and absorber, respectively. For the observed flux density S at frequency ν, the intensity at the absorber is equal to

$$S_{\text{abs}} = S_0\, \nu_0 \frac{z_{\text{em}}^2 (1 + z_{\text{em}})^4}{(z_{\text{em}} - z_{\text{abs}})^2 (1 + z_{\text{em}} - z_{\text{abs}})^4}, \tag{10.39}$$

where S_0 is the measured flux density and ν_0 is the frequency of the corresponding transition.

The line flux density Ly_α can be expressed in terms of the electric field strength E_α as

$$S_\alpha = \frac{1}{2}\sqrt{\frac{\epsilon_0}{\mu_0}} c E_c^2\,, \tag{10.40}$$

where ϵ_0 is the dielectric permittivity of vacuum and μ_0 is the vacuum permeability. In principle, the Rabi frequency for the transition 21 cm can be defined analogously, i.e. as $S_{21} = \frac{1}{2}\sqrt{\frac{\epsilon_0}{\mu_0}} c B_p^2$.

The data used in the calculations are collected in Table 10.8.

Using the data in Table 10.8, the line broadening and frequency shift were estimated. The correction to optical depth $\delta\tau$ for zero and non-zero detuning is calculated using the formula (10.31). The Doppler effect can be accounted

Table 10.8. The first column contains the names of the sources. The second and third columns present the redshifts of the star and absorber, respectively, where the 21 cm absorption combined with Ly_α absorption was observed. The next column shows the density flux at 1.4 GHz (hyperfine splitting of the ground state of the hydrogen atom, $|1\rangle \leftrightarrow |2\rangle$ transition). The fifth column summarizes the flux density and luminosity values at Ly_α. The values of the hydrogen velocity at the 21 cm line are given in the sixth column. Finally, the optical depth values are summarized in the last column of the table. For references to the data used, see [130].

Name	z_{em}	z_{abs}	$S_{1.4\text{ГГц}}$, Jy	$logL_\alpha$, W/Hz	υ, km/s	τ_0
0235+164	0.94	0.523869	1.7	$log[\nu f] \approx -12.5$ erg/(cm^{2}s)	125	$(\frac{1}{f})\int \tau d\upsilon = 13 \pm 0.6$
3C 190	1.1946	1.19565	2.47	0.17, Jy	−37.1	0.0027 ± 0.0002
3C 216	0.668	0.63	3.4	22.699	102	0.38
J0414+0534	2.6365	0.9586	1.82	22.188	205	0.0212(16)
J0414+0534	2.6365	2.63534	3.31	22.188	−94	(0.015 ± 0.002)
0902+343	3.398	3.3968	1.2	22.422	120	–
3C 49	0.621	0.6207	7.28	20.777	−138	0.036 ± 0.003
3C 286	0.849	0.692153	14.7	2.7, Jy	4.2	0.280 ± 0.004
0118-272	0.559	0.558	0.93	0.95, Jy	–	$log[N_{HI}] = 20.3$
0405-331	2.570	2.562	0.63	0.56, Jy	–	$log[N_{HI}] = 20.6$
0537-286	3.104	2.976	0.862	0.90, Jy	–	$(0.41 \pm 0.22) \times 10^{22}$
0957+561A	1.413	1.391	0.59	0.15, Jy	25	$N_{HI} = 7 \times 10^{19} \pm 30\%$
0248+430	1.31	0.3939	1.4	1.5, Jy	40	$N_{HI} = (3.6 \pm 0.4) \times 10^{19}$
0336-017	3.197	3.0619	0.60	0.15, Jy	13	$log[N_{HI}] = 21.25$, $\tau_0 < 0.2$
0528-250	2.813	2.8110	1.16	0.59, Jy	5	$log[N_{HI}] = 21.3 \pm 0.1$
2128-123	0.501	0.430	1.8	0.7, Jy	75	$log[N_{HI}] = 19.37 \pm 0.08$, $\tau_{LL} \simeq 150$

Table 10.9. The first column lists the names of the sources according to Table 10.8. The second column gives the values for the underdoppler broadening. The frequency shift δ_{shift} for the $|1\rangle \leftrightarrow |2\rangle$ transition is presented in the third column. The fourth column shows the relative contributions $\delta\tau$ at detunings $\delta_p \ll \delta_c = \frac{v}{c}\omega_{32}$. The values of $\delta\tau_0$ are given in the last column, in which the values of the correction to the optical depth specified in the Table 10.8 are given after the comma.

Name	γ_{broad}, s^{-1} vs $\Gamma_2 = 2.85 \times 10^{-15}$, s^{-1}	$\delta^{\beta}_{\text{shift}}$, s^{-1}	$\delta\tau$ at $\delta_c = \frac{v}{c}\omega_{32}$	$\delta\tau_0$, $\delta\tau_0 \cdot \tau_0$
0235+164	9.28×10^{-20}	3.87×10^{-23}	1.53×10^{-13}	6.51×10^{-5}, 8.46×10^{-4}
3C 216	2.34×10^{-17}	7.97×10^{-21}	5.805×10^{-11}	0.0164, 6.23×10^{-3}
J0414+0534($z_{abs} = 0.9586$)	4.93×10^{-24}	3.37×10^{-27}	3.02×10^{-18}	3.46×10^{-9}, 7.33×10^{-11}
J0414+0534($z_{abs} = 2.63534$)	5.59×10^{-16}	1.75×10^{-19}	1.63×10^{-9}	0.392, 5.88×10^{-3}
0902+343	8.502×10^{-16}	3.403×10^{-19}	1.52×10^{-9}	0.597
3C 49	3.07×10^{-16}	1.41×10^{-19}	4.15×10^{-10}	0.215, 7.74×10^{-3}
0248+430	6.38×10^{-16}	8.51×10^{-20}	1.03×10^{-8}	0.448
2128-123	1.32×10^{-14}	3.31×10^{-18}	6.07×10^{-8}	0.108, 16.1
3C 190	3.08×10^{-11}	3.798×10^{-15}	5.79×10^{-4}	4.63×10^{-5}, 1.25×10^{-7}
3C 286	8.398×10^{-14}	1.18×10^{-18}	1.23×10^{-4}	0.0169, 0.00475
0118-272	1.72×10^{-10}	–	–	8.29×10^{-6}
0405-331	8.95×10^{-10}	–	–	1.59×10^{-6}
0537-286	2.07×10^{-11}	–	–	6.88×10^{-5}
0957+561A	1.89×10^{-12}	1.58×10^{-16}	7.81×10^{-5}	7.53×10^{-4}, 0.0753
0336-017	3.69×10^{-12}	1.60×10^{-16}	5.63×10^{-4}	3.86×10^{-4}, 7.72×10^{-5}
0528-250	2.41×10^{-8}	4.02×10^{-13}	0.0402	5.91×10^{-8}

for using the sixth column in Table 10.8. It should be noted that due to the smallness of the frequency ω_{21} with respect to Ly_α, the detuning δ_p can be set to zero, since $\delta_p = \beta\omega_p \ll \delta_c = \beta\omega_c$. The numerical results are summarized in Table 10.9, with the designations $\delta\tau_0$ and $\delta\tau$ corresponding to zero and non-zero detuning, respectively.

10.8.4. Results analysis

Correction to optical depth.

Thus, it is shown that the absorption line profile of the $|1\rangle \leftrightarrow |2\rangle$ transition is formed by two contributions: $\Im\{\rho_{21}^{(1)}\}$ and $\Im\{\rho_{21}^{(2)}\}$. The additional contribution to the line profile is proportional to Ω_p and Ω_c, the Rabi frequencies of the

$|1\rangle \leftrightarrow |2\rangle$ and $|2\rangle \leftrightarrow |3\rangle$ transitions, respectively. Its physical interpretation was given in [95] as interfering transitions in the atom. Using this modification, the correction to the optical depth can be found by the formula (10.31). The correction should be small for $\Omega_c \ll \gamma_{21}$. However, due to the smallness of the level width γ_{21} the condition is fulfilled for a very distant source and absorber, while for $z_{\rm em} \approx z_{\rm abs}$ the opposite situation is observed (for a very powerful light source). In this case, the main contribution to the line profile is given by the second term $\Im\{\rho_{21}^{(2)}\}$, and the correction to the optical thickness should be taken as the inverse of the first contribution. Table 10.9 is conditionally divided into two parts, representing just both cases (strongly and slightly distant source and absorber). The numerical results of the correction for optical depth at zero detuning in the cases $\Omega_c \ll \gamma_{21}$ and $\gamma_{21} \ll \Omega_c$ are collected in the first and second parts of Table 10.9 in the form of $\delta\tau_0$.

Although it is always possible to distinguish the case of zero detuning, since the emission of the light source has a continuum character, for a detailed description of the 21 cm absorption line profile in the interstellar medium, the cloud velocity should be taken into account. The latter can be expressed by the approximate equality $\delta_p + \delta_c \approx \frac{\upsilon}{c}\omega_{32}$, where the values of υ are given in Table 10.8. Numerical results for $\delta\tau$ are also given in Table 10.9.

In particular, it follows from Table 10.9 that the $\delta\tau_0$ contribution can be substantial and exceed the accuracy of the experimental determination of τ_0. Although the above analysis is rather rough and does not include the Voigt profile fitting, the main conclusion is that the two-level approximation of the atom is not sufficient. Already in the three-level approximation, additional processes occurring in the atom have to be taken into account with an appropriate fit of the absorption profile. The medium parameters extracted from such a fit can be corrected with the help of the expressions (10.28), (10.31).

Non-Doppler broadening and frequency shift.
According to the expression (10.28), the absorption line profile can be analyzed in terms of line broadening. Regardless of the dominant contribution, $\Im\{\rho_{21}^{(1)}\}$ or $\Im\{\rho_{21}^{(2)}\}$, the absorption line arising from the density matrix element changes by a width $\gamma_{\rm broad}$, see (10.32). The maximum broadening can be estimated as $\Omega_c^2/4\gamma_{31}$, (10.33). The values of $\gamma_{\rm broad}$ at zero detunings are given in Table 10.9.

It is found that the broadening can be significant and several orders of magnitude larger than the natural line width.

A significant interest of such studies is the determination of the frequency shift and hence the refinement of light source distances and cloud sizes. The accuracy of redshift determination is at the level of 10^{-10} [279], and in some cases as high as 10^{-11} [280]. The procedure for determining the redshift can be reduced to finding the maximum of the corresponding line contour. The frequency shift, expression (10.37), was obtained in the same way. The maximum frequency shift occurs when $\delta_p + \delta_c = \gamma_{31}/2$. The numerical values are listed in Table 10.9 in the third column for $\delta^{\beta}_{\text{shift}}$ and are equal to γ_{Broad} at maximum (see the second column of Table 10.9). Then, the redshift uncertainty δz_{shift} can be estimated from the frequency shift δ_{shift} as follows:

$$\delta z_{\text{shift}} = \frac{\delta_{\text{shift}}(1 + z_{\text{abs}})}{\nu_0}, \tag{10.41}$$

where ν_0 is the transition frequency. The values given in Table 10.9 show that this effect is very insignificant and can be excluded from the corresponding analysis.

Thus, although the frequency shift is negligibly small, the width of the line profile can be several orders of magnitude larger than natural. The most significant effect occurs for the optical depth. In particular, the optical depth error for the J0414+0534 source is about 13%, see Table 10.8, while the contribution (10.31) turns out to be about 39%. The same result can be obtained for the 3C 49 light source: the error and correction are about 8% and 20%, respectively. The magnitude of the correction to the optical depth and hence to the column density of hydrogen can be as high as 60%, see Table 10.9. At $z \approx z_{\text{abs}}$, fitting the observed line profile with a one-photon contour for the isolated resonance may overestimate the corresponding values.

In conclusion of this chapter, it is worth paying attention to the fact that the processes of one-photon scattering on the hydrogen atom do not fully reflect the phenomena related to radiation transfer [76, 99]. In the framework of the density matrix formalism, it is shown that the absorption (emission) line profile undergoes significant changes. In particular, the density matrix theory permits

a detailed description of the processes of emission (absorption) by an atom exposed to external radiation. The profile of the one-photon absorption line in this case can be obtained in the framework of the two-level approximation of the atomic system, which is the zero approximation. However, additional emission (absorption) processes should be taken into account. These processes can be evaluated in the framework of the three-level approximation. It is shown that additional interfering transitions lead to a modification of the profile (the line contour is obtained explicitly) of the corresponding line. Also, based on the Sobolev approximation, it is shown how the theory of radiation transfer can be modified to take into account the phenomenon of EIT.

Conclusion

The results presented in the thesis refer to the theoretical study of one- and multiphoton emission and/or absorption processes. As a consequence, the detailed theoretical description presented in the thesis makes it possible to explicitly take into account the role of natural line asymmetry and asymmetry caused by external fields. The application of the obtained results can be attributed at once to three broadest areas of modern physics.

The first of them includes spectroscopy of the hydrogen atom and precision measurements of transition frequencies. Due to the achieved accuracy in spectroscopic experiments for the hydrogen atom, the identification of effects affecting the precision determination of the frequency is extremely important. In particular, the theoretical description of experiments to measure the frequency of the $1s - 2s$ transition in hydrogen has shown that the line asymmetry does not play a decisive role. The experimental error in determining the frequency is several orders of magnitude larger than the expected shift due to the asymmetry of the line profile. However, the picture changes significantly for measuring frequencies for excited states with the principal quantum number $n > 2$. In this case, the role of the line asymmetry may have a crucial role in determining the transition frequency. Within the framework of the theory presented in this thesis, a number of effects leading to asymmetry of the spectral line profile for both the total and differential scattering cross sections have been considered. The most significant is the effect of quantum interference obtained for the differential scattering cross section. In addition to the calculation of the resonant frequency shifts arising due to states close to the resonance state, it is shown that there is an influence of the radiation process on the formation of the absorption profile. In the framework of the one-photon absorption pro-

cess, the role of the profile asymmetry due to the cascade radiation process is clearly demonstrated. Moreover, on the basis of a detailed theoretical analysis, possibilities for further improvement of the experimental accuracy related to the measurement of the transition frequencies for highly excited states are pointed out. Both one- and two-photon absorption processes are discussed in the framework of hydrogen atom spectroscopy.

Another, no less important, area includes the effects arising in the external electric field. Thus, it is shown that the linear field contributions arising in the emission probabilities can lead to a significant difference in the spectral characteristics of hydrogen and anti-hydrogen atoms. At the same time, the analysis presented in the thesis concerns not only the metastable $2s$ state, but also highly excited (Rydberg) states. The latter is due to the experimental conditions. Within the framework of the studies in this direction, it was found that even extremely weak ("stray") fields can lead to the detection of differences in the spectra of H and $\bar{\text{H}}$. In addition, it is shown how the differences in the spectra of H and $\bar{\text{H}}$ atoms arising in external fields can be used to search for anti-matter in the Universe.

The study of the role of the spectral line asymmetry (natural or induced by external fields) necessitates a detailed calculation of two-photon transitions. A non-relativistic theory using different forms and gauges for the corresponding quantities is presented in the framework of the thesis, and estimates of the contribution of the negative energy spectrum are presented. The calculated values are in good agreement with completely relativistic calculations; an appropriate comparative analysis for different gauges is given.

Finally, to the third area, to which the conducted research is applied, belong astrophysical studies of the microwave cosmic background and the interstellar medium. Within the framework of these questions, not only "pure" multiphoton emission processes (discussed in detail in the thesis), but also cascade processes and spectral line asymmetry play a role. In particular, the thesis presents a more "correct" line profile arising from a strictly QED description, demonstrates the impossibility of separating "pure" radiation (leading to a direct "detachment" of radiation), investigates the role of two-photon multipole processes in the emission of highly excited states, and shows the possibility of separating the

two-photon link (in the resonance approximation) in the multiphoton cascade decay. Finally, as an astrophysical application, the influence of external radiation on the line profile is considered; a modified contour is explicitly obtained and a method of accounting for the corresponding effects is shown, accompanied by numerical evaluations.

Acknowledgements

The author of this thesis considers it his honorable responsibility to express his deepest gratitude to his colleagues Labzovsky L.N., Dubrovich V.K., Andreev O.Y., Volotka A.V., Glazov D.A., Kozhedub Yu.S., Plunien G., Soff G. and others. A number of studies were performed jointly with Zalialiutdinov T.A., Anikin A.A., Shchedrin G. and Chernovskaya E., whose contribution should not be underestimated. Prof. Labzovsky L.N. is the founder of line contour asymmetry research and a scientific mentor, without whose guidance this research would not have been possible. This work was supported by grants from the Russian Foundation for Basic Research, the Russian Science Foundation, research funds from SPbSU, grants from the Max Planck Institute (Germany), and other non-commercial funds and programs.

List of Figures

List of Tables

List of abbreviations and symbols

$R_\infty = 10973731.568\ldots$ - Rydberg constant

Z nuclear charge

$\alpha \approx 1/137.036\ldots$ - fine structure constant

$\bar{\mathbf{H}}$ anti-hydrogen atom

$\mu\mathbf{H}$ muonic hydrogen atom

BBR blackbody radiation

CEO covariant evaluation operator method

CMB cosmic microwave background

EIT electromagnetically induced transparency

GFM Green's function method

H hydrogen atom

HCI multicharged ions

He helium atom

HFS hyperfine structure

ISM interstellar medium

LPA Line Profile Approach

NR nonresonant

Ps positronium atom

QED quantum electrodynamics

QIE quantum interference effect

QM quantum mechanics

SE self-energy

TTGF two-time Green's function method

The thesis mainly uses the relativistic system of units, in which $\hbar = c = m = 1$, and the atomic system of units $\hbar = e = m = 1$, where c is the speed of light, e is the electron charge, $\hbar$ is Planck's reduced constant, and m is the electron mass.

Literature

[1] Berestetskii V., Lifshits E., Pitaevskii L. Quantum Electrodynamics. — Oxford Butterworth-Heinemann, 1982.

[2] Akhiezer A.I., Berestetskii V.B. Quantum Electrodynamics. — Wiley-Interscience, New York, 1965.

[3] Labzowsky L., Klimchitskaya G., Dmitriev Yu. Relativistic Effects in the Spectra of Atomic Systems. — Institute of Physics Publishing, 1993.

[4] Greiner W., Reinhart J. Quantum Electrodynamics. — Springer-Werlag Berlin Heidelberg, 2003.

[5] Bethe H.A., Salpeter E.E. Quantum Mechanics of One- and Two-Electron Atoms. — Springer Berlin Heidelberg, 1957.

[6] Sobel'man I.I. Introduction to the Theory of Atomic Spectra. — Pergamon, 1972. — ISBN: 9781483159720.

[7] Shabaev V.M. Two-time Green's function method in quantum electrodynamics of high-Z few-electron atoms // Phys. Rep. — 2002. — Vol. 356, no. 3. — P. 119–228.

[8] Andreev O.Yu., Labzowsky L.N., Plunien G., Solovyev D.A. QED theory of the spectral line profile and its applications to atoms and ions // Phys. Rep. — 2008. — Vol. 455. — P. 135–246.

[9] Lindgren I.P.K., Salomonson S., Åsén B. The covariant-evolution-operator method in bound-state QED // Physics Reports. — 2004. — Vol. 389, no. 4. — P. 161 – 261.

[10] Indelicato P. QED tests with highly charged ions // Journal of Physics B: Atomic, Molecular and Optical Physics. — 2019. — Vol. 52, no. 23. — P. 232001.

[11] Mohr P.J., Newell D.B., Taylor B.N. CODATA recommended values of the fundamental physical constants: 2014 // J. Phys. Chem. Ref. Data. — 2016. — Vol. 45. — P. 043102.

[12] Shabaev V.M., Glazov D.A., Plunien G., Volotka A.V. Theory of Bound-Electron g Factor in Highly Charged Ions // Journal of Physical and Chemical Reference Data. — 2015. — Vol. 44, no. 3. — P. 031205. — 10.1063/1.4921299.

[13] Glazov D.A., Köhler-Langes F., Volotka A.V. et al. g Factor of Lithium-like Silicon: New Challenge to Bound-State QED // Phys. Rev. Lett. — 2019. — Vol. 123. — P. 173001.

[14] Sturm S., Vogel M., Kahler-Langes F. et al. High-Precision Measurements of the Bound Electron's Magnetic Moment // Atoms. — 2017. — Vol. 5, no. 1.

[15] Arapoglou I., Egl A., Höcker M., et al. g Factor of Boronlike Argon $^{40}Ar^{13+}$ // Phys. Rev. Lett. — 2019. — Vol. 122. — P. 253001.

[16] Sturm S., Köhler F., Zatorski J., et al. High-precision measurement of the atomic mass of the electron // Nature. — 2014. — Vol. 506, no. 7489. — P. 467–470. — 1406.5590.

[17] Stajic J. A Better-Known Electron Mass // Science. — 2014. — Vol. 343, no. 6175. — P. 1058–1058.

[18] Andreev Yu.M., Banerjee D., Bernhard J., et al. Constraints on New Physics in Electron g-2 from a Search for Invisible Decays of a Scalar, Pseudoscalar, Vector, and Axial Vector // Phys. Rev. Lett. — 2021. — Vol. 126. — P. 211802.

[19] Abi B., Albahri T., Al-Kilani S., et al. Measurement of the Positive Muon Anomalous Magnetic Moment to 0.46 ppm // Phys. Rev. Lett. — 2021. — Vol. 126. — P. 141801.

[20] Parthey C.G., Matveev A., Alnis J. et al. Improved Measurement of the Hydrogen $1S - 2S$ Transition Frequency // Phys. Rev. Lett. — 2011. — Vol. 107. — P. 203001.

[21] Matveev A., Parthey C.G., Predehl K., et al. Precision Measurement of the Hydrogen $1S - 2S$ Frequency via a 920-km Fiber Link // Phys. Rev. Lett. — 2013. — Vol. 110. — P. 230801.

[22] Grinin A., Matveev A., Yost D.C., et al. Two-photon frequency comb spectroscopy of atomic hydrogen // Science. — 2020. — Vol. 370, no. 6520. — P. 1061–1066.

[23] van Rooij R., Borbely J.S., Simonet J. et al. Frequency Metrology in Quantum Degenerate Helium: Direct Measurement of the $2^3S_1 \rightarrow 2^1S_0$ Transition // Science. — 2011. — Vol. 333, no. 6039. — P. 196–198.

[24] Zheng X., Sun Y.R., Chen J.-J. et al. Laser Spectroscopy of the Fine-Structure Splitting in the 2^3P_J Levels of ^{4}He // Phys. Rev. Lett. — 2017. — Vol. 118. — P. 063001.

[25] Levi F., Calonico D., Calosso C.E. et al. Accuracy evaluation of ITCsF2: a nitrogen cooled caesium fountain // Metrologia. — 2014. — Vol. 51, no. 3. — P. 270–284.

[26] Nicholson T.L., Campbell S.L., Hutson R.B., et al. Systematic evaluation of an atomic clock at 2×10^{-18} total uncertainty // Nature Communications. — 2015. — Vol. 6, no. 1. — P. 6896.

[27] McGrew W.F., Zhang X., Fasano R.J., et al. Atomic clock performance enabling geodesy below the centimetre level // Nature. — 2018. — Vol. 564. — P. 87–90.

[28] Pachucki K., Patkos V., Yerokhin V.A. Testing fundamental interactions on the helium atom // Phys. Rev. A. — 2017. — Vol. 95. — P. 062510.

[29] Pohl R., et al. The size of the proton // Nature. — 2010. — Vol. 466. — P. 213–216.

[30] Antognini A., Nez F., Schuhmann K., et al. Proton Structure from the Measurement of 2S-2P Transition Frequencies of Muonic Hydrogen // Science. — 2013. — Vol. 339, no. 6118. — P. 417–420.

[31] Antognini A., Kottmann F., Biraben F. et al. Theory of the $2S - 2P$ Lamb shift and 2S hyperfine splitting in muonic hydrogen // Annals of Physics. — 2013. — Vol. 331. — P. 127–145.

[32] Beyer A., et al. The Rydberg constant and proton size from atomic hydrogen // Science. — 2017. — Vol. 358, no. 6359. — P. 79–85.

[33] Labzowsky L., Karasiev V., Goidenko I. Importance of the non-resonant corrections for the modern Lamb shift measurements in the multicharged hydrogen-like ions // J. Phys. B: At. Mol. Opt. Phys. — 1994. — Vol. 27, no. 15. — P. L439.

[34] Labzowsky L.N., Goidenko I.A., Liesen D. The non-resonant corrections to the process of the radiative electron capture of highly charged heavy ions // Physica Scripta. — 1997. — Vol. 56, no. 3. — P. 271–274.

[35] Labzowsky L.N., Solovyev D.A., Plunien G., Soff G. Asymmetry of the Natural Line Profile for the Hydrogen Atom // Phys. Rev. Lett. — 2001. — Vol. 87. — P. 143003.

[36] Labzowsky L.N., Solovyev D.A., Plunien G., Soff G. Nonresonant corrections for the hydrogen atom // Canadian Journal of Physics. — 2002. — Vol. 80, no. 11. — P. 1187–1194. — 10.1139/p02-094.

[37] Labzowsky L., Soloviev D., Plunien G., Soff G. Nonresonant corrections to the 1s-2s two-photon resonance for the hydrogen atom // Phys. Rev. A. — 2002. — Vol. 65. — P. 054502.

[38] Labzowsky L., Solovyev D., Sharipov V. et al. One- and two-photon resonant spectroscopy of hydrogen and anti-hydrogen atoms in external electric fields // Journal of Physics B: Atomic, Molecular and Optical Physics. — 2003. — Vol. 36, no. 15. — P. L227–L233.

[39] Labzowsky L., Sharipov V., Solovyev D. et al. Spectroscopy of the hydrogen and anti-hydrogen atoms in external fields // International Journal of Modern Physics B. — 2004. — Vol. 18, no. 30. — P. 3875–3886. — 10.1142/S0217979204026809.

[40] Labzowsky L.N., Schedrin G., Solovyev D., Plunien G. Nonresonant corrections and limits for the accuracy of the frequency measurements in modern hydrogen experiments // Canadian Journal of Physics. — 2007. — Vol. 85, no. 5. — P. 585–595. — 10.1139/p07-014.

[41] Labzowsky L., Schedrin G., Solovyev D., Plunien G. Theoretical study of the accuracy limits of optical resonance frequency measurements // Physical Review Letters. — 2007. — Vol. 98. — P. 2030032.

[42] Labzowsky L., Schedrin G., Solovyev D. et al. Nonresonant corrections for the optical resonance frequency measurements in the hydrogen atom // Phys. Rev. A. — 2009. — Vol. 79. — P. 052506.

[43] Jentschura U.D., Mohr P.J. Nonresonant effects in one- and two-photon transitions // Can. J. of Phys. — 2002. — Vol. 80, no. 6. — P. 633–644.

[44] Horbatsch M., Hessels E.A. Shifts from a distant neighboring resonance // Phys. Rev. A. — 2010. — Vol. 82. — P. 052519.

[45] Horbatsch M., Hessels E.A. Shifts from a distant neighboring resonance for a four-level atom // Phys. Rev. A. — 2011. — Vol. 84. — P. 032508.

[46] Sansonetti C.J., Simien C.E., Gillaspy J.D., et al. Absolute Transition Frequencies and Quantum Interference in a Frequency Comb Based Measurement of the ^{6,7}Li D Lines // Phys. Rev. Lett. — 2011. — Vol. 107. — P. 023001.

[47] Brown R.C., Wu S., Porto J.V., et al. Quantum interference and light polarization effects in unresolvable atomic lines: Application to a precise measurement of the ^{6,7}Li D_2 lines // Phys. Rev. A. — 2013. — Vol. 87. — P. 032504.

[48] Marsman A., Horbatsch M., Hessels E.A. The Effect of Quantum-Mechanical Interference on Precise Measurements of the n = 2 Triplet P Fine Structure of Helium // J. Phys. Chem. Ref. Data. — 2015. — Vol. 44, no. 3. — P. 031207.

[49] Amaro P., Fratini F., Safari L., et al. Quantum interference shifts in laser spectroscopy with elliptical polarization // Phys. Rev. A. — 2015. — Vol. 92. — P. 062506.

[50] Amaro P., Franke B., Krauth J.J., et al. Quantum interference effects in laser spectroscopy of muonic hydrogen, deuterium, and helium-3 // Phys. Rev. A. — 2015. — Vol. 92. — P. 022514.

[51] Udem Th., Maisenbacher L., Matveev A., et al. Quantum Interference Line Shifts of Broad Dipole-Allowed Transitions // Annalen der Physik. — 2019. — Vol. 531, no. 5. — P. 1900044.

[52] Solovyev D., Anikin A., Zalialiutdinov T., Labzowsky L. Importance of nonresonant corrections for the description of atomic spectra // Journal of Physics B: Atomic, Molecular and Optical Physics. — 2020. — Vol. 53, no. 12. — P. 125002.

[53] Anikin A., Zalialiutdinov T., Solovyev D. Angular correlations in two-photon spectroscopy of hydrogen // Phys. Rev. A. — 2021. — Vol. 103. — P. 022833.

[54] Patkos V., Yerokhin V.A., Pachucki K. Complete $\alpha^7\, m$ Lamb shift of helium triplet states // arXiv. — 2021. — 2103.01037.

[55] Yerokhin V.A., Patkos V., Puchalski M., Pachucki K. QED calculation of ionization energies of $1snd$ states in helium // Phys. Rev. A. — 2020. — Vol. 102. — P. 012807.

[56] Dorrer C., Nez F., de Beauvoir B. et al. Accurate Measurement of the $2^3S_1 - 3^3D_1$ Two-Photon Transition Frequency in Helium: New Determination of the 2^3S_1 Lamb Shift // Phys. Rev. Lett. — 1997. — Vol. 78. — P. 3658–3661.

[57] Luo P.-L., Peng J.-L., Hu J., et al. Precision frequency measurements of ^{3,4}He $2\,^3P \rightarrow 3\,^3D$ transitions at 588 nm // Phys. Rev. A. — 2016. — Vol. 94. — P. 062507.

[58] Namba T. Precise measurement of positronium // Progress of Theoretical and Experimental Physics. — 2012. — Vol. 2012, no. 1.

[59] Gurung L., Babij T.J., Hogan S.D., Cassidy D.B. Precision Microwave Spectroscopy of the Positronium $n = 2$ Fine Structure // Phys. Rev. Lett. — 2020. — Vol. 125. — P. 073002.

[60] Ishida, A. New Precise Measurement of the Hyperfine Splitting of Positronium // Journal of Physical and Chemical Reference Data. — 2015. — Vol. 44, no. 3. — P. 031212–03121210.

[61] Vallery R.S., Zitzewitz P.W., Gidley D.W. Resolution of the Orthopositronium-Lifetime Puzzle // Phys. Rev. Lett. — 2003. — Vol. 90. — P. 203402.

[62] Kennedy C.J., Oelker E., Robinson J.M., et al. Precision Metrology Meets Cosmology: Improved Constraints on Ultralight Dark Matter from Atom-Cavity Frequency Comparisons // Phys. Rev. Lett. — 2020. — Vol. 125. — P. 201302.

[63] Roberts B.M., Dzuba V.A., Flambaum V.V., et al. Dark matter scattering on electrons: Accurate calculations of atomic excitations and implications for the DAMA signal // Phys. Rev. D. — 2016. — Vol. 93. — P. 115037.

[64] Gelmini G.B. Light weakly interacting massive particles // Reports on Progress in Physics. — 2017. — Vol. 80, no. 8. — P. 082201.

[65] Kim K.W., Adhikari G., Adhikari P., et al. Limits on interactions between weakly interacting massive particles and nucleons obtained with NaI(Tl) crystal detectors // Journal of High Energy Physics. — 2019. — Vol. 2019, no. 3. — P. 194.

[66] Andresen G.B., Ashkezari M.D., Baquero-Ruiz M. et al. Confinement of antihydrogen for 1,000 seconds // Nature Physics. — 2011. — Vol. 7, no. 7. — P. 558–564.

[67] Hori M., Sótér A., Barna D.and Dax A. et al. Two-photon laser spectroscopy of antiprotonic helium and the antiproton-to-electron mass ratio // Nature. — 2011. — Vol. 475, no. 7357. — P. 484–488. — URL: https://www.nature.com/articles/nature10260.

[68] Korobov V.I. Calculation of transitions between metastable states of antiprotonic helium including relativistic and radiative corrections of order $R_\infty\alpha^4$ // Phys. Rev. A. — 2008. — Apr. — Vol. 77. — P. 042506. — URL: https://link.aps.org/doi/10.1103/PhysRevA.77.042506.

[69] Korobov V.I., Hilico L., Karr J.-Ph. $m\alpha^7$-Order Corrections in the Hydrogen Molecular Ions and Antiprotonic Helium // Phys. Rev. Lett. — 2014. — Mar. — Vol. 112. — P. 103003. — URL: https://link.aps.org/doi/10.1103/PhysRevLett.112.103003.

[70] Baur G., Boero G., Brauksiepe A. et al. Production of antihydrogen // Physics Letters B. — 1996. — Vol. 368, no. 3. — P. 251–258. — URL: https://www.sciencedirect.com/science/article/pii/0370269396000056.

[71] Blanford G., Christian D.C., Gollwitzer K. et al. Observation of Atomic Antihydrogen // Phys. Rev. Lett. — 1998. — Apr. — Vol. 80. — P. 3037–3040. — URL: https://link.aps.org/doi/10.1103/PhysRevLett.80.3037.

[72] Amoretti M., Amsler C., Bonomi G. et al. Production and detection of cold antihydrogen atoms // Nuclear Instruments and Methods in Physics

Research Section A: Accelerators, Spectrometers, Detectors and Associated Equipment. — 2004. — Vol. 518, no. 1-2. — P. 244–248. — URL: https://www.nature.com/articles/nature01096.

[73] Ahmadi M., Alves B., Baker C., et al. Observation of the hyperfine spectrum of antihydrogen // Nature. — 2017. — Vol. 548. — P. 66–69. — URL: https://www.nature.com/articles/nature23446.

[74] Ahmadi M., Alves B.X.R., Baker C.J. et al. Observation of the 1S-2P Lyman-α transition in antihydrogen // Nature. — 2018. — Vol. 561, no. 7722. — P. 211–215. — URL: https://www.nature.com/articles/s41586-018-0435-1.

[75] Baker C.J., Bertsche W .and Capra A., Carruth C. et al. Laser cooling of antihydrogen atoms // Nature. — 2021. — Vol. 592, no. 7852. — P. 35–42. — URL: https://www.nature.com/articles/s41586-021-03289-6.

[76] Seager S., Sasselov D.D., Scott D. A New Calculation of the Recombination Epoch // The Astrophysical Journal. — 1999. — aug. — Vol. 523, no. 1. — P. L1. — URL: https://dx.doi.org/10.1086/312250.

[77] Peebles P.J.E. Recombination of the Primeval Plasma // Ap.J. — 1968. — Vol. 153. — P. 1.

[78] Zel'dovich Ya.B., Kurt V.G., Syunyaev R.A. Recombination of Hydrogen in the Hot Model of the Universe // Soviet Journal of Experimental and Theoretical Physics. — 1969. — Vol. 28. — P. 146. — ZhETF, Vol. 55, No. 1, p. 278, January 1969.

[79] Zeldovich Ya.B., Sunyaev R.A. The Interaction of Matter and Radiation in a Hot-Model Universe // Astrophysics and Space Science. — 1969. — Vol. 4, no. 3. — P. 301–316.

[80] Strukov I.A., Brukhanov A.A., Skulachev D.P., Sazhin M.V. The Relikt-1 experiment - New results // MNRAS. — 1992. — Vol. 258, no. 2. — P. 37P–40P.

[81] Smoot G.F., Bennett C.L., Kogut A., et al. Structure in the COBE Differential Microwave Radiometer First-Year Maps // ApJL. — 1992. — Vol. 396. — P. L1.

[82] Labzowsky L., Solovyev D., Plunien G. Two-photon decay of excited levels in hydrogen: The ambiguity of the separation of cascades and pure two-photon emission // Phys. Rev. A. — 2009. — Vol. 80. — P. 062514.

[83] Solovyev D., Dubrovich V., Volotka A.V. et al. Two-photon decays of highly excited states in hydrogen // Journal of Physics B: Atomic, Molecular and Optical Physics. — 2010. — Vol. 43, no. 17. — P. 175001.

[84] Zalialiutdinov T.A., Solovyev D.A., Labzowsky L.N., Plunien G. QED theory of multiphoton transitions in atoms and ions // Physics Reports. — 2018. — Vol. 737. — P. 1–84. — QED theory of multiphoton transitions in atoms and ions.

[85] Low F. Natural Line Shape // Phys. Rev. — 1952. — Vol. 88. — P. 53.

[86] Landau L.D., Lifshitz E.M. Quantum Mechanics: Non-Relativistic Theory. — Pergamon Press, 1965.

[87] Sucher J. S-Matrix Formalism for Level-Shift Calculations // Phys. Rev. — 1957. — Vol. 107. — P. 1448–1449.

[88] Barbieri R., Sucher J. General theory of radiative corrections to atomic decay rates // Nucl. Phys. B. — 1978. — Vol. 134. — P. 155–168.

[89] Gell-Mann M., Low F. Bound States in Quantum Field Theory // Phys. Rev. — 1951. — Vol. 84. — P. 350–354.

[90] Labzowsky L.N. Adiabatic S-matrix approach in QED theory of highly charged two-electron ions // Journal of Physics B: Atomic, Molecular and Optical Physics. — 1993. — Vol. 26, no. 6. — P. 1039–1069.

[91] Braun M.A., Gurchumelia A.D., Safronova U.I. Relativistic Atom Theory. — Nauka, Moscow, 1984.

[92] Lindgren I., Morrison J. Atomic many-body theory. Springer series on atoms + plasmas. — Springer, 1986. — ISBN: 9783540166498.

[93] Gea-Banacloche J., Li Y.-Q., Jin Sh.-Zh., Xiao M. Electromagnetically induced transparency in ladder-type inhomogeneously broadened media: Theory and experiment // Phys. Rev. A. — 1995. — Jan. — Vol. 51. — P. 576–584. — URL: https://link.aps.org/doi/10.1103/PhysRevA.51.576.

[94] Marangos J.P. Electromagnetically induced transparency // Journal of Modern Optics. — 1998. — Vol. 45. — P. 471–503. — URL: https://api.semanticscholar.org/CorpusID:42159034.

[95] Wielandy S., Gaeta A.L. Investigation of electromagnetically induced transparency in the strong probe regime // Phys. Rev. A. — 1998. — Sep. — Vol. 58. — P. 2500–2505. — URL: https://link.aps.org/doi/10.1103/PhysRevA.58.2500.

[96] Boyd R.W. Nonlinear Optics. — Elsevier Science, 2003. — ISBN: 9780080479750.

[97] Breuer H.P., Petruccione F. The theory of open quantum systems. — Great Clarendon Street : Oxford University Press, 2002.

[98] Keizer, J. On the solutions and the steady states of a master equation // Journal of Statistical Physics. — 1972. — Vol. 6, no. 2. — P. 67–72.

[99] Seager S., Sasselov D.D., Scott D. How Exactly Did the Universe Become Neutral? // The Astrophysical Journal Supplement Series. — 2000. — jun. — Vol. 128, no. 2. — P. 407. — URL: https://dx.doi.org/10.1086/313388.

[100] Sobolev V.V. The Diffusion of L_α Radiation in Nebulae and Stellar Envelopes. // Sov.Ast. — 1957. — oct. — Vol. 1. — P. 678.

[101] Rapoport L.P., Zon B.A., Manakov N.L. Theory of multiphoton processes in atoms. — Atomizdat, Moscow, 1978.

[102] Shabaev V.M., Tupitsyn I.I., Yerokhin V.A. et al. Dual Kinetic Balance Approach to Basis-Set Expansions for the Dirac Equation // Phys. Rev. Lett. — 2004. — Sep. — Vol. 93. — P. 130405. — URL: https://link.aps.org/doi/10.1103/PhysRevLett.93.130405.

[103] Azimov V.I., Ansel'm A.A., Moskalev A.N., Ryndin R.M. Some parity-nonconservation effects in emission by hydrogenlike atoms // Zh. Eksp. Teor. Fiz. — 1974. — Vol. 67. — P. 17–29.

[104] Mohr P.J. $E1 - M1$ Interference in Radiative Decay of Hydrogen-like Atoms in an Electric Field // Phys. Rev. Lett. — 1978. — Mar. — Vol. 40. — P. 854–856. — URL: https://link.aps.org/doi/10.1103/PhysRevLett.40.854.

[105] Hilley M., Mohr P.J. Radiative decay of hydrogenlike atoms in an electric field // Phys. Rev. A. — 1980. — Jan. — Vol. 21. — P. 24–33. — URL: https://link.aps.org/doi/10.1103/PhysRevA.21.24.

[106] Solov'ev D.A., Sharipov V.F., Labzovskii L.N., Plunien G. Probabilities of single-photon 2s - 1s transition in hydrogen and antihydrogen atoms in an external electric field // Optics and Spectroscopy. — 2008. — Vol. 104, no. 4. — P. 509–512.

[107] Anikin A.A., Zalialiutdinov T.A., Solovyev D.A. Nonresonant Effects in the Two-Photon Spectroscopy of a Hydrogen Atom: Application to the Calculation of the Charge Radius of the Proton // JETP Letters. — 2021. — Aug. — Vol. 114, no. 4. — P. 180–187. — URL: https://doi.org/10.1134/S0021364021160037.

[108] Zalialiutdinov T., Anikin A., Solovyev D. Analysis of nonresonant effects in the two-photon spectroscopy of helium // Journal of Physics B: Atomic, Molecular and Optical Physics. — 2021. — sep. — Vol. 54, no. 16. — P. 165002. — URL: https://dx.doi.org/10.1088/1361-6455/ac232c.

[109] Solovyev D., Solovyeva E. Adapted method of moments for determining the transition frequency // Physics Letters A. — 2022. — Vol.

432. — P. 128021. — URL: https://www.sciencedirect.com/science/article/pii/S0375960122001037.

[110] Labzowsky L.N., Shonin A.V., Solovyev D.A. QED calculation of E1M1 and E1E2 transition probabilities in one-electron ions with arbitrary nuclear charge // Journal of Physics B: Atomic, Molecular and Optical Physics. — 2005. — Vol. 38, no. 3. — P. 265–278.

[111] Labzowsky L., Solovyev D., Plunien G., Soff G. Two-photon E1M1 and E1E2 transitions between 2p and 1s levels in hydrogen // The European Physical Journal D - Atomic, Molecular, Optical and Plasma Physics. — 2006. — Vol. 37, no. 3. — P. 335–343.

[112] Solovyev D.A., Labzowsky L.N., Sharipov V.F. Influence of an external electric field on the probabilities of two-photon transitions between 2s, 2p and 1s levels for hydrogen and antihydrogen atoms // Optics and Spectroscopy. — 2009. — Vol. 107, no. 1. — P. 16–24.

[113] Solovyev D.A., Labzowsky L.N., V.F. Sharipov. Odno-, dvuh- i trehfotonny perehody mezhdu 2s-, 2p- i 1s-urovniami dlia atomov vodoroda i antivodoroda vo vneshnem electricheskom pole i bez nego // Vestnik Sankt-Peterburgskogo Universiteta. Fizika i Himia. — 2009. — no. 4. — P. 377–390.

[114] Solovyev D., Sharipov V., Labzowsky L., Plunien G. Influence of external electric fields on multi-photon transitions between the 2s, 2p and 1s levels for hydrogen and antihydrogen atoms and hydrogen-like ions // Journal of Physics B: Atomic, Molecular and Optical Physics. — 2010. — Vol. 43, no. 7. — P. 074005.

[115] Solovyev D., Labzowsky L. Two-photon approximation in the theory of electron recombination in hydrogen // Phys. Rev. A. — 2010. — Vol. 81. — P. 062509.

[116] Solovyev D., Labzowsky L. The two-photon approximation for the four-

photon decay of the 4d excited state in hydrogen // Canadian Journal of Physics. — 2011. — Vol. 89, no. 1. — P. 123–127.

[117] Solovyev D., Labzowsky L., Volotka A., Plunien G. Extension of the sum rule for the transition rates between multiplets to the multiphoton case // The European Physical Journal D. — 2011. — Vol. 61, no. 2. — P. 297–304.

[118] Zalyalyutdinov T.A., Solovyev D.A., Labzovskii L.N. 4s-1s two-photon decay in hydrogen atom with allowance for cascades // Optics and Spectroscopy. — 2011. — Vol. 110, no. 3. — P. 328–334.

[119] Solovyev D., Solovyeva E. Rydberg-state mixing in the presence of an external electric field: Comparison of the hydrogen and antihydrogen spectra // Phys. Rev. A. — 2015. — Vol. 91. — P. 042506.

[120] Zalialiutdinov T., Baukina Yu., Solovyev D., Labzowsky L. Theory of the multiphoton cascade transitions with two photon links: comparison of quantum electrodynamical and quantum mechanical approaches // Journal of Physics B: Atomic, Molecular and Optical Physics. — 2014. — Vol. 47, no. 11. — P. 115007.

[121] Zalialiutdinov T., Solovyev D., Labzowsky L., Plunien G. Two-photon transitions with cascades: Two-photon transition rates and two-photon level widths // Phys. Rev. A. — 2014. — Vol. 89. — P. 052502.

[122] Zalialiutdinov T., Solovyev D., Labzowsky L., Plunien G. Exclusion principle for photons: Spin-statistic selection rules for multiphoton transitions in atomic systems // Phys. Rev. A. — 2015. — Vol. 91. — P. 033417.

[123] Zalialiutdinov T., Solovyev D., Labzowsky L. QED calculations of three-photon transition probabilities in H-like ions with arbitrary nuclear charge // Journal of Physics B: Atomic, Molecular and Optical Physics. — 2016. — Vol. 49, no. 5. — P. 055001.

[124] Zalialiutdinov T., Solovyev D., Labzowsky L., Plunien G. Spin-statistic selection rules for multiphoton transitions: Application to helium atoms // Phys. Rev. A. — 2016. — Vol. 93. — P. 012510.

[125] Zalialiutdinov T., Solovyev D., Labzowsky L. Generalized spin-statistic selection rules for atomic transitions with arbitrary number of equivalent photons // The European Physical Journal Special Topics. — 2017. — Vol. 226, no. 12. — P. 2837–2842.

[126] Labzowsky L., Solovyev D. Resonant spectroscopy of the antihydrogen atom // Phys. Rev. A. — 2003. — Vol. 68. — P. 014501.

[127] Solovyev D., Labzowsky L. The 21 cm absorption line profile as a tool for the search for antimatter in the universe // Progress of Theoretical and Experimental Physics. — 2014. — Vol. 2014, no. 11. — 111E01.

[128] Solovyev D., Dubrovich V.K., Plunien G. Investigation of the electromagnetically induced transparency in the era of cosmological hydrogen recombination // Journal of Physics B: Atomic, Molecular and Optical Physics. — 2012. — Vol. 45, no. 21. — P. 215001.

[129] Solovyev D., Dubrovich V. EIT phenomenon for the three-level hydrogen atoms and its application to the era of cosmological recombination // Central European Journal of Physics. — 2014. — Vol. 12, no. 5. — P. 367–374.

[130] Solovyev D. Analysis of the absorption line profile at 21 cm for the hydrogen atom in the interstellar medium // Journal of Physics B: Atomic, Molecular and Optical Physics. — 2018. — Vol. 51, no. 22. — P. 225004.

[131] Weisskopf V., Wigner E. Berechnung der natürlichen Linienbreite auf Grund der Diracschen Lichttheorie // Zeitschrift für Physik. — 1930. — Jan. — Vol. 63, no. 1. — P. 54–73. — URL: https://doi.org/10.1007/BF01336768.

[132] Labzowsky L. Natural spectral line width and shape in the relativistic theory of the atom // Zh. Eksp. Teor. Fiz. — 1983. — Vol. 85. — P. 869–880. — URL: http://www.jetp.ras.ru/cgi-bin/r/index/e/58/3/p503?a=list.

[133] Karasiev V.V., Labzowsky L.N., Nefiedov A.N. et al. Overlap of the line profiles in the spectra of the heliumlike uranium // Physica Scripta. — 1992. — sep. — Vol. 46, no. 3. — P. 225–229. — URL: https://doi.org/10.1088/0031-8949/46/3/004.

[134] Niering M., Holzwarth R., Reichert J. et al. Measurement of the Hydrogen $1S$- $2S$ Transition Frequency by Phase Coherent Comparison with a Microwave Cesium Fountain Clock // Phys. Rev. Lett. — 2000. — Jun. — Vol. 84. — P. 5496–5499. — URL: https://link.aps.org/doi/10.1103/PhysRevLett.84.5496.

[135] Labzowsky L., Karasiev V., Lindgren I. et al. Higher-order QED corrections for multi-charged ions // Physica Scripta. — 1993. — jan. — Vol. T46. — P. 150–156. — URL: https://doi.org/10.1088/0031-8949/1993/t46/022.

[136] Labzowsky L., Solovyev D. Multiple resonant photon scattering on the hydrogen atom and the shift of the photon intensity distribution // Journal of Physics B: Atomic, Molecular and Optical Physics. — 2004. — Vol. 37, no. 16. — P. 3271–3281.

[137] Eikema K.S.E., Walz J., Hänsch Th.W. Continuous Coherent Lyman-α Excitation of Atomic Hydrogen // Phys. Rev. Lett. — 2001. — Jun. — Vol. 86. — P. 5679–5682. — URL: https://link.aps.org/doi/10.1103/PhysRevLett.86.5679.

[138] Cui Z.-F., Binosi D., Roberts C.D., Schmidt S.M. Fresh Extraction of the Proton Charge Radius from Electron Scattering // Phys. Rev. Lett. — 2021. — Aug. — Vol. 127. — P. 092001. — URL: https://link.aps.org/doi/10.1103/PhysRevLett.127.092001.

[139] Bezginov N., Valdez T., Horbatsch M. et al. A measurement of the atomic hydrogen Lamb shift and the proton charge radius // Science. — 2019. — 09. — Vol. 365. — P. 1007–1012.

[140] Salour M.M. Quantum interference effects in two-photon spectroscopy // Rev. Mod. Phys. — 1978. — Jul. — Vol. 50. — P. 667–681. — URL: https://link.aps.org/doi/10.1103/RevModPhys.50.667.

[141] Matveev A., Kolachevsky N., Adhikari C.M., Jentschura U.D. Pressure shifts in high-precision hydrogen spectroscopy: II. Impact approximation and Monte-Carlo simulations // Journal of Physics B: Atomic, Molecular and Optical Physics. — 2019. — mar. — Vol. 52, no. 7. — P. 075006. — URL: https://doi.org/10.1088/1361-6455/ab08e1-1.

[142] Jentschura U.D., Adhikari Ch.M. Long-Range Interactions for Hydrogen: 6P-1S and 6P-2S Systems // Atoms. — 2017. — Vol. 5, no. 4. — URL: https://www.mdpi.com/2218-2004/5/4/48.

[143] Brandt A.D., Cooper S.F., Rasor C. et al. Measurement of the $2S_{1/2} - 8D_{5/2}$ Transition in Hydrogen // Phys. Rev. Lett. — 2022. — Jan. — Vol. 128. — P. 023001. — URL: https://link.aps.org/doi/10.1103/PhysRevLett.128.023001.

[144] Fleurbaey H., Galtier S., Thomas S. et al. New Measurement of the $1S - 3S$ Transition Frequency of Hydrogen: Contribution to the Proton Charge Radius Puzzle // Phys. Rev. Lett. — 2018. — May. — Vol. 120. — P. 183001. — URL: https://link.aps.org/doi/10.1103/PhysRevLett.120.183001.

[145] Yost D.C., Matveev A., Peters E. et al. Quantum interference in two-photon frequency-comb spectroscopy // Phys. Rev. A. — 2014. — Jul. — Vol. 90. — P. 012512. — URL: https://link.aps.org/doi/10.1103/PhysRevA.90.012512.

[146] Fleurbaey H., Biraben F., Julien L. et al. Cross-damping effects in $1S-3S$ spectroscopy of hydrogen and deuterium // Phys. Rev. A. — 2017. — May. — Vol. 95. — P. 052503. — URL: https://link.aps.org/doi/10.1103/PhysRevA.95.052503.

[147] Marsman A., Horbatsch M., Hessels E.A. Quantum interference effects in saturated absorption spectroscopy of $n = 2$ triplet-helium fine structure // Phys. Rev. A. — 2015. — Jun. — Vol. 91. — P. 062506. — URL: https://link.aps.org/doi/10.1103/PhysRevA.91.062506.

[148] Amaro P., Loureiro U., Safari L. et al. Quantum interference in laser spectroscopy of highly charged lithiumlike ions // Phys. Rev. A. — 2018. — Feb. — Vol. 97. — P. 022510. — URL: https://link.aps.org/doi/10.1103/PhysRevA.97.022510.

[149] Patkóš V., Yerokhin V.A., Pachucki K. Nonradiative $\alpha^7 m$ QED effects in the Lamb shift of helium triplet states // Phys. Rev. A. — 2020. — Jun. — Vol. 101. — P. 062516. — URL: https://link.aps.org/doi/10.1103/PhysRevA.101.062516.

[150] Braskén M., Kyrölä E. Resonance scattering of Lyman alpha from interstellar hydrogen // Astronomy and Astrophysics. — 1998. — Vol. 332. — P. 732–738. — URL: https://api.semanticscholar.org/CorpusID:14622417.

[151] Magnan C., Pecker J.C. Asymmetry in solar spectral lines. // Highlights of Astronomy. — 1974. — jan. — Vol. 3. — P. 171–203.

[152] Jackson J.M., Whitaker J.S., Rathborne J.M. et al. Asymmetric Line Profiles in Dense Molecular Clumps Observed in MALT90: Evidence for Global Collapse // The Astrophysical Journal. — 2018. — dec. — Vol. 870, no. 1. — P. 5. — URL: https://doi.org/10.3847/1538-4357/aaef84.

[153] Lee H.-W. Asymmetric absorption profiles of Lyα and Lyβ in damped Lyα systems // The Astrophysical Journal. — 2013. — jul. — Vol. 772, no. 2. — P. 123. — URL: https://doi.org/10.1088/0004-637x/772/2/123.

[154] Bach K. Radiation-damped profiles of extremely high column density neutral hydrogen: implications of cosmic reionization // Monthly Notices of the Royal Astronomical Society. — 2016. — 09. — Vol. 464,

no. 1. — P. 1137–1145. — https://academic.oup.com/mnras/article-pdf/464/1/1137/18512453/stw2208.pdf.

[155] Lee C.C., Webb J.K., Carswell R.F. Quantum mechanics at high redshift - modelling damped Lyman-α absorption systems // Monthly Notices of the Royal Astronomical Society. — 2019. — 11. — Vol. 491, no. 4. — P. 5555–5571. — https://academic.oup.com/mnras/article-pdf/491/4/5555/31613939/stz3170.pdf.

[156] Wang F., Yang J., Fan X. et al. A Luminous Quasar at Redshift 7.642 // The Astrophysical Journal Letters. — 2021. — jan. — Vol. 907, no. 1. — P. L1. — URL: https://doi.org/10.3847/2041-8213/abd8c6.

[157] Heisenberg W. Über quantentheoretische Umdeutung kinematischer und mechanischer Beziehungen. // Zeitschrift für Physik. — 1925. — Vol. 33, no. 1. — P. 879–893.

[158] Goldman S.P., Drake G.W.F. Relativistic two-photon decay rates of $2s_{\frac{1}{2}}$ hydrogenic ions // Phys. Rev. A. — 1981. — Jul. — Vol. 24. — P. 183–191. — URL: https://link.aps.org/doi/10.1103/PhysRevA.24.183.

[159] Furry W. On Bound States and Scattering in Positron Theory // Phys. Rev. — 1951. — Jan. — Vol. 81. — P. 115–124. — URL: https://link.aps.org/doi/10.1103/PhysRev.81.115.

[160] Anikin A., Zalialiutdinov T., Solovyev D. Natural line profile asymmetry // Physica Scripta. — 2023. — mar. — Vol. 98, no. 4. — P. 045407. — URL: https://dx.doi.org/10.1088/1402-4896/acc28d.

[161] Łach G., DeKieviet M., Jentschura U.D. Enhancement of Blackbody Friction due to the Finite Lifetime of Atomic Levels // Phys. Rev. Lett. — 2012. — Vol. 108. — P. 043005.

[162] Gunn J.E., Peterson B.A. On the Density of Neutral Hydrogen in Intergalactic Space // Astrophysical Journal. — 1965. — nov. — Vol. 142. — P. 1633–1636.

[163] Bach K., Lee H.-W. The Kramers-Heisenberg Formula and the Gunn-Peterson Trough from the First Objects in the Universe // Journal of The Korean Astronomical Society. — 2014. — Vol. 47, no. 47. — P. 187–193.

[164] Chluba J., Sunyaev R.A. Two-photon transitions in hydrogen and cosmological recombination // A&A. — 2008. — Vol. 480, no. 3. — P. 629–645. — URL: https://doi.org/10.1051/0004-6361:20077921.

[165] Chluba J., Sunyaev R.A. Lyα escape during cosmological hydrogen recombination: the 3d-1s and 3s-1s two-photon processes // A&A. — 2010. — Vol. 512. — P. A53. — URL: https://doi.org/10.1051/0004-6361/200912263.

[166] Zel'dovich Y.B., Raizer Y.P. Physics of Shock Waves and High-Temperature Hydrodynamic Phenomena. Dover Books on Physics. — Dover Publications, 2012. — ISBN: 9780486135083.

[167] Santos M.R. Probing reionization with Lyman α emission lines // Monthly Notices of the Royal Astronomical Society. — 2004. — 04. — Vol. 349, no. 3. — P. 1137–1152. — https://academic.oup.com/mnras/article-pdf/349/3/1137/18649003/349-3-1137.pdf.

[168] Hirata Ch.M., Forbes J. Lyman-α transfer in primordial hydrogen recombination // Phys. Rev. D. — 2009. — Jul. — Vol. 80. — P. 023001. — URL: https://link.aps.org/doi/10.1103/PhysRevD.80.023001.

[169] Peebles P.J.E. Principles of Physical Cosmology. — Princeton University Press, 1993.

[170] Lee H.-W., Lee K.W. On the profiles and the polarization of Raman-scattered emission lines in symbiotic stars // Monthly Notices of the Royal Astronomical Society. — 1997. — 05. — Vol. 287, no. 1. — P. 211–220. — https://academic.oup.com/mnras/article-pdf/287/1/211/3166581/287-1-211.pdf.

[171] Veselov M. G., Labzowsky L. N. Teoria atoma. Stroenie elektronnyh obolochek. — Moscow Nauka, 1986.

[172] Labzowsky L.N., Solovyev D.A. Coulomb Green Function and Its Applications in Atomic Theory // Precision Physics of Simple Atomic Systems / Ed. by S.G. Karshenboim, V.B. Smirnov. — Berlin, Heidelberg : Springer Berlin Heidelberg, 2003. — P. 15–34. — ISBN: 978-3-540-45059-7. — URL: https://doi.org/10.1007/978-3-540-45059-7_2.

[173] Wichmann E.H., Kroll N.M. Vacuum Polarization in a Strong Coulomb Field // Phys. Rev. — 1956. — Jan. — Vol. 101. — P. 843–859. — URL: https://link.aps.org/doi/10.1103/PhysRev.101.843.

[174] Martin P.C., Glauber R.J. Relativistic Theory of Radiative Orbital Electron Capture // Phys. Rev. — 1958. — Feb. — Vol. 109. — P. 1307–1325. — URL: https://link.aps.org/doi/10.1103/PhysRev.109.1307.

[175] Gorshkov V.G. On the Coulomb Green's function // JETP. — 1965. — January. — Vol. 20. — P. 234. — URL: http://jetp.ras.ru/cgi-bin/r/index/e/20/1/p234?a=list.

[176] Gorshkov V.G. Relativistic Coulomb Functions // JETP. — 1965. — May. — Vol. 20. — P. 1331. — URL: http://jetp.ras.ru/cgi-bin/r/index/e/20/5/p1331?a=list.

[177] Marmo S.I. Mnogofotonnye perekhody v kulonovskom kontinuume // Diss. doc. fiz.-mat. nauk [Multiphoton transitions in Coulomb continuum. D.Sc. (Physics and Mathematics)], Voronezh, 2006. — 2006. — URL: https://www.dissercat.com/content/mnogofotonnye-perekhody-v-kulonovskom-kontinuume.

[178] Gradshteyn I.S., Ryzhik I.M., Jeffrey A. Table of integrals, series, and products. — 5th ed edition. — San Diego : Academic Press, 1994.

[179] Varshalovich D.A., Moskalev A.N., Khersonskii V.K. Quantum Theory of Angular Momentum. — Singapore : World Scientific, 1988.

[180] Baird P.E.G., Brambley R.J., Burnett K. et al. Optical isotope shifts and hyperfine structure in λ553.5 nm of barium // Proceedings of the Royal Society of London. A. Mathematical and Physical Sciences. — 1979. — Vol. 365, no. 1723. — P. 567–582. — https://royalsocietypublishing.org/doi/pdf/10.1098/rspa.1979.0035.

[181] Korobov V.I., Hilico L., Karr J.-Ph. $m\alpha^7$-Order Corrections in the Hydrogen Molecular Ions and Antiprotonic Helium // Phys. Rev. Lett. — 2014. — Mar. — Vol. 112. — P. 103003. — URL: https://link.aps.org/doi/10.1103/PhysRevLett.112.103003.

[182] Huber A., Gross B., Weitz M., Hänsch Th.W. High-resolution spectroscopy of the $1S-2S$ transition in atomic hydrogen // Phys. Rev. A. — 1999. — Mar. — Vol. 59. — P. 1844–1851. — URL: https://link.aps.org/doi/10.1103/PhysRevA.59.1844.

[183] Tiesinga E., Mohr P.J., Newell D.B., Taylor B.N. CODATA recommended values of the fundamental physical constants: 2018 // Rev. Mod. Phys. — 2021. — Vol. 93. — P. 025010. — URL: https://link.aps.org/doi/10.1103/RevModPhys.93.025010.

[184] Fradkin E. S., Gitman D. M., Shvartsman Sh. M. Quantum electrodynamics with unstable vacuum. — Springer-Verlag, Berlin, Heidelberg, 1991.

[185] Parthey C.G., Matveev A., Alnis J. et al. Precision Measurement of the Hydrogen-Deuterium $1S-2S$ Isotope Shift // Phys. Rev. Lett. — 2010. — Jun. — Vol. 104. — P. 233001. — URL: https://link.aps.org/doi/10.1103/PhysRevLett.104.233001.

[186] Kolachevsky N., Fendel P., Karshenboim S.G., Hänsch Th.W. $2S$ hyperfine structure of atomic deuterium // Phys. Rev. A. — 2004. — Dec. — Vol. 70. — P. 062503. — URL: https://link.aps.org/doi/10.1103/PhysRevA.70.062503.

[187] Horbatsch M., Hessels E.A. Tabulation of the bound-state energies of atomic hydrogen // Phys. Rev. A. — 2016. — Vol. 93. — P. 022513.

[188] Schippers S. Analytical expression for the convolution of a Fano line profile with a gaussian // Journal of Quantitative Spectroscopy and Radiative Transfer. — 2018. — Vol. 219. — P. 33–36. — URL: https://www.sciencedirect.com/science/article/pii/S0022407318304849.

[189] Solovyev D., Zalialiutdinov T., Anikin A., Labzowsky L. Theoretical prerequisites for the upcoming generation of precision spectroscopic experiments // submitted. — 2023. — arXiv: 2311.12606 [physics.atom-ph], 21 Nov 2023. URL: https://doi.org/10.48550/arXiv.2311.12606.

[190] Solovyev D., Anikin A., Zalialiutdinov T., Labzowsky L. Impact of quantum interference in cascade radiation on the absorption profile // Phys. Rev. A. — 2024. — Feb. — Vol. 109. — P. 022806. — URL: https://link.aps.org/doi/10.1103/PhysRevA.109.022806.

[191] Martynenko A.P. $2S$ Hyperfine splitting of muonic hydrogen // Phys. Rev. A. — 2005. — Feb. — Vol. 71. — P. 022506. — URL: https://link.aps.org/doi/10.1103/PhysRevA.71.022506.

[192] Martynenko A.P. Hyperfine structure of the S levels of the muonic helium ion // Journal of Experimental and Theoretical Physics. — 2008. — Apr. — Vol. 106, no. 4. — P. 690–699. — URL: https://doi.org/10.1134/S1063776108040079.

[193] Borie E. Lamb shift in muonic hydrogen // Phys. Rev. A. — 2005. — Mar. — Vol. 71. — P. 032508. — URL: https://link.aps.org/doi/10.1103/PhysRevA.71.032508.

[194] Milotti E. Energy levels and radiative transitions in muonic hydrogen // Atomic Data and Nuclear Data Tables. — 1998. — Vol. 70, no. 2. — P. 137 – 177. — URL: http://www.sciencedirect.com/science/article/pii/S0092640X98907902.

[195] Borie E. Lamb shift in light muonic atoms - Revisited // Annals of Physics. — 2012. — Vol. 327, no. 3. — P. 733–763. — URL: https://www.sciencedirect.com/science/article/pii/S0003491611001904.

[196] Cancio Pastor P., Consolino L., Giusfredi G. et al. Frequency Metrology of Helium around 1083 nm and Determination of the Nuclear Charge Radius // Phys. Rev. Lett. — 2012. — Apr. — Vol. 108. — P. 143001. — URL: https://link.aps.org/doi/10.1103/PhysRevLett.108.143001.

[197] Zheng X., Sun Y.R., Chen J.-J. et al. Measurement of the Frequency of the $2\,^3S - 2\,^3P$ Transition of ^{4}He // Phys. Rev. Lett. — 2017. — Dec. — Vol. 119. — P. 263002. — URL: https://link.aps.org/doi/10.1103/PhysRevLett.119.263002.

[198] Sun Yu.R., Hu Sh.-M. Precision spectroscopy of atomic helium // National Science Review. — 2020. — 08. — Vol. 7, no. 12. — P. 1818–1827. — https://academic.oup.com/nsr/article-pdf/7/12/1818/38880256/nwaa216.pdf.

[199] Morton D.C., Wu Q., Drake G.W.F. Energy levels for the stable isotopes of atomic helium (4He I and 3He I) // Canadian Journal of Physics. — 2006. — Vol. 84, no. 2. — P. 83–105. — https://doi.org/10.1139/p06-009.

[200] Sulai I.A., Wu Q., Bishof M. et al. Hyperfine Suppression of $2\,^3S_1 - 3\,^3P_J$ Transitions in ^{3}He // Phys. Rev. Lett. — 2008. — Oct. — Vol. 101. — P. 173001. — URL: https://link.aps.org/doi/10.1103/PhysRevLett.101.173001.

[201] Weitz M., Huber A., Schmidt-Kaler F. et al. Precision measurement of the 1S ground-state Lamb shift in atomic hydrogen and deuterium by frequency comparison // Phys. Rev. A. — 1995. — Vol. 52. — P. 2664–2681.

[202] Weitz M., Schmidt-Kaler F., Hänsch Th.W. Precise optical Lamb shift measurements in atomic hydrogen // Phys. Rev. Lett. — 1992. — Feb. — Vol. 68. — P. 1120–1123. — URL: https://link.aps.org/doi/10.1103/PhysRevLett.68.1120.

[203] Nez F., Plimmer M. D., Bourzeix S. et al. Precise frequency measurement of the 2S-8S/8D transtions in atomic hydrogen: New determi-

nation of the Rydberg constant // Phys. Rev. Lett. — 1992. — Oct. — Vol. 69. — P. 2326–2329. — URL: https://link.aps.org/doi/10.1103/PhysRevLett.69.2326.

[204] Schwob C., Jozefowski L., de Beauvoir B. et al. Optical Frequency Measurement of the 2S-12D Transitions in Hydrogen and Deuterium: Rydberg Constant and Lamb Shift Determinations // Phys. Rev. Lett. — 1999. — Vol. 82, no. 25. — P. 4960–4963.

[205] de Beauvoir B., Schwob C., Acef O. et al. Metrology of the hydrogen and deuterium atoms: Determination of the Rydberg constant and Lamb shifts // Eur. Phys. J. D. — 2000. — Vol. 12, no. 1. — P. 61–93.

[206] de Beauvoir B., Nez F., Julien L. et al. Absolute Frequency Measurement of the $2S-8S/D$ Transitions in Hydrogen and Deuterium: New Determination of the Rydberg Constant // Phys. Rev. Lett. — 1997. — Vol. 78. — P. 440–443.

[207] Schwob C., Jozefowski L., Acef O. et al. Frequency measurement of the 2S-12D transitions in hydrogen and deuterium, new determination of the Rydberg constant // IEEE Transactions on Instrumentation and Measurement. — 1999. — Vol. 48, no. 2. — P. 178–181.

[208] Patkóš V., Yerokhin V.A., Pachucki K. Complete $\alpha^7 m$ Lamb shift of helium triplet states // Phys. Rev. A. — 2021. — Apr. — Vol. 103. — P. 042809. — URL: https://link.aps.org/doi/10.1103/PhysRevA.103.042809.

[209] Schmoranzer H., Roth H., Volz U., Marger D. Radiative lifetimes of He I 3^3S_1 and 3^3D_J by beam-gas dye-laser spectroscopy // Journal of Physics B: Atomic, Molecular and Optical Physics. — 1991. — feb. — Vol. 24, no. 3. — P. 595–604. — URL: https://doi.org/10.1088/0953-4075/24/3/015.

[210] Riehle F. Frequency Standards: Basics and Applications. — Wiley Verlag, Weinheim, 2004.

[211] Drake G.W.F. Atomic, Molecular and Optical Physics Handbook. — Springer, New York, NY, 1996.

[212] Hlousek L., Lee S.A., Fairbank W.M. Precision Wavelength Measurements and New Experimental Lamb Shifts in Helium // Phys. Rev. Lett. — 1983. — Jan. — Vol. 50. — P. 328–331. — URL: https://link.aps.org/doi/10.1103/PhysRevLett.50.328.

[213] Theodosiou C.E. Lifetimes of singly excited states in He I // Phys. Rev. A. — 1984. — Dec. — Vol. 30. — P. 2910–2921. — URL: https://link.aps.org/doi/10.1103/PhysRevA.30.2910.

[214] Farley J.W., Wing W.H. Accurate calculation of dynamic Stark shifts and depopulation rates of Rydberg energy levels induced by blackbody radiation. Hydrogen, helium, and alkali-metal atoms // Phys. Rev. A. — 1981. — Vol. 23. — P. 2397.

[215] Solovyev D., Labzowsky L., Plunien G. QED derivation of the Stark shift and line broadening induced by blackbody radiation // Phys. Rev. A. — 2015. — Vol. 92. — P. 022508.

[216] Solovyev D. Thermal QED theory for bound states // Annals of Physics. — 2020. — Vol. 415. — P. 168128.

[217] Collisional Effects on Molecular Spectra / Ed. by J.-M. Hartmann, C. Boulet, D. Robert. — Second Edition edition. — Elsevier, 2021. — P. 1–557. — ISBN: 978-0-12-822364-2.

[218] Kolachevsky N., Haas M., Jentschura U.D. et al. Photoionization broadening of the $1S-2S$ transition in a beam of atomic hydrogen // Phys. Rev. A. — 2006. — Nov. — Vol. 74. — P. 052504.

[219] Dubessy J., Caumon M.-C., Rull F., Sharma Sh. Instrumentation in Raman spectroscopy: elementary theory and practice // Raman spectroscopy applied to Earth sciences and cultural heritage. — Mineralogical Society of Great Britain and Ireland, 2012. — 01.

[220] Yuan X., Mayanovic R.A. An Empirical Study on Raman Peak Fitting and Its Application to Raman Quantitative Research // Applied Spectroscopy. — 2017. — Vol. 71, no. 10. — P. 2325–2338. — PMID: 28665140.

[221] Bakker R.J. The perfection of Raman spectroscopic gas densimeters // Journal of Raman Spectroscopy. — 2021. — Vol. 52, no. 11. — P. 1923–1948.

[222] Nims, Ch. and Cron, Br. and Wetherington, M. and Macalady, J. and Cosmidis, J. Low frequency Raman Spectroscopy for micron-scale and in vivo characterization of elemental sulfur in microbial samples // Scientific Reports. — 2019. — Vol. 9, no. 1. — P. 7971.

[223] Holzscheiter M.H., Bendiscioli G., Bertin A. et al. Antihydrogen production and precision experiments // Nuclear Physics B - Proceedings Supplements. — 1997. — Vol. 56, no. 1. — P. 336–348. — Proceedings of the Fourth Biennial Conference on Low Energy Antiproton Physics. URL: https://www.sciencedirect.com/science/article/pii/S092056329700296X.

[224] Cesar, Cl.L. Trapping and spectroscopy of hydrogen // Hyperfine Interactions. — 1997. — Vol. 109, no. 1. — P. 293–304.

[225] Meshkov, I.N. Antihydrogen generation and studies in storage rings // Hyperfine Interactions. — 1997. — Vol. 109, no. 1. — P. 225–232.

[226] Regenfus, C. Antihydrogen production and precision experiments on trapped cold antihydrogen // Hyperfine Interactions. — 1999. — Vol. 119, no. 1. — P. 301–304.

[227] Bluhm R., Kostelecký V.A., Russell N. *CPT* and Lorentz Tests in Hydrogen and Antihydrogen // Phys. Rev. Lett. — 1999. — Mar. — Vol. 82. — P. 2254–2257. — URL: https://link.aps.org/doi/10.1103/PhysRevLett.82.2254.

[228] Hellwig H., Vessot R.F.C., Levine M.W. et al. Measurement of the Unperturbed Hydrogen Hyperfine Transition Frequency // IEEE Transactions

on Instrumentation and Measurement. — 1970. — Vol. 19, no. 4. — P. 200–209.

[229] Zel'dovich Ya.B. Dipole Moment of Unstable Elementary Particles // JETP [ZhETF 39(5), 1483 (1961)]. — 1961. — Vol. 12, no. 1. — P. 1030. — URL: http://jetp.ras.ru/cgi-bin/e/index/e/12/5/p1030?a=list.

[230] Aleksandrov E.B., Khodovoy V.A. Note on Dehmelt's Experiment // Optics and Spectroscopy. — 1963. — jun. — Vol. 14. — P. 437.

[231] Aleksandrov E.B., Kaliteevski N.I.B, ChaBika M.P. Superhigh-resolution spectroscopy based on interference of states // Soviet Physics Uspekhi. — 1979. — sep. — Vol. 22, no. 9. — P. 760. — URL: https://dx.doi.org/10.1070/PU1979v022n09ABEH005611.

[232] Andrae H.J. Stark-induced quantum beats in H Ly alpha emission // Physical Review A. — 1970. — Vol. 2. — P. 2200–2207. — URL: https://api.semanticscholar.org/CorpusID:124112337.

[233] Labzowsky L., Sharipov V. Quantum Beats in Hydrogen and Antihydrogen Atoms in an External Electric Field // Phys. Rev. Lett. — 2004. — Mar. — Vol. 92. — P. 133003. — URL: https://link.aps.org/doi/10.1103/PhysRevLett.92.133003.

[234] Labzowsky L., Sharipov V., Solovyev D., Plunien G. Coherent beam-foil excitation of 2s1/2 and 2p1/2 states of hydrogen and antihydrogen atoms in an external electric field // Journal of Physics B: Atomic, Molecular and Optical Physics. — 2006. — Vol. 39, no. 24. — P. 5091–5096.

[235] Labzowsky L., Sharipov V. Antihydrogen atom in external electric and magnetic fields // Phys. Rev. A. — 2005. — Jan. — Vol. 71. — P. 012501. — URL: https://link.aps.org/doi/10.1103/PhysRevA.71.012501.

[236] Kanekar N., Briggs F.H. 21-cm absorption studies with the Square Kilometer Array // New Astronomy Reviews. — 2004. — Vol. 48,

no. 11. — P. 1259–1270. — Science with the Square Kilometre Array. URL: https://www.sciencedirect.com/science/article/pii/S1387647304001125.

[237] Ishwara-Chandra, C.H. and Dwarakanath, K.S. and Anantharamaiah K.R. GMRT detection of HI 21 cm associated absorption towards thez = 1.2 red quasar 3C 190 // Journal of Astrophysics and Astronomy. — 2003. — Vol. 24, no. 1. — P. 37–43.

[238] Roberts D.A., Dickel H.R., Goss W.M. High-Resolution Observations of H I Zeeman Absorption toward DR 21 // The Astrophysical Journal. — 1997. — feb. — Vol. 476, no. 1. — P. 209. — URL: https://dx.doi.org/10.1086/303602.

[239] Sarma A.P., Momjian E., Troland T.H., Crutcher R.M. Very Large Array H I Zeeman Observations of NGC 1275 (Perseus A) // The Astronomical Journal. — 2005. — dec. — Vol. 130, no. 6. — P. 2566. — URL: https://dx.doi.org/10.1086/497637.

[240] Cooray A., Furlanetto S.R. Polarization signals of the 21-cm background from the era of reionization // Monthly Notices of the Royal Astronomical Society: Letters. — 2005. — 05. — Vol. 359, no. 1. — P. L47–L52. — https://academic.oup.com/mnrasl/article-pdf/359/1/L47/6404218/359-1-L47.pdf.

[241] Weisberg J.M., Cordes J.M., Kuan B. et al. Arecibo 430 MHz Pulsar Polarimetry: Faraday Rotation Measures and Morphological Classifications // The Astrophysical Journal Supplement Series. — 2004. — jan. — Vol. 150, no. 1. — P. 317. — URL: https://dx.doi.org/10.1086/379802.

[242] Nikitin A.A., Rudzikas Z.B. Osnovy teorii spectrov atomov i ionov. — Moscow: Nauka, 1983. — in Russian.

[243] Sucher J. Magnetic dipole transitions in atomic and particle physics: ions and psions // Reports on Progress in Physics. — 1978. — nov. — Vol. 41,

no. 11. — P. 1781. — URL: https://dx.doi.org/10.1088/0034-4885/41/11/002.

[244] Labzowsky L.N. Teoria atoma. Kvantovaia electrodinamika electronnyh obolochek i processy izluchenia. — Moscow: Nauka, FIZMATLIT, 1996. — ISBN: 5-02-015016-9. — in Russian.

[245] Zon B.A., Manakov N.L., Rapoport L.I. Two-photon Bound-bound Transitions in a Coulomb Field // JETP. — 1969. — mar. — Vol. 28, no. 3. — P. 480. — URL: http://www.jetp.ras.ru/cgi-bin/r/index/e/28/3/p480?a=list.

[246] Jentschura U.D. Self-energy correction to the two-photon decay width in hydrogenlike atoms // Phys. Rev. A. — 2004. — May. — Vol. 69. — P. 052118. — URL: https://link.aps.org/doi/10.1103/PhysRevA.69.052118.

[247] Page L., Hinshaw G., Komatsu E. et al. Three-Year Wilkinson Microwave Anisotropy Probe (WMAP) Observations: Polarization Analysis // The Astrophysical Journal Supplement Series. — 2007. — Jun. — Vol. 170, no. 2. — P. 335. — URL: https://dx.doi.org/10.1086/513699.

[248] Hinshaw G., Nolta M.R., Bennett C.L. et al. Three-Year Wilkinson Microwave Anisotropy Probe (WMAP) Observations: Temperature Analysis // The Astrophysical Journal Supplement Series. — 2007. — Jun. — Vol. 170, no. 2. — P. 288–334.

[249] Labzowsky L.N., Shonin A.V. QED theory of cascades and two-photon transitions and calculation of the $E1 - M1$ transition probability in two-electron highly charged ions // Phys. Rev. A. — 2004. — Jan. — Vol. 69. — P. 012503. — URL: https://link.aps.org/doi/10.1103/PhysRevA.69.012503.

[250] Drake G.W.F. Energy level calculations and E1M1 two photon transition rates in two electron U90+ // Nuclear Instruments and Methods in Physics Research Section B: Beam Interactions with Materials and

Atoms. — 1985. — Vol. 9, no. 4. — P. 465–470. — URL: https://www.sciencedirect.com/science/article/pii/0168583X85903489.

[251] Savukov I.M., Johnson W.R. Two-photon $E1M1$ decay of 2^3P_0 states in heavy heliumlike ions // Phys. Rev. A. — 2002. — Dec. — Vol. 66. — P. 062507. — URL: https://link.aps.org/doi/10.1103/PhysRevA.66.062507.

[252] Hirata Ch.M. Two-photon transitions in primordial hydrogen recombination // Phys. Rev. D. — 2008. — Jul. — Vol. 78. — P. 023001. — URL: https://link.aps.org/doi/10.1103/PhysRevD.78.023001.

[253] Jentschura U.D., Surzhykov A. Relativistic calculation of the two-photon decay rate of highly excited ionic states // Phys. Rev. A. — 2008. — Apr. — Vol. 77. — P. 042507. — URL: https://link.aps.org/doi/10.1103/PhysRevA.77.042507.

[254] Jentschura U.D. Non-uniform convergence of two-photon decay rates for excited atomic states // Journal of Physics A: Mathematical and Theoretical. — 2007. — feb. — Vol. 40, no. 9. — P. F223. — URL: https://dx.doi.org/10.1088/1751-8113/40/9/F02.

[255] Jentschura U.D. Two-photon decays reexamined: cascade contributions and gauge invariance // Journal of Physics A: Mathematical and Theoretical. — 2008. — apr. — Vol. 41, no. 15. — P. 155307. — URL: https://dx.doi.org/10.1088/1751-8113/41/15/155307.

[256] Jentschura U.D. Virtual resonant states in two-photon decay processes: Lower-order terms, subtractions, and physical interpretations // Phys. Rev. A. — 2009. — Feb. — Vol. 79. — P. 022510. — URL: https://link.aps.org/doi/10.1103/PhysRevA.79.022510.

[257] Sapirstein J., Pachucki K., Cheng K.T. Radiative corrections to one-photon decays of hydrogenic ions // Phys. Rev. A. — 2004. — Feb. — Vol. 69. — P. 022113. — URL: https://link.aps.org/doi/10.1103/PhysRevA.69.022113.

[258] Amaro P., Santos J.P., Parente F. et al. Resonance effects on the two-photon emission from hydrogenic ions // Phys. Rev. A. — 2009. — Jun. — Vol. 79. — P. 062504. — URL: https://link.aps.org/doi/10.1103/PhysRevA.79.062504.

[259] Labzovskii L.N. Electron Correlation in the Relativistic Theory of Atoms // JETP. — 1971. — Jan. — Vol. 32. — P. 94. — URL: http://jetp.ras.ru/cgi-bin/e/index/r/59/1/p168?a=list.

[260] Bogoliubov N.N., Shirkov D.V. Introduction to the theory of quantized fields by N.N. Bogoliubov and D.V. Shirkov. Translated from the Russian by G.M. Volkoff. — New York : Interscience Publishers, Inc., 1959.

[261] Gallagher Th.F. Rydberg Atoms. Cambridge Monographs on Atomic, Molecular and Chemical Physics. — Cambridge University Press, 1994.

[262] Jitrik O., Bunge C.F. Transition Probabilities for Hydrogen-Like Atoms // Journal of Physical and Chemical Reference Data. — 2005. — 01. — Vol. 33, no. 4. — P. 1059–1070. — https://pubs.aip.org/aip/jpr/article-pdf/33/4/1059/8183662/1059_1_online.pdf.

[263] Wiese W.L., Fuhr J.R. Accurate Atomic Transition Probabilities for Hydrogen, Helium, and Lithium // Journal of Physical and Chemical Reference Data. — 2009. — 06. — Vol. 38, no. 3. — P. 565–720. — https://pubs.aip.org/aip/jpr/article-pdf/38/3/565/15667142/565_1_online.pdf.

[264] Puchkov A.M., Labzovskiĭ L.N. Probabilities of forbidden magnetic-dipole transitions in the hydrogen atom and hydrogen-like ions // Optics and Spectroscopy. — 2009. — Vol. 106, no. 2. — P. 153–157.

[265] Alijah A., Broad J.T., Hinze J. Stark effect and field ionisation of atomic hydrogen // Journal of Physics B: Atomic and Molecular Physics. — 1986. — sep. — Vol. 19, no. 17. — P. 2617. — URL: https://dx.doi.org/10.1088/0022-3700/19/17/011.

[266] Feranchuk I.D., Hai L.X. Analytical estimation of the energies and widths of the Rydberg states of a hydrogen atom in an electric field // Physics Letters A. — 1989. — Vol. 137, no. 7. — P. 385–388. — URL: https://www.sciencedirect.com/science/article/pii/0375960189909109.

[267] Fernández-Menchero L., Summers H.P. Stark effect in neutral hydrogen by direct integration of the Hamiltonian in parabolic coordinates // Phys. Rev. A. — 2013. — Aug. — Vol. 88. — P. 022509. — URL: https://link.aps.org/doi/10.1103/PhysRevA.88.022509.

[268] Kolosov V.V. A hydrogen atom in a strong electric field // Journal of Physics B: Atomic and Molecular Physics. — 1987. — jun. — Vol. 20, no. 11. — P. 2359. — URL: https://dx.doi.org/10.1088/0022-3700/20/11/008.

[269] Damburg R.J., Kolosov V.V. A hydrogen atom in a uniform electric field. III // Journal of Physics B: Atomic and Molecular Physics. — 1979. — aug. — Vol. 12, no. 16. — P. 2637. — URL: https://dx.doi.org/10.1088/0022-3700/12/16/011.

[270] Drake G.W.F., Farago P.S., van Wijngaarden A. Test of the anisotropy method for Lamb-shift measurements—theory and experiment // Phys. Rev. A. — 1975. — May. — Vol. 11. — P. 1621–1628. — URL: https://link.aps.org/doi/10.1103/PhysRevA.11.1621.

[271] Kuroda N., Ulmer S., Murtagh D.J. et al. A source of antihydrogen for in-flight hyperfine spectroscopy // Nature Communications. — 2014. — Vol. 5, no. 1. — P. 3089.

[272] Ficek Z., Drummond P.D. Three-level atom in a broadband squeezed vacuum field. I. General theory // Phys. Rev. A. — 1991. — Jun. — Vol. 43. — P. 6247–6257. — URL: https://link.aps.org/doi/10.1103/PhysRevA.43.6247.

[273] Ficek Z., Drummond P.D. Three-level atom in a broadband squeezed vacuum field. II. Applications // Phys. Rev. A. — 1991. — Jun. —

Vol. 43. — P. 6258–6271. — URL: https://link.aps.org/doi/10.1103/PhysRevA.43.6258.

[274] Weiner J., Nunes F. Light-matter interaction: physics and engineering at the nanoscale. — Oxford University Press, 2017.

[275] Kaplan S.A., Khaplanov G.M., Khronopulo Yu.G. On the nonlinear absorption coefficient of electromagnetic radiation under astrophysical conditions // Astrophysics. — 1971. — Vol. 7, no. 3. — P. 294–296.

[276] Whitley R.M., Stroud C.R. Double optical resonance // Phys. Rev. A. — 1976. — Oct. — Vol. 14. — P. 1498–1513. — URL: https://link.aps.org/doi/10.1103/PhysRevA.14.1498.

[277] Grachev S.I., Dubrovich V.K. Hydrogen recombination in an expanding universe // Astrophysics. — 1991. — Vol. 34, no. 2. — P. 124–134.

[278] Gupta N., Salter C.J., Saikia D.J. et al. Probing radio source environments via HI and OH absorption // Monthly Notices of the Royal Astronomical Society. — 2006. — dec. — Vol. 373, no. 3. — P. 972–992.

[279] Darling J. Toward a direct measurement of the cosmic accelaration // The Astrophysical Journal Letters. — 2012. — dec. — Vol. 761, no. 2. — P. L26. — URL: https://dx.doi.org/10.1088/2041-8205/761/2/L26.

[280] Wolfe A.M., Jorgenson R.A., Robishaw T. et al. Spectral polarization of the redshifted 21 cm absorption line toward 3C 286 // The Astrophysical Journal. — 2011. — apr. — Vol. 733, no. 1. — P. 24. — URL: https://dx.doi.org/10.1088/0004-637X/733/1/24.

Author's list of publications included in the defense

[35] Labzowsky L. N., Solovyev D. A., Plunien G., Soff G. Asymmetry of the Natural Line Profile for the Hydrogen Atom // Phys. Rev. Lett. 2001. Vol. 87, no. 14. P. 143003-1–143003-4.

[36] Labzowsky L. N., Solovyev D. A., Plunien G., Soff G. Nonresonant corrections for the hydrogen atom // Canadian Journal of Physics. 2002. Vol. 80, no. 11. P. 1187–1194. 10.1139/p02-094.

[37] Labzowsky L., Soloviev D., Plunien G., Soff G. Nonresonant corrections to the 1s-2s two-photon resonance for the hydrogen atom // Phys. Rev. A. 2002. Vol. 65, no. 5. P. 054502-1–054502-3.

[38] Labzowsky L., Solovyev D., Sharipov V. et al. One- and two-photon resonant spectroscopy of hydrogen and anti-hydrogen atoms in external electric fields // Journal of Physics B: Atomic, Molecular and Optical Physics. 2003. Vol. 36, no. 15. P. L227–L233.

[126] Labzowsky Leonti, Solovyev Dmitri. Resonant spectroscopy of the antihydrogen atom // Phys. Rev. A. 2003. Vol. 68, no. 1. P. 014501-1– 014501-3.

[39] Labzowsky L., Sharipov V., Solovyev D. et al. Spectroscopy of the hydrogen and anti-hydrogen atoms in external fields // International Journal of Modern Physics B. 2004. Vol. 18, no. 30. P. 3875–3886. 10.1142/S0217979204026809.

[110] Labzowsky L. N., Shonin A. V., Solovyev D. A. QED calculation of E1M1 and E1E2 transition probabilities in one-electron ions with arbitrary nuclear charge // Journal of Physics B: Atomic, Molecular and Optical Physics. 2005. Vol. 38, no. 3. P. 265–278.

[111] L. Labzowsky, D. Solovyev, G. Plunien, G. Soff. Two-photon E1M1 and E1E2 transitions between 2p and 1s levels in hydrogen // The European Physical Journal D - Atomic, Molecular, Optical and Plasma Physics. 2006. Vol. 37, no. 3. P. 335–343.

[40] Labzowsky L. N., Schedrin G., Solovyev D., Plunien G. Nonresonant corrections and limits for the accuracy of the frequency measurements in modern hydrogen experiments // Canadian Journal of Physics. 2007. Vol. 85, no. 5. P. 585–595. 10.1139/p07-014.

[41] Labzowsky L., Schedrin G., Solovyev D., Plunien G. Theoretical study of the accuracy limits of optical resonance frequency measurements // Physical Review Letters. 2007. Vol. 98, no. 20. P. 2030032-1–2030032-4.

[106] Solov'ev D. A., Sharipov V. F., Labzovskii L. N., Plunien G. Probabilities of single-photon 2s - 1s transition in hydrogen and antihydrogen atoms in an external electric field // Optics and Spectroscopy. 2008. Vol. 104, no. 4. P. 509–512.

[8] Andreev O. Yu., Labzowsky L. N., Plunien G., Solovyev D. A. QED theory of the spectral line profile and its applications to atoms and ions // Phys. Rep. 2008. Vol. 455, no. 4. P. 135–246.

[42] Labzowsky L., Schedrin G., Solovyev D. et al. Nonresonant corrections for the optical resonance frequency measurements in the hydrogen atom // Phys. Rev. A. 2009. Vol. 79, no. 5. P. 052506-1–052506-14.

[82] Labzowsky L., Solovyev D., Plunien G. Two-photon decay of excited levels in hydrogen: The ambiguity of the separation of cascades and pure two-photon emission // Phys. Rev. A. 2009. Vol. 80, no. 6. P. 062514-1–062514-15.

[112] Solovyev D. A., Labzowsky L. N., Sharipov V. F. Influence of an external electric field on the probabilities of two-photon transitions between 2s, 2p and 1s levels for hydrogen and antihydrogen atoms // Optics and Spectroscopy. 2009. Vol. 107, no. 1. P. 16–24.

[113] Solovyev, D.A., Labzowsky, L.N., Sharipov V.F. Odno-, dvuh- i trehfotonnye perehody mezhdu 2s-, 2p- i 1s-urovniami dlia atomov vodoroda i antivodoroda vo vneshnem electricheskom pole i bez nego (in Russian) // Vestnik Sankt-Peterburgskogo Universiteta. Fizika i Khimia 2009. no. 4. P. 377-390.

[114] Solovyev D., Sharipov V., Labzowsky L., Plunien G. Influence of external electric fields on multi-photon transitions between the 2s, 2p and 1s levels for hydrogen and antihydrogen atoms and hydrogen-like ions // Journal of Physics B: Atomic, Molecular and Optical Physics. 2010. Vol. 43, no. 7. P. 074005-1–074005-16.

[83] Solovyev D., Dubrovich V., Volotka A. V. et al. Two-photon decays of highly excited states in hydrogen // Journal of Physics B: Atomic, Molecular and Optical Physics. 2010. Vol. 43, no. 17. P. 175001-1–175001-8.

[115] Solovyev D., Labzowsky L. Two-photon approximation in the theory of electron recombination in hydrogen // Phys. Rev. A. 2010. Vol. 81, no. 6. P. 062509-1–062509-10.

[116] Solovyev D., Labzowsky L. The two-photon approximation for the four-photon decay of the 4d excited state in hydrogen // Canadian Journal of Physics. 2011. Vol. 89, no. 1. P. 123–127.

[117] Solovyev D., Labzowsky L., Volotka A., Plunien G. Extension of the sum rule for the transition rates between multiplets to the multiphoton case // The European Physical Journal D. 2011. Vol. 61, no. 2. P. 297–304.

[118] Zalyalyutdinov T. A., Solovyev D. A., Labzovskii L. N. 4s-1s two-photon decay in hydrogen atom with allowance for cascades // Optics and Spectroscopy. 2011. Vol. 110, no. 3. P. 328–334.

[128] Solovyev D., Dubrovich V. K., Plunien G. Investigation of the electromagnetically induced transparency in the era of cosmological hydrogen recombination // Journal of Physics B: Atomic, Molecular and Optical Physics. 2012. Vol. 45, no. 21. P. 215001-1–215001-7.

[120] Zalialiutdinov T., Baukina Yu., Solovyev D., Labzowsky L. Theory of the multiphoton cascade transitions with two photon links: comparison of quantum electrodynamical and quantum mechanical approaches // Journal of Physics B: Atomic, Molecular and Optical Physics. 2014. Vol. 47, no. 11. P. 115007-1–115007-11.

[129] Solovyev D., Dubrovich V. EIT phenomenon for the three-level hydrogen atoms and its application to the era of cosmological recombination // Central European Journal of Physics. 2014. Vol. 12, no. 5. P. 367–374.

[127] Solovyev D., Labzowsky L. The 21 cm absorption line profile as a tool for the search for antimatter in the universe // Progress of Theoretical and Experimental Physics. 2014. Vol. 2014, no. 11. P. 111E01-1–111E01-6.

[121] Zalialiutdinov T., Solovyev D., Labzowsky L., Plunien G. Two-photon transitions with cascades: Two-photon transition rates and two-photon level widths // Phys. Rev. A. 2014. Vol. 89, no. 5. P. 052502-1–052502-15.

[122] Zalialiutdinov T., Solovyev D., Labzowsky L., Plunien G. Exclusion principle for photons: Spin-statistic selection rules for multiphoton transitions in atomic systems // Phys. Rev. A. 2015. Vol. 91, no. 3. P. 033417-1–033417-12.

[119] Solovyev D., Solovyeva E. Rydberg-state mixing in the presence of an external electric field: Comparison of the hydrogen and antihydrogen spectra // Phys. Rev. A. 2015. Vol. 91, no. 4. P. 042506-1–042506-8.

[123] Zalialiutdinov T., Solovyev D., Labzowsky L. QED calculations of three-photon transition probabilities in H-like ions with arbitrary nuclear

charge // Journal of Physics B: Atomic, Molecular and Optical Physics. 2016. Vol. 49, no. 5. P. 055001-1–055001-8.

[124] Zalialiutdinov T., Solovyev D., Labzowsky L., Plunien G. Spin-statistic selection rules for multiphoton transitions: Application to helium atoms // Phys. Rev. A. 2016. Vol. 93, no. 1. P. 012510-1–012510-7.

[125] Zalialiutdinov T., Solovyev D., Labzowsky L. Generalized spin-statistic selection rules for atomic transitions with arbitrary number of equivalent photons // The European Physical Journal Special Topics. 2017. Vol. 226, no. 12. P. 2837–2842.

[130] Solovyev D. Analysis of the absorption line profile at 21 cm for the hydrogen atom in the interstellar medium // Journal of Physics B: Atomic, Molecular and Optical Physics. 2018. Vol. 51, no. 22. P. 225004-1–225004-13.

[84] Zalialiutdinov T. A., Solovyev D. A., Labzowsky L. N., P. Gunter. QED theory of multiphoton transitions in atoms and ions // Physics Reports. 2018. Vol. 737. P. 1–84.

[52] Solovyev D., Anikin A., Zalialiutdinov T., Labzowsky L. Importance of nonresonant corrections for the description of atomic spectra // Journal of Physics B: Atomic, Molecular and Optical Physics. 2020. Vol. 53, no. 12. P. 125002-1–125002-14.

[53] Anikin A., Zalialiutdinov T., Solovyev D. Angular correlations in two-photon spectroscopy of hydrogen // Phys. Rev. A. 2021. Vol. 103, no. 2. P. 022833-1–022833-11.

[107] Anikin A. A., Zalialiutdinov T. A., Solovyev D. A. Nonresonant Effects in the Two-Photon Spectroscopy of a Hydrogen Atom: Application to the Calculation of the Charge Radius of the Proton // JETP Letters. 2021. Aug. Vol. 114, no. 4. P. 180–187.

[108] Zalialiutdinov T., Anikin A., Solovyev D. Analysis of nonresonant effects in the two-photon spectroscopy of helium // Journal of Physics B: Atomic,

Molecular and Optical Physics. 2021. sep. Vol. 54, no. 16. P. 165002-1–165002-6.

[109] Solovyev D., Solovyeva E. Adapted method of moments for determining the transition frequency // Physics Letters A. 2022. Vol. 432. P. 128021-1–128021-7.